VOLUME [illegible]
DECEMBER 19[illegible]
PART

JOURNAL of the

A[illegible]

D[illegible]

PROCEEDINGS OF THE

ASSETS AND SPECIAL

OF PAYNE AND PAYNE

Journal of the
HYDRAULICS DIVISION
Proceedings of the American Society of Civil Engineers

HYDRAULICS DIVISION
EXECUTIVE COMMITTEE
Harold M. Martin, Chairman; Carl E. Kindsvater, Vice-Chairman;
Wallace M. Lansford; Arthur T. Ippen; Joseph B. Tiffany, Jr., Secretary

COMMITTEE ON PUBLICATIONS
James W. Hall, Chairman; Wallace M. Lansford; Joseph B. Tiffany

CONTENTS

December, 1957

Papers

Number

The Hydraulic Jump at an Abrupt Drop
by Walter L. Moore and Carl W. Morgan 1449

Transition from Laminar to Turbulent Flow in a Pipe
by M. R. Carstens 1450

Flood Frequencies Derived from Rainfall Data
by Joseph L. H. Paulus and John F. Miller 1451

Flow Characteristics on the Ogee Spillway
by Robert B. Jansen 1452

Discharge Characteristics of Rectangular Thin-Plate Weirs
by Carl E. Kindsvater and Rolland W. Carter 1453

Air Binding in Large Pipelines Flowing Under Vacuum
by R. T. Richards 1454

Flow Through Circular Weirs
by J. C. Stevens 1455

Discussion 1456

Divided Flow Through a Divergent Inlet Conduit
by Stavros Tsakonas 1492

Copyright 1957 by the American Society of Civil Engineers.

Paper 1449 December, 1957 HY 6

Journal of the
HYDRAULICS DIVISION
Proceedings of the American Society of Civil Engineers

THE HYDRAULIC JUMP AT AN ABRUPT DROP[1]

Walter L. Moore,* A.M., ASCE and Carl W. Morgan,** A.M., ASCE
(Proc. Paper 1449)

SYNOPSIS

The hydraulic jump may form at various locations relative to a low abrupt drop in a rectangular channel. The role of the drop in determining the form of the jump and in stabilizing its position is clarified by analysis and experiment. An example illustrates the application of the results to the analysis of a stilling basin.

INTRODUCTION

In many types of hydraulic structures a considerable portion of the kinetic energy of the flowing water must be dissipated to prevent erosion of the channel downstream from the structure. Various methods of energy dissipation have been used to achieve tranquil flow conditions as the flow enters the downstream channel. The primary purpose of all such methods is to convert as much as possible of the kinetic energy of the flow into turbulent energy and ultimately into heat. The required energy dissipation is frequently most effectively accomplished by means of a hydraulic jump which may assume several different forms depending on the geometry of the channel boundaries. In an effort to reduce the length of stilling basins and to insure that the jump will not be swept from the stilling basins and to insure that the jump will not be swept from the stilling basin under varying flow conditions, an abrupt drop or rise in the channel bottom may be introduced.

For economic reasons, there has been a tendency in practical design to make the length of the stilling pool considerably less than the length of the jump. This paper presents information concerning the characteristics of the

Note: Discussion open until May 1, 1958. Paper 1449 is part of the copyrighted Journal of the Hydraulics Division of the American Society of Civil Engineers, Vol. 83, No. HY 6, December, 1957.

1. Paper presented at a meeting of the American Society of Civil Engineers in Knoxville, Tenn., June, 1956.

* Prof., Dept. of Civ. Eng., Univ. of Texas, Austin, Tex.
** Asst. Prof., Dept. of Civ. Eng., Univ. of Texas, Austin, Tex.

jump at an abrupt drop in the channel bottom with particular emphasis on the characteristics when the drop is located within the length of the jump.

Previous Study

Basic information concerning the characteristics of the hydraulic jump on a level surface is published in many books on hydraulics and fluid mechanics. Mr. Edward A. Elevatorski[1] has compiled a bibliography of published information concerning the hydraulic jump under various channel and flow conditions. This publication lists some 504 references arranged by years starting in 1819 and extending to 1954.

Information concerning flow problems closely allied with those discussed in this article have been published. Moore[2] made an analytical and experimental study of a free overfall and determined the energy, velocity, and surface profiles for various conditions of flow. Forster and Skrinde[3] studied both theoretically and experimentally the stabilizing effect of an abrupt rise at the end of a jump and developed a composite graphical summary of results by which the downstream depth after the rise could be computed. Valuable contributions to the flow analysis were also made by the several persons discussing this paper. Rouse, Bhoota, and Hsu[4] investigated the stabilizing characteristics of an abrupt drop in a channel bottom. They found that two different types of flow may occur at a given drop, the transition from one to the other being characterized by an undular wave. The type of flow which will form is dependent upon whether the downstream depth is above or below that which produces the undular standing wave. The conditions which produce the undular stage (critical transition zone) cannot be foretold by equations utilizing only the momentum and continuity relationships but must be obtained by experimental measurements. Rouse, Bhoota, and Hsu presented such data which verified their analysis and indicated a systematic transition between the two regimes of flow depending on the Froude number. To simplify the analysis for the two types of jumps, the pressure on the face of the drop was assumed to be hydrostatically distributed and assumed to be dependent on the downstream depth if the jump is upstream from the drop and dependent on the upstream depth if the jump is downstream from the drop. Experimental data was not presented for intermediate positions of the jump which were not subject to a simple analysis based on the two assumed hydrostatic pressure distributions on the face of the drop.

Analysis

The different forms of a hydraulic jump which will occur at an abrupt drop in a rectangular channel are shown in the definition sketch, Fig. 1. For convenience the different forms are identified as A, W, and B as indicated on the sketch. The relative height of a stationary jump $\frac{Y_2}{Y_1}$, will be dependent upon the dimensionless parameters $\frac{\Delta Z_o}{Y_1}$, $\frac{h_D}{Y_1}$ and the Froude number $\frac{V_1}{\sqrt{gY_1}}$ of the entering flow. As the jump changes from one form to the other, the value of

y_1 = Depth upstream from drop
y_2 = Depth downstream from drop
Δz_o = Height of drop
h_D = Piezometric head on drop

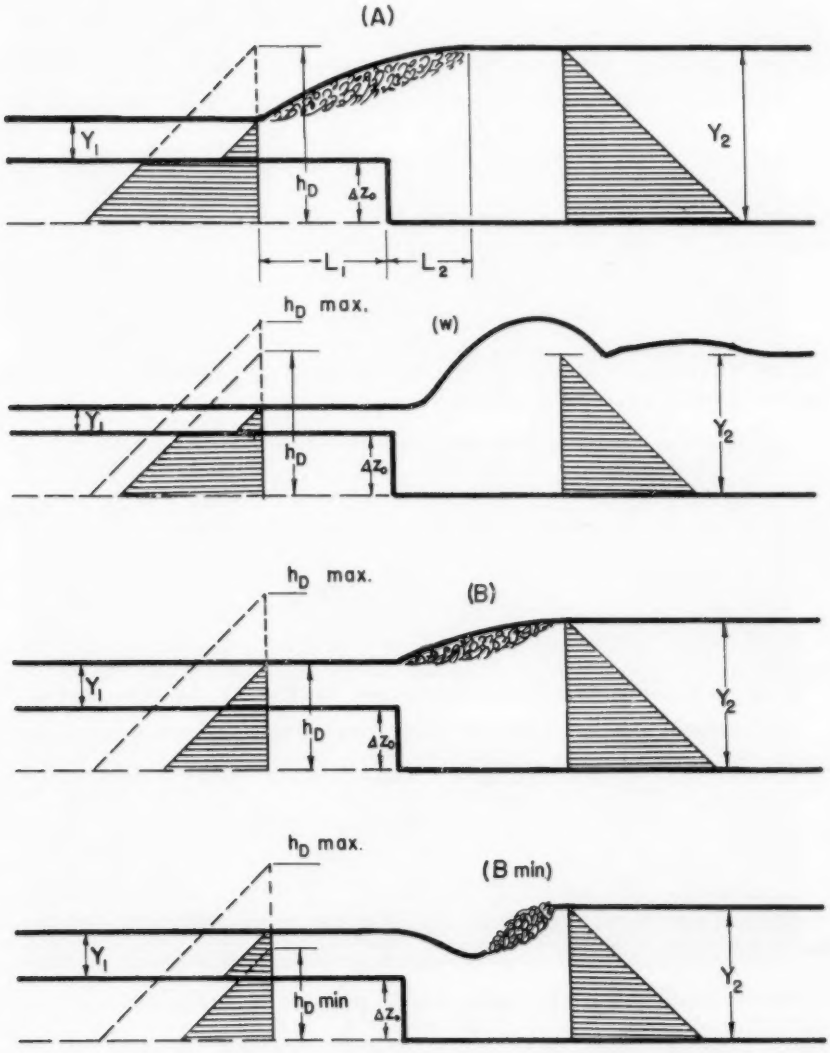

FIG. 1. FORMS OF HYDRAULIC JUMP AT AN ABRUPT DROP.

the hydrostatic head, h_D, will change causing the pressure on the face of the drop to change from a maximum value of $\gamma h_D = \gamma Y_2$ when the jump forms upstream from the drop to a minimum value of $\gamma h_D < \gamma (\Delta Z_o + Y_1)$ when the jump forms downstream from the drop. Photographs illustrating various forms of the jump are shown as Fig. 2.

If the pressure distribution on the face of the drop is assumed to be hydrostatic under a head of h_D, if the shear stress along the solid boundaries between section 1 and 2 is neglected, and if the momentum coefficients β_1 and β_2 are assumed as unity, the momentum equation for sections (1) and (2) is

$$\frac{\gamma Y_1^2}{2} + \gamma\left(h_D - \frac{\Delta Z_o}{2}\right)\Delta Z_o - \frac{\gamma Y_2^2}{2} = \frac{\gamma}{g} q(V_2 - V_1) \tag{1}$$

in which γ is the specific weight of the fluid and q is the discharge per unit width of the channel. If the continuity equation,

$$q = V_1 Y_1 = V_2 Y_2 \tag{2}$$

and Eq. 1 are combined and reorganized, the following general equation relating the several variables is obtained.

$$F_1^2 = \frac{\left(\frac{Y_2}{Y_1}\right)^2 - \left(1 + \frac{\Delta Z_o}{Y_1}\right)^2 - 2\frac{\Delta Z_o}{Y_1}\left(\frac{h_D}{Y_1} - \frac{\Delta Z_o}{Y_1} - 1\right)}{2\left(1 - \frac{Y_1}{Y_2}\right)} \tag{3}$$

Plots of Eq. 3 for different values of the variables are shown as Figs. 3, 4, and 5.

It can be shown that for the condition $h_D = Y_2$ (Fig. 1A) Eq. 3 reduces to

$$F_1^2 = \frac{\left(\frac{Y_2}{Y_1} - \frac{\Delta Z_o}{Y_1}\right)^2 - 1}{2\left(1 - \frac{Y_1}{Y_2}\right)} \tag{4}$$

A plot of this equation gives the upper limiting curve (plotted as a dashed line) for Figs. 3, 4, and 5.

For the condition $h_D = Y_1 + \Delta Z_o$, that is $\frac{h_D}{Y_1} = 1 + \frac{\Delta Z_o}{Y_1}$ (Fig. 1B) the general equation reduces to

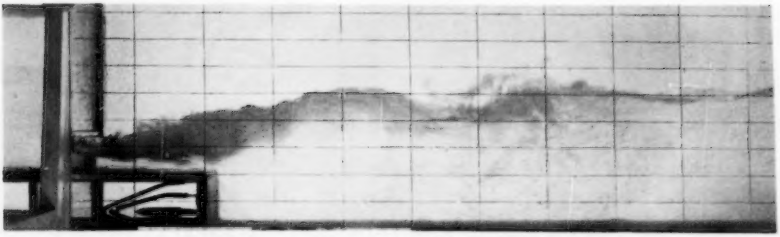

JUMP A

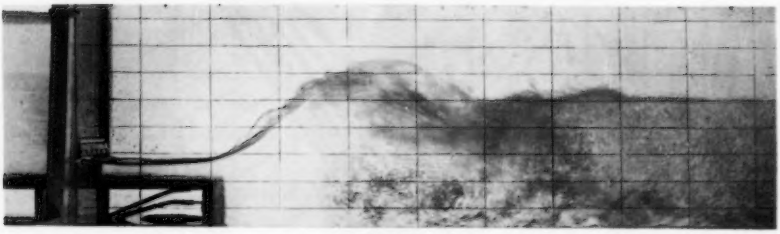

WAVE

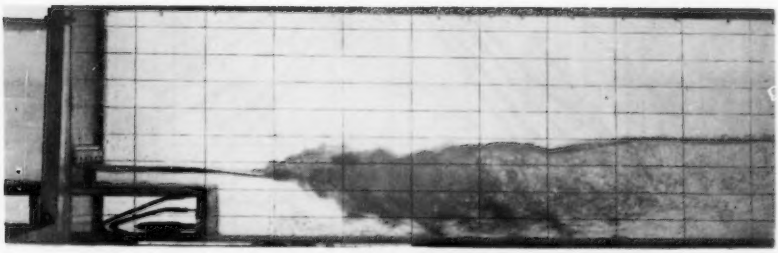

JUMP B

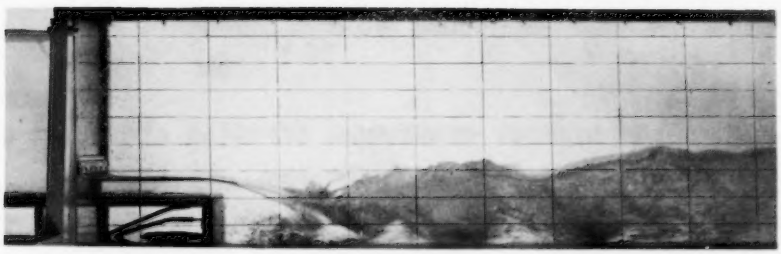

MIN. JUMP B

FIG. 2. PHOTOGRAPHS SHOWING FORMS OF THE HYDRAULIC JUMP AT AN ABRUPT DROP

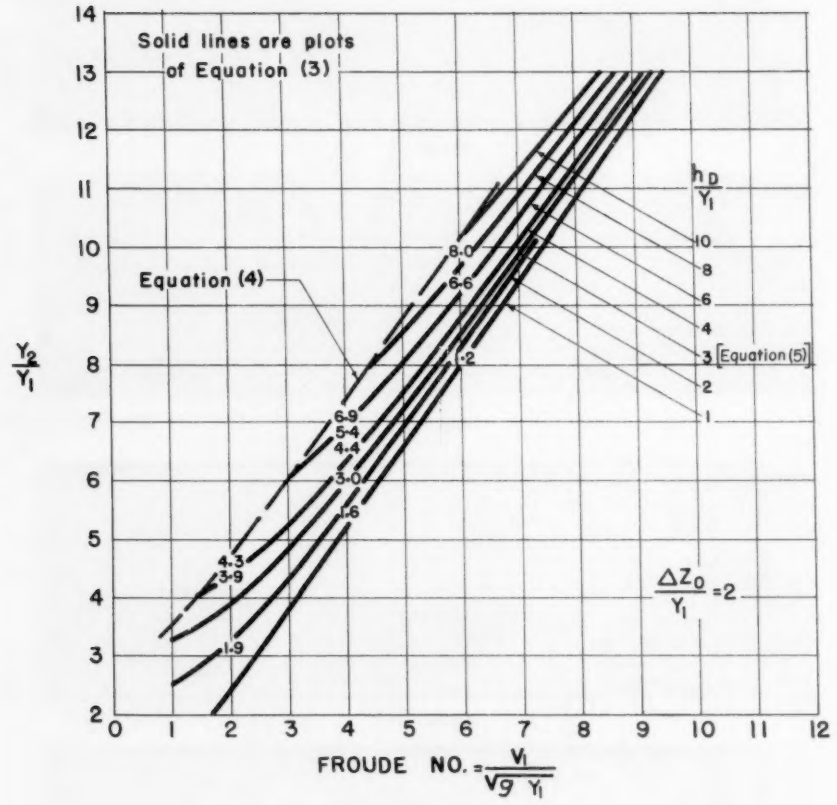

FIG. 3 RELATIVE DOWNSTREAM DEPTH AS A FUNCTION OF FROUDE NO. AND PIEZOMETRIC HEAD AT THE DROP.

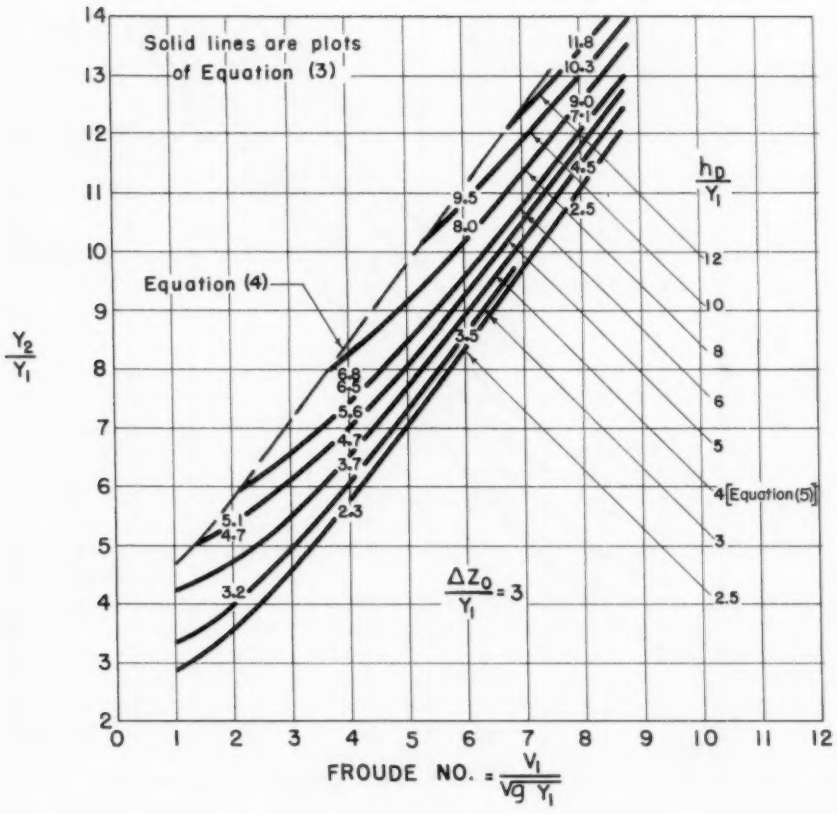

FIG. 4 RELATIVE DOWNSTREAM DEPTH AS A FUNCTION OF FROUDE NO. AND PIEZOMETRIC HEAD AT THE DROP.

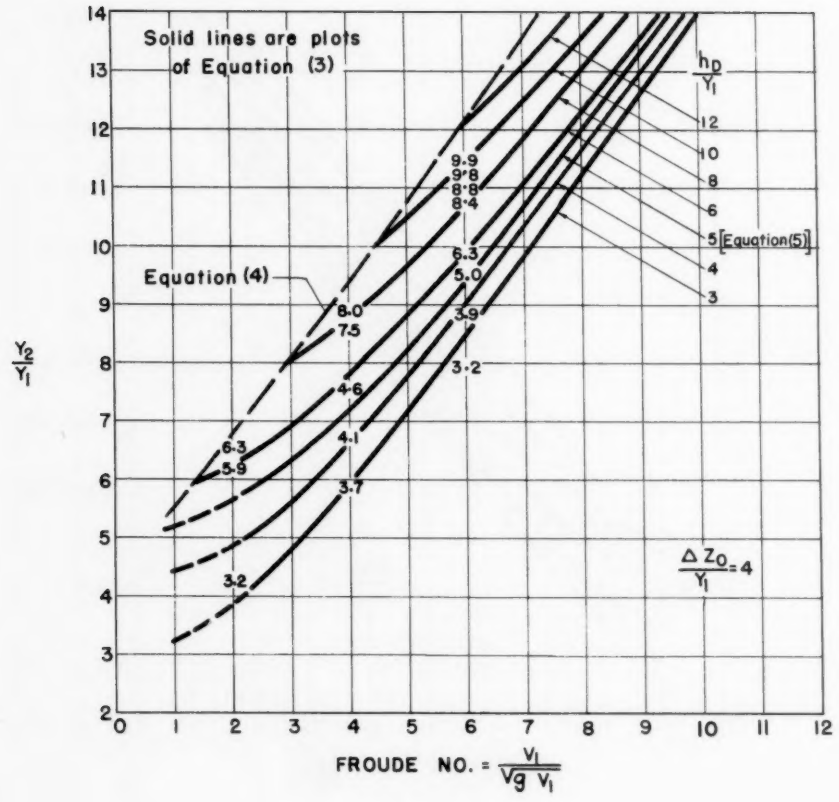

FIG.5 RELATIVE DOWNSTREAM DEPTH AS A FUNCTION OF FROUDE NO. AND PIEZOMETRIC HEAD AT THE DROP.

$$F_1^2 = \frac{\left(\frac{Y_2}{Y_1}\right)^2 - \left(1 + \frac{\Delta Z_o}{Y_1}\right)^2}{2\left(1 - \frac{Y_1}{Y_2}\right)} \quad (5)$$

Equation 4 and 5 are equivalent to the equations given by Hsu, et al,[5] for the two values of h_D which were assumed to determine the characteristics analytically.

It is noted that a reduction of $\frac{h_D}{Y_1}$ causes a shift to the right in the curves of Figs. 3, 4 and 5. That is, for a given condition of the entering flow, the jump can be held in place with a reduced downstream depth Y_2. The converse is, of course, equally true.

Experimental Apparatus

Experimental observations were made on two drops which were constructed of 3/4 inch waterproof plywood and each in turn mounted in a one-foot wide glass walled flume. One drop was 0.400 ft. deep and the other was 0.200 ft. deep. Each was 3 ft. long with an elliptical section at the upstream end and a vertical section at the downstream end. A brass sluice gate adjustable by an attached screw device could be positioned to 0.001 ft. The sluice gate had a carefully machined 1/2 inch rounded edge which gave only a slight contraction in the jet.

Water was supplied from a constant head tank through an 8 in. pipe to the forebay of the flume. The discharge was regulated with an 8 in. gate valve, and the flow rate was measured by a 5 1/4 x 8 in. Venturi-Orifice Meter with a 4 3/8 in. sharp edged orifice plate inserted in the throat section. The differential head on the meter could be read to $\pm$ .001 ft. which made it possible to set the rate of flow with an error less than 1%.

Surface elevations were determined with an electric point gage mounted upon an instrument carriage that could slide along rails above the channel. The vertical position of the gage was read with a direct vernier reading to 0.001 ft. The depth of water in the downstream channel was controlled by a wicket type gate, which caused a minimum disturbance to the flow pattern upstream. It was located 17.5 feet downstream from the last section at which measurements were taken.

Velocities were measured with a standard Prandtl pitot-static tube that had a coefficient of 1.00. The pitot tube was fitted to the same instrument carriage which held the point gage and could be positioned to 0.001 ft. Velocities were measured near the bottom of the channel at several positions downstream from the drop. Distances were measured on a section of engineers steel tape with an error of no more than $\pm$ 0.002 ft.

Values of h_D were measured by means of piezometers attached to piezometric holes drilled in a 1/2 in. x 1 in. brass strip set into the face of the drop so as to be flush with the vertical surface. The openings were set at 0.073 ft., 0.200 ft. and 0.327 ft. from the bottom of the 0.400 ft. drop and at 0.100 ft. from the bottom of the 0.200 ft. drop.

The following flow conditions were chosen for observations.

Z	Y_1	$\frac{\Delta Z}{Y_1}$	F_1	Type of Jump
0.400	0.100	4	2, 4, 6, 8	B, W, A
0.400	0.133	3	2, 4	B, W, A
0.200	0.067	3	6, 8	B, W, A
0.200	0.100	2	2, 4, 6	B, W, A

Values of the depth Y_2, the piezometric head at each piezometer, and velocity along the bottom were read for each of the flow conditions listed.

Results

It was found that the pressure on the face of the drop was hydrostatically distributed under a piezometric head, h_D, which varied with the location of the pump relative to the drop. The measured values of $\frac{h_D}{Y_1}$ are shown on Figs. 3, 4, and 5 at the values of $\frac{Y_2}{Y_1}$ and F_1 at which they were observed. The decimal point indicates the plotted point. These observed values confirm the analytical calculations within the limits of accuracy of the observation and clearly indicate the variation of h_D with the change in the flow conditions.

The limiting values of $\frac{Y_2}{Y_1}$ within which each type of jump would form at given entering flow conditions are shown in Figs. 6, 7, and 8. The conditions under which Jump A will form are shown as a very narrow band, but actually Jump A may form at values of $\frac{Y_2}{Y_1}$ greater than the upper bound being limited only by the free distance upstream and the slope and resistance of the channels. The undular wave will form at values of the variables which fall within the middle band. The height of this wave may exceed the value of Y_2 by as much as 50 per cent and might cause considerable damage unless adequate training walls were provided. Jump B will form when values of the variables are those within the lower band (dotted). The narrow gap between the intermediate and lower bands in Figs. 6, 7, and 8 represents a transition zone where there is uncertainty as to whether the wave or Jump B will form. For values of $\frac{Y_2}{Y_1}$ and F_1 which would lie below the lower band, the jump would be swept downstream from the drop. Perhaps the most important characteristic presented is that the jumps can form over a wide range of $\frac{Y_2}{Y_1}$ for the entire range of entering Froude numbers covered by the experiments. This might be anticipated from the previous analysis because the hydrostatic head, h_D, should vary continuously between its limiting values. Visual observation of the gradual change in curvature of the main stream of the flow as it crossed

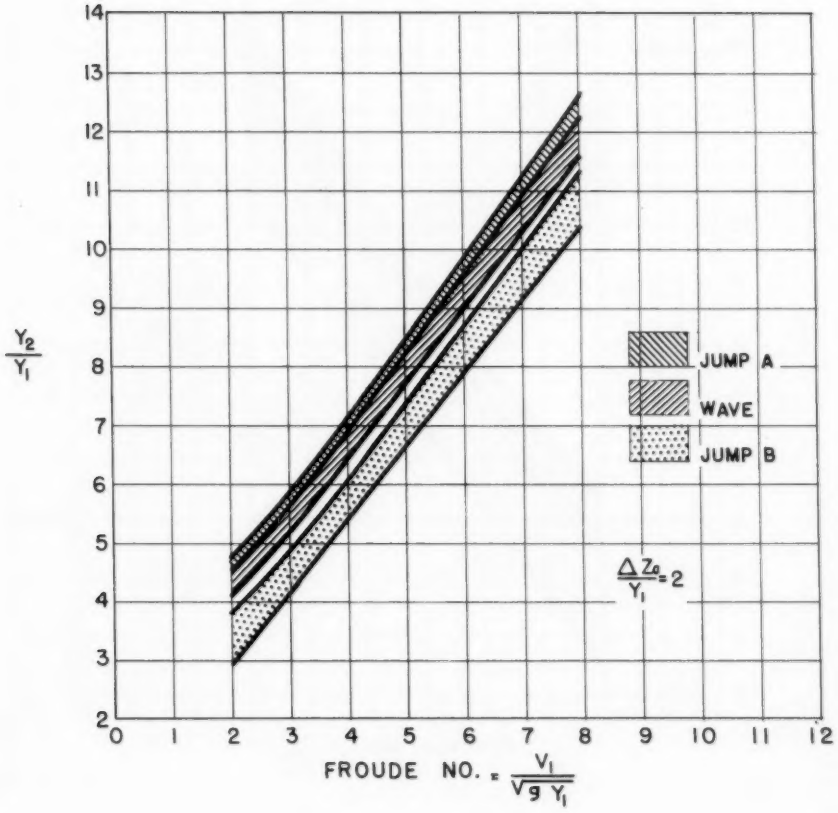

FIG. 6 FORMS OF THE HYDRAULIC JUMP AS A FUNCTION OF FROUDE NO. AND RELATIVE DOWNSTREAM DEPTH.

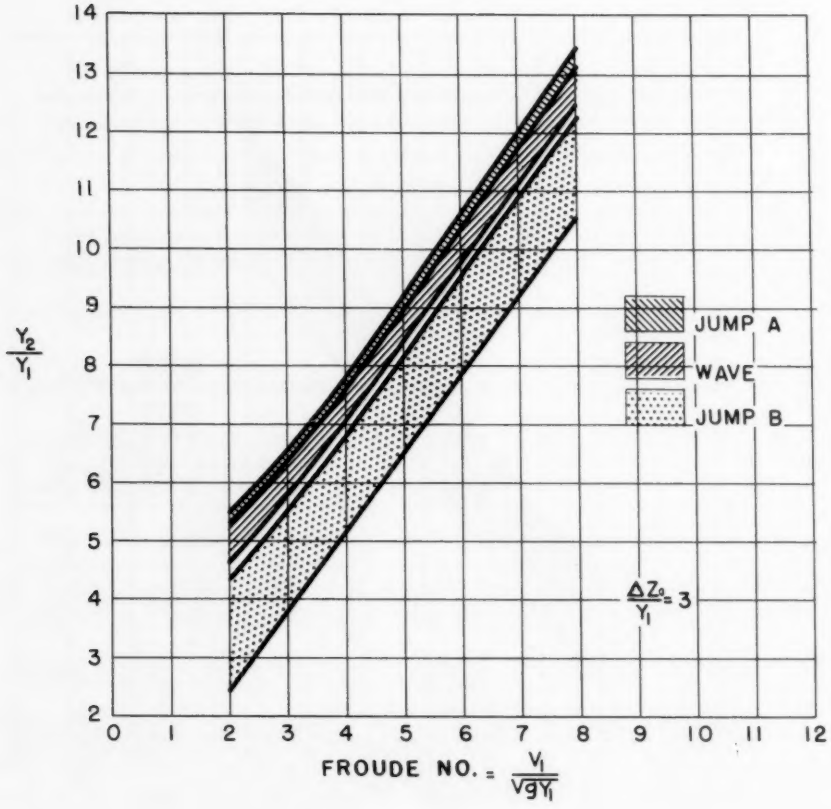

FIG. 7 FORMS OF THE HYDRAULIC JUMP AS A FUNCTION OF FROUDE NO. AND RELATIVE DOWNSTREAM DEPTH.

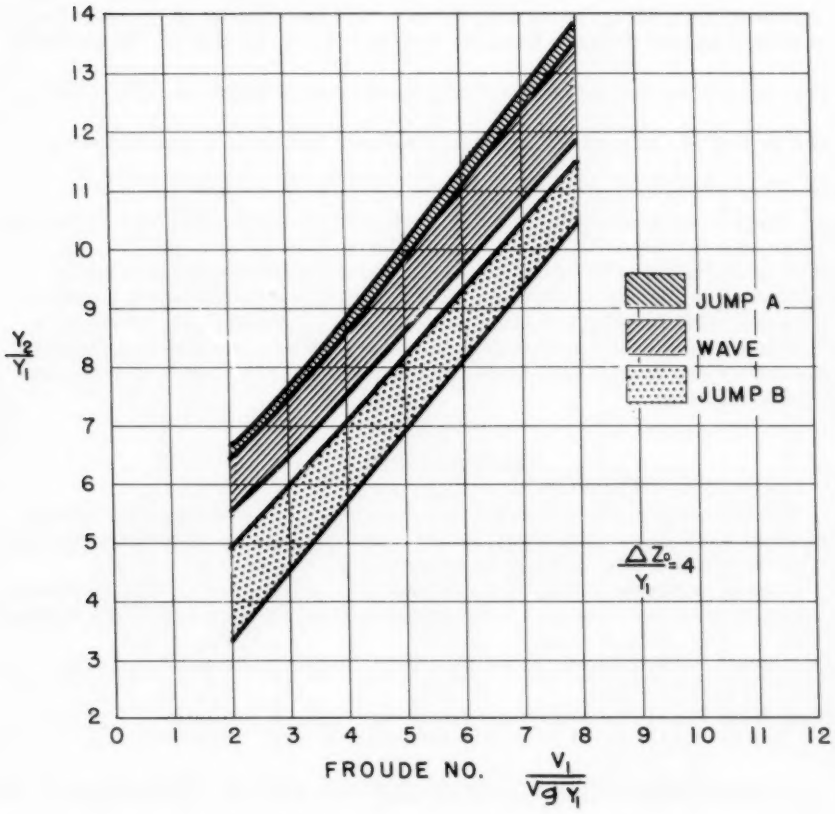

FIG. 8 FORMS OF THE HYDRAULIC JUMP AS A FUNCTION OF FROUDE NO. AND RELATIVE DOWNSTREAM DEPTH.

the drop also indicated a continuous variation of h_D. As indicated by Eq. 3, a continuous variation of h_D implies a continuous variation of $\frac{Y_2}{Y_1}$ between its extreme values.

To demonstrate the effectiveness of the different types of jumps in reducing the velocity along the channel bottom, the velocity near the channel bottom is plotted against distance from the drop in Figs. 9, 10, and 11. Of particular interest are the high velocities produced by Jump B which may give ratios $\frac{V_b}{V_2}$ of 5 or 6 at $\frac{L}{Y_2}$ of approximately 2. The wave and Jump A give values of $\frac{V_b}{V_2}$ from 2 to 3 in the upstream direction near the drop. The return flow results from the reverse roller produced by both the wave and the Jump A. Jump A gives the smallest values of velocities along the bottom in the downstream direction. This condition would be expected since the greater pressure on the face of the drop causes the entering flow to be directed slightly upward and the violent eddy motion to occur in the upper levels of the downstream channel.

Application of Results

The investigation has clarified the action of an abrupt drop in stabilizing the position of a hydraulic jump. The results obtained are directly applicable to the design of a stilling basin incorporating an abrupt drop.

If the downstream depth, Y_2, is required for given entering flow conditions, it may be read from Fig. 6, 7, or 8 using the chart with the applicable relative drop height. For example, given $Y_1 = 2$ ft., Froude No. = 4 and $\frac{\Delta Z_o}{Y_1} = 3$. Then, from Fig. 7, the following information could be obtained:

Type of Jump	Range of $\frac{Y_2}{Y_1}$	Range of Y_2
Jump B	5.1 - 6.8	10.2 - 13.6 ft.
Wave	7.0 - 7.6	14.0 - 15.2 ft.
Jump A	7.6 - 7.8	15.2 - 15.7 ft.

The results may be applied to analyze the performance of a stilling basin for a range of discharges and tailwater elevations. For example, assume a spillway with a crest 100 ft. long at elevation 460 and a coefficient of 4.0. Let the apron be at elevation 400 with a drop of 8 ft. to elevation 392. For a series of values for the head on the spillway, discharge may be determined as well as the depth and Froude number at the base of the spillway; i.e., Y_1 and F_1. (For convenience, the effects of resistance and air entrainment were neglected in the example.) By use of Figs. 6, 7, and 8, and by interpolating for

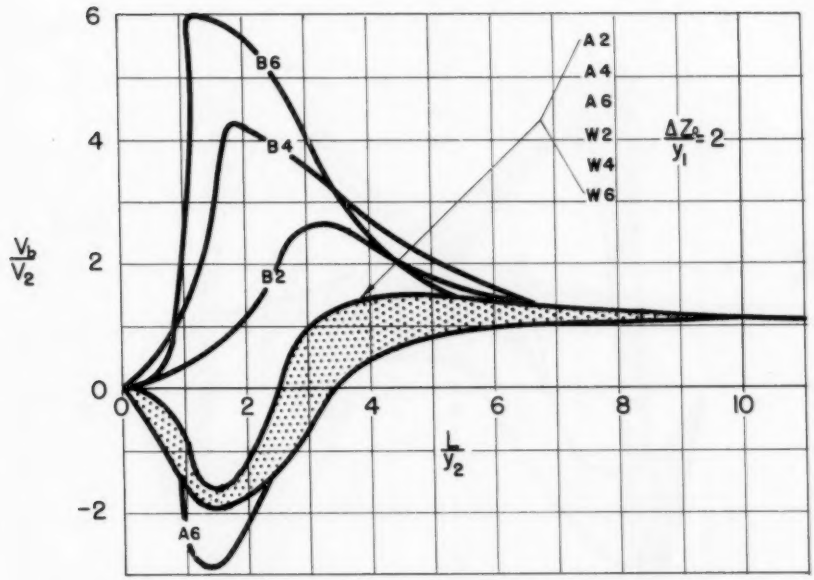

FIG. 9. VELOCITY ALONG BOTTOM Vs. DISTANCE FROM DROP

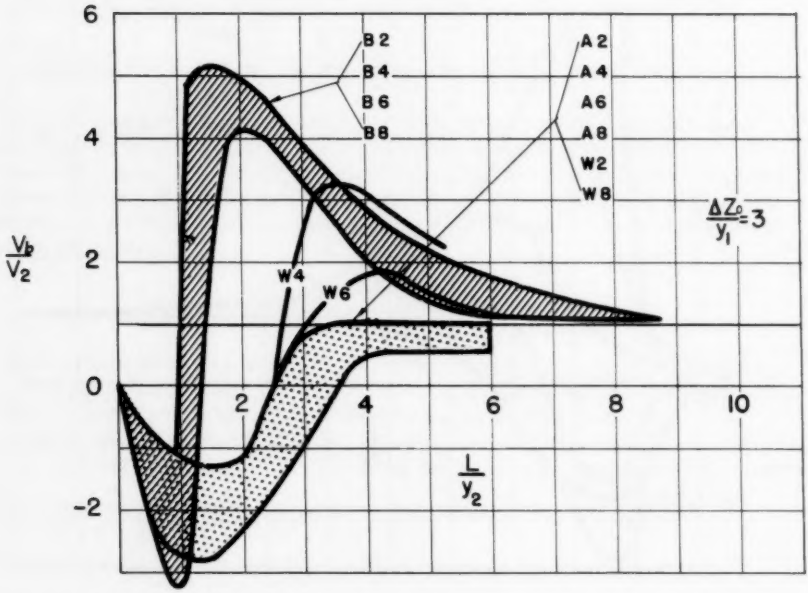

FIG.10. VELOCITY ALONG BOTTOM Vs. DISTANCE FROM DROP

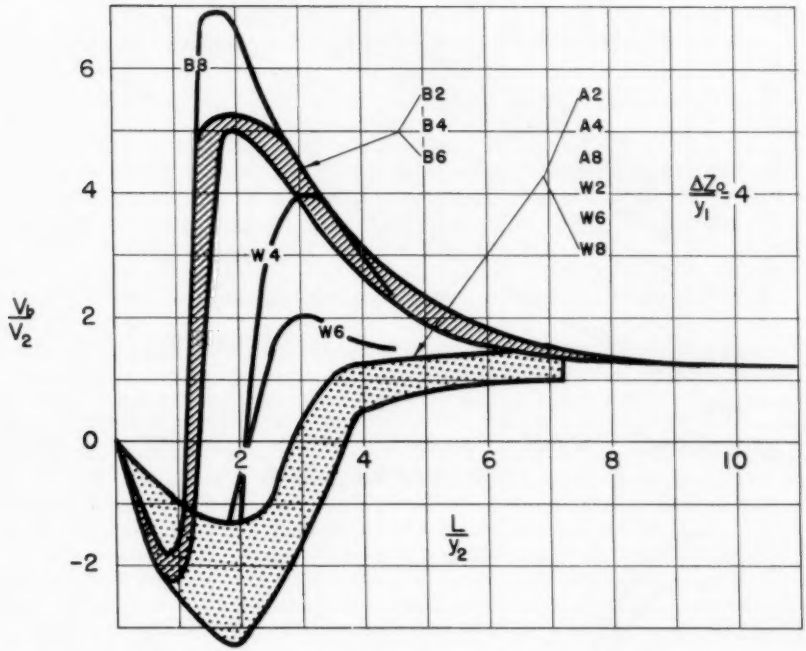

FIG. II. VELOCITY ALONG BOTTOM Vs. DISTANCE FROM DROP

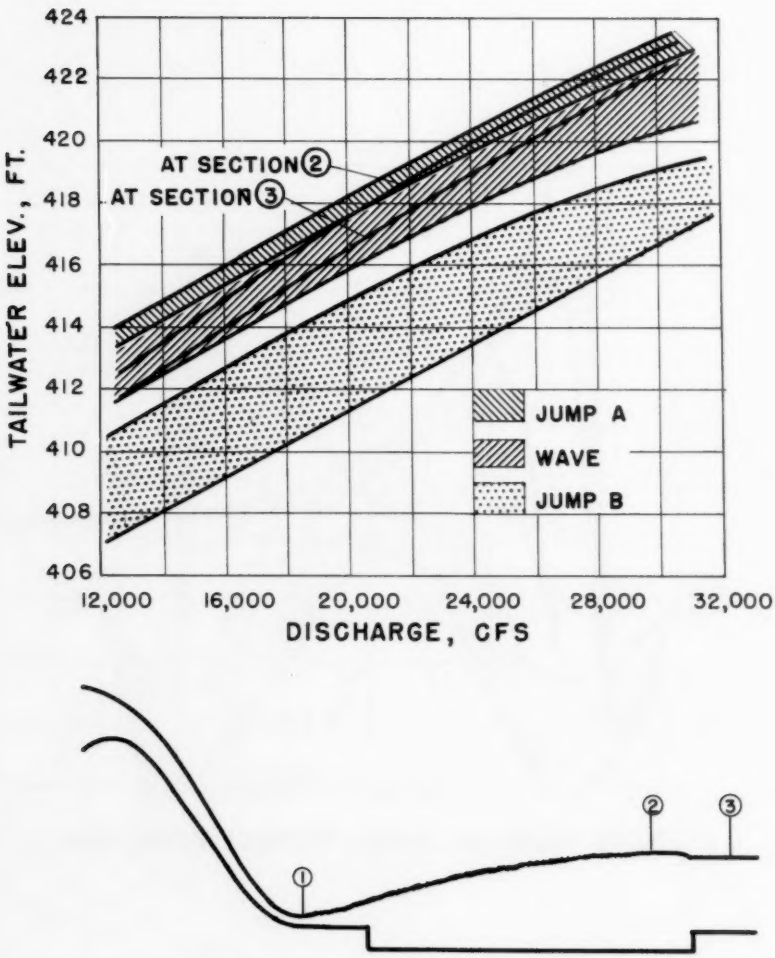

FIG. 12 TAILWATER ELEVATIONS AND JUMP CHACTERISTICS FOR DOWNSTREAM CHANNEL I

intermediate values of $\frac{\Delta Z_o}{Y_1}$, the range of values of Y_2 for each type of jump can be determined. These results are shown in Fig. 12 in which the depths Y_2 have been converted into elevations. Also shown in Fig. 12 are curves of the tailwater elevations at sections 2 and 3 for a rectangular downstream channel 100 ft. wide with its bottom at elevation 398.5, a slope of 0.0016, and a Manning n of 0.03. This is referred to as Channel I. In making the computations it was assumed that the depressed apron (elevation 392) was 125 ft. long which would allow tranquil flow to develop at section 2. If the depressed apron were shorter so that high velocity flow would impinge on the step at the end of the apron, dynamic pressures would develop on the face of the step adding an additional upstream force component tending to stabilize the jump. Since it is not yet possible to evaluate the effect of this force, it was eliminated from consideration by choosing a long apron.

From Fig. 12, it is apparent that the type A jump will occur at discharges above about 20,000 cfs with the form changing to the wave at lower rates of discharge. There is no danger of the jump washing downstream for these conditions and from Figs. 9, 10, and 11, it is apparent that the velocity near the bottom would be negligible while the type A jump forms; i.e., $Q > 20{,}000$ cfs. At lower discharges when the wave forms the velocity near the bottom at the end of the depressed apron would not exceed $3V_2$ or about $3 \times 7 = 21$ ft./sec.

Figure 13 shows what would happen if the same spillway discharged into a channel 100 ft. wide with its bottom at the same elevation as the depressed apron (392) and with a slope of 0.0010 and a Manning n of 0.035. This is referred to as Channel II. From Fig. 13, it is apparent that type A jump would form at the maximum discharge with the form changing successively through the wave to type B as the discharge decreases. As the form of the jump changes, it would move progressively down over the drop but, even at the lowest tailwater, it would remain close to the location of the drop.

These examples illustrate the type of analysis made possible by the results of these experiments. By making it possible to determine the jump characteristics for a wide range of Froude number and tailwater conditions, the effect of both upstream and downstream geometry on the jump characteristics can be determined.

CONCLUSION

1. An abrupt drop in the bottom of a rectangular channel is effective in stabilizing the hydraulic jump over a broad and continuous range of values of the relative downstream depth.

2. As the relative downstream depth is reduced from its upper limit, the jump shifts progressively downstream resulting in a corresponding continuous decrease in the pressure on the face of the drop as the jump passes through three different forms.

3. A momentum analysis which includes a term for the pressure force on the vertical face of the drop gives results which are consistent with the experimental observations.

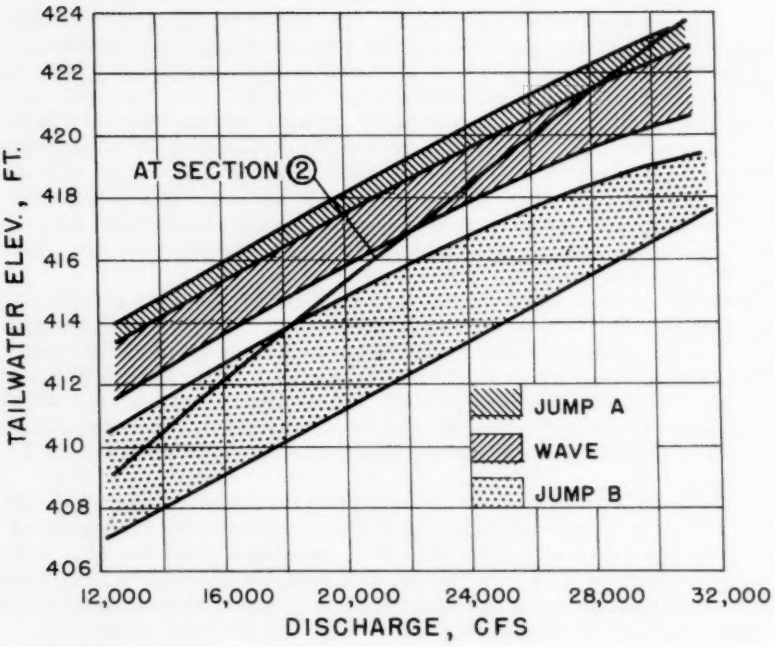

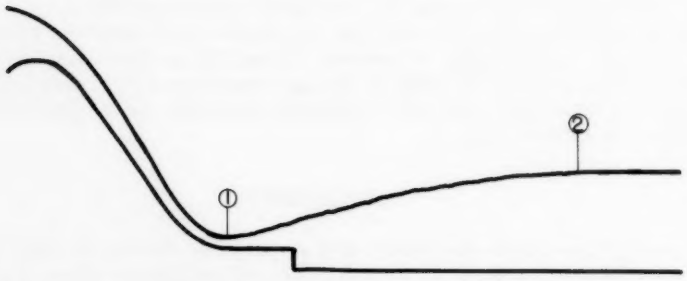

FIG. 13 TAILWATER ELEVATIONS AND JUMP CHACTERISTICS FOR DOWNSTREAM CHANNEL III

4. The maximum velocity attained near the channel bottom, which may be considered as an index of the scouring power of the flow leaving the jump, varies over a wide range and depends mainly on the form of the jump. For the type B jump (Fig. 1) this velocity may attain a value several times greater than the downstream velocity, but for the type A jump, the maximum velocity near the bottom exceeds only slightly the average velocity in the downstream channel.

ACKNOWLEDGMENT

The authors are grateful to the Bureau of Engineering Research of the University of Texas for sponsoring the investigation and for aid in preparing the manuscript and figures. Charles Schmidt, a senior student, made many of the experimental measurements; Robert Pollak and John Phillips prepared the figures; and Dolores Cobb and Wanda Potter typed the manuscript.

REFERENCES

1. Elevatorski, Edward A., "The Hydraulic Jump—A Bibliography," Copyright, First Edition, Albuquerque, New Mexico, (May, 1955).
2. Moore, Walter L., "Energy Loss at the Base of a Free Overfall," Transactions, ASCE, p. 1343, (1943).
3. Forster, John W. and Skrinde, Raymond A., "Control of the Hydraulic Jump by Sills," Transactions, ASCE, p. 973, (1950).
4. Rouse, Hunter; Bhoota, B. V.; Hsu, En-Yun, "Design of Channel Transitions," Proceedings, ASCE, p. 1382, (Nov., 1949).
5. Hsu, En-Yun, Discussion of "Control of the Hydraulic Jump by Sills," by John W. Forster and Raymond Skrinde, Transactions, ASCE, p. 990.

Paper 1450 December, 1957 HY 6

Journal of the
HYDRAULICS DIVISION
Proceedings of the American Society of Civil Engineers

TRANSITION FROM LAMINAR TO TURBULENT FLOW IN A PIPE

M. R. Carstens[1]
(Proc. Paper 1450)

ABSTRACT

Transition from laminar to turbulent flow was experimentally observed during flow establishment in a smooth straight pipe. Turbulence originated as spots. The downstream face of the turbulent spots was transported with the centerline velocity of the preceding laminar flow. Turbulent spot formation was in qualitative agreement with the Tollmein-Schlichting theory of small disturbances.

INTRODUCTION

A study of flow establishment in a pipe was performed in the Hydraulics Laboratory, School of Civil Engineering, Georgia Institute of Technology. The experiments were performed with a smooth, straight, circular pipe which was horizontally aligned. The upstream extremity of the pipe was a well-rounded inlet which was located in a large reservoir. The downstream extremity of the pipe was unobstructed so that a liquid jet was formed in the atmosphere downstream from the pipe. The flow was established by rapid (effectively instantaneous) release of a disk valve placed against the square-edged downstream end of the pipe. Velocity-time data were obtained from a motion picture record of the jet. Pressure-time data were obtained at selected stations along the pipe. These data were recorded as an oscillograph record of the output signals of pressure transducers.

The experiments were performed with a systematic variation of the independent dimensionless variables in the equations:

Note: Discussion open until May 1, 1958. Paper 1450 is part of the copyrighted Journal of the Hydraulics Division of the American Society of Civil Engineers, Vol. 83, No. HY 6, December, 1957.

1. Assoc. Prof., School of Civ. Eng., Georgia Inst. of Technology, Atlanta, Ga.

$$\frac{V}{\sqrt{2gh_o}} = \phi\left[\frac{t\sqrt{gh_o}}{L}, \frac{L}{D}, \frac{gh_oD^3}{L\nu^2}\right]$$

and

$$\frac{h}{h_o} = \phi\left[\frac{t\sqrt{gh_o}}{L}, \frac{L}{D}, \frac{gh_oD^3}{L\nu^2}, \frac{x}{D}\right]$$

The letter symbols are defined as follows:

- D - inside diameter of pipe;
- g - acceleration of gravity;
- h - piezometric head in the pipe, referenced to the pipe centerline;
- h_o - piezometric head in the reservoir, referenced to the pipe centerline;
- L - length of pipe;
- ν - kinematic viscosity of the fluid;
- t - time since opening of the valve;
- V - mean velocity in the pipe; and,
- x - axial distance from the inlet.

Results obtained from ten experimental runs (Runs 20-29, inclusive) are reported in this paper. The value of L/D was 380.3 in Runs 20-24 and was 475.3 in Runs 25-29. The other externally controlled variable, $gh_oD^3/L\nu^2$, was established at values of $6(10^6)$, $12(10^6)$, $18(10^6)$, $24(10^6)$, and $30(10^6)$.

In this paper only the phenomenon of the transition from laminar to turbulent flow is considered. The specific objectives of this study are (1) to determine the position of turbulence formation, (2) to determine the manner of expansion of the turbulence, and (3) to determine the requisite flow conditions for the formation of the turbulence.

Experimental Equipment and Technique

Figure 1 is a schematic drawing of the equipment. The description of the equipment is presented from the upstream section to the downstream.

The reservoir was a sealed cylindrical steel tank with a diameter of 42 inches. The air pressure in the reservoir above the water was controlled to any desired magnitude by means of an air overflow line. The air overflow was allowed to bubble into the bottom of a standpipe. Thus by controlling the water level in the standpipe, the air pressure in the reservoir could be maintained so as to obtain the desired magnitude of the reservoir piezometric head, h_o. No water was added to the reservoir during a run, and no run was made without allowing the reservoir to be quiescent for at least four hours. Since the tank cross section was large and the volume of air above the water was large, the piezometric-head change was negligible ($\Delta h_o/h_o < 0.06\%$) during the short time required for a run. With this arrangement, the value of $gh_oD^3/L\nu^2$ was determined within an estimated accuracy of $\pm$ 0.4% and the magnitude was controlled within $\pm$ 1.0% of the desired value.

The pipe leading from the reservoir consisted of coupled sections of extra-heavy smooth brass pipe. In order to vary the pipe length easily and

systematically, five sections approximately 95 diameters in length were machined and fitted to insure close abutment and proper alignment when forced into the machined-brass sleeve couplings. Each pipe length was carefully aligned along a straight horizontal axis.

The extruded brass pipe proved to be extremely uniform in diameter. Micrometer measurements were taken on orthogonal diameters at each end section. The mean diameter of these twenty measurements was 0.544 inch with all readings being within $\pm$ 0.001 inch of this value. The average diameter of each pipe length was also checked by weighing the water that would fill each length.

The rounded pipe inlet was located in the reservoir. The inlet piece was attached to the first pipe length by a machined connection similar to the sleeve coupling. The machined brass inlet piece was made with a radius of rounding equal to 1.13 pipe diameters. A band of non-uniform sand roughness approximately 1/8-inch wide was cemented to the inlet piece slightly upstream from the tangent point of the inlet roundness.

Wall piezometer holes were placed 1/2-inch from the downstream end of each pipe length. Four piezometer openings were drilled on orthogonal diameters with a No. 45 (0.0820 inch) drill. The holes were carefully inspected, and any burrs caused by drilling were carefully removed. The four piezometer openings were connected by a piezometer ring which was machined in the pipe sleeve coupling.

Pressure-time measurements were obtained by means of pressure transducers, the signal of which was electrically amplified and recorded. These differential-pressure transducers were mounted on a transducer collar in order that the water passage from the pressure transducer to the piezometer ring was large in cross section and short in length. The pressure transducers were of the unbounded-resistance-wire type. The transducer impulses were amplified and recorded on an oscillograph. The oscillograph contained an independent timing mechanism with the result that the oscillograph record consisted of the timing pips as well as the output record of the two pressure transducers. Because of the cost of the transducers and the recording equipment, only two transducers with a two-channel recorder were utilized. Runs with four and five pipe sections (Runs 20-29, inclusive) were duplicated in order to obtain pressure-time records at all piezometer stations.

In order to simplify the boundary conditions associated with the flow establishment, a downstream valve was required which could be instantaneously opened and which in the opening process would not influence the resulting fluid motion. The physical requirements of such a valve are (a) in a negligible time after valve release the piezometric head, h, at the pipe outlet must drop from the value, h_o, to zero, and (b) the valve must be moved in the same direction and with a faster motion than the fluid particles issuing from the pipe outlet. The type of valve selected was a flat disk, which was positioned flush against the downstream end of the pipe. The force of a stressed tension spring was utilized to remove rapidly the valve disk from the oncoming fluid.

Velocity determinations were made from individual frames of a 35 mm motion-picture camera record of the jet. The exposure time for each frame was 0.0015 second. The camera was run at a speed of approximately 36 frames per second. Rear lighting was used in order to eliminate the shadow of the jet. Also, a clock image was recorded in each motion picture frame. Time could be determined to the nearest 0.001 second. A horizontal and a vertical grid scale were also photographed. These scales were positioned in the plane of the jet to avoid parallax.

Transformation of Data into a Form Suitable for Analysis

With this experimental equipment, the time-dependent data were available in the form of a 35 mm motion-picture film strip of the jet and the oscillograph records from the pressure-transducer circuit. The reduction of the pressure data into a useable form was straightforward. The reduction of the film strip data into a useable form was not straightforward. In order to explain the process of data transformation, the data of Run 29 is used throughout the following description. In Run 29 all five pipe lengths were utilized, that is, the value of L/D was 475. The other independent variable, $gh_oD^3/L\nu^2$, was established at the value, $30(10^6)$.

Pressure Transducer Data

In each run the pressure data as recorded by the oscillograph was replotted in the form of the dimensionless piezometric head ratio, h/h_o, as a function of dimensionless time, $t\sqrt{gh_o}/L$. Time, t, was measured from the instant of opening of the valve. The very rapid change in piezometric head, h, from the initial value, h_o, at the instant the valve was opened could be easily discerned on the oscillograph record. Time was measured from this point on the record by the pips made by the independent timing stylus. Figure 2 is a graph of h/h_o at each of the five measuring stations as a function of $t\sqrt{gh_o}/L$ for Run 29. The position of measurement is given by the dimensionless distance from the inlet, x/D. Runs 29 and 29a were duplicate runs in order to obtain pressure measurements at four stations with the two pressure transducers. The pressure at the outlet, x/D = 475, is zero for $t>0$.

Film Strip Data

Six frames of the film strip of Run 29 are shown in Fig. 3.

Two assumptions were used to determine fluid velocity from the photographically recorded jet. First, air resistance was considered negligible. Second, the jet was considered to be a succession of fluid masses composed of individual fluid particles each having the velocity characteristics of this larger group. If the velocity characteristics of the individual particles of a fluid mass are identical, the motion can be completely described by the motion of the mass center of that fluid mass. In Fig. 4 the dimensionless "observed velocity," $V'/\sqrt{2gh_o}$, is plotted as a function of $t\sqrt{gh_o}/L$.

The magnitude of the error involved in assuming negligible air resistance can be determined by observing the same fluid mass on successive film strip frames. The relationships between V' and t determined at + 0.5 ft. and + 2.50 ft. below the pipe were identical, indicating negligible air resistance.

The correctness of the assumption that the jet can be visualized as a series of individual fluid masses is confirmed by the appearance of the jet (Fig. 3). In all the photographs, discrete masses of fluid appear to be forming in the jet. A logical explanation of why the jet can be considered to be a series of fluid masses is as follows. During the time the fluid is in the pipe, the external force of boundary shear acts on the fluid at the pipe wall. This boundary-shear force results in a system of internal shear forces within the fluid and results in a radial variation of linear momentum. The fluid particles close to the wall are deficient in momentum. As the fluid issues from the pipe into the atmosphere, the external boundary-shear force becomes zero. However the internal shear forces are reduced to zero only if the

linear momentum is constant in a cross section. The internal shear forces persist until the jet has constant linear momentum in the cross section. Thus the internal shear forces are the implement for effecting the radial transfer of linear momentum. The result of this process is a jet with uniform linear momentum in a cross section which is, of course, the assumption utilized in determining the "observed velocity," V'.

However, the "observed velocity," V', is not the mean velocity, V, of the pipe flow. Because of the boundary-shear force between the fluid and the pipe wall the velocity distribution is not uniform within the pipe. Thus the fluid upon leaving the pipe has a greater linear momentum than if the velocity of all particles were equal to the mean velocity, V. Since the linear momentum is constant in a fluid mass after this fluid mass leaves the pipe, the fluid mass attains the velocity, V', which is greater than V. The two velocities are related by the relationship, $V = V'/C_m$, in which C_m is the momentum correction coefficient. C_m is a function only of velocity distribution and is defined by the relationship, $C_m = (1/A) \int_A (v/V)^2 \, dA$, in which v is the point velocity and A is the cross sectional area of the pipe. Therefore in order to utilize quantitatively the data of Fig. 4 in a study of pipe flow, the velocity distribution had to be determined as a function of time.

The velocity distribution, or specifically the value of C_m, in unsteady laminar flow was determined by a combination of theoretical analysis and empirical results.

A solution of the Navier-Stokes equations was obtained in which the experimentally determined data relating piezometric head and time were introduced. If the pipe flow is uniform, that is, the velocity is axial, two of the Navier-Stokes equations are indicative that (a) the piezometric head is constant in a fluid cross section which is normal to the flow and (b) the axial piezometric-pressure gradient $\partial p^*/\partial x$ is only a function of time. The remaining equation is

$$\frac{\partial v}{\partial t} = \nu \left[\frac{\partial^2 v}{\partial r^2} + \frac{1}{r} \frac{\partial v}{\partial r} \right] - \frac{1}{\rho} \frac{\partial p^*}{\partial x} \qquad (1)$$

in which v is the point velocity and ρ is the mass density. The boundary conditions are that the velocity, v, is zero at the boundary and that the velocity gradient, $\partial v/\partial r$, is zero at the pipe centerline. The initial condition is that the velocity, v, is zero when time, t, is zero.

The analogous equation with analogous boundary and initial conditions has been solved for temperature distribution in a cylindrical rod.(1) The solution for the pipe flow problem is

$$v = 2/\rho \sum_{n=1}^{\infty} \left[J_o(a_n \beta)/a_n J_1(a_n) \right] e^{-a_n^2 \nu t/r_o^2} \int_o^t g(\tau) e^{a_n^2 \nu \tau/r_o^2} \, d\tau \qquad (2)$$

The various terms are as follows: J_0 and J_1 are Bessel functions of the first kind of orders zero and one, respectively; the positive numbers a_n are the zero roots of J_0; r_0 is the value of the radius, r, at the pipe wall; β is the dimensionless radial coordinate, r/r_0; τ is a dummy variable of integration; $g(\tau)$ is $-\partial p^*/\partial x$; and α is $\nu t/r_0^2$.

In order to apply Eq. (2) in the analysis of the experimental results, the existence and location of a uniform laminar flow region must be determined and, then, the time variation of the piezometric-pressure gradient, $\partial p^*/\partial x$, in this region must be determined from the pressure-time data of Fig. 2.

A physical interpretation of the pressure-time data (Fig. 2) is requisite to locating a laminar flow region. Since the fluid starts from rest, the flow is laminar in the entire pipe during the initial period after the downstream valve is opened. The first external indication of a change in flow regime is the abrupt pressure increase at the piezometers. For example, as shown in Fig. 2, the first of these abrupt pressure increases occurred at the location x/D of 189 at the time $t\sqrt{gh_0}/L$ of 0.616. The interpretation of these pressure increases is that an interface between laminar flow and turbulent flow is passing the piezometer at that instant. The reason for the rapid change is that the mean kinetic energy of the cross section is greater in the laminar flow than in the turbulent flow even though the mean velocity, V, is identical on both sides of the interface. The difference in these kinetic energies is due to the different velocity distributions. Thus at x/D of 189 the flow was laminar prior to $t\sqrt{gh_0}/L$ of 0.616 and was turbulent during the remainder of the run.

The time when turbulence passes through the outlet can also be determined from the pressure record. In Figs. 2 and 4, the time coincidence of the rapid pressure drops and the rapid drop in the "observed velocity" V' is apparent. Both occurrences are a manifestation that the laminar-turbulent interface is passing the pipe outlet at x/D of 475. Prior to $t\sqrt{gh_0}/L$ of 1.38 the flow is laminar at the outlet. During this time a laminar-turbulent interface is moving toward the outlet. The flow is turbulent upstream from the interface. As explained in the preceding paragraph, the piezometric head is greater in the turbulent flow immediately behind the interface than in the laminar flow immediately preceding the interface. The outlet of the pipe is a station of fixed piezometric head since the liquid jet is projected into the atmosphere. Thus as the laminar-turbulent interface passes the outlet, the piezometric-head line is rapidly lowered just upstream from the outlet. The effect is a pivoting of the piezometric-head line. This rapid pivoting of the piezometric-head line results in a piezometric-head drop at every measuring station. The magnitude of this drop is directly proportional to the distance from the inlet. This effect is clearly illustrated in Fig. 2 at the time, $t\sqrt{gh_0}/L$, of 1.38.

With this preliminary knowledge concerning the movement of turbulence, regions can be definitely located in which the flow is laminar. For example, in Fig. 2 between the time, $t\sqrt{gh_0}/L$, of 0.715 and 1.06 the flow is laminar between the x/D stations 379 and 475, and prior to $t\sqrt{gh_0}/L$ of 0.715 the flow is laminar between the x/D stations 284 and 475.

The piezometric-head lines are indicative that the laminar flow regions are uniform. At constant values of time, $t\sqrt{gh_0}/L$, the measured values of piezometric head were plotted as a function of x/D. Since each plotted piezometric-head line was straight at a given time in this laminar flow region, the conclusion was that the region was also a uniform flow region as visualized in the derivation of Eq. (2). A contributing factor in the existence of this uniform downstream laminar flow region is the presence of upstream

turbulent flow regions, since an upstream turbulent flow region has the effect of isolating the inlet. Thus the downstream laminar flow region is similar to flow in an infinitely long pipe since the boundary-layer thickness, piezometric-head gradient, and developing velocity profile are functions only of time.

The slopes of the piezometric-head lines of the uniform laminar flow were determined and plotted. These slope values are shown as points on Fig. 5 for the run being discussed. In order to incorporate this experimental data into Eq. (2), an analytic function for $g(\tau)$ must be selected that approximates the empirical results. A very simple function was selected, that is, $\partial p^*/\partial x$ is proportional to $\cos(\pi t/2t^*)$ in which $t^*\sqrt{gh_o}/L$ is empirically defined as shown on Fig. 5. The value of $t^*\sqrt{gh_o}/L$ is dependent upon the experimental parameters as well as the time and position of turbulence inception. The function for $g(\tau)$ was introduced into Eq. (2) and the integration performed. The resulting expression for the time-developing velocity profile is

$$\frac{v}{V} = \frac{\displaystyle\sum_{n=1}^{\infty} \frac{J_o(a_n\beta)\left[\cos(\pi/2)(t/t^*) + (\pi/2a_n^2\alpha^*)\sin(\pi/2)(t/t^*) - e^{-a_n^2\alpha^*(t/t^*)}\right]}{a_n^3 J_1(a_n)\left[1 + (\pi/2a_n^2\alpha^*)^2\right]}}{2\displaystyle\sum_{n=1}^{\infty} \frac{1\left[\cos(\pi/2)(t/t^*) + (\pi/2a_n^2\alpha^*)\sin(\pi/2)(t/t^*) - e^{-a_n^2\alpha^*(t/t^*)}\right]}{a_n^4\left[1 + (\pi/2a_n^2\alpha^*)^2\right]}} \qquad (3)$$

All terms of Eq. (3) have been previously defined except α^* which is $\nu\, t^*/r_o^2$.

Values of v/V were computed in systematic steps so that by interpolation of the computed results, these results could be applied to all experimental runs. The first nine zero-roots of the Bessel function were used in the numerical computations. The range of the other variables were as follows: $0<\beta<1$, $0.01<\alpha^*<0.05$, and $0.2<t/t^*<1.0$. Values of the linear momentum correction coefficient, C_m, were then computed using numerical-graphical methods. Hence to determine the temporal variation of C_m for any experimental run only the value of $t^*\sqrt{gh_o}/L$ was required.

The analytical solution does not cover the complete temporal range of laminar flow. An empirical method was used to extrapolate the analytical solution. The method is based upon the "observed velocity" data. At the time of transition from laminar flow to turbulent flow at the pipe outlet, there is a sharp discontinuity in the "observed velocity," as shown in Fig. 4. However there can be no discontinuity in the mean velocity. Thus the observed discontinuity must be due to the difference in C_m of the laminar flow and turbulent flow. Hence at the time of transition

$$(C_m)_{laminar} = 1.02\,\frac{(V'/\sqrt{2gh_o})_{laminar}}{(V'/\sqrt{2gh_o})_{turbulent}}$$

since $(C_m)_{turbulent}$ is equal to 1.02. The value of C_m of 1.02 for turbulent flow is based upon the seventh-root law of velocity distribution.

The mean velocity, V, was then computed from the "observed velocity," V'. The displacement boundary-layer thickness was also computed using the following relationship

$$v_c(r_o - \delta^*)^2 \pi = \int_o^{r_o} v\, 2\pi r\, dr \qquad (4)$$

in which v_c is the centerline velocity and δ^* is the displacement boundary-layer thickness. The values of $V/\sqrt{2gh_o}$, δ^*/r_o, and v_c/V of Run 29 are presented in Fig. 6 as a function of time.

Analysis of Results

The specific objectives of this paper pertain to the determination of the manner of turbulence inception and the manner in which the turbulent flow zones are expanded until the pipe is filled with turbulently flowing fluid.

Downstream Movement of Turbulence

The pressure-time records, of which Fig. 2 is an example, of all the runs are indicative that the turbulent flow region is moved toward the outlet in a systematic manner. As previously explained, the abrupt pressure increase at the measuring station is an indication that the laminar-turbulent interface is passing the piezometer, and the simultaneous pressure decrease at all measuring stations is an indication that the laminar-turbulent interface is passing the pipe outlet. A systematic movement of the turbulence is indicated in Fig. 2 between stations at which x/D is 284 and 379 and between stations 379 and 475. The mean transport velocity, V*, (between the measuring stations) of the laminar-turbulent interface was computed. The results are presented in Table I. These results are indicative that the downstream movement of turbulence is a physical transport phenomenon in which the turbulent eddies are transported downstream with a velocity equal to the centerline velocity of the preceding laminar flow.

Nature of the Downstream Face of the Turbulent Zones

A qualitative picture of the nature of the downstream face of a turbulent zone can be constructed from the occurrences recorded as the interface is moved past the pipe outlet. The appearance of a typical jet shortly after the interface has passed the outlet is shown on Fig. 3 (e). The simultaneous pressure decrease at all measuring stations as shown in Fig. 2 occurs during the time the interface is passing the outlet. The rapid decrease in the "observed velocity," V', as shown in Fig. 4 also occurs when the laminar-turbulent interface passes the outlet.

In order to establish the chronological order of events, the times of various occurrences are presented in Table II. Columns 2, 3, and 4 of Table II are based upon motion picture data. In columns 2 and 3 are recorded times of passage through this outlet of the last laminar flow and of the first turbulent flow, respectively. The fluid that passed the outlet in the interveing time is presumably in the interface region. Based upon this time increment the

computed lengths of the interface region are presented in column 4. These computed lengths are useful only to establish the order of magnitude of the length of the interface region because the time interval between the last laminar flow and the first turbulent flow is too short to be determined with precision. The time of passage of the last laminar flow through the outlet as indicated by the pressure record is presented in column 5. The time of passage of the first turbulent flow through the outlet as indicated by the pressure record was not tabulated because the rate of pressure decrease as indicated on the record was of the same order of magnitude as the capability of the oscillograph to follow rapid changes. The interpretation was that the rapid pressure drop was at least as rapid as indicated and was probably more rapid than indicated.

Based upon the previously determined transport velocity and the recorded data (Table II) at the time the laminar-turbulent interface passed through the pipe outlet, a possible configuration of the interface can be conceived which is in basic agreement with the data. Fig. 7 is a schematic drawing of the interface region. The flow is from left to right with laminar flow preceding the turbulent flow. The turbulence in region (a) of Fig. 7 is transported downstream at a velocity, V*, equal to the centerline velocity, v_c, of the laminar flow. The turbulence diffuses radially outward from the central region (a) into the boundary layer (b). In this advanced stage of laminar boundary-layer development, the boundary layer is unstable for a wide range of disturbance frequencies. As the turbulence is diffused into the laminar boundary layer, a point is reached at which the entire laminar boundary layer (c) suddenly becomes turbulent. The last indication of laminar flow from the pressure record (Table II, Column 5), most closely corresponds with the first indication of turbulent flow from the motion picture data (Table II, Column 3). The wall piezometric head, h, probably does not rapidly change (d) until the entire laminar boundary layer becomes turbulent (c). The deceleration of the velocity in the central region as the turbulence penetrates the boundary layer (b) is the cause of the radial piezometric head gradient, (e) to (d), necessary to effect the radial mass transfer involved in changing from the laminar velocity distribution to the turbulent velocity distribution.

Delineation of the Turbulent Flow Regions

The spatial and temporal location of the turbulent regions within the pipe can be determined from the piezometric-head lines. The details of this process are illustrated with the data of Run 29 (Figs. 2 and 6). The values of the piezometric-head ratio, h/h_o, were determined from Fig. 2 at each of the measuring stations at constant values of the time parameter, $t\sqrt{gh_o}/L$. Since the time that a laminar-turbulent interface passed a measuring station could be determined from the pressure record and since this interface was moved with the centerline velocity of the laminar flow, the position of the downstream extremity of a turbulent region could be calculated at the constant values of the time parameter for which the piezometric-head lines were to be plotted. The piezometric-head changes at the laminar-turbulent interfaces were calculated as being the difference in the mean kinetic energy of the laminar and turbulent flow. The piezometric-head lines were then plotted as shown in Fig. 8 A.

A rather complex plotting procedure was adopted in Fig. 8 in order to show both the temporal and spatial location of the turbulent flow regions. The

constant value of $t\sqrt{gh_o}/L$ for each piezometric-head line is shown at the right hand margin. The position of the zero value of h/h_o was lowered with increasing values of $t\sqrt{gh_o}/L$ in order to avoid a superposition of many piezometric-head lines. Since the plotted points at the largest values of x/D are for the pipe outlet, the zero value of each piezometric-head line is at this level. With the known positions of the downstream extremity of the turbulent regions and with the slopes of the piezometric-head lines of the laminar and turbulent flow, the upstream extremity of the turbulent regions could be graphically determined. The regions of turbulent flow are clearly delineated in both time and space on Fig. 8. The turbulent flow regions are below the dashed line and the laminar flow regions are above the dashed line. As a matter of incidental interest, the last laminar flow of Run 29 (Fig. 8A) attained a pipe Reynolds number, VD/ν, of 5.1 $(10)^4$.

Inception of Turbulence

With the turbulent flow regions located both spatially and temporally as shown in Fig. 8, the flow conditions at the time of origin of the turbulent spots can be qualitatively analyzed with reference to the stability of small disturbances.(2) Basically, the method is to introduce a two-dimensional periodic disturbance into the Navier-Stokes equations and to determine whether the disturbance is amplified or diminished as the disturbance is moved downstream. The neutral curve which separates the regions of amplification and decay is presented on Fig. 9 for Blasius flow over a flat plate.(3) The ordinate value is a ratio of the displacement boundary-layer thickness δ^* to the disturbance wave length λ. The abscissa value of Fig. 9 is the boundary-layer Reynolds number R_{δ^*}.

The salient features of turbulence inception are apparent in Fig. 8, and the pertinent flow parameters are presented in Table III. The most prominent characteristic is that turbulence started as spots in laminar flow. The downstream face of these spots was transported downstream in a systematic manner as shown previously. The upstream face of the turbulent spots did not indicate a systematic movement along the pipe; but even for the spots in which the upstream face moved downstream, this movement was at a lesser velocity than for the downstream face. The result is a joining together of the spots as shown clearly in Fig. 8A. The pattern of turbulent spot generation was approximately the same for equal values of the independently controlled parameter, $gh_oD^3/L\nu^2$. That is, in Runs 29 and 24 the value of $gh_oD^3/L\nu^2$ was $30(10)^6$, in Runs 28 and 23 the value was $24(10)^6$, in Runs 27 and 22 the value was $18(10)^6$ in Runs 26 and 21 the value was $12(10)^6$, and in Runs 25 and 20 the value was $6(10)^6$.

Since the flow throughout the pipe was laminar prior to turbulent spot generation, the initial transition from a laminar boundary layer to a turbulent boundary layer must have been aided by an instability of the laminar boundary layer rather than the external source of free-stream turbulence. The magnitude of R_{δ^*}, $v_c\delta^*/\nu$, at turbulence inception (Table III) in comparison with the magnitude of R_{δ^*} required for boundary-layer instability (Fig. 9) is indicative that turbulence exists soon after the boundary layer is unstable. Direct numerical comparison between the values of R_{δ^*} in Table III and Fig. 9 is not possible for two reasons. Firstly, the curve of neutral stability of Fig. 9 is for Blasius flow over a flat plate rather than for a temporally growing boundary layer in a circular pipe. Secondly, the experimentally

determined values of $R\delta^*$ of Table III are the values at the time of turbulence inception; whereas, the values of $R\delta^*$ of Fig. 9 are the values at which disturbances are either amplified or diminished. Since a disturbance undoubtedly must undergo some amplification before the disturbance is transformed into turbulence, turbulence inception occurs at a later time and at a farther downstream position than the time and place of disturbance generation.

The location of the points of turbulence inception (Fig. 8 and Table III) is indicative of the source of the disturbances.

Turbulent spot number 1 occurred in all runs and in the position range of $0 < x/D < 62$. The source of disturbances for turbulent spot number 1 was the band of sand grain roughness which was cemented to the bellmouth inlet. Since the source of disturbances was at the inlet, the value of x/D at the position of turbulence generation is evidence of the distance required to amplify the disturbance before turbulence is actually generated. The flow pattern is complex in the region just downstream from the inlet since the boundary layer is expanding both with increasing time and increasing distance from the inlet. Because the disturbance is generated in a region of small boundary-layer thickness, the disturbance may first diminish in amplitude due to the small and hence stable value of $R\delta^*$. Since the boundary layer increases in thickness both with distance and time, the disturbance which was initially diminishing may pass into the region of instability or amplification. The disturbance is moved further downstream during amplification. At some point the disturbance attains a sufficient amplitude to break into turbulence. The heterogeneous mixture of disturbance wavelengths from the nonuniform sand grain roughness as well as the spatially varying laminar boundary-layer thickness precluded the possibility of avoiding the unstable region (Fig. 9) with the result that turbulent spot number 1 existed in all runs.

Turbulent spot number 2 occurred in all runs except Run 25 and in the position range $99 < x/D < 134$. This position is indicative that the source of disturbances was the pipe junction at x/D of 95. In spite of the care of preparing the pipe junctions, the pipe edges could have been mismatched as much as 0.001 inch because of diameter variations between the ends of each pipe length. With the pipe junction as the source of disturbances for turbulent spot number 2, the distance required for amplification of the disturbance was from 4 to 39 pipe diameters. More significantly, this distance for amplification varies between $130\delta^*$ and $650\delta^*$. In order to determine the minimum possible wavelength the maximum value of $2\pi\delta^*/\lambda$ of 0.409 is utilized from Fig. 9. Thus the minimum wave length, λ, is approximately $15\delta^*$. With this minimum wavelength and the distance for amplification, the maximum number of disturbance waves between the disturbance source and the point of turbulence inception would be approximately 40.

The existence of turbulent spot number 2 (Table III) in all runs except Run 25 can be qualitatively explained by reference to the neutral stability curve. The dimensionless boundary-layer thickness, δ^*/r_o, and the boundary-layer Reynolds number, $R\delta^*$, were computed for each run. In Fig. 10 the value of δ^*/r_o is presented as a function of $R\delta^*$, $v_c\delta^*/\nu$ for the early portion of all runs. The boundary-layer parameters as shown in Fig. 10 are very similar for Runs 29 and 24, Runs 28 and 23, and so forth. This similarity of boundary-layer parameters is the reason for the similarity of the turbulent spot patterns which was mentioned previously. With the hypothesis that the disturbance wave length λ is proportional to the roughness height at the pipe junction, a possible neutral stability curve for turbulent spot number 2 is shown

on Fig. 10. This neutral stability curve is for a disturbance wavelength, λ, of approximately 2.1 r_o. This neutral stability curve is for the longest disturbance wavelength which originates at the pipe junction. Thus, the neutral stability curves for shorter wavelengths would be below the curve shown in Fig. 10. With this concept there is no conflict in that some of the points of turbulence inception (indicated by the circular symbols on Fig. 10) are below the lower branch of the curve shown. The curve of neutral stability is a line of zero amplification. Other lines of constant amplification are similar in shape to the neutral curve and resemble the contour lines of the end of a ridge on a topographic map. Since the boundary layer is undergoing essentially temporal growth, the boundary-layer curves of Fig. 10 can be visualized as pertaining to a single wave or disturbance. Thus a disturbance of Runs 20 and 25 (Fig. 10) would be subjected to lesser amplification in crossing the unstable zone than for the other runs. The disturbance of Run 20 received sufficient amplification to break into turbulence, whereas the disturbance of Run 25 passed into the upper stable zone before breaking into turbulence. Once a disturbance is in the upper stable zone, this disturbance will diminish without breaking into turbulence.

Turbulent spot number 3 occurred in only Runs 24 and 29 at the x/D position of 200 and 213. This position is indicative that the source of the disturbances was the pipe junction at x/D of 190. This axial distance is equivalent to $310\delta^*$ and $600\delta^*$. The maximum number of disturbance waves between the source and the point of turbulence would be approximately 40. A possible neutral stability curve for the longest wavelength, equal to 1.5 r_o, is shown in Fig. 10 for turbulent spot number 3. The interpretation is the same as before except that only in Runs 24 and 29 was a disturbance amplified sufficiently to break into turbulence. In all other runs a disturbance was not sufficiently amplified in crossing the unstable zone to break into turbulence.

Upstream Face of a Turbulent Spot

The experimental data are of little use in defining the nature of the upstream face of the turbulent zones. Since every individual turbulent eddy is transported downstream, new turbulence would have to be generated even for the upstream face of the turbulent zone to remain in a fixed position. Since the position of the upstream face of the turbulent zones depends upon the generation of new turbulence, the probability is that this face has an erratic motion. If two turbulent spots are joined before the downstream face of the upstream spot passed a pressure transducer station, the presence of the upstream spot could not be detected from the data. In fact, it is probable that turbulent spot number 1 of Fig. 8B and Fig. 8D is formed from two or more spots which are soon joined. The upstream face of the turbulent zone would move downstream if no new turbulence were generated. In a temporally growing boundary layer, a single burst of turbulence might be generated, subsequent disturbances from a fixed source of disturbance being insufficiently amplified to break into turbulence. Referring to Fig. 10, this occurrence appears to be probable for turbulent spot number 2 in Run 20 and for turbulent spot number 3 in Runs 24 and 29. The definite downstream movement of the upstream face of these turbulent spots, as shown in Figs. 8A, 8B, and 8J, is indicative of this occurrence.

CONCLUSIONS

Based upon an experimental study of unsteady flow, the following conclusions concerning transition from laminar to turbulent flow in a pipe are considered to be significant:

1. In an experimental investigation of laminar boundary-layer transition the effects of free-stream turbulence can be avoided entirely with a temporally expanding boundary layer.

2. Transition from laminar to turbulent flow in a pipe occurs in spots.

3. The magnitudes of the laminar boundary layer Reynolds number at turbulence inception was in reasonable agreement with the theoretical values determined for Blasius flow over a flat plate.

4. The downstream movement of a turbulent zone into a laminar zone is that of physical transport. The transport velocity is that of the centerline velocity of the laminar flow. In the region of this interface the free stream turbulence is the disturbance source for laminar boundary layer transition.

5. The regions of laminar and turbulent flow in a pipe can be defined from the piezometric-head lines.

6. From the standpoint of boundary shear, the pipe utilized in the experiment would be classified as smooth. However, from the standpoint of laminar boundary-layer transition, disturbance sources were found at the pipe junction as well as at the sand-roughened inlet.

7. With a systematic variation of boundary-layer parameters, the presence or absence of boundary-layer transition at the pipe junctions was found to be in qualitative agreement with the laminar boundary-layer stability theory.

ACKNOWLEDGMENTS

The experiments on which this paper is based were conducted under the writer's supervision by Messrs. Christopher and Trimble in the Hydraulic Laboratory, School of Civil Engineering, Georgia Institute of Technology. Four graduate theses have been submitted based upon this study. The authors of the theses are Messrs. Christopher, Trimble, Roller, and Olive. Financial assistance for the study was granted by the National Science Foundation, Washington, D. C.

REFERENCES

1. "Fourier Transforms," by Ian N. Sneddon, McGraw-Hill Book Co., Inc., New York, N. Y., 1951, p. 202.

2. "Boundary Layer Theory," by H. Schlichting, translated by J. Kestin, McGraw-Hill Book Co., Inc., New York, 1955, Chapter XVI, pp. 308-336.

3. "On the stability of two-dimensional parallel flows, Part III," by C. C. Lin, Quarterly of Applied Mathematics, Vol. 3, January 1946, p. 277.

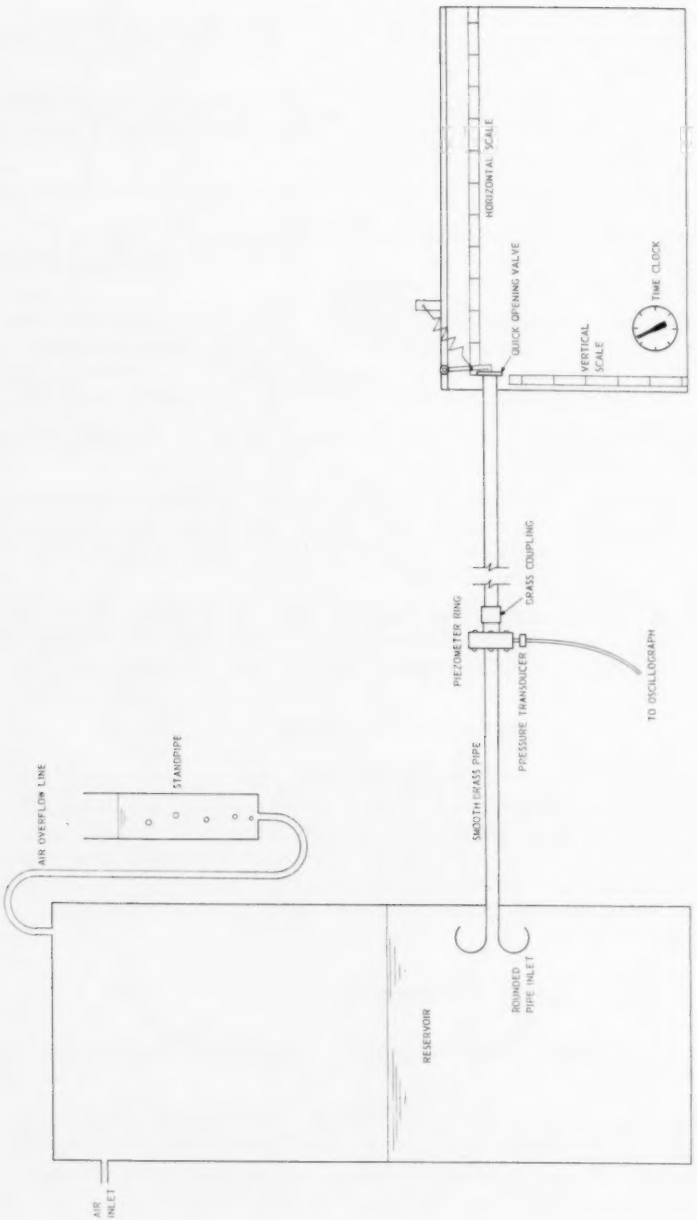

Figure 1. Schematic Drawing of Equipment.

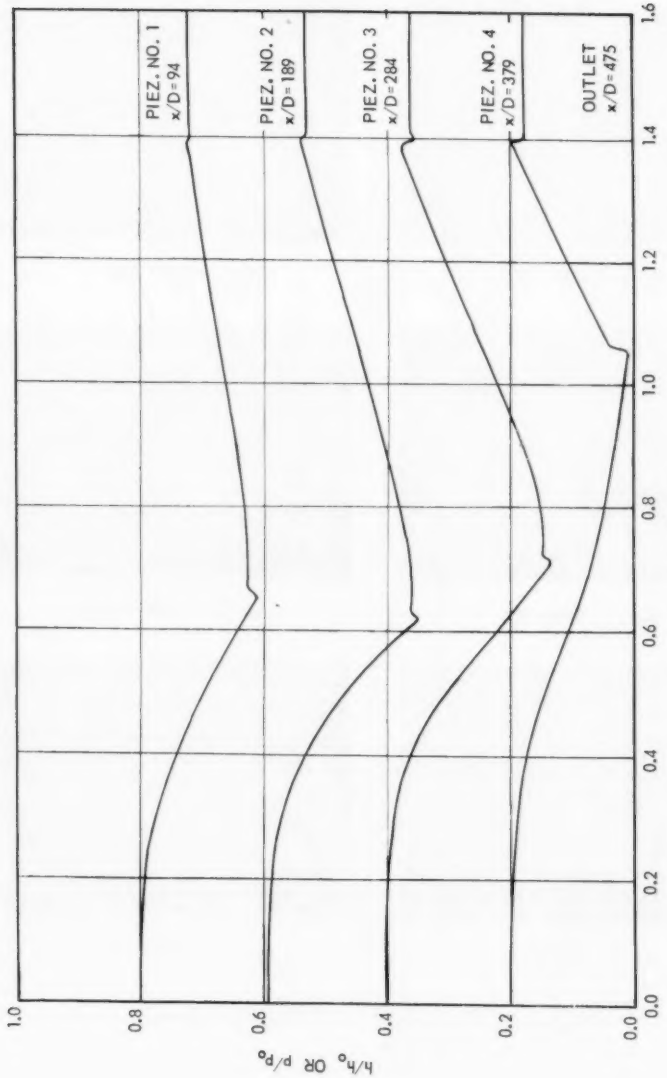

Figure 2. Pressure-time Curves of Runs 29 and 29a.

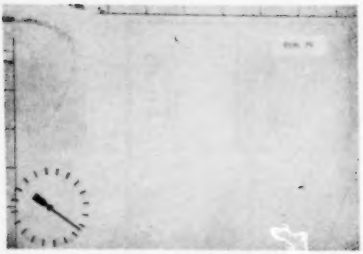

(a) T = 0.355 SEC.

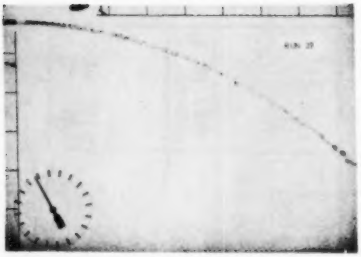

(d) T = 1.222 SEC.

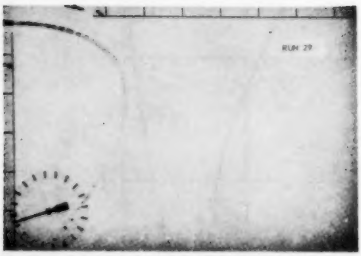

(b) T = 0.466 SEC.

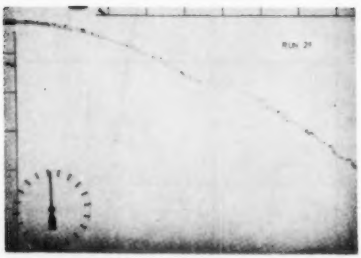

(e) T = 1.607 SEC.

(c) T = 0.511 SEC.

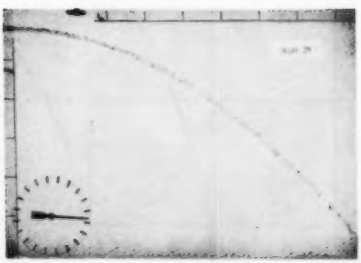

(f) T = 1.953 SEC.

Figure 3. Selected Film Strip Data of Run 29.

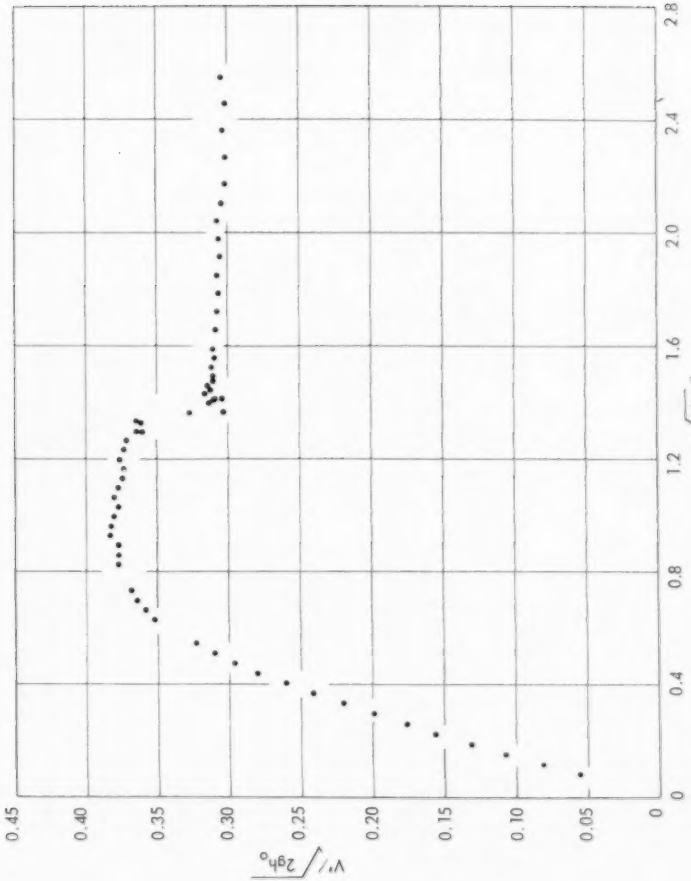

Figure 4. Observed Velocity-time Data of Run 29.

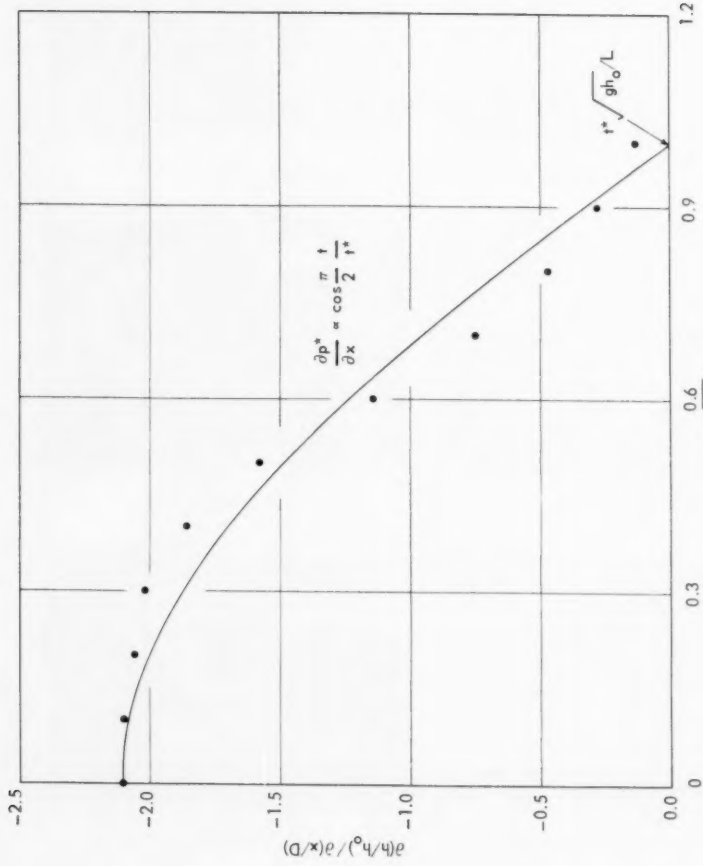

Figure 5. Temporal Variation of The Piezometric-Head Line Slope in the Uniform Laminar Flow of Run 29.

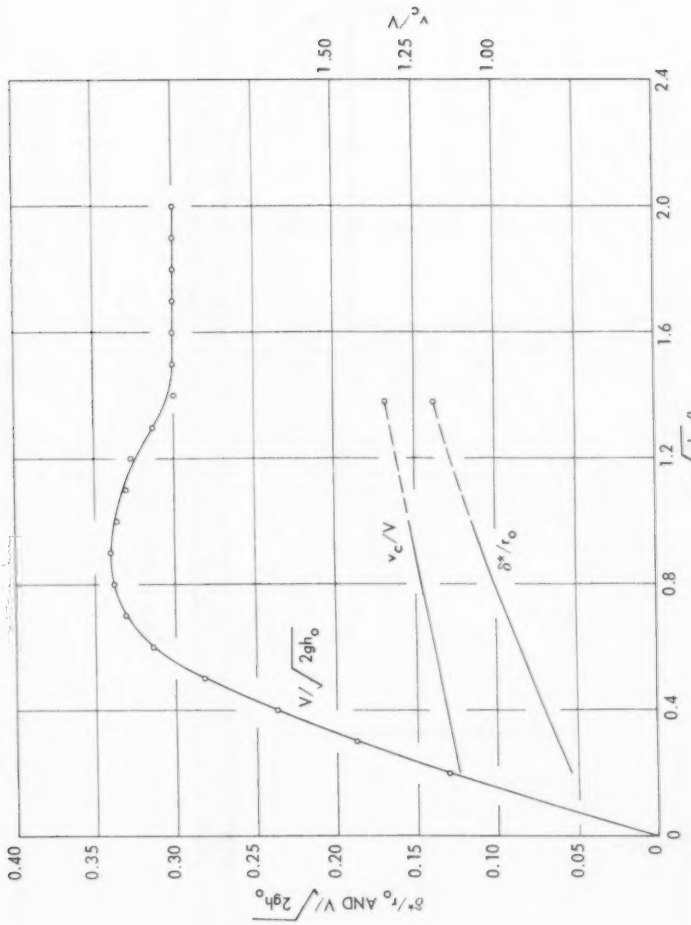

Figure 6. Temporal Variation of $V/\sqrt{2gh_o}$, δ^*/r_o, and v_c/V of Run 29.

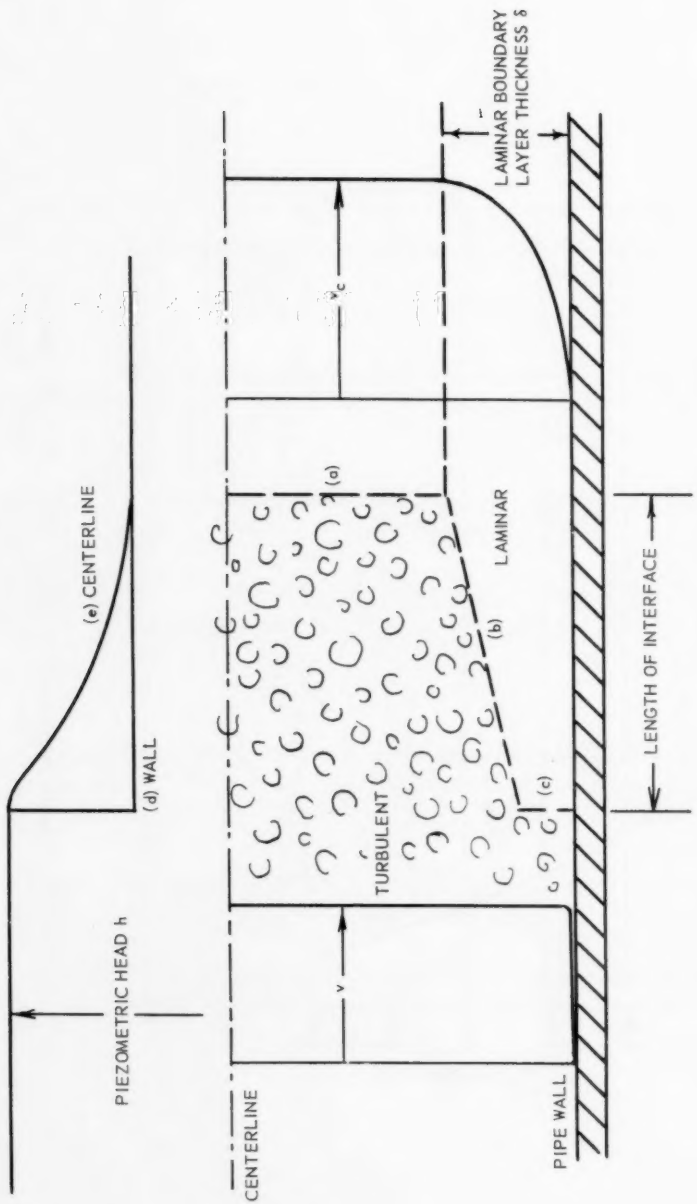

Figure 7. Schematic Drawing of the Laminar-Turbulent Interface Within the Pipe.

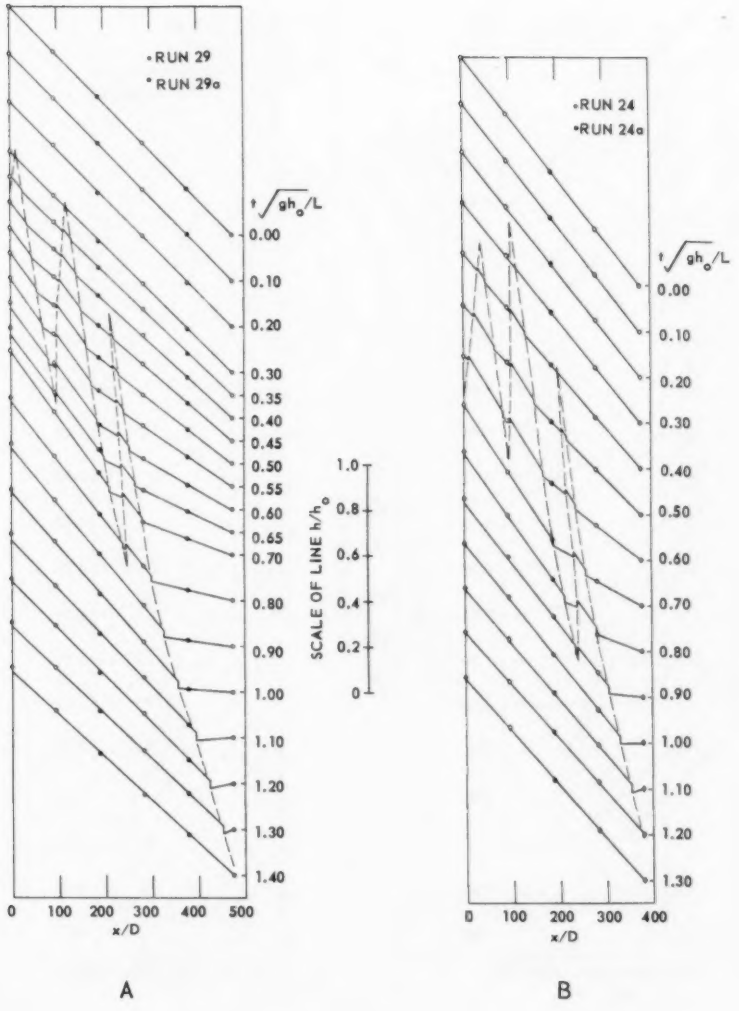

Figure 8. Piezometric Head Lines of Runs 20-29, Inclusive. (Continued)

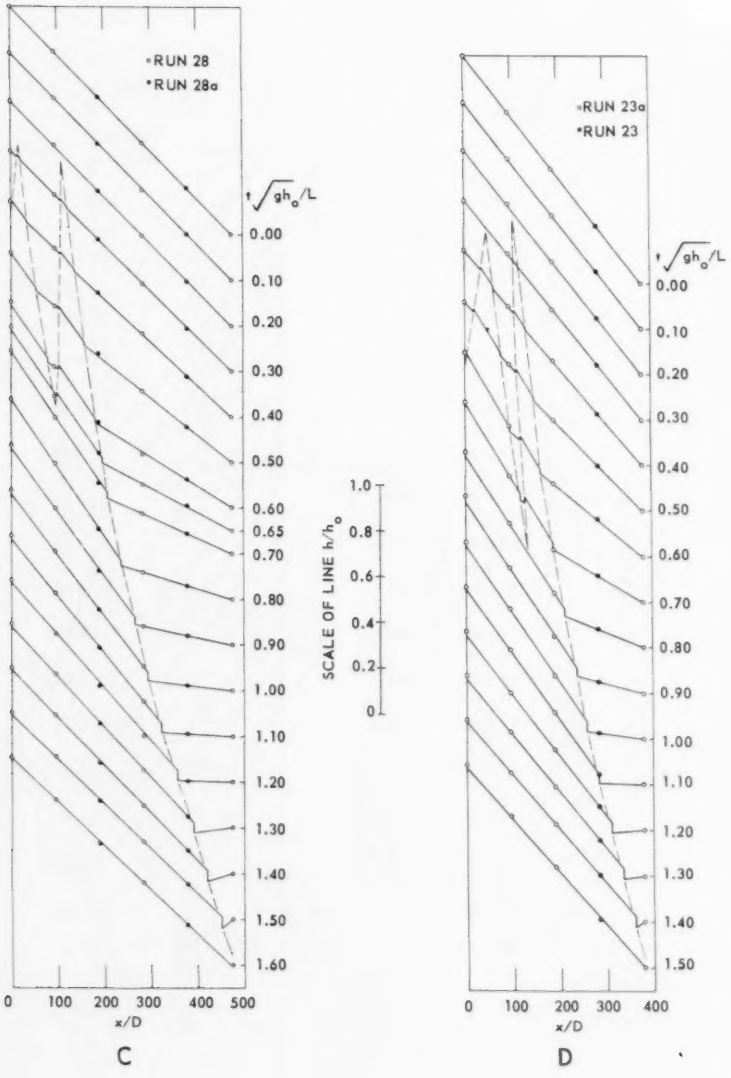

Figure 8. Piezometric Head Lines of Runs 20-29, Inclusive. (Continued)

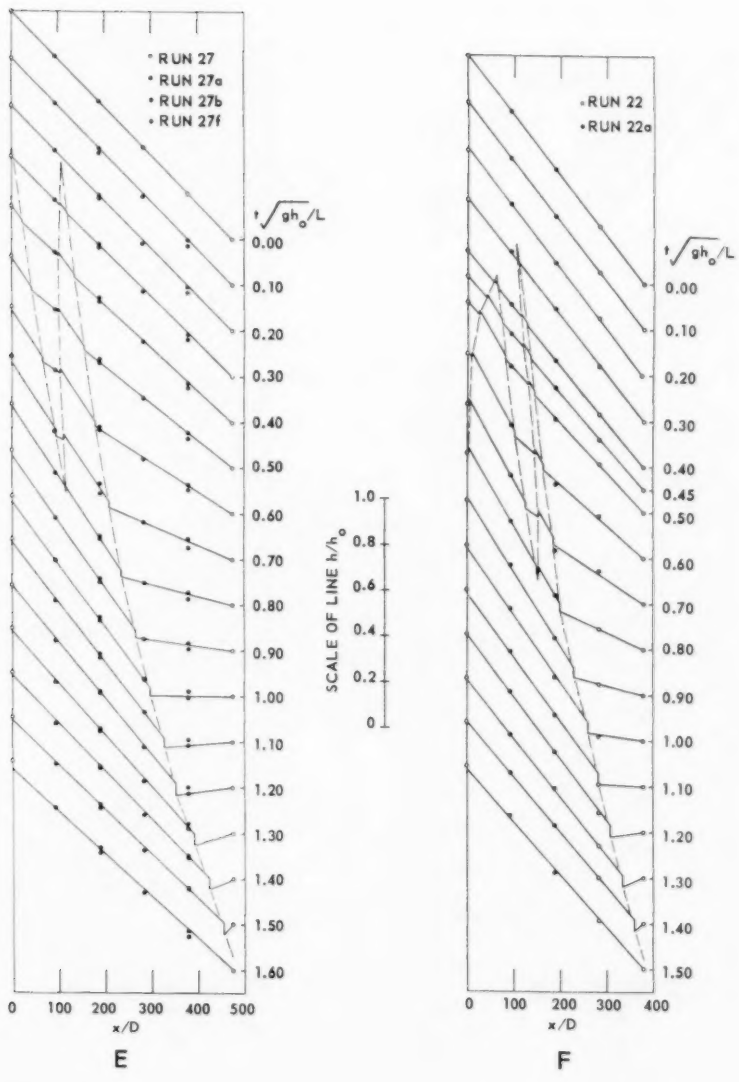

Figure 8. Piezometric Head Lines of Runs 20-29, Inclusive. (Continued)

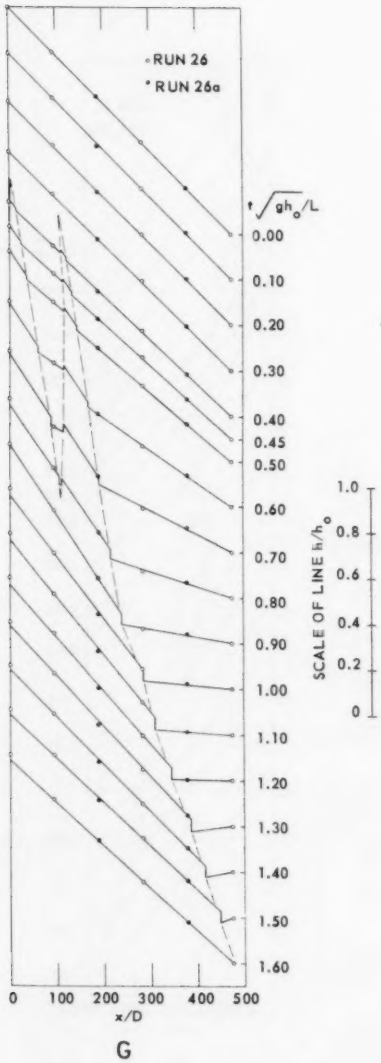

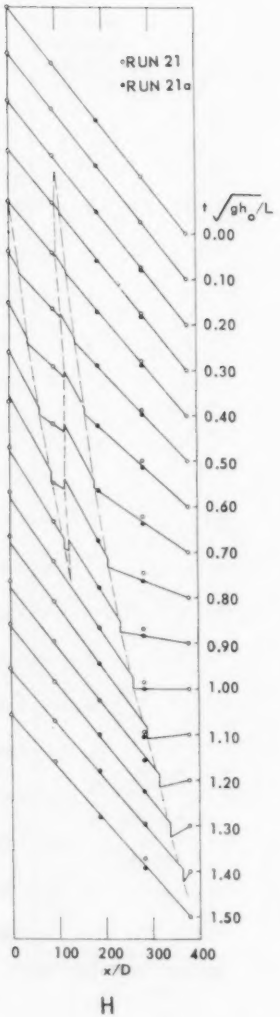

Figure 8. Piezometric Head Lines of Runs 20-29. Inclusive. (Continued)

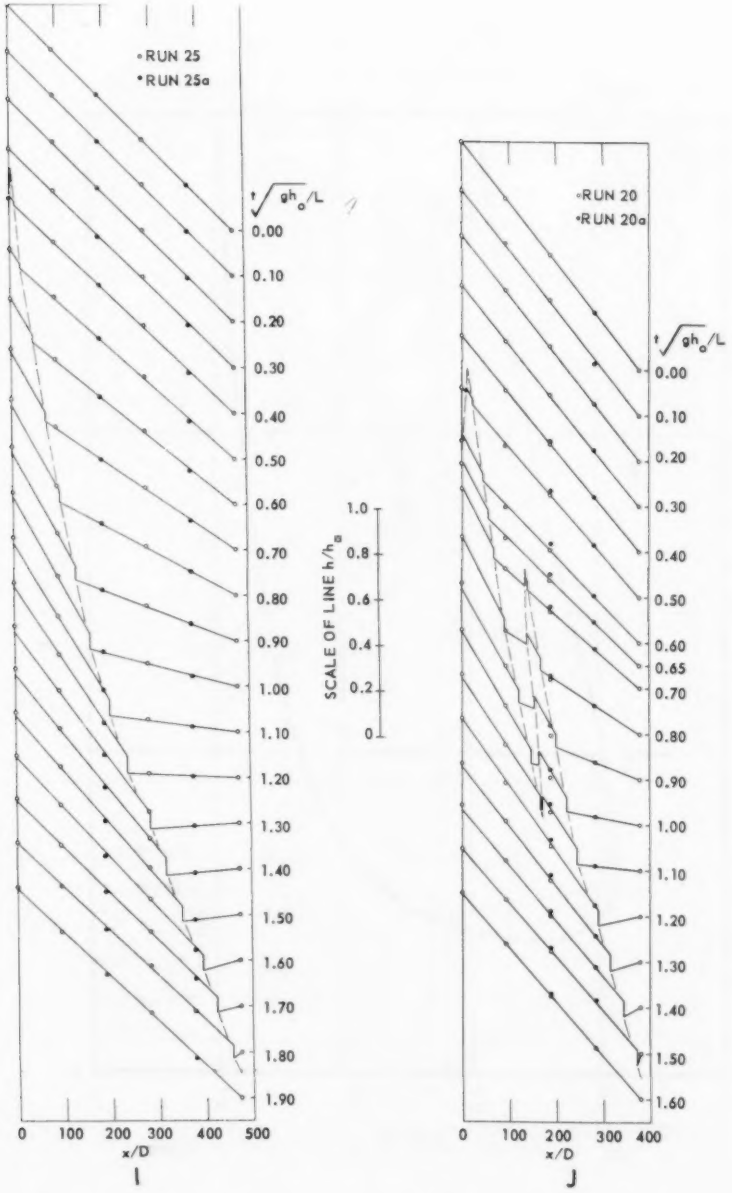

Figure 8. Piezometric Head Lines of Runs 20-29, Inclusive. (Concluded)

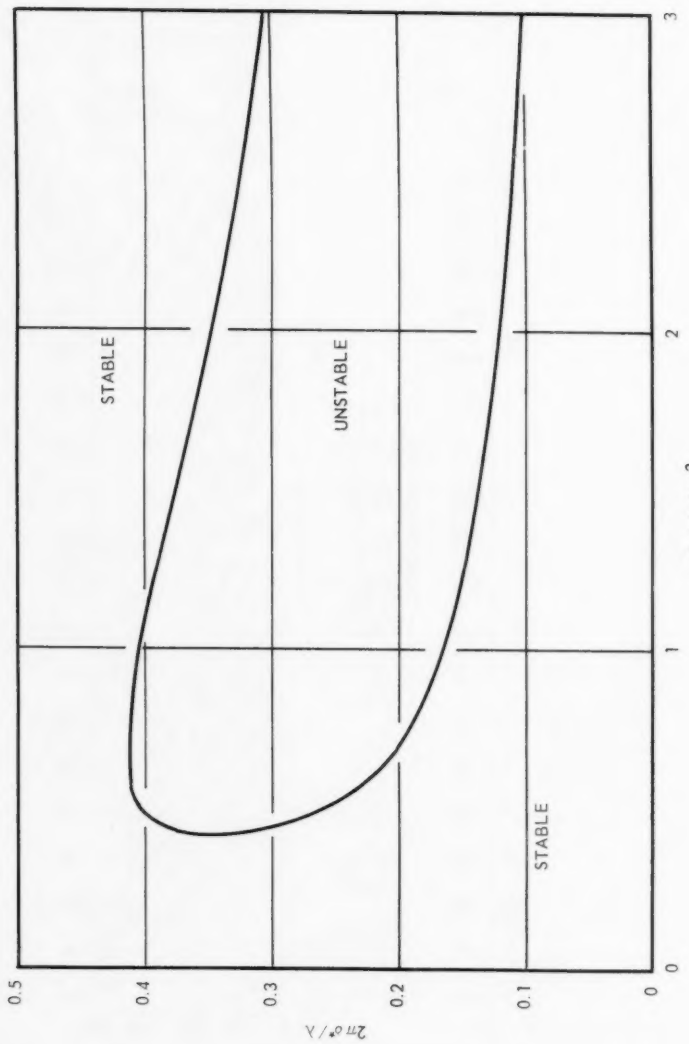

Figure 9. Neutral Stability Curve of Blasius Flow Over a Flat Plate.

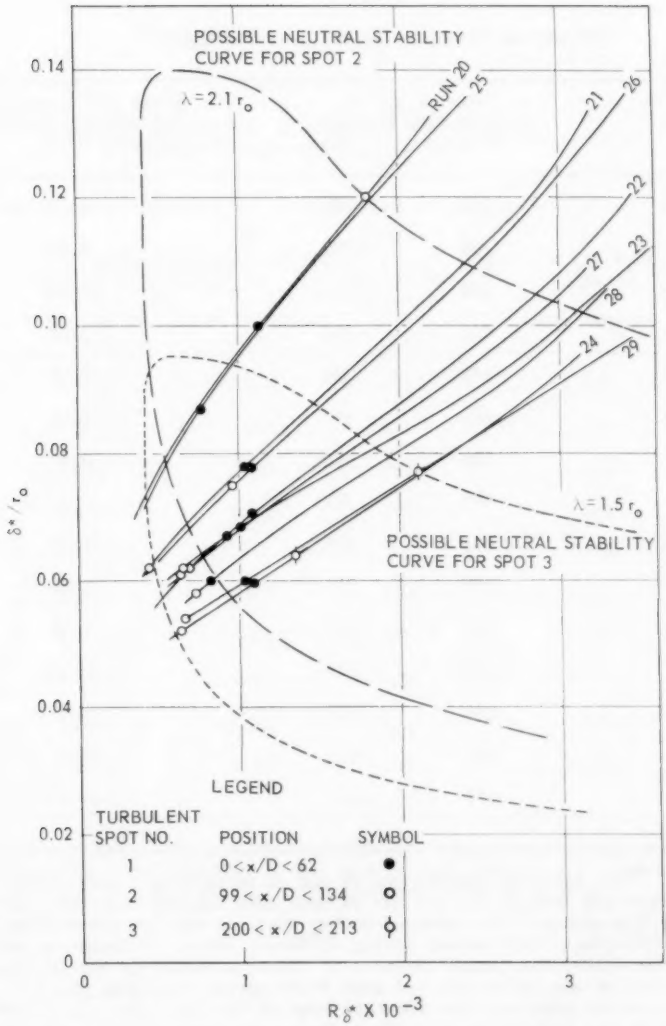

Figure 10. Boundary-Layer Thickness as a Function of Boundary-Layer Reynolds Number of Runs 20-29, Inclusive.

Table I

Downstream Transport Velocity of Turbulence*

Run No.	Value of x/D at Measuring Station From	To	Ratio of Transport Velocity to Centerline Velocity V^*/v_c
21a	189	284	0.97
22	284	380	0.99
22a	189	380	0.96
23	284	380	1.00
23a	189	380	0.98
23b	284	380	1.01
24	284	380	0.97
27	189	379	0.97
27b	189	379	1.01
27c	189	379	1.00
27d	189	379	1.02
27f	189	379	1.03
28a	189	379	1.00
29	284	475	1.01
29a	379	475	1.02

*Data from Run Numbers 20, 25 and 26 as well as a portion of the data from Run Numbers 21, 27, and 28 have been omitted from this tabulation. The omitted data occurred during the time the jet was separating into individual fluid masses having different values of linear momentum. In other words, the radial transfer of linear momentum by the internal shear forces was incomplete and some fluid masses fell from the jet with a lesser momentum than the main body of the jet. The calculated values of the centerline velocity v_c were questionable during this type of jet separation.

Table II

Laminar - Turbulent Interface at the Time of Passage Through the Pipe Outlet

1 Run No.	2 Data from Motion Pictures $t\sqrt{gh_o}/L$ Last Laminar	3 Data from Motion Pictures $t\sqrt{gh_o}/L$ First Turbulent	4 Length of Interface	5 Data from Pressure Record $t\sqrt{gh_o}/L$ Last Laminar
20	1.532	1.566	9D	1.587
21	1.447	1.493	11D	1.501
22	1.386	1.479	23D	1.468
23	1.433	1.462	7D	1.460
24*	- -	- -	- -	1.214
25	1.781	1.835	17D	1.844
26	1.531	1.553	7D	1.583
27	1.526	1.567	13D	1.579
28	1.530	1.567	11D	1.584
29	1.333	1.365	9D	1.386

*The length of the interface region was very short with the result that meaningful determinations of the time of last laminar flow passage and of the time of first turbulent flow passage were impossible.

Table III

Flow Parameters at the Inception of Turbulence

Run No.	Turbulent Spot Number	Position of Turbulence Inception in Diameters	Boundary Layer Thickness δ^*/r_o	Boundary Layer Reynolds Number $R_{\delta^*} = v_c \delta^*/\nu$
20	1	112	0.100	1140
	2	134	0.120	1810
21	1	0	0.078	1030
	2	99	0.062	440
22	1	62	0.070	1100
	2	105	0.062	710
23	1	48	0.068	1020
	2	105	0.062	650
24	1	37	0.060	1090
	2	100	0.052	640
	3	200	0.064	1340
25	1	4	0.087	770
26	1	4	0.078	1080
	2	110	0.075	960
27	1	3	0.067	920
	2	102	0.061	630
28	1	13	0.060	810
	2	109	0.058	730
29	1	16	0.060	1030
	2	105	0.054	660
	3	213	0.076	2130

Paper 1451 December, 1957 HY 6

Journal of the
HYDRAULICS DIVISION
Proceedings of the American Society of Civil Engineers

FLOOD FREQUENCIES DERIVED FROM RAINFALL DATA

Joseph L. H. Paulhus,[1] A.M. ASCE, and John F. Miller[2]
(Proc. Paper 1451)

ABSTRACT

The feasibility of using rainfall data to obtain flood frequencies has been demonstrated before. Most investigations, however, utilized rainfall data and rainfall-runoff relations specific to the basins for which the flood-frequency data were desired. The present study, involving 36 basins, shows that the rainfall data need not be from the problem basin and that the data from one precipitation network can be used to synthesize streamflow data for a number of basins. Similarly, rainfall-runoff relations already derived for other basins may be easily modified to apply to the problem basin. The transposition of rainfall data and rainfall-runoff relations not only make it possible to extend the streamflow record of basins not having rainfall data, but greatly reduces the cost of synthesizing streamflow data.

INTRODUCTION

Among the procedures for extending streamflow records for design purposes is that reported by Kresge and Nordenson,(1) who demonstrated that streamflow data, specifically annual flood peaks, could be synthesized from rainfall data by means of a rainfall-runoff relation and unit hydrograph. Using the Hocking River at Athens, Ohio, area 944 sq. mi., which had a 4-station precipitation network and a 37-year period of concurrent precipitation and streamflow records, they showed that the flood-frequency characteristics of the basin could be reproduced from rainfall data. The procedure requires a great deal of work and the cost of application on a broad scale might be considered prohibitive, especially in connection with the design of low-cost hydraulic structures, such as highway culverts. The results were so encouraging, however, that in 1954-56 the U. S. Weather Bureau and the Bureau of

Note: Discussion open until May 1, 1958. Paper 1451 is part of the copyrighted Journal of the Hydraulics Division of the American Society of Civil Engineers, Vol. 83, No. HY 6, December, 1957.

1. Chief, Cooperative Studies Section, U. S. Weather Bureau, Washington, D.C.
2. U. S. Weather Bureau, Washington, D. C.

Public Roads jointly undertook further investigations along these lines to determine if the procedure could be modified to lower the cost of application when used on a broad scale.

A preliminary study based on three basins: Delaware River at Valley Falls, Kans. (922 sq. mi.); Meramec River near Steelville, Mo. (781 sq. mi.); and Ralston Creek at Iowa City, Iowa (3 sq. mi.), showed that their flood-frequency characteristics could be satisfactorily reproduced from rainfall data outside the basins. The tests were made by taking rainfall data from a number of networks around each basin and comparing the results of the frequency analysis of the 30 years of annual flood peaks at each basin with those of the annual flood peaks synthesized from the rainfall data for the corresponding networks for the same period as the streamflow record. It was found that a precipitation network would yield satisfactory results provided (1) its area roughly approximated the size of the problem basin, (2) its rainfall-intensity—frequency characteristics were similar to those of the basin, and (3) the seasonal distribution of rainfall was the same as that of the basin.

These preliminary studies thus led to the large-scale undertaking of synthesizing streamflow data for 36 basins (Table 1). These 36 basins, ranging in size from 2.2 to 521 sq. mi., are scattered in a long, narrow region having homogeneous physiographic characteristics* and extending from northern New Jersey to northern Georgia (Fig. 1). Each basin has at least 15 years of streamflow record.

Procedure

Selection of Precipitation Networks

As it had been decided to synthesize streamflow data for no less than a 50-year period for each problem basin, the basic precipitation networks were made up of stations with at least 50 years of concurrent rainfall data. This restriction severely limited the number of networks available. Because of the relatively wide scatter of stations with 50-year rainfall records, the individual networks were limited to no more than 3 stations, since a larger number would have made the network area incompatible in size with the problem basins.

The effect of the size of the network area on synthesized peak discharges was investigated. For this purpose the West Fork River Basin at Clarksburg, W. Va., 384 sq. mi., was used. This basin contains a fairly evenly distributed precipitation network of 8 stations, and is surrounded by other stations not far outside its boundaries. Fig. 2 shows the equation used to obtain an index of the effective area of the 1-, 2- and 3-station networks selected for this investigation and the effect of network area on synthesized 2-year peak discharges. The 2-year peak discharge synthesized from the storm-precipitation averages of the basin's 8-station network served as the control. The curve of Fig. 2 indicates that for network areas of about 40 to 600 sq. mi., a difference up to 350 sq. mi. between network and basin areas affects the results by no more than 5 percent. The range of network area from 0 to 40 sq. mi.,

*As indicated by the map of Problem Areas in Soil Conservation, published by the U. S. Soil Conservation Service in July 1950. Most of the problem basins were in the area designated as the Piedmont Plateau, or B-10, region.

Table 1

PROBLEM BASINS

No. (From Fig. 1)	STREAM AND GAGING STATION	AREA (Sq. Mi.)
1	Whippany River at Morristown, N. J.	29.4
2	North Branch Raritan River nr Far Hills, N. J.	26.2
3	Walnut Brook nr Flemington, N. J.	2.24
4	Neshanic River nr Reaville, N. J.	25.7
5	Tohickon Creek nr Pipersville, Pa.	94.4
6	Perkiomen Creek at Graterford, Pa.	279.
7	Chester Creek nr Chester, Pa.	61.1
8	Codorus Creek at Spring Grove, Pa.	74.3
9	Octoraro Creek nr Rising Sun, Md.	193.
10	Piney Run nr Sykesville, Md.	11.4
11	Linganore Creek nr Frederick, Md.	82.3
12	Seneca Creek at Dawsonville, Md.	101.
13	Northwest Branch Anacostia River nr Colesville, Md.	21.3
14	Goose Creek nr Leesburg, Va.	338.
15	Slate River nr Arvonia, Va.	235.
16	Tye River nr Lovingston, Va.	92.
17	Appomattox River at Farmville, Va.	306.
18	Goose Creek nr Huddleston, Va.	187.
19	Sandy River nr Danville, Va.	113.
20	Mayo River nr Price, N. C.	260.
21	Fishing Creek nr Enfield, N. C.	521.
22	Dial Creek nr Bahama, N. C.	4.9
23	Eno River at Hillsboro, N. C.	66.5
24	Horsepen Creek at Battleground, N. C.	15.9
25	East Fork Deep River nr High Point, N. C.	14.2
26	Deep River nr Randleman, N. C.	124.
27	Fisher River nr Copeland, N. C.	121.
28	South Yadkin River nr Mocksville, N. C.	313.
29	Uwharrie River nr Eldorado, N. C.	347.
30	Brown Creek nr Polkton, N. C.	110.
31	South Tyger River nr Woodruff, S. C.	174.
32	South Tyger River nr Reidville, S. C.	106.
33	Middle Tyger River at Lyman, S. C.	68.3
34	Apalachee River nr Buckhead, Ga.	436.
35	Little Tallapoosa River at Carrollton, Ga.	89.
36	Tobesofkee Creek nr Macon, Ga.	182.

however, encompasses a rapid change in selectivity, suggesting that synthesized peak discharges should be adjusted when there is any appreciable difference between basin and network area within this range. The data of Fig. 2 also suggest that 2-station networks yield results as satisfactory as those obtained from 3-station networks. Use of the 2-station instead of the 3-station network results in a great saving of time in making storm surveys and determining time distribution of rainfall. Best results for very small basins, i.e., under about 15 sq. mi., were obtained from single stations. This is true, of course, only because closely-spaced long-record precipitation stations were not available. Another important consideration in the selection of precipitation networks was their geographic proximity to groups of problem basins, the objective being to effect economy by applying one network to a group of basins.

Storm Surveys

After the precipitation networks had been selected, their records of daily precipitation were scrutinized to select the major rainstorms of each water year. A base value of daily precipitation was arbitrarily selected (usually one inch) and whenever one or more stations in the network exceeded the base value, precipitation was tabulated for all stations for the entire storm period, including days with less than the base value. If fewer than 10 or 12 storms were obtained in any one water year, the base was lowered and the record reexamined.

The runoff for each major rainstorm was then roughly estimated by means of a rainfall-runoff relation (Fig. 3) as described by Kohler and Linsley.[2] The four or five storms producing the highest runoff in any one water year were then set aside for a detailed analysis of the time distribution of the rainfall, because the relatively small size of the problem basins required a breakdown of rainfall into increments no longer than 6 hours for accurate estimates of runoff and computations of peak discharge.

Time Distribution of Rainfall

The time distribution of rainfall in the several storms selected for each year was determined from the records of a recording-gage station in or near the network involved. The hourly data were scanned to determine the maximum 6-hour rainfall increment for a storm, and the entire storm was divided into 6-hour increments synchronizing with the maximum. The average storm rainfall for the network was distributed into 6-hour increments in accordance with the indicated distribution for the recording-gage station. Six-hour increments of runoff were then obtained from a rainfall-runoff relation. For basins smaller than about 15 sq. mi., the peak discharges generally result from short-duration, high-intensity rainfall. Consequently, 1-hour increments of rainfall were used for such basins, the 1-hour runoff increments being estimated by means of a special rainfall-runoff relation.[3]

Rainfall-Runoff Relations

Rainfall-runoff relations were available for very few of the problem basins. Development of these relations is a time-consuming procedure. In order to keep the cost of the study to a minimum, available rainfall-runoff relations from other basins were utilized. In order to determine which of several

relations was best suited to a particular problem basin, the runoff for 25 or more storms over the basin was computed from the hydrographs. The runoff for the same storms was also estimated by means of the rainfall-runoff relation being tested, and plotted against the corresponding observed runoff. The relation yielding values nearest to a 45° line was the most representative of the rainfall-runoff characteristics of the problem basin. The mean curve for the points yielded by this most representative relation was used to adjust all runoff values obtained from that particular rainfall-runoff relation for use on the problem basin involved. Fig. 4 presents such a mean curve indicating so high a degree of representativity for the rainfall-runoff relation that no adjustment was considered necessary.

Unit Hydrographs

Unit hydrographs of 1-hour or 6-hour duration were derived from discharge data obtained from the original records of the U. S. Geological Survey for converting runoff increments into peak discharge.[4] It is generally recognized that one unit hydrograph for a basin may not properly reproduce the stream hydrograph for all magnitudes of floods.[5] Different unit hydrographs are often required for low and high runoff, and sometimes for intermediate values. No matter what criteria are established for the choice of the proper unit hydrograph, situations will exist where almost equal values of runoff will require different unit hydrographs, probably resulting in appreciable differences in the peak discharges obtained. In order to avoid such discontinuities, only one unit hydrograph was constructed for each basin, and a curve was then developed to adjust the peak discharges yielded by the unit hydrograph.

The unit-hydrograph adjustment curve for a particular basin was derived by first obtaining from observed flood hydrographs the total storm runoff for a good range of peak discharges. The next step was the breakdown of storm runoff into 1- or 6-hour incremental runoff on the basis of the chronological distribution of the rainfall producing the runoff. The peak discharge was then computed by applying a unit hydrograph like that of Fig. 5 to the runoff increments. The computed peak discharge for each storm was then plotted against the observed peak discharge for the storm. The mean curve (Fig. 6) was used to adjust the synthesized peak discharges estimated by the unit hydrograph.

In addition to eliminating the need for several unit hydrographs for one basin, the peak-discharge adjustment curve also allowed for base flow. Base flow was not included in synthesizing the peak flow from the unit hydrograph, but it was included in the observed values of peak discharge used to derive the adjustment curve. Consequently, a part of the adjustment provided by application of the curve was for base flow.

Results

Comparative Test

After selection of the most representative rainfall-runoff relation and unit hydrograph and their adjustment curves for a particular basin, peak discharges corresponding to the rainstorms for the period of discharge measurements were estimated. The estimated or synthesized annual peak discharges, i.e., the maximum for each water year, were arrayed in decreasing order of

magnitude and then compared with the observed, similarly arrayed. If the average difference between the two was less than 20 percent, the record of synthesized peak discharges was considered to be representative of the streamflow record. Annual peak discharges were then synthesized for the remainder of the precipitation record.

Synthesized Annual Peak Discharges for Codorus Creek, Pa.

Table 2 shows such a comparison between synthesized and observed annual peak discharges (annual floods) for Codorus Creek Basin above Spring Grove, Pa., area 74.3 sq. mi. Codorus Creek has a streamflow record starting with water year 1933, and annual flood peaks were available through water year 1954. Peak discharges were therefore synthesized for the corresponding period.

The peak discharges for Codorus Creek were synthesized from major rainstorms observed by a 3-station network (Ephrata, Lancaster and Lebanon, Pa.) about 45 miles northeast of the basin. The time distribution of the rainfall in the selected storms subsequent to 1940 was determined from either or both of the recording gages (Lancaster, Lebanon) and prior to 1940 from the recording gage at Harrisburg, about 30 miles west of the network. The runoff from these storms was estimated by means of a rainfall-runoff relation previously developed for the Anacostia River Basin, about 50 miles south of the problem basin. This rainfall-runoff relation was so well adapted to the problem basin that no adjustment was considered necessary (see Fig. 4).

The 6-hour unit hydrograph (Fig. 5) used to estimate the peak discharge from the computed runoff was based on five storms of approximately 6 hours' duration in the problem basin. An adjustment curve was required (Fig. 6).

The first three columns of Table 2 show poor agreement on an annual basis between observed and synthesized annual floods. This is not surprising as it would indeed be strange if floods of the same approximate frequency occurred simultaneously over the problem basin and over the network 45 miles away. Tests based on two pairs of adjoining basins showed poor agreement between observed annual peak discharges for adjoining basins on a year-to-year basis.

The last two columns of Table 2, showing observed and synthesized annual floods in decreasing order of magnitude, suggest that the two may well represent samples of the same population. The synthesized annual floods are generally well within the 20-percent limit of acceptability. A frequency analysis of the observed and synthesized annual floods for the 22-year period by the Gumbel method yielded the results shown in Table 3.

The frequency data of Table 3 might be criticized by some statisticians because they were based on all annual floods for the 1933-54 water years. Referring to Table 2, it is seen that the 1933 observed and synthesized annual floods were both extremely high, being about twice the second highest. Some would argue that the 1933 annual floods are not of the same population as the lesser floods and should therefore not be included in the frequency analysis. Table 4 shows the results of the frequency analysis of observed and synthesized annual floods for water years 1934-54. This table shows even better agreement between observed and synthesized annual floods than when the 1933 data were included. In any event, it appears that the record of synthesized annual floods compares reasonably well with that of observed annual floods for Codorus Creek Basin.

Table 2

ANNUAL FLOODS FOR CODORUS CREEK AT SPRING GROVE, PA.
(74.3 Sq. Mi.)

CHRONOLOGICAL LISTING			STATISTICAL ARRAY		
Water Year	Observed (cfs)	Synthesized (cfs)	Order No.	Observed (cfs)	Synthesized (cfs)
1954	1910	2890	1	11200	11600
1953	2180	2240	2	6070	5370
1952	1750	2340	3	4880	4900
1951	3200	4900	4	4180	4800
1950	1610	2590	5	3200	3910
1949	1730	1640	6	3180	3670
1948	1810	1930	7	3070	2890
1947	1430	1320	8	2710	2810
1946	3070	4800	9	2490	2730
1945	2490	2810	10	2380	2590
1944	2380	3910	11	2210	2360
1943	4180	1750	12	2180	2340
1942	2710	5370	13	1910	2240
1941	870	1340	14	1810	1970
1940	4880	1970	15	1750	1940
1939	1620	1940	16	1730	1930
1938	3180	2730	17	1620	1780
1937	2210	2360	18	1610	1750
1936	1380	1780	19	1430	1640
1935	1110	1330	20	1380	1340
1934	6070	3670	21	1110	1330
1933	11200	11600	22	870	1320

The suitability of the above precipitation network, rainfall-runoff relation and unit hydrograph for synthesizing peak discharges for Codorus Creek Basin having been established, the next step was to synthesize annual floods for the remainder of the precipitation record. The results are given in Table 5.

The results of a frequency analysis of the 55-year period of synthesized annual floods of Table 5 are given in Table 6. Also listed are the results obtained with the 1933 flood eliminated. Both sets of data suggest that the 1933 observed flood peak of 11,200 cfs is an unusual event with a return period probably much greater than 100 years.

Synthesized Annual Floods for the Other 35 Project Basins

Synthesized annual floods for the other 35 project basins (Table 1) provided comparable degrees of agreement with the observed for the respective basins. Altogether, only 13 precipitation networks and 17 rainfall-runoff relations were used in synthesizing annual flood records for all 36 basins.

CONCLUSIONS

This study substantiates the conclusion that reasonably reliable flood-frequency data may be synthesized from rainfall records. Moreover, the precipitation stations need not be in the basin for which the synthesized flood peaks are required. The fact that the rainfall record from one network and one rainfall-runoff relation can apparently be used to synthesize flood-frequency data for a number of basins makes the procedure economically practicable.

One point that must not be overlooked, however, is that there were no adequate precipitation networks in the project basins. This meant that there were no entirely suitable controls for determining whether the synthesizing procedure was yielding reliable values of peak discharge storm by storm. It is obvious that tests involving even but a few years of streamflow data with concurrent rainfall observations from an adequate network in the basin proper are to be preferred to the tests employed in these investigations.

In spite of this shortcoming, the results of the studies made thus far strongly suggest that the synthesizing of peak discharges from rainfall is practicable and economically feasible.

ACKNOWLEDGMENTS

These studies were conducted by the Weather Bureau's Hydrologic Services Division, W. E. Hiatt, Chief, in cooperation with the Bureau of Public Roads, whose coordinating officials were Messrs. C. F. Izzard and W. D. Potter. Mr. Max A. Kohler, Chief Research Hydrologist, Weather Bureau, served as consultant. Messrs. A. L. Shands, T. J. Nordenson and W. T. Wilson read the manuscript and made several beneficial suggestions. Mrs. Emma L. Weaver, Mrs. Pauline J. Fagan and Mrs. Marie M. McGonegal typed the manuscript.

Table 3

FREQUENCY ANALYSIS OF OBSERVED AND SYNTHESIZED ANNUAL FLOODS FOR 1933-1954

Return period (years)	Observed (cfs)	Synthesized (cfs)
2	2530	2730
5	4850	5040
10	6380	6570
25	8320	8500
50	9750	9940
100	11180	11360

Table 4

FREQUENCY ANALYSIS OF OBSERVED AND SYNTHESIZED ANNUAL FLOODS FOR 1934-54

Return period (years)	Observed (cfs)	Synthesized (cfs)
2	2280	2470
5	3610	3730
10	4500	4560
25	5610	5610
50	6440	6390
100	7260	7160

Table 5

SYNTHESIZED ANNUAL FLOODS FOR CODORUS CREEK AT SPRING GROVE, PA. FOR 1900-1954

CHRONOLOGICAL LISTING		:	STATISTICAL ARRAY		
Water Year	Annual Flood		Order No.	Annual Flood	Water Year
1954	2890	:	1	11600	1933
1953	2240	:	2	5420	1908
1952	2340	:	3	5370	1942
1951	4900	:	4	4900	1951
1950	2590	:	5	4800	1946
1949	1640	:	6	4270	1902
1948	1930	:	7	4100	1913
1947	1320	:	8	3910	1944
1946	4800	:	9	3670	1934
1945	2810	:	10	3420	1916
1944	3910	:	11	3040	1915
1943	1750	:	12	2950	1927
1942	5370	:	13	2890	1954
1941	1340	:	14	2850	1903
1940	1970	:	15	2810	1945
1939	1940	:	16	2730	1938
1938	2730	:	17	2660	1926
1937	2360	:	18	2590	1950
1936	1780	:	19	2360	1937
1935	1330	:	20	2340	1952
1934	3670	:	21	2240	1953
1933	11600	:	22	2210	1906
1932	2200	:	23	2200	1932
1931	1390	:	24	2200	1924
1930	2030	:	25	2140	1919
1929	1380	:	26	2120	1907
1928	1530	:	27	2030	1930
1927	2950	:	28	1970	1940
1926	2660	:	29	1960	1900
1925	1380	:	30	1950	1917
1924	2200	:	31	1940	1939
1923	1200	:	32	1930	1948
1922	1400	:	33	1820	1910
1921	1220	:	34	1810	1905
1920	1260	:	35	1780	1936

(Continued next page)

Table 5 - Con.

SYNTHESIZED ANNUAL FLOODS FOR CODORUS CREEK AT SPRING GROVE, PA.
FOR 1900-1954

CHRONOLOGICAL LISTING		:	STATISTICAL ARRAY		
Water Year	Annual Flood	:	Order No.	Annual Flood	Water Year
1919	2140	:	36	1750	1943
1918	1520	:	37	1730	1911
1917	1950	:	38	1640	1949
1916	3420	:	39	1600	1904
1915	3040	:	40	1590	1914
1914	1590	:	41	1530	1928
1913	4100	:	42	1520	1918
1912	1250	:	43	1470	1901
1911	1730	:	44	1400	1922
1910	1820	:	45	1390	1931
1909	1270	:	46	1380	1929
1908	5420	:	47	1380	1925
1907	2120	:	48	1340	1941
1906	2210	:	49	1330	1935
1905	1810	:	50	1320	1947
1904	1600	:	51	1270	1909
1903	2850	:	52	1260	1920
1902	4270	:	53	1250	1912
1901	1470	:	54	1220	1921
1900	1960	:	55	1200	1923

Table 6

FREQUENCY ANALYSES OF SYNTHESIZED ANNUAL FLOODS

Return period (years)	1900-54	1900-32 1934-54
2	2240	2160
5	3840	3220
10	4890	3920
25	6230	4810
50	7220	5470
100	8200	6130

REFERENCES

1. Kresge, R. F., and Nordenson, T. J., Flood Frequencies Derived from River Forecasting Procedures, ASCE Proc., Vol. 81, Separate No. 630, 1955.

2. Kohler, M. A., and Linsley, R. K., Predicting the Runoff from Storm Rainfall, Weather Bureau Research Paper No. 34, 1951.

3. Miller, J. F., and Paulhus, J. L. H., Rainfall-Runoff Relation for Small Basins, Trans. Amer. Geophys. Union, Vol. 38, pp. 216-218, Apr. 1957.

4. Sherman, L. K., Streamflow from Rainfall by the Unit Graph Method, Engineering News-Record, Vol. 108, p. 501, 1932.

5. Corps of Engineers, Department of the Army, Engineering Manual Civil Works Construction; Part CXIV, Hydrologic and Hydraulic Analyses; Chap. 5, Flood-Hydrograph Analyses and Computations; Sect. 5-22, pp. 15-16, March, 1948.

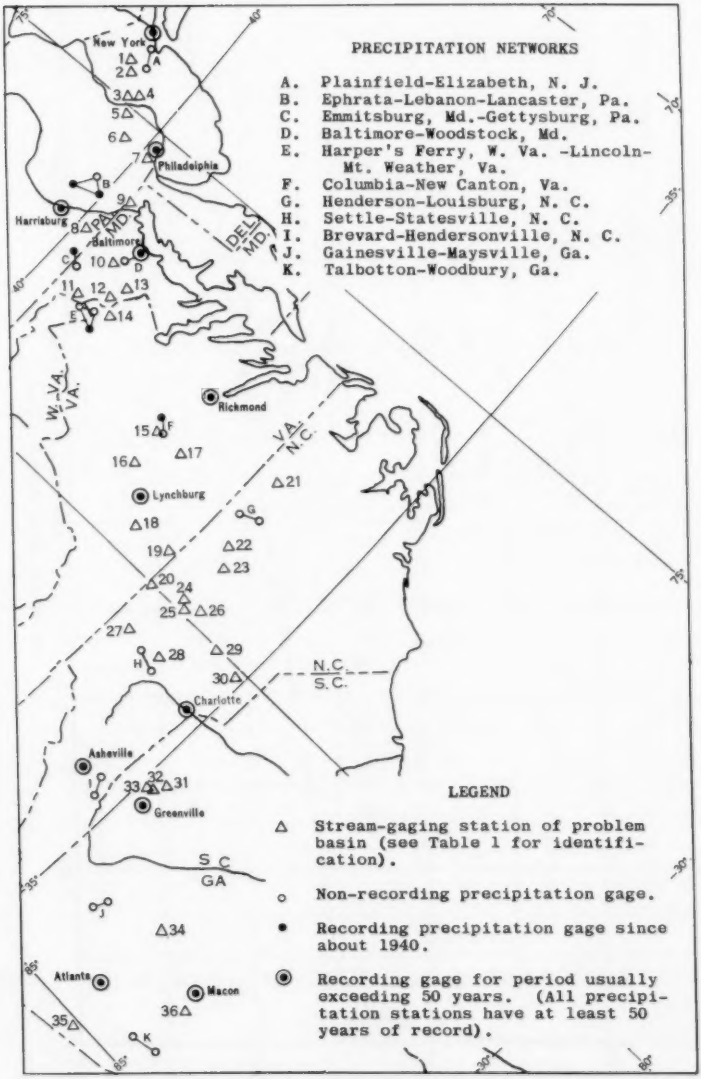

LOCATIONS OF PROBLEM BASINS AND PRECIPITATION NETWORKS

FIGURE 1

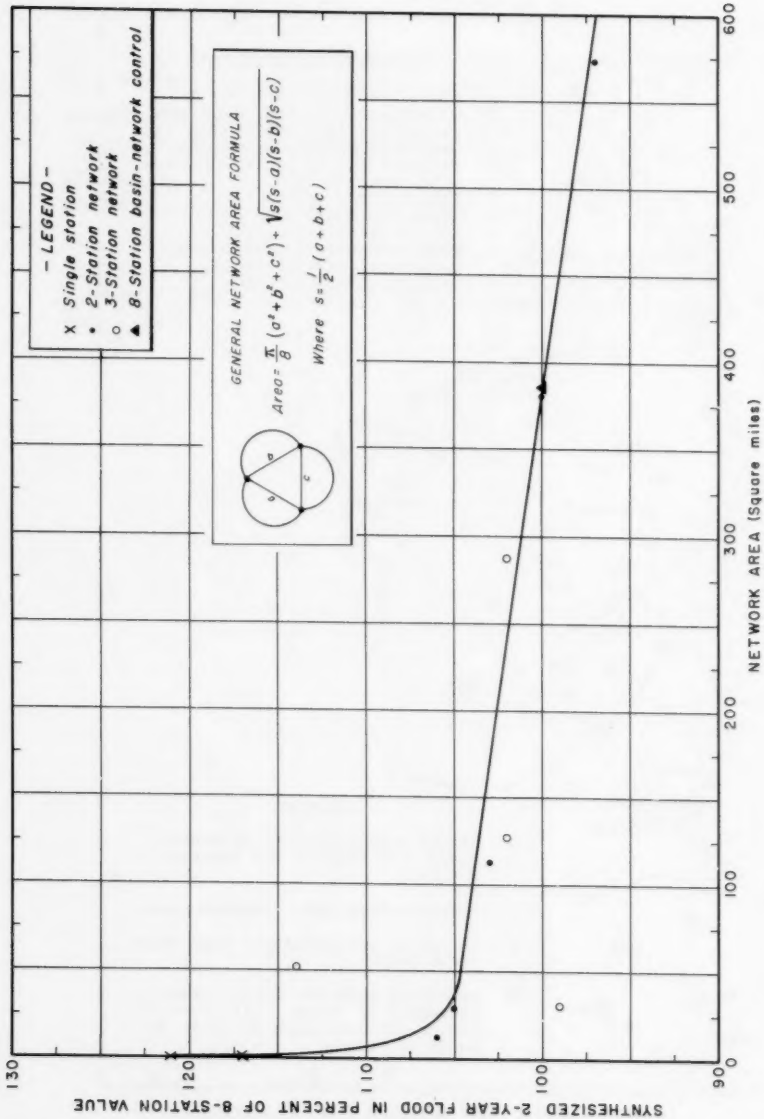

EFFECT OF NETWORK AREA ON SYNTHESIZED PEAK DISCHARGE

FIGURE 2

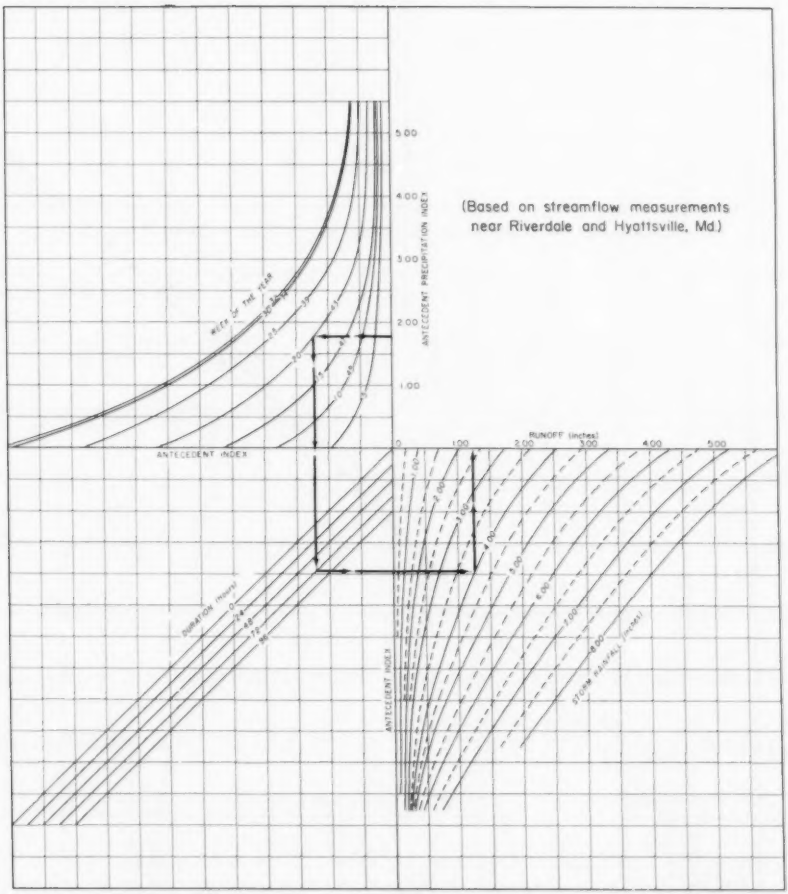

RAINFALL-RUNOFF RELATION FOR ANACOSTIA RIVER

FIGURE 3

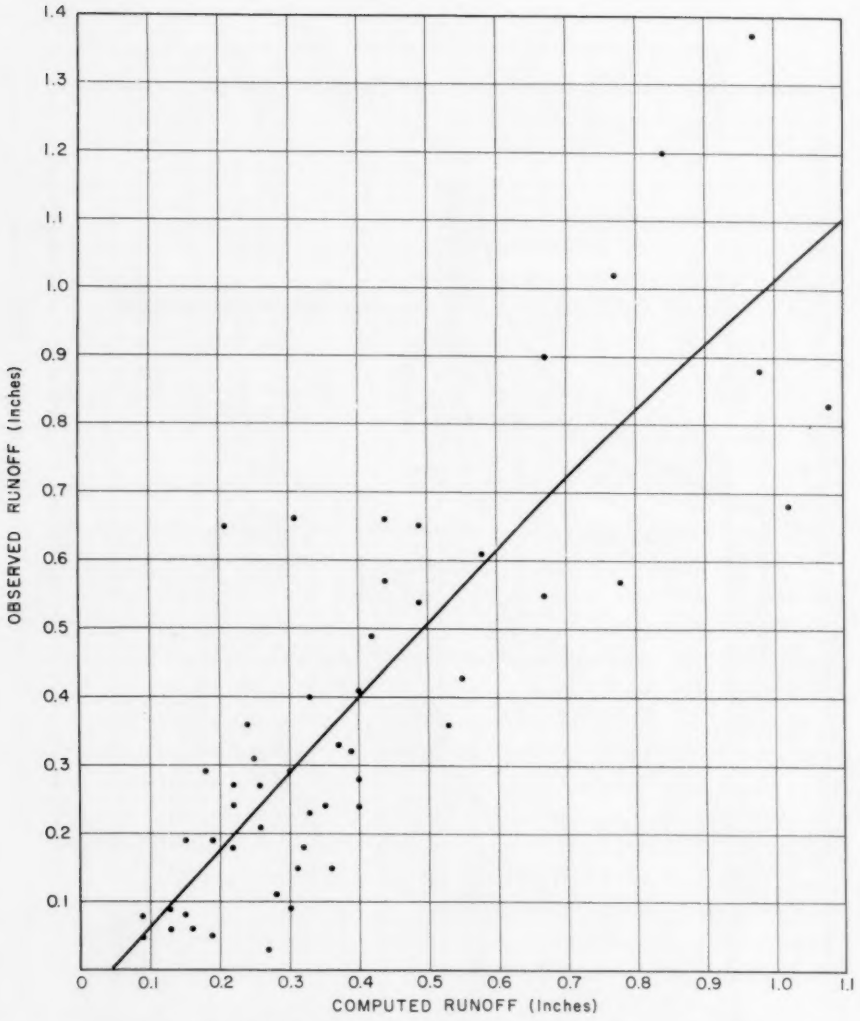

COMPUTED VS OBSERVED STORM RUNOFF

CODORUS CREEK AT SPRING GROVE, Pa. (74.3 Sq. Miles)

FIGURE 4

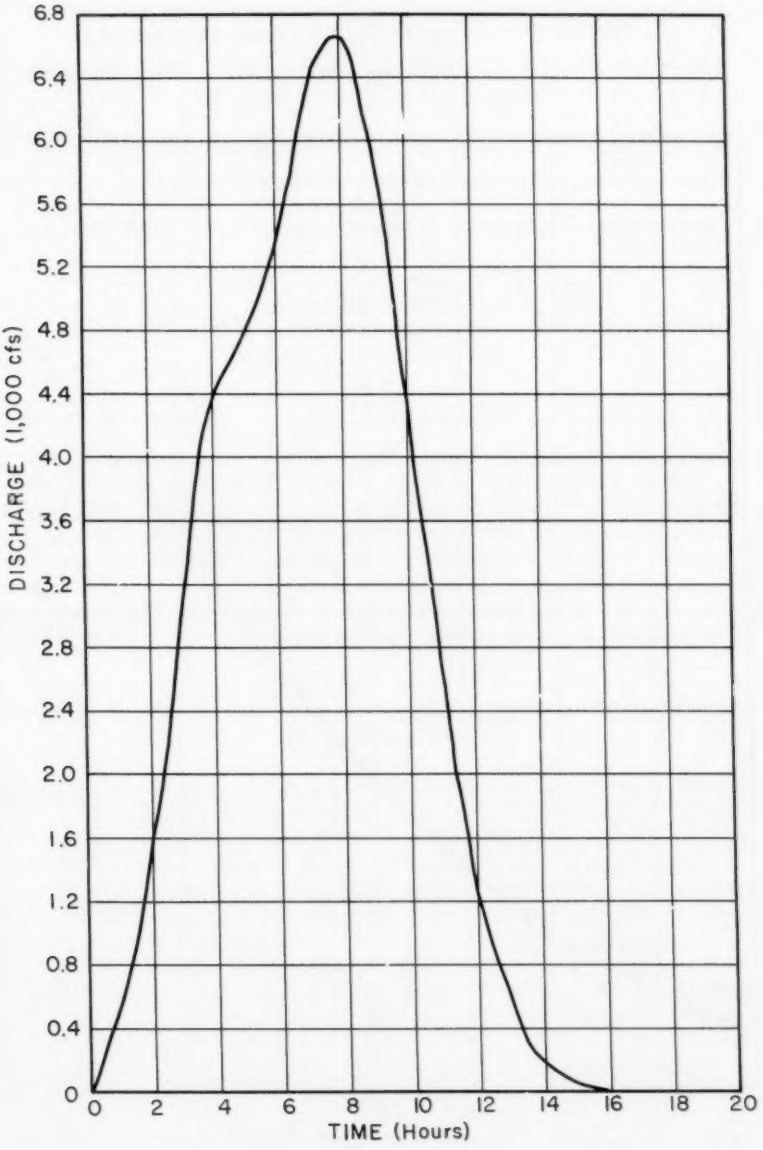

SIX-HOUR UNIT HYDROGRAPH
CODORUS CREEK AT SPRING GROVE, PA., (74.3 Sq. Miles)

FIGURE 5

COMPUTED VS OBSERVED PEAK DISCHARGE
CODORUS CREEK AT SPRING GROVE, PA., (74.3 Sq. Miles)

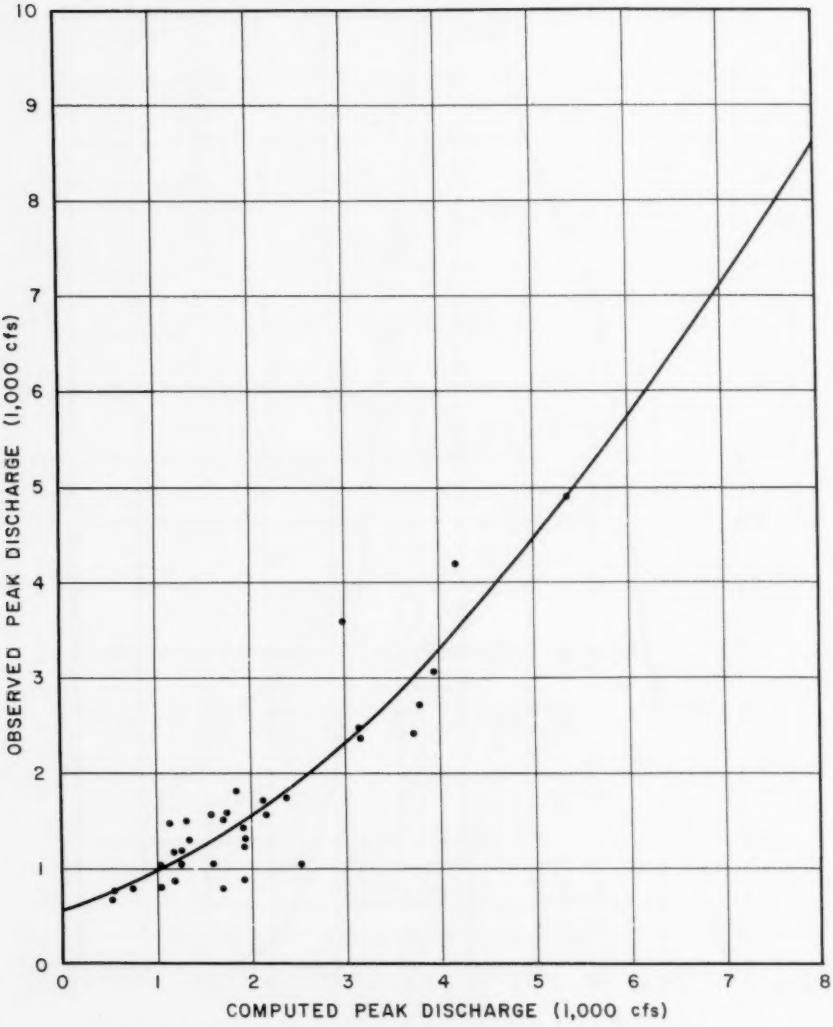

COMPUTED VS OBSERVED PEAK DISCHARGE
CODORUS CREEK AT SPRING GROVE, PA. (74.3 Sq. Miles)

FIGURE 6

Paper 1452 December, 1957 HY 6

Journal of the
HYDRAULICS DIVISION
Proceedings of the American Society of Civil Engineers

FLOW CHARACTERISTICS ON THE OGEE SPILLWAY

Robert B. Jansen,* A.M. ASCE
(Proc. Paper 1452)

SYNOPSIS

Although the ogee spillway has been the subject of more research than perhaps any other hydraulic structure, there are still deficiencies in our knowledge of its functioning. There is more to be learned about the process of energy loss on the spillway face and about the effects of submergence of the spillway jet. A general formula is here suggested for calculation of the spillway energy loss, and a theoretical derivation is presented defining the limit between the true hydraulic jump and the drowned jump. A criterion for estimating bottom velocities along a level spillway apron is considered.

INTRODUCTION

The determination of energy losses in flow on the face of an ogee spillway and the solution of the energy dissipation problem on the spillway apron often have been approached by means of hydraulic models. The reliability of such tests is universally accepted. The hydraulic laboratory plays a most important role in the design of these structures. The wealth of data on spillway energy loss produced by the many laboratories offers a good source of material for use in the development of general mathematical criteria. This paper attempts to bring this potentiality into focus.

Experience gained thus far in design of the overflow spillway indicates that this hydraulic structure has certain elements which lend themselves to standardization. In shaping the ogee crest, for example, it has become widely accepted practice to conform to the lower nappe of a stream issuing over a sharp-edged weir. Uniformity has been obtainable in this case because of

Note: Discussion open until May 1, 1958. Paper 1452 is part of the copyrighted Journal of the Hydraulics Division of the American Society of Civil Engineers, Vol. 83, No. HY 6, December, 1957.

*Supervising Hydr. Engr., Dept. of Water Resources, State of California, Sacramento, Calif.

the easily predictable nature of the phenomenon of overflow. Probably due to the relative difficulties of measurement, the prediction of flow characteristics on the spillway face and apron has not been simplified to this extent. However, by correlation of the results of experimentation by our hydraulic laboratories, such simplification should be possible.

Energy Loss on Spillway Face

A simple and exact criterion for determining the energy loss which will occur on the face of an overflow spillway would be a valuable design tool. Various mathematical procedures are now employed for this purpose. The application of the Manning formula has many advocates and is believed by them to yield satisfactory results. Solution by this means, though, is not direct and there are differences of opinion as to how the formula can best be applied. For example, in using the Manning equation, a common practice has been to determine the friction loss that would occur for flow at the depth without air entrainment, but to allow for an assumed lower actual loss by reducing the value of the Manning coefficient of roughness. Yet, in the words of one reviewer of this paper, it is not even universally agreed that entrainment of air in the water has the effect of reducing the friction loss.

Flow characteristics on the apron below the dam will depend, among other factors, upon the energy that remains in the jet when it enters the tail water. The height of the spillway, the head on the crest, the shape of the crest, and the position of the tail water will all affect the amount of energy thus involved. The theoretical energy content of the jet will obviously vary directly with the vertical distance of travel. The amount of water involved, and therefore the total energy rate, will depend primarily upon the crest head and the crest form.

It is reasonable to assume that the energy loss on the spillway face is determined by a simple natural law. The factors involved are few, and their influences are relatively uncomplicated. The principal components of the formula would be the rate of discharge and the height of fall. The roughness and slope of the spillway face also affect the energy loss, and would have to be taken into account. The influence of these factors could probably be incorporated into a coefficient in the formula.

In the Madden Dam spillway prototype tests,[1] Pitot-tube measurements of jet velocities were made for a range of crest heads. The loss in energy head on the spillway face was taken as the difference in elevation between the reservoir water surface and the energy grade line calculated on the basis of the Pitot-tube readings. In order to appraise the accuracy of these velocity tests, the method of construction of the Pitot tubes should be noted. As described by Mr. Randolph, each installation consisted of a plate steel pedestal embedded in the concrete of the spillway apron, and projecting from 14 to 20 inches above the floor. The Pitot tube itself was a length of 1-inch pipe protruding 4 inches from the nose of the pedestal at a height between 3 inches and 18 inches from the floor. Although readings on these Pitot tubes were thoroughly and carefully taken, it can not be assured that the resulting accuracy is comparable with that obtained with laboratory instruments. Also, since the tubes were located close to the floor, they gave indications of the maximum velocity rather than the mean. Despite these apparent limitations, the writer considers the Madden Dam velocity tests to be reliable enough to

serve in a preliminary general analysis of basic relationships.

The head loss between the spillway crest and any point on the spillway face, for a given concrete roughness, should be a function of the height of fall and the rate of discharge over the crest. It is suggested, therefore, that the free-flow loss on the spillway face may be defined by the general expression:

$$h_L = K \frac{(P + H)^a}{q^b} \tag{1}$$

wherein K is a coefficient, P is the height of crest above the downstream apron, H is the total head on the crest, q is the discharge per unit length of crest, and "a" and "b" are constant exponents. Fig. 1 shows the relationship of the basic dimensions.

Application of this general formula to the prototype observations on the spillway of the Madden Dam shows encouraging possibilities. Using values of K = 1/8, a = 3/2, and b = 1/3, an acceptably close correlation can be obtained. However, the face of the Madden spillway has a roughness somewhat greater than average. For a typical concrete spillway of common roughness and comparable in other respects to Madden Dam, it is believed that the following equation will give a reasonably close measure of the head loss.

$$h_L = \frac{0.10(P + H)^{3/2}}{q^{1/3}} \tag{2}$$

Substitution of $CH^{3/2}$ for q in Equation (2) leads to

$$h_L = \frac{0.10(P + H)^{3/2}}{C^{1/3}H^{1/2}} \tag{3}$$

in which C is the coefficient of discharge over the crest at the given head.

Mr. Randolph in his paper attempted to derive an expression for the friction loss on the ogee spillway face. The following two formulas, converted to the notation used herein, were developed by him for the Madden Dam spillway:

$$h_L = 0.02 \frac{P}{H} (P + H) \tag{4}$$

and

$$h_L = \frac{0.00934\ P(P + H)}{H^{0.623}} \tag{5}$$

Equation (4) is dimensionally correct but Equation (5) is not. The deficiencies of these expressions, either individually or comparatively, are demonstrated by the substitution of the Madden Dam spillway height of 172 feet and a crest head of one foot. The result in each case is an energy loss greater than the actual head available. It is believed that Equation (3) will be found to be a more generally applicable conclusion. The implication is not intended, however, that Equation (3) itself is a final refinement. It is merely an approximation independently drawn from the basic data presented by Mr. Randolph in his highly commendable work.

Mr. Randolph, in his paper on the Madden Dam tests, stated that he was suggesting the installation of Pitot tubes on the aprons of other dams designed

by the U. S. Bureau of Reclamation. If data from such Pitot-tube measurements are available for a full range of heights of prototype dams, a formula probably of a form similar to Equation (1) can likely be derived which will remove the uncertainties from this design problem. The use of data obtained from high prototype spillways will enable the extension of the criteria to include the effect of air insufflation.

Type of Flow on Spillway Apron

In order to provide full assurance against structural failure at the toe of an overflow dam, the desirable flow characteristics on the spillway apron must be known, along with the means of maintaining these characteristics. Formation of a true hydraulic jump may be desired, but not always feasible to attain. When the tailwater depth exceeds a certain limit, the jump can be expected to become submerged and the efficiency of energy dissipation accordingly reduced. Of importance to the designer, therefore, is the determination of the limiting condition at which the jump will lose its true characteristics.

The criterion of demarcation between the true hydraulic jump and the drowned jump can be established theoretically. This is demonstrated in the analysis which follows.

Using the term H to denote the total energy head on the crest (including velocity head) and D_1 as the depth of flow at the base of the overfall, the velocity at the base of the overfall is

$$V_1 = \sqrt{2g(P + H - D_1 - h_L)} \tag{6}$$

wherein h_L is the total head loss from the crest to the apron, and g is the acceleration of gravity.

The depth of flow at the base of the fall can be expressed as

$$D_1 = \frac{q}{V_1} = \frac{CH^{3/2}}{\sqrt{2g(P + H - D_1 - h_L)}} \tag{7}$$

The hydraulic jump will become drowned at a tailwater depth greater than the sequent depth D_2 which would occur at the downstream end of a true jump. The limit between the true jump and the submerged jump can therefore be defined by this sequent depth. The theory of conservation of momentum gives

$$D_2 = \frac{D_1}{2}\left[\sqrt{\frac{8q^2}{gD_1^3} + 1} - 1\right] \tag{8}$$

By substitution of terms derived above, the following dimensionless ratio is obtained:

$$\frac{D_2}{P} = \frac{D_1}{2P}\left[\sqrt{\frac{16(P + H - D_1 - h_L)}{D_1} + 1} - 1\right] \quad (9)$$

By plotting the ratios H/P versus D_2/P, obtained through application of Equations (7) and (9), a family of limiting curves for various values of the coefficient of discharge can be developed. Fig. 2 serves as an illustration. For convenience in determining the depth at the end of the overfall, Fig. 3 may be used instead of Equation (7).

In planning for the design of the Boulder Canyon Project, the U. S. Bureau of Reclamation conducted an extensive hydraulic model testing program, much of which was devoted to a study of performance of overflow spillways. This program has provided experimental data relating to the limit between the true jump and the drowned jump.(2) Fig. 4 was derived from these observations by the Bureau of Reclamation. Comparison of Figs. 2 and 4 indicates that the limiting depth observed in the laboratory was somewhat higher than that obtained by the theoretical formulas. This difference is noted even when the loss on the spillway face is neglected in applying Equations (7) and (9). It is suggested that perhaps Fig. 2 defines the limit at which the jump first tends to move upstream, and that the limiting curve of Fig. 4 marks the tailwater depth at which the drowning process is complete.

Bottom Velocities on Spillway Apron

Of primary concern to the designer is the distance traveled by the high-velocity stream under the tail water. On this will depend the extent of the works necessary for protection of the streambed against erosion. It is important that a criterion be established to locate the point at which the velocity of the jet has been reduced to a safe magnitude.

In the testing program for the spillway of Madden Dam, a set of measurements was taken of bottom velocities along a horizontal apron below a model overflow dam. An analysis has been made of the data reported from these tests. The relations drawn in Fig. 5 show the most promise in interpreting the experimental results. The graph is dependent upon limited data and therefore should not be applied to general use. It is presented here to illustrate the possibilities of such analysis. The curves in Fig. 5 apply to a level apron without baffle piers or deflector sill. The variables used in the graph are defined as follows: The term "x" is the horizontal distance from the intersection of the downstream spillway slope with the level apron (neglecting the curve of the bucket); V_o is the velocity of flow at the point where the stream on the spillway face passes the elevation of the tail water at the downstream end of the apron; d_o is the depth of flow, measured perpendicular to the spillway face, at the same point as V_o; h_{vo} is the velocity head corresponding to V_o; D is the depth of tail water at the downstream end of the apron; and V is the bottom velocity of the jet on the apron.

CONCLUSION

This presentation has been exploratory in nature. The primary factors affecting the characteristics of spillway flow have been considered, along with

suggested means of relating them. Basic relations developed here are dependent upon a limited experimental foundation and are therefore intended to serve only for comparison with other model or prototype observations. It is expected that the discussions which are invited will produce further records from observed spillway flows that may enable the formulation of more widely usable criteria.

Particular emphasis has been placed herein on the determination of velocities of flow on the spillway face and apron, and on the phenomena influenced by these velocities. It is believed that a simple natural law governs flow on the face of an ogee spillway, although the exact relationship has not yet been written. The formula for energy loss here offered for comparison may help in the writing of a dependable rule that can be applied generally to overflow spillways of any shape or size.

It is hoped that this paper will provoke discussions which will contribute knowledge not yet available to the profession at large. If the skeleton of criteria appearing here is given sustenance drawn from the experience of others, the purpose of this work will be served.

REFERENCES

1. Randolph, Richard R., Jr., "Hydraulic Tests on the Spillway of the Madden Dam," Transactions, ASCE, Vol. 103, 1938, p. 1080.
2. "Studies of Crests for Overfall Dams," Bulletin No. 3, Pt. VI, Boulder Canyon Final Reports, Bureau of Reclamation, U. S. Dept. of the Interior, Denver, Colorado, 1948.

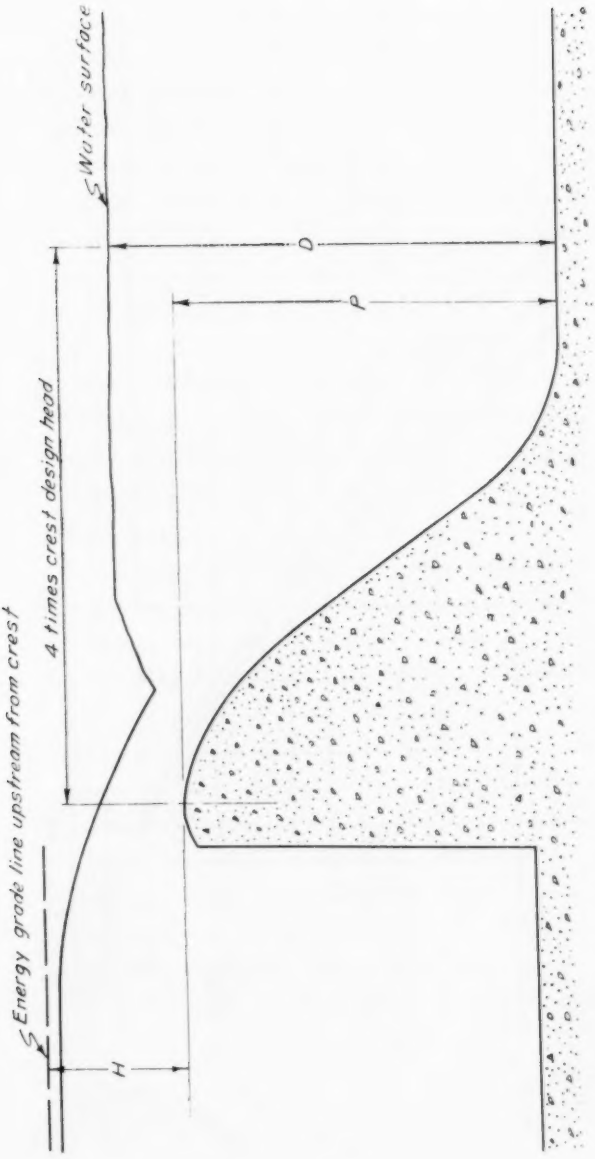

FIG.1-OVERFLOW SPILLWAY

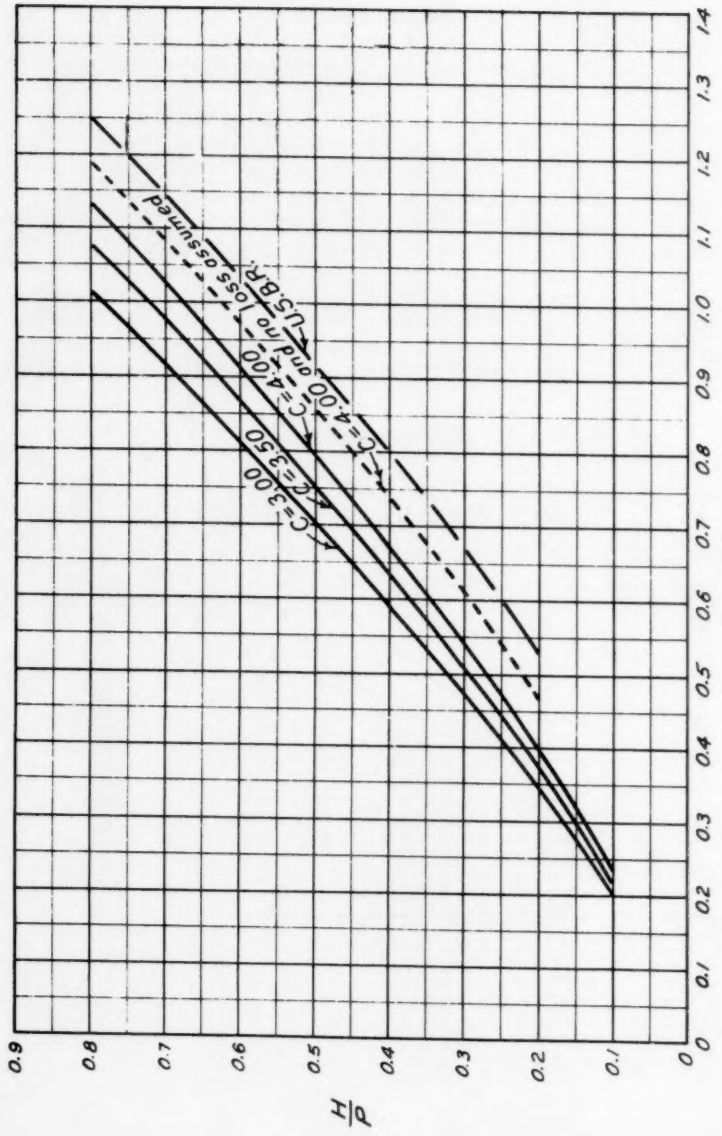

FIG. 2 - LIMIT BETWEEN TRUE AND DROWNED JUMPS

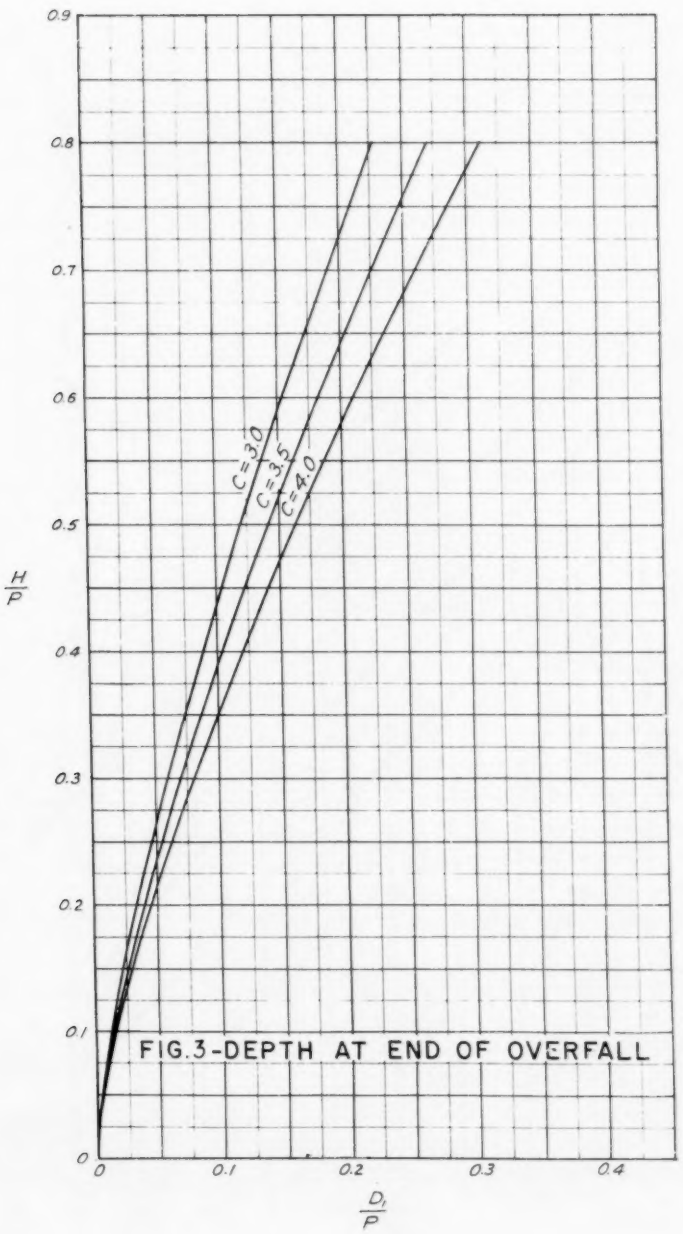

FIG.3-DEPTH AT END OF OVERFALL

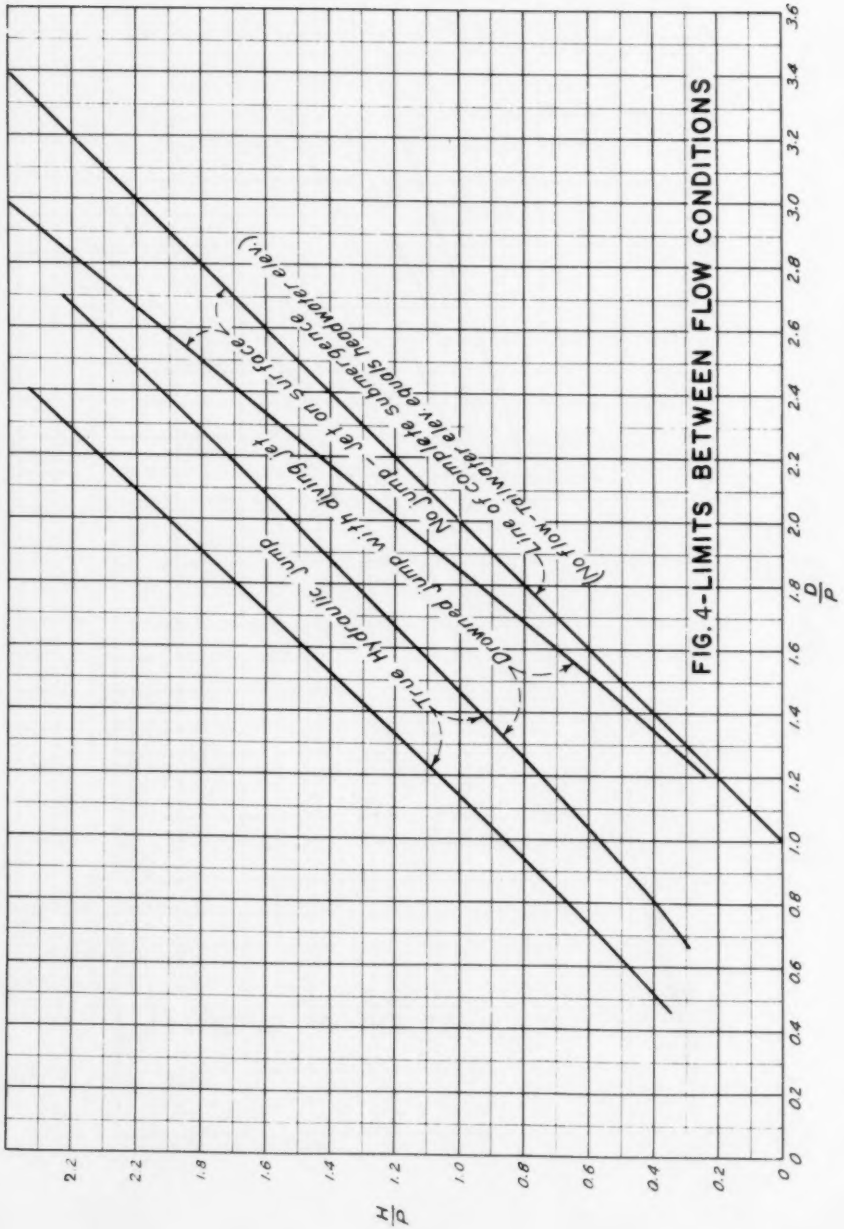
FIG. 4-LIMITS BETWEEN FLOW CONDITIONS
d/D
D/H
(No flow - tailwater elev. equals headwater elev.)
Line of complete submergence
No jump - jet on surface
Drowned jump with diving jet
True Hydraulic jump

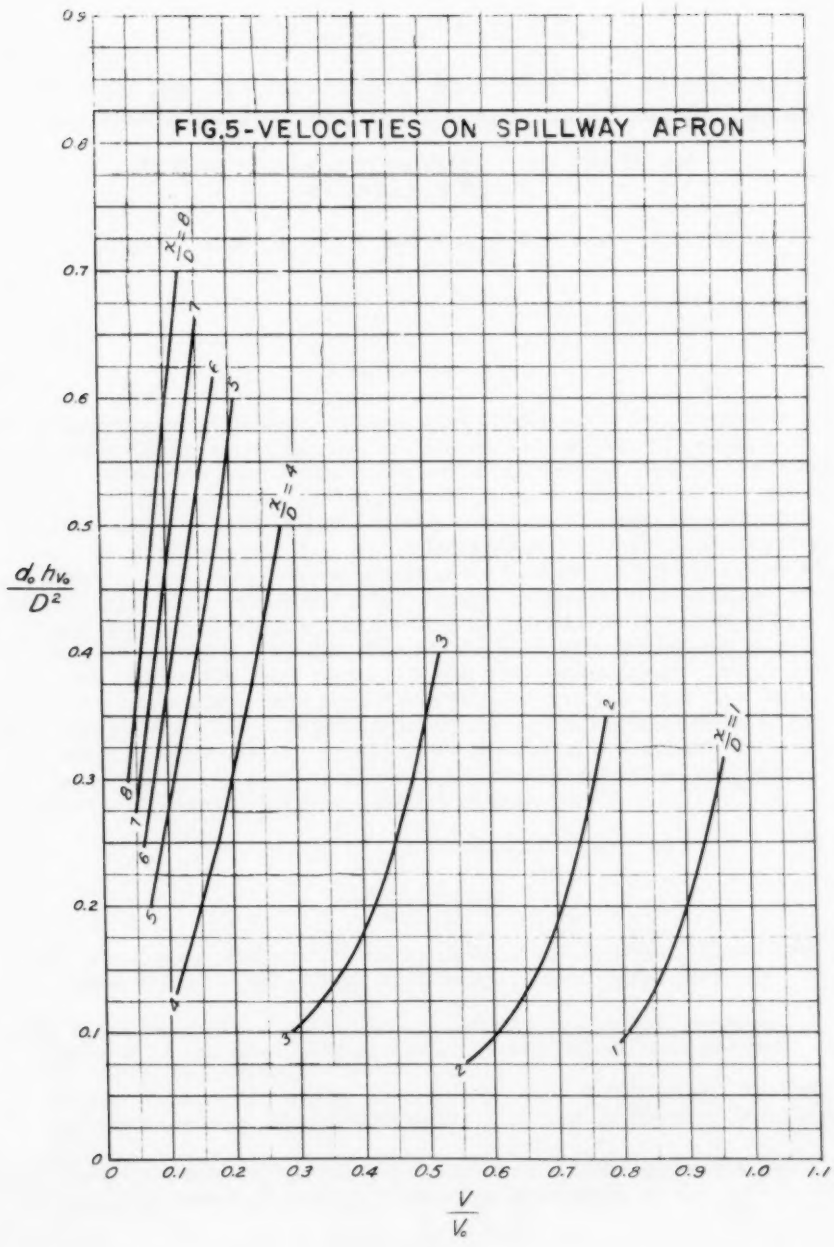
FIG.5-VELOCITIES ON SPILLWAY APRON
$\frac{d_o\, h v_o}{D^2}$
$\frac{V}{V_o}$
x/D = 8
x/D = 4
x/D = 1
0
0.1
0.2
0.3
0.4
0.5
0.6
0.7
0.8
0.9
1.0
1.1

Paper 1453 December, 1957 HY 6

Journal of the

HYDRAULICS DIVISION

Proceedings of the American Society of Civil Engineers

DISCHARGE CHARACTERISTICS OF RECTANGULAR THIN-PLATE WEIRS

Carl E. Kindsvater,[1] M. ASCE, and Rolland W. Carter,[2] A.M. ASCE
(Proc. Paper 1453)

SYNOPSIS

A comprehensive solution is proposed for the discharge characteristics of rectangular, thin-plate weirs. The solution is based on a simple equation of discharge and experimentally derived coefficients which account for the influence of the fluid properties and the physical characteristics of the weir and the weir channel. The effects of viscosity and surface tension are related to an increase in the effective head and an increase or decrease in the effective notch width. Thus, the combined effects of the fluid properties are accounted for with adjustment coefficients which are applied to measured values of the head and width. Consequently, the coefficient of discharge is defined as a function of the width-contraction ratio and the head-weir-height ratio only.

Values of the coefficients required to describe the discharge of water over rectangular, thin-plate weirs are determined from original tests covering a wide range of the significant geometric ratios. Additional data needed to confirm the proposed method of analysis are obtained from the published results of experiments by other investigators. The proposed discharge equation is compared with some of the most widely used formulas.

INTRODUCTION

The rectangular, thin-plate weir is defined in this report as a basic weir form which includes rectangular-notch weirs as well as full-width or

Note: Discussion open until May 1, 1958. Paper 1453 is part of the copyrighted Journal of the Hydraulics Division of the American Society of Civil Engineers, Vol. 83, No. HY 6, December, 1957.

1. Regents Prof., School of Civ. Eng., Georgia Inst. of Technology, Atlanta, Ga., and Consultant, Geological Survey, U. S. Dept. of Interior, Washington, D. C.
2. Chief, Research Section, Surface Water Branch, Water Resources Div., Geological Survey, U. S. Dept. of Interior, Washington, D. C.

"suppressed" weirs. A typical rectangular-notch weir in a rectangular channel is shown in Fig. 1.

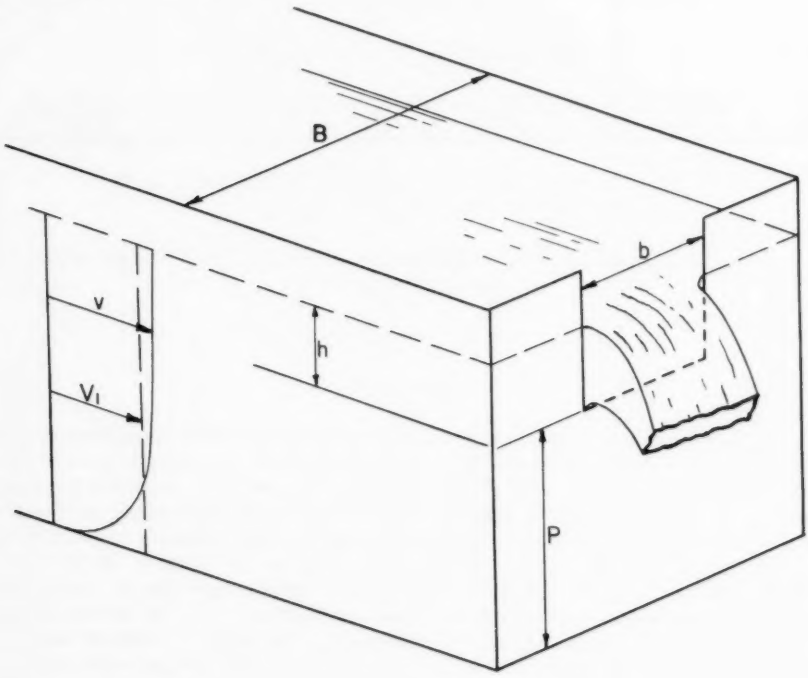

FIG. 1.—THE BASIC THIN-PLATE NOTCH WEIR

For many years hydraulicians have sought a comprehensive equation that would describe the discharge characteristics of rectangular weirs for a full range of fluid, flow, and geometric variables. Because weir discharge involves free, curvilinear flow and the combined influences of several fluid properties, it is not subject to complete mathematical description. Most investigators have resolved their difficulties by restricting their research to the flow of water over full-width weirs of considerable height and width. Unfortunately, however, different workers continue to disagree regarding the physical limitations as well as the discharge characteristics of even this so-called standard measuring weir. Thus, there still exists a variety of weir formulas, each based on a different set of experimental data, which disagree so much that the weir is questioned as an accurate measuring instrument.

Most published weir formulas are related to a quasi-rational analysis in which the weir is described as a limiting example of the two-dimensional orifice. The traditional form of the basic equation of discharge is obtained by integrating an approximate velocity equation over an approximate area. The result is a complex equation which must be modified to make it practicable and adjusted to make it agree with a particular set of experimental data.

The fact that a large number of different empirical formulas have been evolved by this procedure is evidence that the "theoretical" equation is inadequate. The obvious reason for the inadequacy is the fact that the basic assumptions are inaccurate.

Because the flow pattern for the weir is not yet subject to mathematical description, the most direct solution for the discharge function involves a combination of dimensional analysis and experiment. Such an approach to the problem is used in this report.

Analysis of the Discharge Function

Description of the Weir

Fig. 1 shows a typical example of the basic weir form which is the subject of this investigation—a symmetrical, sharp-edge, horizontal-crest, rectangular notch in a smooth, vertical, thin plate located in a smooth, horizontal, rectangular channel. The nappe is fully ventilated and unsubmerged. The channel upstream from the weir, described hereafter as the approach channel, is assumed to be of sufficient length to develop the normal velocity distribution for all discharges. This ideal condition is seldom realized in practice. In fact, the use of short channels with various arrangements of baffles to control the velocity distribution is a major cause of disagreements in the results of experiments made by different investigators.

Dimensional Analysis

The geometry of the flow pattern shown in Fig. 1 is described by the width of the notch (b), the width of the approach channel (B), the height of the weir crest above the bottom of the channel (P), and the piezometric head (h) referred to the level of the crest and measured in the uniform flow section upstream from the weir. The fluid properties involved are the specific weight (γ), the density (ρ), the viscosity (μ), and the surface tension (σ). Only one independent flow characteristic is involved, and it can be represented by either the discharge (Q) or the head (h). However, h is already involved as an independent geometric variable, and Q is conveniently selected as the dependent variable. Thus, a complete statement of the discharge function will include both h and Q, as in the expression

$$Q = f_1(b, B, P, h, \gamma, \rho, \mu, \sigma) \tag{1}$$

From Eq. 1, dimensionless ratios which describe the discharge function can be formed as follows:

$$\frac{Q}{bh\sqrt{gh}} = f_2\left(\frac{b}{B}, \frac{b}{h}, \frac{h}{P}, R, W\right) \tag{2}$$

in which $g = \gamma/\rho$, the acceleration due to gravity. The dependent ratio in Eq. 2 is a coefficient of discharge. The first three independent ratios describe the geometry of the flow boundaries, and the last two symbols represent the Reynolds and Weber numbers.

In American engineering practice the acceleration due to gravity is included in the definition of the coefficient of discharge. Thus, for practical purposes, a convenient definition of the coefficient (C) is

$$C = \frac{Q}{bh^{3/2}} = f_3\left(\frac{b}{B}, \frac{b}{h}, \frac{h}{P}, R, W\right) \quad (3)$$

from which

$$Q = C\, bh^{3/2} \quad (4)$$

The dimensions of C in Eqs. 3 and 4 are the dimensions of $\sqrt{g}$. Because of its obvious simplicity, and despite its lack of dimensional purity, Eq. 4 is used as the basic discharge equation in this report.

The discharge function represented by Eq. 3 cannot be evaluated by analytical procedures. Accordingly, the relative influence of each of the independent ratios must be evaluated by experiment.

Significance of the Geometric Ratios in Eq. 3.

One of the most significant ratios in Eq. 3 is b/B. It is a measure of the channel-width-contraction characteristic of the weir. In combination with h/P, it is also an area-contraction ratio. The influence of b/B is similar to that of the corresponding width or diameter ratios which are used to describe the geometry of orifices. A better analogy is the width ratio which is used to describe open-channel constrictions.(1) Strangely, in view of the great volume of recorded research on weirs, the relative influence of b/B has received little attention. The weir which has been investigated most extensively in the laboratory is the full-width weir, for which b/B = 1.0.

The b/h ratio can be described as a shape parameter. The independent influence of this ratio is believed to be negligible over the full practical range of the other variables. An earlier investigation(2) at the Georgia Institute of Technology supports this conclusion. The fact that most of the published results of research on full-width weirs ignore the b/h ratio indicates either that it was not recognized as an independent ratio or that its influence was not evident from the experimental data. A few recorded efforts to incorporate the b/h ratio in discharge formulas are believed to be based on misinterpretations of influences related separately to the magnitudes of b and h.

The h/P ratio is a measure of the depth-contraction characteristic of the weir. It is complementary to b/B as an area-contraction ratio. Its influence is said to be represented by a velocity-of-approach term in several published formulas. It has also been described as a Froude number for the flow in the approach channel. Actually, for the boundary conditions specified, the flow in the approach channel is always tranquil, and flow with minimum specific energy always occurs in the vicinity of the weir crest. In other words, the Froude number is not a significant independent ratio. (The Froude number would be significant if, for example, the approach channel were sloped or if the weir were located at the foot of a spillway or sluice.) Thus, to describe the h/P ratio as anything but a geometric parameter is to disguise its fundamental significance in the discharge function.

Significance of R and W in Eq. 3

Very little is known about the separate influences of viscosity and surface tension which are represented by the Reynolds and Weber numbers in Eq. 3. It is known, however, that the relative influence of the two fluid properties increases as the head on the weir and the size of the weir decrease.

The Reynolds number (R) is a measure of the relative influence of viscosity. It is usually expressed as

$$R = \frac{VL\rho}{\mu} = \frac{VL}{\nu} \tag{5}$$

in which V is a typical velocity, L is a conveniently evaluated and physically significant length, and ν is the kinematic viscosity of the fluid. For large, full-width weirs the most significant length is the head. For small, narrow weirs, however, the width (and possibly the height) of the weir, as well as the head, are independently significant. In general, therefore, because the Reynolds number must be related to both the head and the width of the weir, there are at least two forms of R. Furthermore, because velocities in the vicinity of the weir crest are proportional to the square root of the head, $\sqrt{h}$ can be substituted for V in Eq. 5, whence $\sqrt{h}(h)/\nu$ and $\sqrt{h}(b)/\nu$ are independent ratios which have the significance of Reynolds numbers. Thus, for a given fluid (ν constant), the total influence of viscosity on a given weir can be expressed in terms of the absolute magnitudes of h and b, or h alone.

The Weber number (W) is a measure of the relative influence of surface tension. It is usually expressed as

$$W = \frac{V\sqrt{L}}{\sqrt{\sigma/\rho}} \tag{6}$$

in which the surface tension (σ) and the density (ρ) are essentially constant for a given liquid. Because V is proportional to $\sqrt{h}$, and because either h or b, or both, can be significant lengths (L), the ratios $\sqrt{h}(\sqrt{h})/\sqrt{\sigma/\rho}$ and $\sqrt{h}(\sqrt{b})/\sqrt{\sigma/\rho}$ are independent ratios which have the significance of Weber numbers. Thus, there are at least two independent forms of the Weber number as well as the Reynolds number. Furthermore, the effects of both viscosity and surface tension for a given weir and liquid are related to the absolute magnitudes of h and b. Therefore, it is impossible to distinguish the separate effects of the two fluid properties from experiments with a single liquid.

Because the Reynolds number for any flow pattern is inversely proportional to a typical viscous-shear force, the relative influence of viscosity decreases as R increases. Similarly, because the Weber number is inversely proportional to a typical surface-tension force, the relative influence of surface tension decreases as W increases. It follows from the foregoing definitions of R and W in terms of h and b that the relative influence of the combined fluid properties diminishes as either h or b becomes larger. Thus, for large heads on large weirs, the influence of viscosity and surface tension is negligible. This conclusion is substantiated, for example, by the observation that the coefficient of discharge for large weirs is essentially constant for all heads above a certain minimum. In other words, C is independent of the fluid-property parameters for large values of h and b. Here the distinction between "small" and "large" must be based on systematic experimental investigations of the independent relationships between C and h and between C and b. Many investigators have attempted to determine the relationship between the absolute head and the discharge coefficient for full-width weirs. The writers know of no systematic effort to evaluate the independent effects related to the absolute width of the weir.

If attention is henceforth restricted to water at ordinary temperatures, it follows from the preceding discussion that the quantities h and b can be used effectively to replace both R and W in Eq. 3. Furthermore, if the b/h ratio

is discarded on the basis of experimental evidence that it is insignificant, the discharge function represented by Eq. 3 can be changed to

$$C = f_4(\frac{b}{B}, \frac{h}{P}, h, b) \tag{7}$$

which must be evaluated by experiment.

Evaluation of Eq. 7

The function represented by Eq. 7 involves four independent variables, a condition which precludes the presentation of experimental data in simple graphical form. However, if the relatively minor effects represented by h and b are described by an approximate, independent, empirical equation, the coefficient of discharge (C) can be expressed as a function of b/B and h/P alone. In other words, if the parameters representing the influence of viscosity and surface tension are effectively "removed" from Eq. 7, the relationship between the coefficient of discharge and the principal geometric ratios can be shown by a family of plane curves.

The effects of viscosity and surface tension cannot be described by exact physical equations. Nevertheless, any procedure whereby these effects are eliminated from the discharge function must be based on a general understanding of the manner in which the fluid properties influence the flow pattern.

The Influence of Viscosity

A flow pattern which is determined by boundary conditions alone is described as a potential-motion pattern. The influence of viscosity in a real fluid motion can be illustrated by comparison with its potential-motion counterpart.

One of the effects of viscosity which can be ignored in many accelerated fluid motions is the energy loss which results from internal shear. The total loss of energy between the section of head measurement and the crest of a weir, for example, is generally insignificant. Therefore, the principal effects of viscosity on weir flow are those which are associated with flow-pattern modifications due to boundary resistance and separation.

A separation zone occupied by a large eddy occurs in the corner between the weir plate and the bottom of the approach channel, as shown in Fig. 2(a). The effect of this occurrence on a low weir, in comparison with the potential pattern for the same weir, is similar to the effect of sloping the weir plate downstream. That is, compared with its potential-motion counterpart, the vertical trajectory of the nappe is lower and the coefficient of discharge, being virtually a coefficient of contraction, is larger. The comparable effect on the discharge, therefore, is the same as an increase in head.

A separation zone similar to that shown in Fig. 2(a) also occurs in the corner between the sides of a notch-weir plate and the walls of the approach channel. The effect of this occurrence, in comparison with potential motion, is to reduce the width contraction of the weir nappe. Its influence on the discharge, therefore, is the same as an increase in the width of the notch.

Viscous shear causes the flow to be retarded in the vicinity of the boundaries. This condition can be described with respect to potential motion by means of the discharge-displacement, boundary-layer thickness, δ^*, shown schematically in Fig. 2. The cross-hatched areas in the figure represent the virtual displacement of the potential motion due to boundary resistance. On the surface of the weir plate, near the vertical edges of the notch as well as

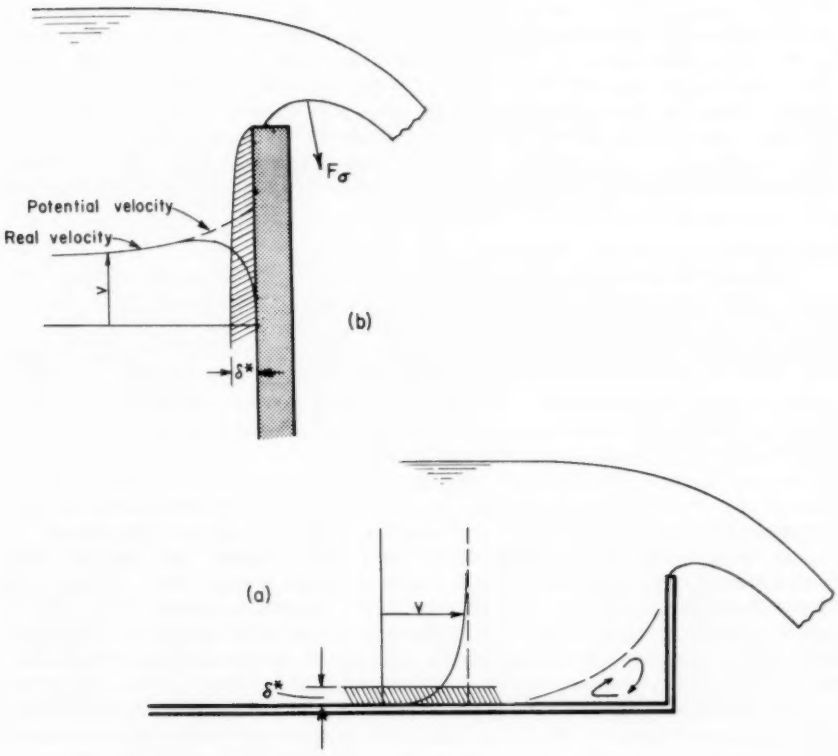

FIG. 2.—INFLUENCE OF VISCOSITY AND SURFACE TENSION (SCHEMATIC)

the horizontal crest, the effect of the boundary layer is similar to the effect of rounding the upstream corners of the notch. Compared with potential flow through a sharp-edged notch, therefore, the coefficient of contraction for the real fluid motion is larger. The effect on the discharge, on the other hand, is similar to the effect of increasing both h and b.

A boundary layer is also formed on the bottom and side walls of the approach channel. The effect of this occurrence is particularly significant for large values of h/P and b/B. For example, the flow through full-width weirs (b/B = 1.0) is characterized by displacement boundary layers on both sides of the channel at the weir section. The effect of this occurrence on the discharge is similar to the effect of a reduction in the width of the weir (b). For values of b/B less than 1.0 the effect of the side-wall boundary layers is to increase the effective value of b/B by decreasing the effective channel width (B). Similarly, the influence of the boundary layer on the bottom of the approach channel resembles the influence of a decrease in P. The effect of this occurrence on the discharge function, therefore, is similar to the effect of an increase in h/P.

The influence of viscosity has been associated with the occurrence of boundary layers and separation zones. It should be emphasized, however, that the thickness of the boundary layers and the size of the separation zones are not directly proportional to the magnitude of the head or the size of the weir. (For this reason, the effects of viscosity are often described as "scale" effects.) Thus, for example, considering the small absolute magnitude of δ^*, the relative effect of each of the several boundary layers depends on the absolute magnitudes of h, b, and P. This observation is consistent with the previous conclusion that the relative effects of viscosity diminish as the size of the weir and the head on the weir increase.

The Influence of Surface Tension

Lindquist,[3] discussing the influence of surface tension on thin-plate, full-width weirs, described two significant phenomena. He observed, first, that the nappe clings to the top edge of the crest as shown in Fig. 2. Thus, compared with its potential-motion counterpart, a real fluid flow is characterized by a lower trajectory and a larger coefficient of contraction because of this surface-tension phenomenon. The effect of the occurrence is similar to the effect of rounding the upstream edge of the plate. Therefore, the effect on the discharge is the same as an increase in head.

The second phenomenon described by Lindquist is the result of surface tension in both the upper and lower nappe surfaces. The effect of this occurrence is a resultant force, F_σ, shown schematically in Fig. 2(b), which acts in the direction of the center of curvature of the nappe. Because the radii of curvature of the nappe surfaces decrease with decreasing head, and because the surface-tension force varies inversely with the radius of curvature, the resultant force F_σ increases as the head decreases. Furthermore, because the resultant surface-tension force has a dominant downward component, it has the same effect on the discharge as an increase in head.

The surface-tension phenomena described for full-width weirs are equally effective on notch weirs. In addition, similar phenomena occur at the vertical sides of the notch as well as the crest. Thus, the total influence of surface tension on the discharge through rectangular-notch, thin-plate weirs can be compared with an increase in the width of the notch as well as an increase in the head on the crest. It should be emphasized, however, that the relative influence of surface tension depends on the absolute magnitudes of h and b. Therefore, like the influence of viscosity, the influence of surface tension diminishes as the size of the weir and the head increase

A Comprehensive Discharge Equation

By comparing the flow of a real fluid with the potential flow for the same boundary conditions, the influence of the fluid properties has been related to an increase in the effective head, an increase or decrease in the effective width of the weir, and a decrease in the effective height of the weir. It has been suggested also that the coefficient of discharge can be expressed in terms of the principal geometric variables alone if the effects of the fluid properties are described by approximate, empirical equations. It is proposed, therefore, that the effective values of h and b be defined as

$$h_e = h + k_h \tag{8}$$

$$b_e = b + k_b \tag{9}$$

in which the quantities k_h and k_b represent the combined effects of the several phenomena attributed to viscosity and surface tension. It is also proposed that a coefficient of discharge which is independent of the size of the weir or the magnitude of the head be defined as

$$C_e = \frac{Q}{b_e h_e^{3/2}} = f_5\left(\frac{b}{B}, \frac{h}{P}\right) \tag{10}$$

It is assumed that k_h and k_b as well as C_e can be defined by experiment. Thus, from Eq. 10, the equation

$$Q = C_e b_e h_e^{3/2} \tag{11}$$

is proposed as a comprehensive equation of discharge for all rectangular, thin-plate weirs. The adequacy of this equation, and, in fact, the adequacy of the effective-head and effective-width concepts, must be examined in the light of experimental data.

Sources of Verification Data

Experiments of Bazin

The classic experiments of Henri Bazin[4, 5] on full-width, thin-plate weirs were made in 1886 and 1887 in a flume located on the bank of the Canal de Bourgogne, near Dijon, France. Bazin's setup included a sluice-controlled forebay and a concrete flume 6.56 ft wide and approximately 700 ft long. His weirs consisted of a crest plate mounted on a timber bulkhead. The nappes were fully ventilated on the downstream side. The crest pieces were described as being iron, carefully straightened, 0.276 in. thick, sharp-edged, and with top surface perpendicular to the plane of the weir. Several different weirs were actually used in making the tests, but they were described as being "perfectly comparable with each other." All of the weirs were of the full-width type ($b/B = 1.0$). In order to cover a full range of values of h/P, Bazin made ten series of tests. The scope of his work is shown in Table 1.

Series 1, 2, and 3 of the Bazin experiments were described as reference tests, because they alone involved volumetric measurements of discharge. For all other tests the weirs were calibrated by comparison with the reference weirs. Head measurements were made with hook gages in stilling wells connected to large orifices in the walls of the flume 16.4 ft upstream from the weirs.

In general, Bazin's instrumentation was good and his technique was meticulous. His results differ considerably from those of most other investigators, however, and this is usually attributed to the conclusion that, for different reasons, the crest pieces were not effectively thin and sharp-edged.[6]

Experiments of Schoder and Turner

One of the most extensive investigations of full-width weirs reported in the literature is that performed under the direction of E. W. Schoder and K. B. Turner at Cornell University from 1911 to 1920.[7] Nearly 2500 tests were made in this investigation, but many of these involved velocity distributions which were not uniform and crest plates which were not sharp-edged. The two series of tests which have been selected for use in this report are believed

TABLE 1. - SCOPE OF THE BAZIN EXPERIMENTS (b/B = 1.0)

Series	P in feet	b in feet	h in feet
1	3.72	6.56	0.19 to 1.01
2	3.72	3.28	0.19 to 1.34
3	3.30	1.64	0.19 to 1.78
4	2.47	6.54	0.48 to 1.28
5	2.47	6.55	0.49 to 1.44
6	1.64	6.54	0.31 to 1.22
7	1.64	6.55	0.34 to 1.40
8	1.16	6.53	0.29 to 0.94
9	1.14	6.55	0.30 to 1.34
10	0.79	6.55	0.30 to 1.34

to have been made with "normal" velocity distributions. The scope of the tests used (Series E and F) is shown in Table 2.

TABLE 2. - SCOPE OF THE SCHODER-TURNER SERIES E AND F TESTS (b/B = 1.0).

Series	P in feet	b in feet	h in feet
E	0.50	4.22	0.029 to 1.41
F	1.00	4.22	0.029 to 2.21

The Cornell tests described in Table 2 were made in a wooden flume 4.22 ft.wide and approximately 30 ft.long. Because of the short length of the flume, baffles were provided at the inlet to control the velocity distribution. A movable bottom was used to obtain different weir heights. Discharges were measured volumetrically. The crest piece for this group of tests was made of rolled brass, 1/4 in. thick. It was described as having a straight, square, and sharp upstream top corner, with a machined 3/32-in. wide top surface and a beveled downstream face. The crest piece was mounted on a timber bulkhead. Head measurements were made with a float gage connected to piezometers 11.74 ft.upstream from the weir. Complete details are given in the paper cited.(7)

Experiments of the U. S. Bureau of Reclamation

Experiments on full-width weirs were performed by the U. S. Bureau of Reclamation in connection with hydraulic investigations for the Boulder Canyon Project.[8] A distinctive feature of the equipment used for the tests was a knife-edge, stainless-steel crest piece. The purpose of this innovation was to prevent the clinging-nappe phenomenon described previously in this report. The crest piece was mounted on a steel plate located in a sheet-metal-lined wooden flume 2 ft.wide and effectively 18 ft.long. A movable floor was used to obtain different values of weir height. Baffles located at the upstream end were used to produce a uniform velocity distribution in the flume. Discharges were measured with venturi meters in the supply line. Heads were measured with a hook gage in a stilling well connected to a piezometer in the movable floor 9.9 ft.upstream from the weir. The scope of the USBR tests is shown in Table 3.

TABLE 3. - SCOPE OF THE USBR EXPERIMENTS (b/B = 1.0).

Series	P in feet	b in feet	h in feet
1	5.00	2.007	0.14 to 1.26
2	4.60	2.007	0.46 to 1.25
3	3.50	2.007	0.14 to 1.22
4	2.50	2.007	0.14 to 1.25
5	2.00	2.007	0.24 to 1.19
6	1.50	2.007	0.28 to 1.20
7	1.01	2.007	0.25 to 1.18
8	0.57 to 0.65	2.007	0.44 to 1.11
9	0.32 to 0.41	2.007	0.40 to 1.04
10	0.13 to 0.14	2.007	0.35 to 0.89
11	0.08 to 0.09	2.007	0.34 to 0.71

New Data on Rectangular Weirs

Original experiments on rectangular weirs were performed in 1955 in the Hydraulics Laboratory of the Georgia Institute of Technology at Atlanta. For the Georgia Tech tests the weirs were located at the downstream end of a steel flume 30 in. deep, 10 ft. wide, and 25 ft.long. The floor of the flume was level and smooth. Its width was varied by means of movable walls faced with 1/4-in. aluminum plates. For tests on full-width weirs the wall plates were made to project through the notch and past the crest a distance of 6 in. Baffles in the forebay and curved guide walls at the upstream ends of the movable walls were adjusted to produce a uniform velocity distribution. Surface floats were used at the entrance to damp waves in the flume.

The basic weir bulkhead was made of 3/8-in. aluminum plate. The width and height of the weir notch was varied by means of lap-joined plate sections made of the same material. The notch edges, including the crest piece, were made of 1/8-in. stainless-steel plates which were fastened to the aluminum plates with the upstream surfaces flush. The edge pieces were machined on a flat-bed planer to be smooth and flat on the upstream side and beveled on the downstream side. The top surface of the notch edges was 1/16-in. wide and perpendicular to the upstream face of the weir. The upstream corners of the edge pieces were sharp.

Water was supplied to the flume from a constant-head system. Discharges were measured in an electrically operated weighing tank at the upstream end of the flume. Heads were measured with a hook gage in a stilling well which was connected to piezometers located in both movable walls 2 in. above the floor and 5 ft.upstream from the weir.

The purpose of the Georgia Tech tests was to obtain the additional experimental data necessary to describe the discharge function over the full, practical range of the variables shown in Eq. 7. The scope of the 249 tests which were made at Georgia Tech is shown in Table 4.

TABLE 4. - SCOPE OF THE GEORGIA TECH TESTS.

P in feet	b in feet	b/B	h in feet
1.44	2.68	1.00	0.16 to 0.53
1.44	1.80	0.90, 0.80, 0.60, 0.40, 0.20	0.14 to 0.58
0.56	2.68	1.00	0.10 to 0.66
0.56	1.80	0.90, 0.80, 0.60, 0.40, 0.20	0.10 to 0.72
0.30	2.68	1.00	0.17 to 0.68
0.30	1.80	0.90, 0.80, 0.60, 0.40, 0.20	0.10 to 0.76
0.30	1.20	0.13	0.11 to 0.66
0.30	0.577	0.06	0.28 to 0.71
0.30	0.281	0.03	0.27 to 0.64
0.30	0.118	0.01	0.08 to 0.65
0.30	0.400	1.00, 0.80, 0.50	0.15 to 0.72
0.30	0.200	1.00, 0.80, 0.50	0.10 to 0.62
0.30	0.100	1.00, 0.80, 0.50	0.10 to 0.60

Verification of the Proposed Solution

Recapitulation

The coefficient C_e in the proposed discharge equation (Eq. 11) is defined in Eq. 10 in terms of the effective head, h_e, and the effective notch width, b_e. It is also defined as a function of the geometric ratios h/P and b/B. Unlike C (Eqs. 4 and 7), therefore, C_e is expected to be independent of the fluid-property effects represented by the magnitudes of h and b in Eq. 7.

It is assumed that C_e can be determined from laboratory data if the measured values of h and b are adjusted as indicated in Eqs. 8 and 9. In Eq. 8 the effective head is defined as the measured head plus a quantity k_h. Similarly, in Eq. 9 the effective width is defined as the measured width plus a quantity k_b. It is reasonable to conclude that the proposed discharge equation will be practicable and convenient to use only if k_h and k_b are constants or functions of not more than one independent variable. Thus, verification of the proposed solution is critically related to the experimental evaluation of the k quantities.

Evaluation of k_h

The quantities k_h and k_b are evaluated from experimental data by a trial computation procedure. For a series of tests in which h is the principal variable, k_h is determined by successive approximations as the quantity which will "remove" the correlation between the coefficient of discharge and the head. The procedure is illustrated by its application to the results of the Schoder-Turner tests.

Fig. 3(a) shows C as a function of h/P for two series of tests made by Schoder and Turner on full-width weirs (Table 2). The scatter in values of C, which is most apparent at lower values of h/P, is systematically related to the magnitude of h. If a small quantity (k_h) is added to h, the value of the coefficient is reduced by an amount which is inversely related to the value of h. Values of the adjusted coefficient (C_e) from a trial computation, using k_h = 0.003 ft, are shown in Fig. 3(b). A second trial, with k_h = 0.004 ft, is shown in Fig. 3(c). From Figs. 3(a) and 3(c) it is apparent that a constant value of k_h = 0.004 ft effectively eliminates the correlation between the coefficient of discharge and the head for Series E and F in the Schoder and Turner tests. From Fig. 3(c), furthermore, C_e is conveniently related to h/P by a straight-line equation.

The Schoder and Turner Series E and F were selected for two reasons. First, they included some tests with very low values of h. For these tests, therefore, the effects of viscosity and surface tension which are related to the magnitude of h are relatively large. Second, the width of the weir used for the tests was large enough (4.22 ft) that the influence of k_b and C_e could be assumed to be negligible. Proof of this conclusion is based on results of Georgia Tech tests which are described subsequently (See Fig. 12).

Fig. 4(a) shows C as a function of h/P for the Bazin tests on full-width weirs (Table 1). Fig. 4(b) shows the same data in a plot of C_e as a function of h/P. The value of k_h used for computing C_e for these tests was 0.012 ft. This value was selected on the basis of trial computations as the value required to eliminate the correlation (evident in Fig. 4(a)) between the coefficient of discharge and the head. The effect of the width-adjustment factor, k_b, was assumed to be negligible for all the Bazin tests. This assumption is believed to have had a small effect on the computed values of C_e for only one group of

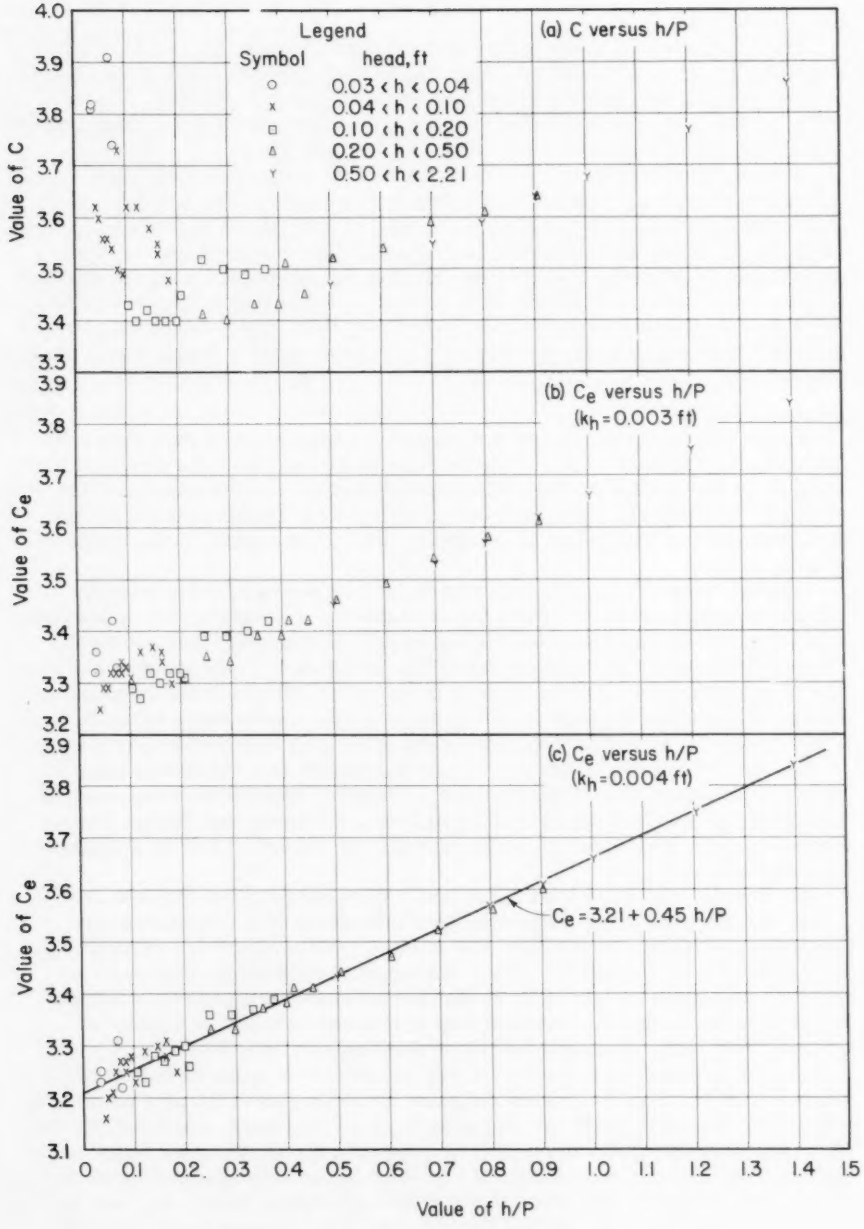
Legend
Symbol head, ft
0.03 < h < 0.04
0.04 < h < 0.10
0.10 < h < 0.20
0.20 < h < 0.50
0.50 < h < 2.21
(a) C versus h/P
(b) Ce versus h/P
(kh = 0.003 ft)
(c) Ce versus h/P
(kh = 0.004 ft)
Ce = 3.21 + 0.45 h/P
Value of C
Value of Ce
Value of h/P

FIG. 3.–SCHODER AND TURNER SERIES E AND F (b/B = 1.0)

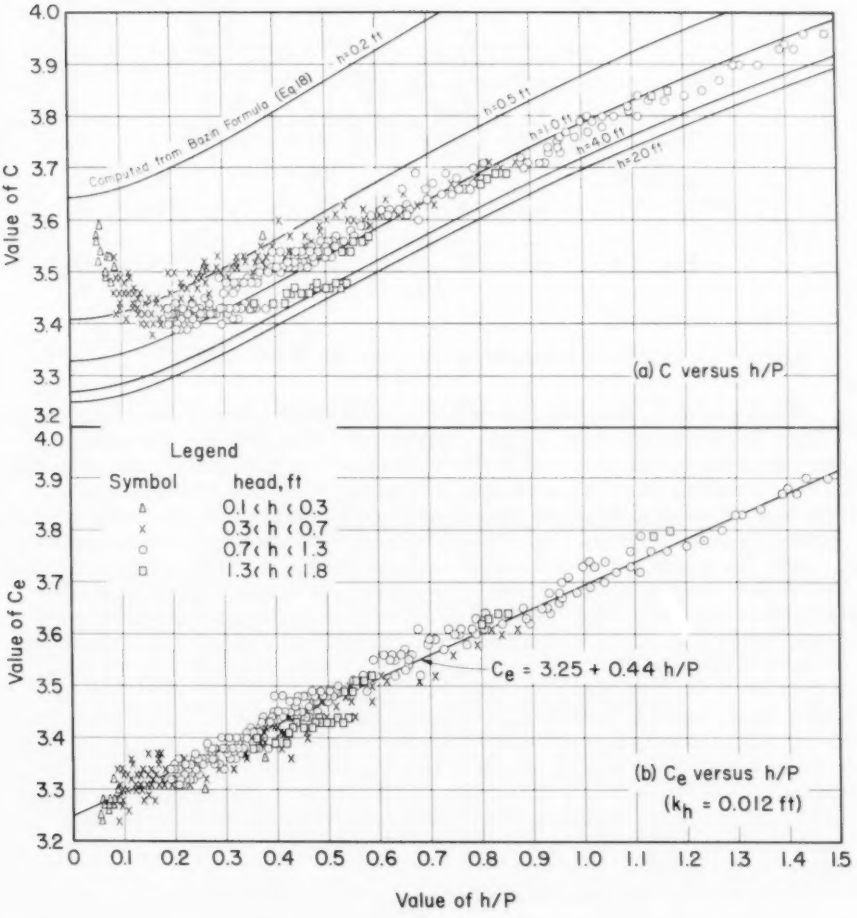

FIG. 4.–BAZIN SERIES 1 TO 10, INCLUSIVE (b/B = 1.0)

tests, Series 3, for which b was 1.64 ft. From Fig. 4(b) it is apparent, again, that C_e is a simple, linear function of h/P.

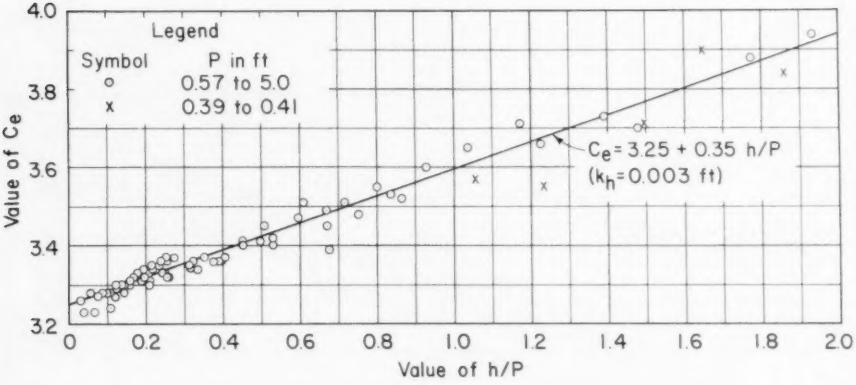

FIG. 5.-U. S. BUREAU OF RECLAMATION TESTS (b/B = 1.0)

Fig. 5 shows C_e as a function of h/P for the USBR tests on full-width weirs (Table 3). For these tests, k_h was determined to be 0.003 ft. The scatter in the points for larger values of h/P is believed to be indicative of experimental errors resulting from observational difficulties related to low values of P. Symbols are used in Fig. 5 to indicate different values of P. The width of the flume was approximately 2 ft. The effect of k_b was assumed to be negligible.

Only full-width weirs (b/B = 1.0) were involved in the tests made by Schoder and Turner, Bazin, and the USBR. Therefore, one of the principal purposes of the Georgia Tech tests (Table 4) was to determine the validity of the proposed solution as applied to notch weirs. Tests made specifically to evaluate k_h included a complete series for each of the following values of b/B: 0.20, 0.40, 0.60, 0.80, 0.90, and 1.00. For the tests on notch weirs, the width (b) was 1.80 ft. For the tests on full-width weirs, b was 2.68 ft. Thus, for all of the k_h tests the relative influence of effects related to b were negligible. Both h and P were varied in each series of tests in order to cover a full range of values of h/P. Values of h varied from 0.10 to 0.76 ft, and values of P varied from 0.30 to 1.44 ft. Sufficient tests were made to define the coefficient of discharge from h/P = 0 to h/P = 2.4. Fig. 6 shows the results of a typical series (b/B = 0.80).

The successive approximations procedure was used to evaluate k_h for each of the series of tests described above. Remarkably, the value of k_h required to satisfy the effective-head criteria was the same for all values of b/B and all values of h/P included in the Georgia Tech tests. In other words, for a full practical range of the significant variables a constant value of k_h (0.003ft) is adequate to compensate for the fluid-property effects related to the head. This conclusion was subsequently verified by successfully applying the same value of k_h to additional tests covering values of b/B from 0.01 to 1.00 and values of b as small as 0.10 ft. Thus, the effective-head concept is substantiated as an important part of the proposed solution.

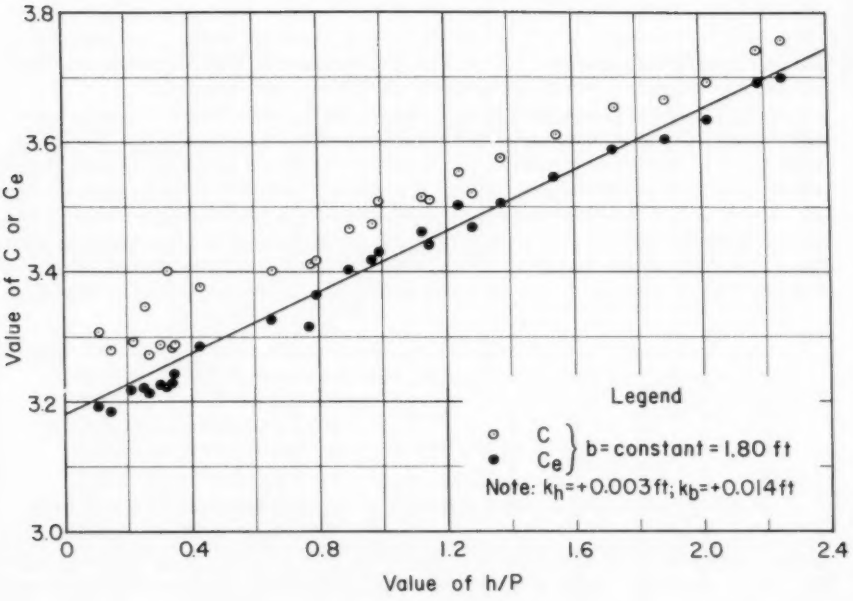

FIG. 6.—GEORGIA TECH TESTS (b/B = 0.80)

Differences in values of k_h and in the C_e curves determined from Schoder and Turner, Bazin, USBR, and Georgia Tech tests on full-width weirs are believed to have been caused by differences in test equipment. The larger value of k_h which characterizes the Bazin tests, for example, is believed to be another indication that Bazin's weir plate was not effectively thin and sharp. This conclusion is supported by the reasoning that the effect of crest-rounding is similar to some of the effects of surface tension and viscosity. The results of the USBR tests are doubtless influenced by the fact that the crest piece of the weir was knife-edged. The Schoder and Turner tests may have been influenced by the fact that their flume was very short and entrance conditions were poor for large values of P. Most of Bazin's tests, on the other hand, were made in flumes long enough to develop a normal, open-channel velocity distribution. Thus, the results of each investigation are characterized by the equipment used in making the experiments.

A constant value of k_h was found to be adequate for all weirs tested in the Georgia Tech investigation. Different values of k_h were determined for full-width weirs tested by other investigators. Therefore, although it is indicated that the same value of k_h can be used for all values of b/B, the value of k_h to be used is also dependent on the physical characteristics of the weir and weir channel.

Evaluation of k_b

The weirs investigated by Bazin, Schoder and Turner, and the Bureau of Reclamation were too wide to reveal the fluid-property effects related to small values of b. Therefore, the results of these tests could not be used to evaluated k_b. Some tests on weirs of relatively small width were included in the Georgia Tech experiments. It was the purpose of these tests to evaluate k_b and to investigate the validity of the effective-width concept.

In Fig. 6 the total displacement of values of C_e with respect to corresponding values of C is a measure of the combined effects of k_h and k_b. However, only a few points at low values of h/P represent heads so small that the adjustment caused by k_h was appreciable. The nearly uniform displacement at higher values of h/P, therefore, is the result of using a value of k_b = 0.014 ft in the computation of C_e. This value was determined from trial computations as the value of k_b which would eliminate the correlation between b and C_e in the results from a special series of tests with b/B = 0.80 (not shown in Fig. 6).

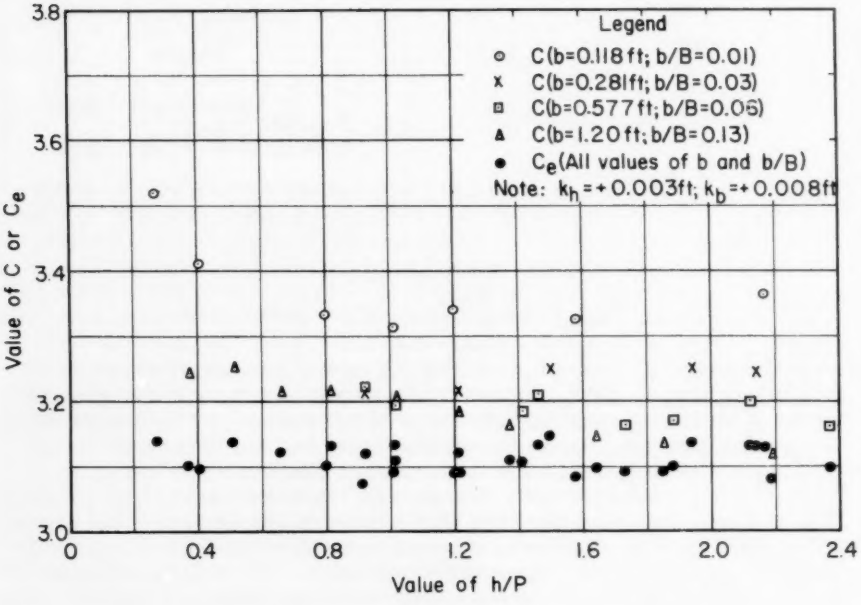

FIG. 7.—GEORGIA TECH TESTS (b/B ≤ 0.13)

Fig. 7 shows the results of special tests made to evaluate k_b for another value of b/B. Actually, several values of b/B are represented on the figure, but the results of the tests indicated that k_b is essentially constant for values of b/B less than 0.2. In Fig. 7, as in Fig. 6, the effect of the k_b adjustment is shown by the displacement of values of C_e with respect to corresponding values of C. The value of k_b used in computing C_e for this example was 0.008 ft.

Fig. 8 shows the results of all tests made to evaluate k_b. The figure

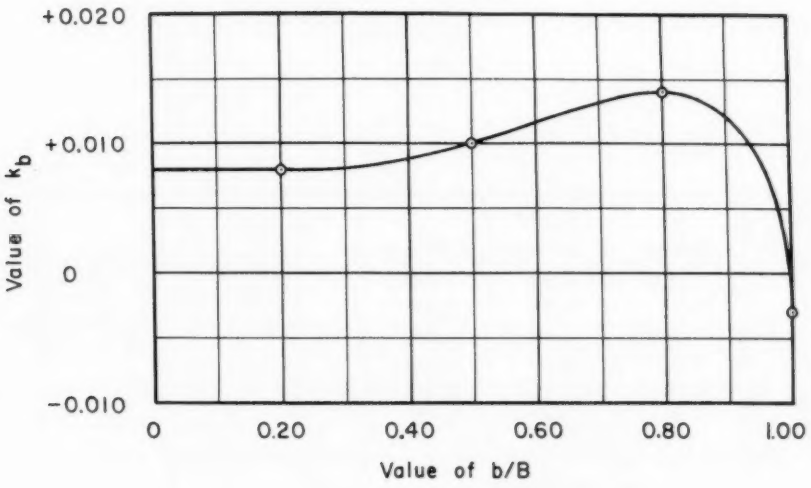

FIG. 8.—VALUE OF k_b DERIVED FROM GEORGIA TECH TESTS

indicates that k_b is a function of b/B, that it increases with increasing values of b/B until it reaches a maximum positive value of 0.014 ft at b/B = 0.80, and that it decreases rapidly thereafter, reaching a minimum value of -0.003 ft at b/B = 1.0. The authors acknowledge some uncertainty regarding the generality of the curve in Fig. 8. It is believed that the value of k_b obtained from the Georgia Tech tests may have been influenced, to an unknown extent, by the physical characteristics of the equipment used. Tests made especially to evaluate k_b involved very small values of b and correspondingly small values of B and Q. Thus, unavoidable errors of measurement may account for comparatively large relative errors in the computed results. Nevertheless, the adequacy of the effective-width concept was demonstrated by the successful elimination of b as an independent variable in the experimentally determined relationship between C_e, h/P, and b/B.

A remarkable example of the experimental evidence which substantiates both the effective-head and the effective-width concepts is shown in Fig. 9. In this figure a single, straight line satisfactorily represents the relationships between C_e and h/P for full-width weirs involving values of b from 0.10 to 2.68 ft and values of h from 0.10 to 0.72 ft.

Evaluation of C_e

The results of the tests from all sources indicate that C_e, the "effective" coefficient of discharge, is a function of b/B and h/P alone. Thus, in confirmation of Eq. 10, C_e is independent of the influences of viscosity and surface tension. Furthermore, the results show that the relationship between C_e and h/P for all values of b/B is conveniently defined by a family of straight lines.

Fig. 10 shows a summary of the results of the Georgia Tech tests. The information on this figure, in combination with values of k_h and k_b (Fig. 8) determined from the same tests, is the information needed to evaluate the

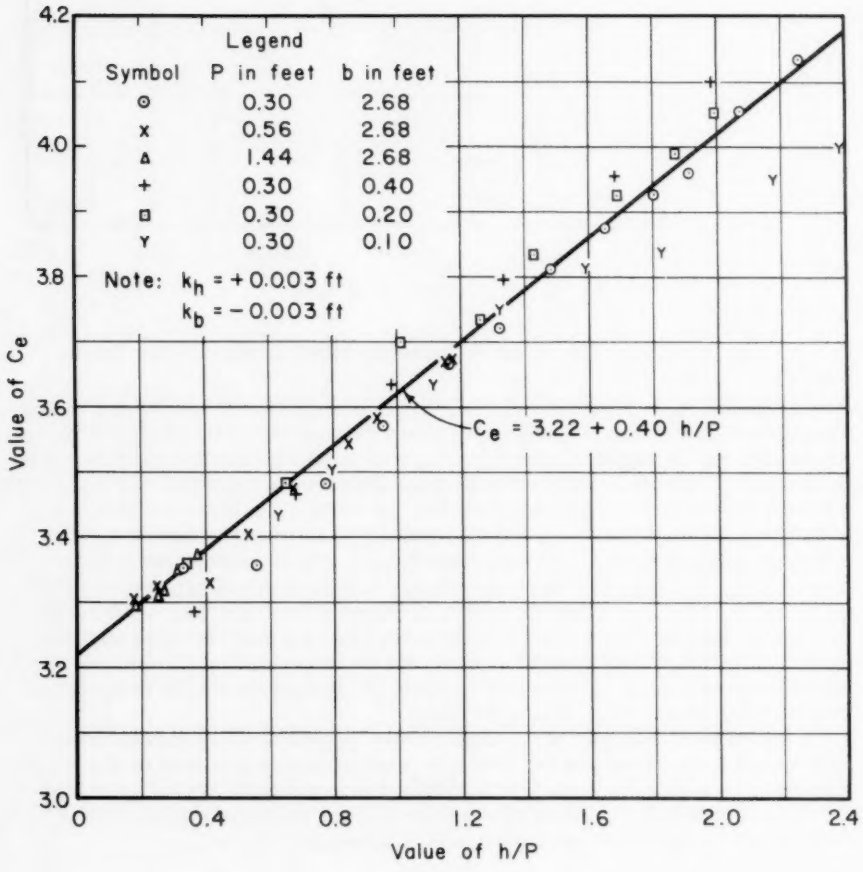

FIG. 9.—GEORGIA TECH TESTS (b/B = 1.0)

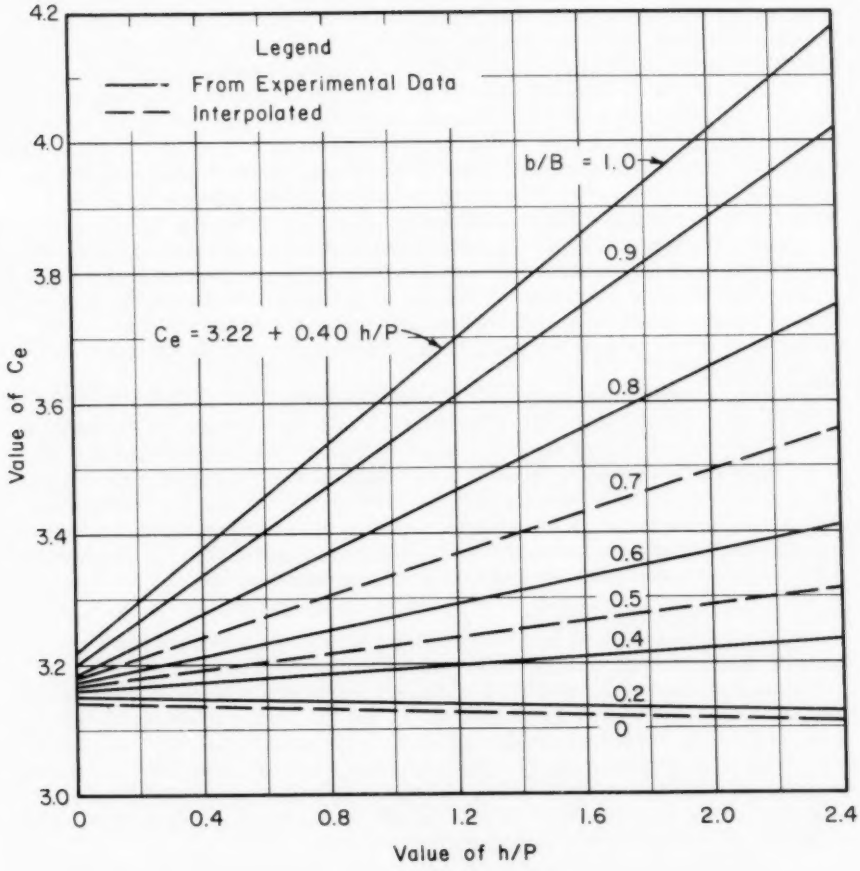

FIG. 10. — C_e FOR ALL VALUES OF b/B, FROM GEORGIA TECH TESTS

proposed discharge equation. Thus, Eq. 11, complemented by the effective-head and effective-width concepts, is confirmed as a comprehensive equation of discharge for all rectangular, thin-plate weirs.

Summary

Experimental Results

The proposed discharge equation (Eq. 11) and the concepts of effective head and effective width (Eqs. 8 and 9) have been substantiated by experiments from various sources covering a wide range of test conditions. It has been demonstrated that C_e is a linear function of h/P for each value of b/B, that k_h is a constant for all values of b/B and h/P, and that k_b is a function of b/B.

From the results of tests made at the Georgia Institute of Technology, values of C_e, k_h and k_b have been determined for water at ordinary temperatures. Fig. 10 shows C_e for a full range of values of b/B, with h/P from 0 to 2.0. From the information contained in this figure, simple equations for C_e can be written if desired. The constant value of k_h determined from the Georgia Tech tests is 0.003 ft. Values of k_b are shown in Fig. 8.

Comparisons of values of C_e and k_h obtained from tests made by different investigators of full-width weirs confirm the general conclusion that weir discharge is critically influenced by the physical characteristics of the experimental setup. Especially critical are the weir-notch edges and the channel properties which control the velocity distribution and turbulence upstream from the weir.

Neither superior equipment nor superior technique is claimed for the Georgia Tech tests. However, it is believed that the over-all quality of these data is as good as that of any other data available. Furthermore, this is the only investigation known to cover a full, practical range of the significant variables. Therefore, as a reasonably accurate solution for the comprehensive discharge characteristics of rectangular weirs with effectively sharp, thin crests, the authors recommend the use of the proposed discharge equation and the coefficients derived from the Georgia Tech experiments.

Effect of Neglecting k_h and k_b

It has been established that the relative influence of viscosity and surface tension diminishes as both the head and the notch width becomes larger. In the proposed discharge equation the fluid-property effects are represented by the head- and width-adjustment factors, k_h and k_b. Thus, the relative influence of k_h decreases as the head increases in magnitude, and the relative influence of k_b decreases as the width increases in magnitude. It follows that for "large" heads on "large" weirs the influence of the adjustment factors is negligible. The experimental results can be used to evaluate the influence of k_h and k_b in relation to the magnitudes of h and b.

A convenient approximation for the discharge can be obtained from Eq. 11, using C_e from Fig. 10, with the unadjusted (measured) values of h and b. The relative accuracy of this approximation is a significant measure of the influence of k_h and k_b. It is also a measure of the influence of the combined effects of viscosity and surface tension. Thus, if the absolute error (ΔQ) due to neglecting k_h and k_b is

$$\Delta Q = C_e b_e h_c^{3/2} - C_e b h^{3/2} \qquad (12)$$

the relative error is

$$\frac{\Delta Q}{Q} = 1 - \frac{b}{b_e}\left(\frac{h}{h_e}\right)^{3/2} \tag{13}$$

The influence of k_h alone can be demonstrated by assuming that the notch width is very large, whence $b \approx b_e$ in Eq. 13. Then, from Eqs. 8 and 13,

$$\frac{\Delta Q}{Q} = 1 - \left(\frac{h}{h + k_h}\right)^{3/2} \tag{14a}$$

which is shown in Fig. 11 for $k_h = 0.003$ ft. Similarly, the separate influence of k_b can be demonstrated by assuming that $h \approx h_e$. Thus, from Eqs. 9 and 13,

$$\frac{\Delta Q}{Q} = 1 - \left(\frac{b}{b + k_b}\right) \tag{14b}$$

which is shown in Fig. 12 for values of k_b from Fig. 8. Figs. 11 and 12 are recommended for use in connection with Eq. 11 as a means of determining when (depending on the accuracy desired) the influence of the fluid properties may be neglected.

Upper Limit of h/P

Bõss[11] has shown that critical depth will occur in the uniform flow upstream from a weir with h/P greater than about 5. For values of h/P greater than 5, therefore, the weir is not a control, and the ordinary weir discharge equations are not applicable. A lower, practical limit on h/P is imposed by observational difficulties and measurement errors. For precise measurements the writers recommend that h/P be limited to values less than 2.0.

Influence of Weir Height

The weir height, P, was acknowledged as a possible third significant length parameter in the discharge function. There is disagreement in the literature, however, regarding experimental evidence of a systematic correlation between P and the coefficient of discharge. Bazin[9] warned against the use of his discharge formulas for a "very low weir. . . which should always be avoided." Rehbock[10] acknowledged "some disturbance, which is not yet clearly understood (and because of which) the coefficient C is not exactly the same for any two sharp-crested weirs of different absolute heights, P, even if the ratios, h/P, are identical." Weirs as low as 0.08 ft were used in the USBR tests in order to achieve the higher values of h/P. The results of these tests show a definite correlation between C_e and P for values of h/P greater than 2 (not included on Fig. 5). The Georgia Tech tests, however, failed to show a similar correlation for values of P as low as 0.30 ft and values of h/P as high as 2.4.

It is generally acknowledged that observational difficulties and errors in measurement may account for appreciable errors in the results of experiments involving small values of P and large values of h/P. For this reason alone, weirs lower than 0.3 ft are not recommended for precise measurement of discharge. Nevertheless, although questions regarding the influence of weir heights less than 0.3 ft may be academic, additional experiments are needed to resolve the contradictions to be found in the literature.

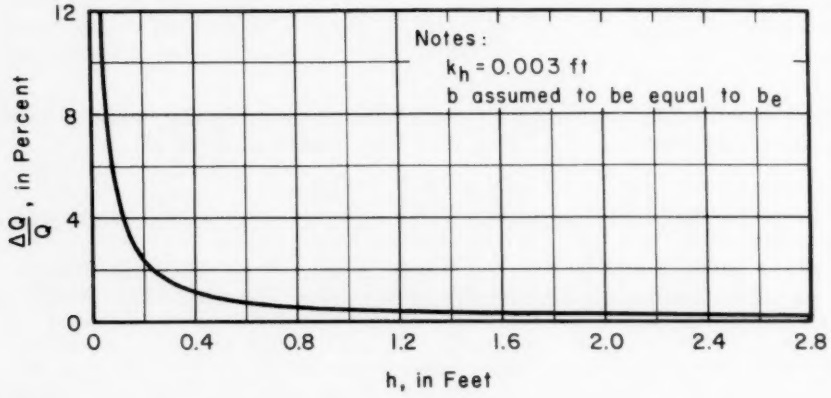

FIG. 11.—EFFECT OF VISCOSITY AND SURFACE TENSION RELATED TO h

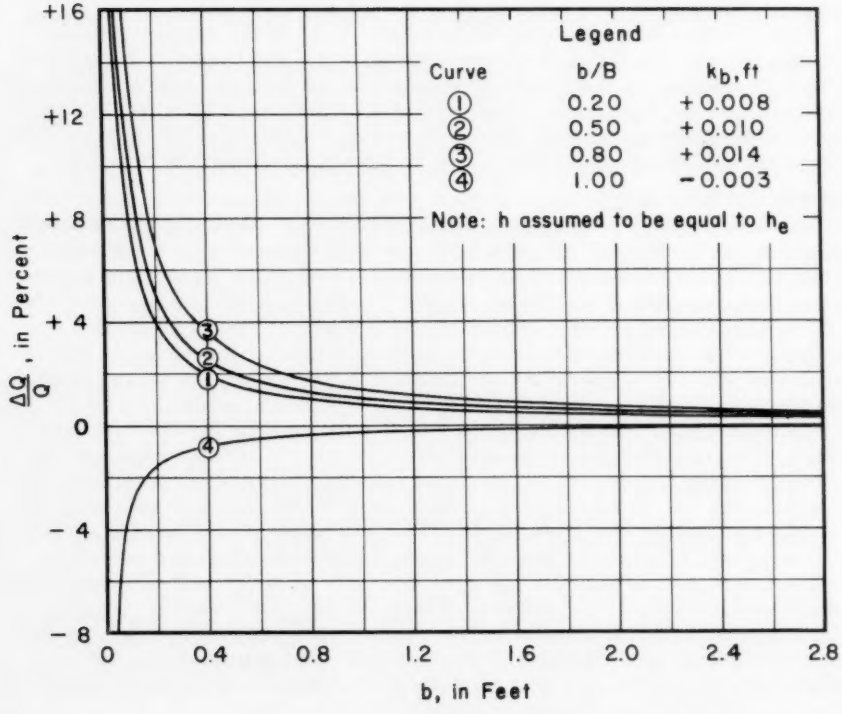

FIG. 12.—EFFECT OF VISCOSITY AND SURFACE TENSION RELATED TO b

Comparison with Other Experiments and Formulas

Some Classic Formulas

One equation is frequently described as the basic equation of discharge for all weirs. It is founded on an assumed analogy between the weir and the two-dimensional orifice. In its derivation an approximate velocity equation is integrated over the approximate area limits of the nappe in the plane of the weir. The effects of viscosity and surface tension are ignored. The result, in the form usually ascribed to Weisbach, is

$$Q = C_c \frac{2}{3}\sqrt{2g}\, b \left[\left(h + \frac{V_1^2}{2g}\right)^{3/2} - \left(\frac{V_1^2}{2g}\right)^{3/2}\right] \tag{15}$$

in which C_c is a coefficient of contraction and V_1 is the average velocity in the approach channel.

Some writers have erroneously implied that Eq. 15 is a comprehensive and theoretically correct equation of discharge. It is claimed, for example, that the velocity-head terms account for the influence of approach-channel geometry. From this viewpoint h/P is eliminated as an independent variable, and C_c is a function of b/B alone. These conclusions are not substantiated by experiment.

The inadequacy of Eq. 15 can be attributed partly to the fact that the effects of viscosity and surface tension are ignored in its derivation. However, experiments show conclusively that these effects are appreciable only when h or b, or both, are relatively small. Eq. 15 is deficient largely because its derivation was based on several erroneous assumptions.

Unjustifiable alterations of Eq. 15 have been made for the purpose of improving agreement between the equation and experimental data. Thus, it is quite common to omit the second velocity-head term in the brackets, and, subsequently, to attribute great significance to the "total head" term which remains. The result is an equation such as that proposed by Hamilton Smith, Jr., in 1884,[12]

$$Q = C_s \frac{2}{3}\sqrt{2g}\, b \left[h + k_1 \left(\frac{V_1^2}{2g}\right)\right]^{3/2} \tag{16}$$

in which both C_s and k_1 are coefficients determined from experiment. Smith described the coefficient k_1 as a number which represents "the portion of the kinetic energy [which] produces a useful effect at the opening of discharge." He recognized that k_1 is a variable which depends on the velocity distribution in the approach channel. Nevertheless, he recommended a constant value of 1.33 for all full-width weirs and 1.40 for all "fully contracted" weirs. He described C_s as a discharge coefficient, and he concluded that it was a function of the head, the notch width, and the width-contraction ratio (b/B). Actually, both k_1 and C_s are functions also of the ratio h/P, and they are critically dependent on the physical characteristics of the weir and the approach channel. Therefore, Eq. 16 is little more than a basis for the experimental definition of the discharge function. It is obviously not the most convenient formula for this purpose, nor is it the comprehensive solution which is needed.

Hamilton Smith's exhaustive study and detailed exposition of the influence of the velocity of approach was subsequently ignored or misinterpreted by others. Some writers have inferred that his k_1 coefficient can be associated

with the kinetic-energy coefficient (α_1). Accordingly, they have perpetuated the misconception that the coefficient of discharge is a constant when the quantity within the brackets (Eq. 16) is evaluated as the true total energy head in the approach channel $[h + \alpha_1 (V_1^2/2g)]$.

The coefficient α is defined as the ratio of the true average velocity head in a cross section to the velocity head computed on the basis of the average velocity in the section. It is a dimensionless measure of the degree of velocity nonuniformity, but it does not account specifically for the shape of the velocity-distribution curve. Smith, Schoder and Turner,[7] and others who have studied the influence of the velocity distribution in the approach channel have shown conclusively that the pattern of nonuniformity is more critical than the degree of nonuniformity. Thus, experiments performed in a large variety of weir channels have failed to reveal a satisfactory correlation between α_1 and k_1.

Most of the defects of Eq. 16 are common also to a large number of equations in the form suggested by Weisbach in 1844,

$$Q = C_w \frac{2}{3}\sqrt{2g}[k_2 + k_3(\frac{h}{P+h})^2]bh^{3/2} \qquad (17)$$

in which C_w, k_2 and k_3 are experimentally determined coefficients which account for the influence of the fluid properties, the velocity distribution, and the physical characteristics of the weir and approach channel. The principal advantage of Eq. 17 is that the velocity-head term in Eq. 16 is replaced by a term which involves the h/P ratio. The effect of this modification is to avoid a successive-approximations solution for discharge. Equations of this general variety include some of the most widely used formulas for full-width weirs (b/B = 1.0). Among these are the Bazin formula,[5]

$$Q = (3.25 + \frac{0.079}{h})[1 + 0.55(\frac{h}{P+h})^2]bh^{3/2} \qquad (18)$$

the Rehbock formula of 1912,[13]

$$Q = (3.24 + 0.43\,\frac{h}{P} + \frac{0.018}{h})\,bh^{3/2} \qquad (19)$$

and the S.I.A. (Swiss Society of Engineers and Architects) formula,[14]

$$Q = (3.29 + \frac{0.011}{h + 0.005})[1 + 0.5(\frac{h}{P+h})^2]\,bh^{3/2} \qquad (20)$$

The complex expressions which are the coefficients of the quantity $bh^{3/2}$ in each of these equations are equivalent to C in the simple equation of discharge (Eq. 4). The numerical quantities are experimentally derived coefficients which account for the influence of the fluid properties as well as the weir and channel characteristics. Specifically, a term involving and having the dimensions of h is now recognized as a means of compensating for the combined effects of viscosity and surface tension. Because it is a dimensional quantity, the h term restricts the application of Eqs. 18, 19, and 20 to the fluid used for the experiments (water at ordinary temperatures). However, it is apparent that the influence of the head term is negligible except when h is relatively small.

An alternate formula for full-width weirs was proposed by Rehbock in 1929[15]:

$$Q = (3.22 + 0.44 \frac{h}{P}) \, bh_e^{3/2} \tag{21}$$

This was the first formula known to involve the effective head ($h_e = h + 0.004$ ft). The quantity 0.004 ft, corresponding to k_h in Eq. 8, was apparently derived by Rehbock from an analysis of his own experiments.

Rehbock did not associate the h term in Eq. 19 or the effective-head term in Eq. 21 with the influence of the fluid properties. He described both terms as a means of accounting for a disturbance related to the magnitude of P. He hesitated to endorse Prandtl's suggestion that they were related to the effect of capillarity.[10]

Various restrictions were placed on Eqs. 18, 19, 20, and 21 by their authors. Bazin[9] specified that "the arrangement of our standard weir [must be] exactly reproduced." Rehbock[15] required that the head be large enough to ensure a free nappe, but he claimed a high degree of accuracy for both of his formulas when applied to full-width weirs of all sizes. The S.I.A., in its Standards for Water Measurement,[14] restricts the application of Eq. 20 to values of P not less than 1 ft, values of h between 0.08 and 2.6 ft, and values of h/P not greater than 1.0.

One of the new formulas developed for rectangular-notch weirs ($b/B < 1.0$) is that proposed by the S.I.A.:[14]

$$Q = [3.09 + 0.20(\frac{b}{B})^2 + \frac{0.063 - 0.053(\frac{b}{B})^2}{h + 0.005}] \, [1 + 0.5(\frac{b}{B})^4 \, (\frac{h}{P + h})^2] \, bh^{3/2} \tag{22}$$

The application of this formula is restricted to values of P not less than 1 ft, values of h between 0.08(B/b) and 2.6 ft, values of h/P not greater than 1.0, and values of b/B not less than 0.3. Eq. 22 is widely quoted in European technical literature, but correspondence and library research failed to reveal the source of the data on which it was based. The formula is virtually unknown in this country.

In American practice, approximate formulas for notch weirs are adapted from formulas for full-width weirs by means of the contracted-width equation ascribed to James B. Francis:[16, 17]

$$b_c = b - 0.2 \, h \tag{23}$$

In this equation b_c is the width of the contracted stream, b is the gross width of the notch, and the quantity 0.2 is a coefficient recommended by Francis for "fully contracted" rectangular-notch weirs. Thus, from Eqs. 4 and 23, the Francis discharge formula for notch weirs is

$$Q = C_1 \, (b - 0.2 \, h) \, h^{3/2} \tag{24}$$

in which C_1 is the coefficient of discharge in any of the formulas for full-width weirs ($b/B = 1.0$).

Hamilton Smith, Jr., after reviewing the experiments of Francis, Fteley

and Stearns, and others, described the requirements for "full contraction" as follows:[17] The weir height (P) should be not less than twice the head (h) or not less than 1 ft; the width from the side of the approach channel to the end of the notch should be not less than twice the head or twice the width of the notch (b). Thus, Smith's recommendations included the requirement that h/P be not greater than 0.5 and that b/B be not greater than 0.2. Francis[17] added the requirement that b/h be not less than 3.0. It is recognized now that the concept of "full contraction" is inconsistent with the true significance of b/B as an independent variable.

Comparison of Experiments and Formulas for Full-Width Weirs

The experiments of Schoder and Turner, Bazin, and the Bureau of Reclamation, as well as the Georgia Tech experiments, were used to confirm the method of analysis and the discharge equation proposed in this report. Consequently, values of C_e and k_h were determined, and these values can be used to compare the results of the tests made by the different investigators. Comparable values of k_b could not be determined because only the Georgia Tech experiments included tests on weirs narrow enough to reveal the fluid-property effects associated with small values of b.

From the results of the Georgia Tech tests on full-width weirs, $k_h = 0.003$ ft, $k_b = -0.003$ ft, and C_e is given by the simple equation,

$$C_e = 3.22 + 0.40 \frac{h}{P} \tag{25}$$

From the Schoder and Turner tests (Series E and F) in Fig. 3(c), $k_h = 0.004$ ft, and

$$C_e = 3.21 + 0.45 \frac{h}{P} \tag{26}$$

The results of the Bazin tests on full-width weirs are shown in Fig. 4. The value of k_h required for the Bazin tests is considerably larger than that determined from the other experiments. From Fig. 4(a), $k_h = 0.012$ ft, and

$$C_e = 3.25 + 0.44 \frac{h}{P} \tag{27}$$

The results of the USBR tests (Fig. 5), in comparison with the others, are characterized by smaller values of C_e at the larger values of h/P. For the USBR tests, $k_h = 0.003$ ft, and

$$C_e = 3.25 + 0.35 \frac{h}{P} \tag{28}$$

Rehbock's 1929 formula is also based on the effective-head concept. Furthermore, his equation for C_e is in the linear form of Eqs. 25 to 28, inclusive. Thus, for comparison with those equations, Rehbock's 1929 formula gives

$$C_e = 3.22 + 0.44 \frac{h}{P} \tag{29}$$

with $k_h = 0.004$ ft. Rehbock did not recognize the existence of k_b, although

some writers have indicated that his experiments were made in a very narrow flume. Therefore, it is possible that Eq. 29 would be modified if k_b were taken into account. This conclusion could not be verified because Rehbock's experimental data were not available.

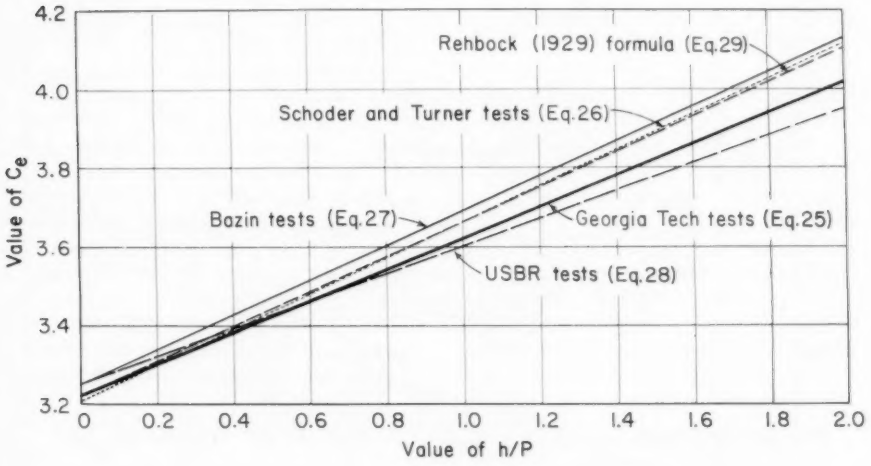

FIG. 13.- COMPARISON OF EXPERIMENTAL DATA (b/B=1.0)

Eqs. 25 to 29, inclusive, are compared in Fig. 13. The Schoder and Turner, Bazin, and Rehbock curves agree reasonably well. The curve determined from the Georgia Tech tests lies below these curves and above the USBR curve. It was suggested previously that the differences in the results of the experiments shown in Fig. 13 were caused by differences in the test equipment. Thus, the distinctive character of the C_e curve from the USBR tests can be associated with the fact that the crest piece for these tests was knife-edged. Similarly, the larger value of k_h determined from Bazin's tests can be related to the conclusion that his crest was not truly thin and sharp. Such details as these, frequently unknown or uncontrollable, are believed to be the cause of the variance shown in Fig. 13. Nevertheless, it is noteworthy that the equations for C_e derived from various sources are all simple, linear functions of the h/P ratio.

Fig. 14 shows a comparison of the results of the Georgia Tech tests with some of the most widely used formulas for full-width weirs. The comparison is made for two values of h and a full range of values of h/P. The Bazin formula (Eq. 18), the Rehbock 1912 formula (Eq. 19), and the S.I.A. formula (Eq. 20) are in the non-linear form suggested by Weisbach. For these formulas C was computed as $Q/bh^{3/2}$ from Eqs. 18, 19, and 20. For the Georgia Tech tests and the Rehbock 1929 formula, C was computed from the relationship

$$C = \frac{Q}{bh^{3/2}} = \frac{C_e b_e (h + k_h)^{3/2}}{bh^{3/2}} \approx \left(\frac{h + k_h}{h}\right)^{3/2} C_e \qquad (30)$$

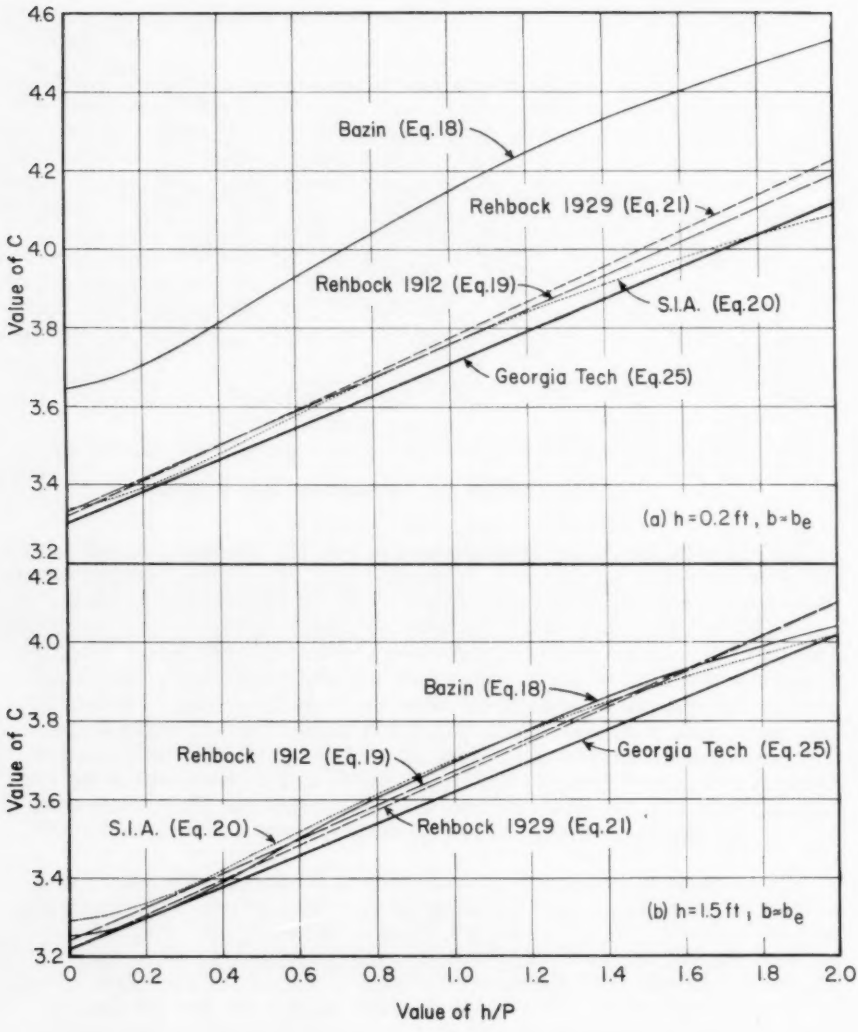

FIG. 14.- COMPARISON OF FORMULAS (b/B=1.0)

in which b is assumed to be so large that the influence of k_b can be neglected, whence $b \approx b_e$. Values of C_e in Eq. 30 were computed from Eq. 25 for the Georgia Tech tests and from Eq. 29 for the Rehbock 1929 formula.

Fig. 14(a) shows a comparison of the different formulas for h = 0.2 ft. For this condition the influence of the fluid properties and effects of differences in the experimental equipment are relatively large. Fig. 14(b) shows a comparison of the formulas for h equal to 1.5 ft. For this condition the effects related to small values of h are negligible (See Fig. 11). The curves in Fig. 14(b) show reasonably good agreement.

In general, the comparisons of experiments and formulas shown in Figs. 13 and 14 cast doubt on the adequacy of some of the widely used formulas and on the reproducibility of the test conditions from which they were derived. In particular, the relatively complex Weisbach-type formulas are not justified as comprehensive discharge equations. This conclusion is emphatically demonstrated in Fig. 4. From the family of curves shown in Fig. 4(a), it is apparent that the Bazin formula compares unfavorably with the results of the Bazin tests for all but the intermediate values of h included in the experiments. In Fig. 4(b), however, a single, straight-line curve fits the data reasonably well for all values of h and h/P. Thus, the simple, linear equation for C_e, complemented by the effective-head concept, is substantiated as an improved method of defining the discharge function.

Comparison of Formulas for Notch-Weirs

Fig. 10, based on the Georgia Tech tests, shows the relationship between C_e, h/P, and b/B for notch weirs. A comparable family of curves can be plotted from the S.I.A. formula for notch weirs (Eq. 22) if the term involving the absolute head is omitted. For relatively large values of h (and b), the influence of the h term is negligible, and values of C from Eq. 22 can be compared with values of C_e from Fig. 10. The comparison is shown in Fig. 15. The maximum difference between corresponding values of C_e shown in Fig. 15 is about 4 percent. However, within the limits of applicability specified by the S.I.A. ($b/B \geq 0.3$, $h/P \leq 1.0$), the maximum difference between the two families of curves is about 2 percent. It is emphasized that Fig. 15 does not include a comparison of the different methods of compensating for the fluid-property effects. However, it is believed that the advantages of the effective-head concept were clearly demonstrated in the previous comparisons of formulas and experiments for full-width weirs.

The results of the Georgia Tech tests on notch weirs (Fig. 10) indicate that C_e is a function of b/B and h/P. In the Francis contracted-width formula (Eq. 23), however, a correction for "end contractions" is assumed to be a function of h alone. Because of this fundamental difference, the Francis discharge formula (Eq. 24) cannot be compared with the Georgia Tech tests or the S.I.A. formula on a graph such as Fig. 15. Nevertheless, it is possible to show that the Francis formula is not substantiated by the curves shown in Fig. 10.

Eq. 23 can be written in the form

$$b_c = b - Kh \tag{31}$$

in which, according to Francis, K is a constant equal to 0.2 for "fully contracted" rectangular-notch weirs. From Eqs. 11, 24, and 31,

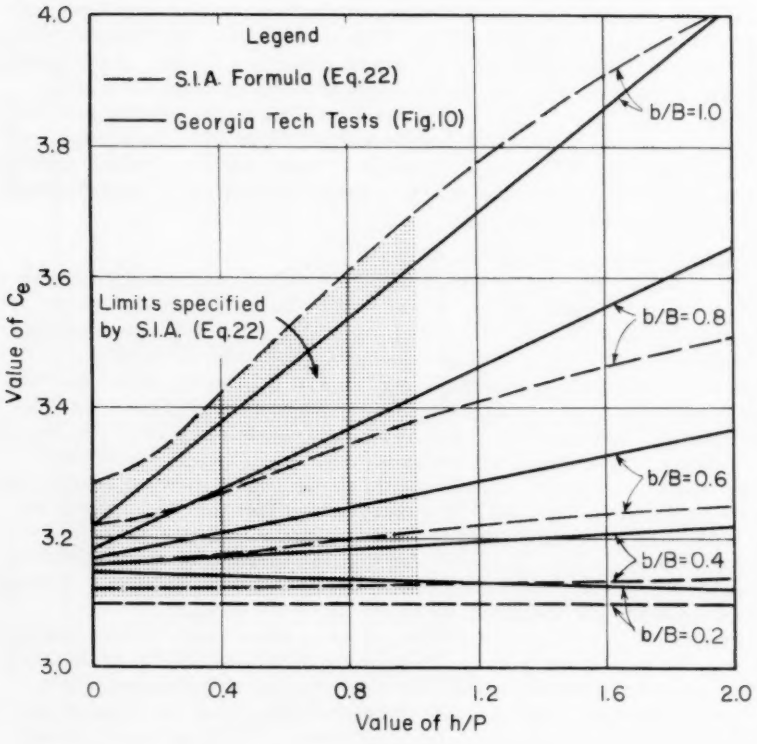

FIG. 15.- COMPARISON WITH S.I.A. FORMULA FOR NOTCH WEIRS

$$Q = C_e b_e h_e^{3/2} = C_{e_1}(b - Kh)h^{3/2} \tag{32}$$

in which C_e is the coefficient of discharge for notch weirs and C_{e1} is the corresponding coefficient for full-width weirs (b/B = 1.0). If the fluid-property effects related to small heads and widths are neglected, $h \approx h_e$ and $b \approx b_e$. Thus, from Eq. 32,

$$K = \left(\frac{C_{e_1} - C_e}{C_{e_1}}\right)\frac{b}{h} \tag{33}$$

Fig. 16 shows K as a function of h/P and b/h. Values of K shown in this figure were computed from Eq. 33, using values of C_e and C_{e1} from Fig. 10. It is apparent that the constant value of K recommended by Francis is not substantiated, even within the limits specified by Smith and Francis for "fully contracted" weirs.

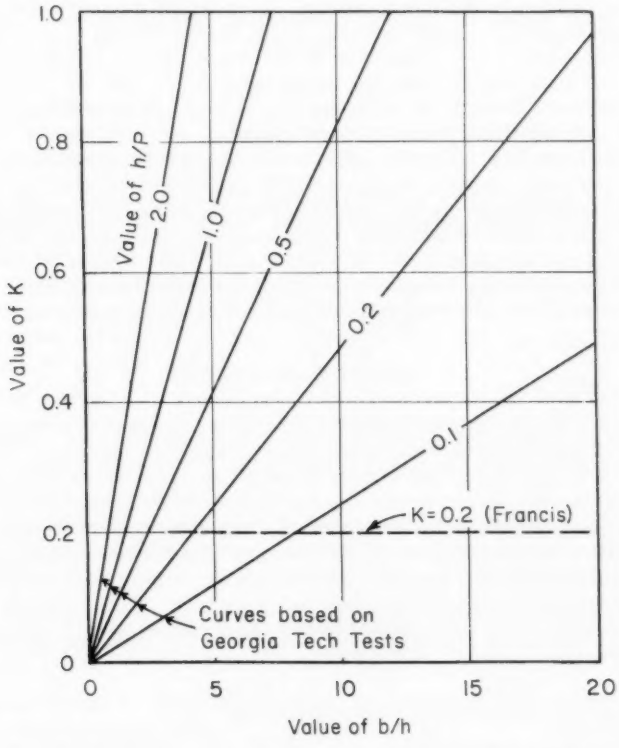

FIG. 16.- COMPARISON WITH FRANCIS FORMULA FOR NOTCH WEIRS

The comparison shown in Fig. 15 indicates that the S.I.A. formula for notch weirs agrees reasonably well with the results of the Georgia Tech tests. However, the complexity of the formula is a deterrent to its use, and the limits of applicability specified by the S.I.A. prevent its being a comprehensive solution for a full, practical variety of notch weirs. Furthermore, the effective-head

and effective-width concepts which are complementary to the simple C_e equations derived from the Georgia Tech tests are believed to be superior to any other method of accounting for the influence of viscosity and surface tension.

CONCLUSIONS

The flow pattern for rectangular, thin-plate weirs is not subject to complete mathematical analysis. Consequently, an analytical solution for the discharge characteristics has not been developed. A comprehensive solution based on dimensional analysis and experiment is presented in this report. It provides a simple, direct solution for the discharge and a convenient method of compensating for the influence of viscosity and surface tension. It is substantiated by experimental data from various sources.

Widely used formulas adapted from the classic Weisbach equation are not justified as comprehensive solutions. In fact, they do not satisfy the need for a simple equation which can be used to correlate experimental data covering a full range of the significant variables. Unjustified emphasis has been placed on the significance of the orifice analogy in the derivation of weir equations. Furthermore, there is no logical basis for the assumption that formulas involving the true total-energy head are independent of the h/P ratio. The Francis contracted-width formula is fundamentally inadequate as a means of adapting formulas for full-width weirs to notch weirs.

Weir discharge is critically influenced by the physical characteristics of the weir and weir channel. It is especially dependent on features which control the velocity distribution in the approach channel. For this reason the results of experiments made by different, capable investigators do not agree, and formulas based on a particular set of data reflect the individual characteristics of those data. For this reason, too, a truly reproducible, standard measuring weir and a precise, universal discharge formula are impractical.

ACKNOWLEDGMENTS

The investigation on which this report is based is part of a comprehensive study of the discharge characteristics of weirs and spillways which is being carried out by the Water Resources Division (Surface Water Branch) of the Geological Survey, United States Department of the Interior. Original experimental data on notch weirs were obtained from a thesis investigation[18] conducted at the Georgia Institute of Technology. The thesis was originally undertaken to substantiate the analysis proposed by the senior author in unpublished reports prepared for the USGS. Engineer personnel of the Research Section, USGS, at Atlanta, Ga., participated in the computations and in the preparation of this report.

REFERENCES

1. Kindsvater, Carl E. and Carter, Rolland W., "Tranquil Flow through Open-Channel Constrictions," Transactions, ASCE, Vol. 120, 1955, p. 969.

2. Wells, James Robert, "Discharge Characteristics of Rectangular Notch Weirs in Rectangular Channels," thesis presented to the Georgia Institute

of Technology, Atlanta, Ga., 1954, in partial fulfillment of the requirements for the degree of Master of Science in Civil Engineering.

3. Discussion by Eric Lindquist of "Precise Weir Measurements," by Ernest W. Schoder and Kenneth B. Turner, Transactions, ASCE, Vol. 93, 1929, p. 1168.

4. Bazin, H., "Experiences nouvelles sur l'ecoulement en deversoir," Annales des Ponts et Chaussees, October, 1888, p. 393.

5. Bazin, H., "Recent Experiments on the Flow of Water Over Weirs," English translation by Arthur Marichal and John C. Trautwine, Jr., Proceedings, Engineers Club of Philadelphia, Vol. VII, 1889, pp. 259-310.

6. Discussion by Ernest W. Schoder of "Precise Weir Measurements," by Ernest W. Schoder and Kenneth B. Turner, Transactions, ASCE, Vol. 93, 1929, p. 1189.

7. Schoder, Ernest W. and Turner, Kenneth B., "Precise Weir Measurements," Transactions, ASCE, Vol. 93, 1929, pp. 999-1110.

8. "Studies of Crests for Overfall Dams," Bulletin 3, Boulder Canyon Project, Final Reports, Bureau of Reclamation, U. S. Department of the Interior, Denver, Colo., 1948.

9. Bazin, H., "Recent Experiments on the Flow of Water Over Weirs," English translation by Arthur Marichal and John C. Trautwine, Jr., Proceedings, Engineers Club of Philadelphia, Vol. VII, 1889, p. 309.

10. Discussion by Th. Rehbock of "Precise Weir Measurements," by Ernest W. Schoder and Kenneth B. Turner, Transactions, ASCE, Vol. 93, 1929, p. 1148.

11. Bõss, Paul, "Berechnung der Abflussmengen und der Wasserspiegellage bei Abstũrzen und Schwellen unter besonderer Berũcksichtigung der dabei auftretenden Zusatzspannungen," Wasserkraft und Wasserwirtschaft, Vol. 22, 1929, pp. 13-33.

12. Smith, Hamilton, Jr., Hydraulics, John Wiley and Sons, New York, 1884.

13. Discussion by Th. Rehbock of "Precise Weir Measurements," by Ernest W. Schoder and Kenneth B. Turner, Transactions, ASCE, Vol. 93, 1929, p. 1147.

14. Normen für Wassermessungen, Normen des Schweizerischen Ingenieur- und Architekten-Vereins (Swiss Society of Engineers and Architects), No. 109, 1924.

15. Discussion by Th. Rehbock of "Precise Weir Measurements," by Ernest W. Schoder and Kenneth B. Turner, Transactions, ASCE, Vol. 93, 1929, p. 1149.

16. Francis, James B., Van Nostrand, D., Lowell Hydraulic Experiments, New York, fourth edition, 1883.

17. Horton, Robert E., "Weir Experiments, Coefficients, and Formulas," Water-Supply Paper 200, U. S. Geological Survey, 1907.

18. Carter, Rolland W., "A Comprehensive Discharge Equation for Rectangular-Notch Weirs," thesis presented to the Georgia Institute of Technology, Atlanta, Ga., 1956, in partial fulfillment of the requirements for the degree of Master of Science in Civil Engineering.

Paper 1454 December, 1957 HY 6

Journal of the
HYDRAULICS DIVISION
Proceedings of the American Society of Civil Engineers

AIR BINDING IN LARGE PIPELINES FLOWING UNDER VACUUM[a]

R. T. Richards,* A.M. ASCE
(Proc. Paper 1454)

SYNOPSIS

Air Binding is a potentially serious cause of excess head loss in water pipelines flowing under less than atmospheric pressure. This paper discusses the phenomenon of air binding and methods of control, with emphasis on the accumulation of air in sloping pipes. The specific installations described are circulating water systems of steam-electric stations, but the principles discussed are applicable to any water pumping station with similar profile.

INTRODUCTION

Air binding in a pipeline is the trapping of air within the water passage in a manner which prevents the pipe from flowing full. In poorly laid out or poorly vented pipelines air binding may be the source of head losses which can seriously reduce the pipeline capacity.

The accumulation of air is particularly severe in a pipeline flowing as a siphon under less than atmospheric pressure. Such a condition may occur, for example, where the pipe passes over a hill.

Important water pumping installations which normally utilize a siphon are the circulating water systems of steam-electric generating stations. These pumping plants may move as much as 150,000 gallons per minute through the condenser of each large generating unit. Large-diameter circulating water pipelines, several hundred feet long, are often designed to flow under a vacuum between minus 20 and minus 30 feet of water. The phenomenon of air binding is illustrated in this paper by two examples of circulating water systems which were seriously obstructed by air. Excess head losses due to

Note: Discussion open until May 1, 1958. Paper 1454 is part of the copyrighted Journal of the Hydraulics Division of the American Society of Civil Engineers, Vol. 83, No. HY 6, December, 1957.

a. Paper prepared for presentation at a meeting of the American Society of Civil Engineers, New York, N. Y., October, 1957.

* Civ. Engr., Ebasco Services Inc., New York, N. Y.

entrapped air were 15 feet and 19 feet for systems designed originally to pump against normal pressures of 43 and 36 feet.

It will become apparent by study of these examples that the air binding problem may be applicable to any other pipeline with similar profile.

Basic Elements of the Air Binding Problem

Air accumulation in a pumping system may originate from several sources: air exists in the empty pipeline before it is filled, air is entrained in the water carried into the system and, at sections under negative pressure, it can leak in at joints and fittings. This air will be present in varying concentrations from very small, widely dispersed bubbles to large pockets.

The air is carried along the pipeline by the moving water. However, where the pipe slopes downward from a high point, the bubbles tend to collect along the top of the pipe. When the buoyancy of the air accumulation becomes greater than the water force pushing it down the pipe the pipeline becomes air bound.

The most severe head losses encountered in circulating water systems flowing under vacuum are the result of large air pockets lying along downward slopes and creating a condition similar to open channel flow. The energy gradient thus roughly parallels the actual slope of the pipeline instead of representing only the friction losses in a pipe flowing full. Figure 1 is a diagrammatic view of the phenomenon of airbound slopes. The air pocket terminates in a hydraulic jump which absorbs further energy.

Generally speaking, for a given water velocity and pipe slope air binding difficulties increase with the pipe size. For example, an 8-foot-per-second velocity may be sufficient to carry all accumulating air out of a 12-inch pipe on a given slope, but is not sufficient to move such air through an 84-inch pipe on the same slope. For large-size pipe there is very little published information relating the factors of air entrainment, air release, water velocity, pipe size, pipe slope and natural air removal.

The author has been concerned particularly with conduits of such a size that water velocities up to approximately 10 feet per second have not been sufficient to move air down a slope. Pipes of five feet or more in diameter fall into this class. The discussion is, of course, applicable to smaller conduit where water velocities are low.

Experience indicates that where a large diameter pipe normally flows under vacuum there will be air binding in any non vented section which slopes downstream from the high point in the system. Accumulating air must be continuously removed or the efficiency of the system will be impaired. Exceptions to this general rule have been at slopes immediately following sharp horizontal bends; the turbulence induced by the horizontal bend may break up large air pockets into more easily transported smaller bubbles.

Self-Priming Vertical Drops

When a change in grade is made with a vertical or nearly vertical drop the possibilities of air binding are much reduced. Such a vertical drop is generally "self-priming." The turbulence created by the abrupt change in water direction breaks up and disperses large pockets of air. The smaller bubbles are then carried away by the moving water. See Figure 2.

Vertical Versus Sloping Pipelines

It is apparent from the comments above that air evacuation equipment must be used unless the change in grade is made with a vertical drop. This equipment, discussed briefly below, is expensive and requires constant maintenance. However, vertical drops have disadvantages also, and in many cases may be more costly to install and operate than a continuously evacuated sloping pipeline.

First, the turbulence which entrains and carries away the air at a vertical bend will also create a permanent loss of head which raises the cost of pumping water. This loss for one vertical drop with two reverse 90° bends may amount to 1 foot of head and represent an annual excess pump operating cost of several hundred dollars and a capitalized cost of several thousand dollars. One company solved a potential air binding problem in one of their older plants by traversing a downgrade with a series of three vertical drops, a total of six 90° bends. At a large plant the cost of head lost in such an arrangement would be considerably more than the cost for the installation and maintenance of an air removal system on a sloping pipeline.

A second serious objection to the vertical drop is the thrust produced at 90° bends. Massive thrust blocks must be provided to anchor such a bend securely in the event of water hammer surges. At one large power station the thrust block required at a vertical drop in twin 84-inch conduits contained over 400 cubic yards of concrete and required complicated formwork. A new circulating water system at this same station has a sloping conduit equipped with an air removal system at a fraction of the cost of the thrust block.

Methods of Air Removal

Air taps at high points are standard practice on pipelines, but it is apparent from the previous discussion and a knowledge of laboratory observation that the air carried by moving water will be found along the downstream slope. Air removal systems on the conduits discussed below were not effective when they were connected to the high point taps alone. Accordingly, a system of taps along the downstream slope was provided. These taps were connected to a common header which in turn was connected to the air removal system.

Where a vertical drop is used a single air removal connection should be placed at the high point at the outside edge of the bend. Generally, this tap will not be required during operation unless water velocities are very low.

Where an airbound pipe flows under vacuum some type of air evacuator will be required to remove the air accumulations. Such an installation may consist of one or more vacuum pumps, a control system, power supply and, for water-sealed pumps, a continuous supply of clean water (or a closed-circuit sealing system using some other fluid). The author's firm has recently installed a water jet evacuation system which is considerably less complex and costly than vacuum pumps. Operating water for the jets is supplied from the power station elevated water tank, but could be supplied by booster pump taking suction from the pipeline itself.

The primary consideration in sizing air removal equipment is to provide enough capacity to maintain the line free of air during operation. A secondary consideration is the rate of initial priming of the system.

The determination of capacity requirements is a difficult matter. Uncertainty is caused by several factors. A first unknown is the quantity of air which may leak in through joints and fittings in long conduits under vacuum. Also, experimental data for these large-size pipes is not sufficient to permit determination of the amount of entering air which will be carried out naturally for given velocities, slopes and pipe sizes.

It may be desirable to install one fairly large vacuum pump for initial priming, then a smaller pump in parallel to maintain the prime. The smaller one can be selected and installed after actual operating experience with the large vacuum pump has indicated the air binding characteristics of the pipeline.

The details of two typical circulating water systems are described below. Both of these are older stations at which air binding problems had to be corrected. For all new stations the original design should provide for air removal if the profile indicates a potential problem.

Station A - 132,000-KW Power Plant Installation on a Large River

Station "A" has a 1,750-foot condenser discharge conduit, all of which should normally operate under a partial vacuum. The majority of the pipe is 78-inch diameter, the design velocity is 7.3 feet per second. The profile of this conduit is shown on Figure 3. The head recovery in this discharge siphon line was very poor and caused considerable concern because of the loss in water pumping capacity.

The vacuum measured at the condenser discharge should be minus 22.9 feet of water for river elevation 718. The actual measurement at the north condenser was minus 7.9 feet, an unexplained loss of 15 feet. It was determined that with river water levels at 719 or above air accumulated along the 57:1 sloping section shown on Figure 3, giving a head loss at water level 719 of about 7.5 feet. This represented the approximate difference in elevation between the top and bottom of the slope, and indicated that the pressure gradient was parallel with the pipe slope as could be expected for open channel flow down a similar incline. At water levels under 719 the air pocket also extended along the entire top of the horizontal section and into the 45° sloping condenser discharge pipe, thereby reducing the siphon an additional 7.5 feet.

When the river level was at 709, flow through the pipeline was recorded as follows:

	Design Flow With Proper Venting	Actual Flow in Pipeline No Venting	Total Loss of Capacity
Two Pumps	70,000 gpm	58,000 gpm	12,000 gpm
Three Pumps	89,000 gpm	74,000 gpm	15,000 gpm

The points of air evacuation had been installed in accordance with original design, but proved to be inefficient. A 95-cfm, 15-inch Hg vacuum pump was located at Point A where the discharge line passed the intake structure. It worked continuously and was of insufficient capacity. Two-inch air-powered ejectors at the condensers were also ineffective.

As a result of investigation, a 200-cfm vacuum pump was installed at Point B on Figure 3. Additional taps were also installed on either side of Point B, and on the upper end of the 45° condenser piping. These all take

suction from the same pump. The 95-cfm pump at the intake structure was also replaced with a 200-cfm pump.

This arrangement was effective in eliminating the air binding problem.

Station "B" - 166,000-KW Power Plant Installation on a Large River

The circulating water system of this station has three pronounced high points, the usual one at the condensers, and two where the intake and discharge conduits pass over a flood protection levee. The principal airbound section is 66-inch diameter, design velocity is 10.7 feet per second. An approximate profile is shown on Figure 4.

The pressure at the crest of the discharge levee crossing was about minus 3.5 feet without venting. The design pressure was minus 23 feet, a difference of 19.5 feet representing excess lost head. A vacuum pump taking suction from a single tap at the crest had been able to maintain a maximum vacuum of slightly less than 15 feet, even though the gage glass at the air receiving tank showed full prime at this point. Taps were therefore drilled at three additional points on the downstream slope of the pipe and connected to the vacuum pump. Maximum design siphon of minus 23 feet was obtained within less than one hour and could be maintained indefinitely with a 6-cfm pump. The air had been trapped on the slope beyond the levee crest as could be expected from previous discussion in this paper.

With the increased vacuum provided by the air evacuation system four-pump flow in the system was increased from 115,000 gpm to 134,000 gpm. This increased flow was so great that the pump impellers had to be redesigned to prevent excessive impeller pitting due to cavitation.

The amount of air to be removed from this system was very small since little leakage of air could take place. The only section under vacuum was that section of welded steel pipe over the levee.

When only one or two of the four circulating water pumps were operating at low water conditions a slight vacuum also occurred at the intake levee crest and a similar air-binding condition arose. Vacuum pump connections were run to this point also. A completely separate parallel circulating water system has recently been installed for Units 3 and 4 of this power plant. A bank of vacuum pumps with interconnected controls and suction lines draws air from both circulating water systems at the intake and discharge levees. The maximum length of air suction line is about 600 feet.

CONCLUSION

These two examples clearly indicate the extent of capacity loss which may be experienced in pipelines flowing downhill under a vacuum. This phenomenon probably occurs much more frequently than records show. In many steam plant circulating water systems overdesigned pumps have made up for lack of hydraulic efficiency. Air binding may well have gone unnoticed at Station B if the extent of head loss had been a little less severe. At Station A, on the other hand, air binding threatened to reduce the efficiency of the entire power station as summer weather brought a greater demand for cooling water.

There is a particular need for experimental air-binding data applying to large diameter pipelines. Observations at Station "B" for several different

pumping conditions have indicated that the pipe may be self-evacuating at velocities slightly above the design. Empirical formulas based on enough carefully evaluated field data may well permit the confident design of a self-evacuating sloping pipeline flowing under vacuum.

REFERENCES

1. Van Hengel, G. H., "Analysis and Tests on Hydraulic Circuits of Surface Condensers," Transactions of the American Society of Mechanical Engineers, FSP-59-3, pp. 156-160, 1937.

2. Kalinske, A. A. and Robertson, James M., "Air Entrainment in Closed Conduit Flow," Transactions of the American Society of Civil Engineers, Vol. 108, pp. 1435-1516, 1943.

3. Kent, Joseph Chan, "The Entrainment of Air by Water Flowing in Circular Conduits with Downgrade Slopes," Doctoral Dissertation submitted June, 1952, to the University of California.

4. Moors, A. Joseph, "Design Criteria for Development for Siphonic Action in Pumping Plant Discharge Lines," paper presented before the Hydraulic Division of the American Society of Civil Engineers, Annual Convention October 15, 1957.

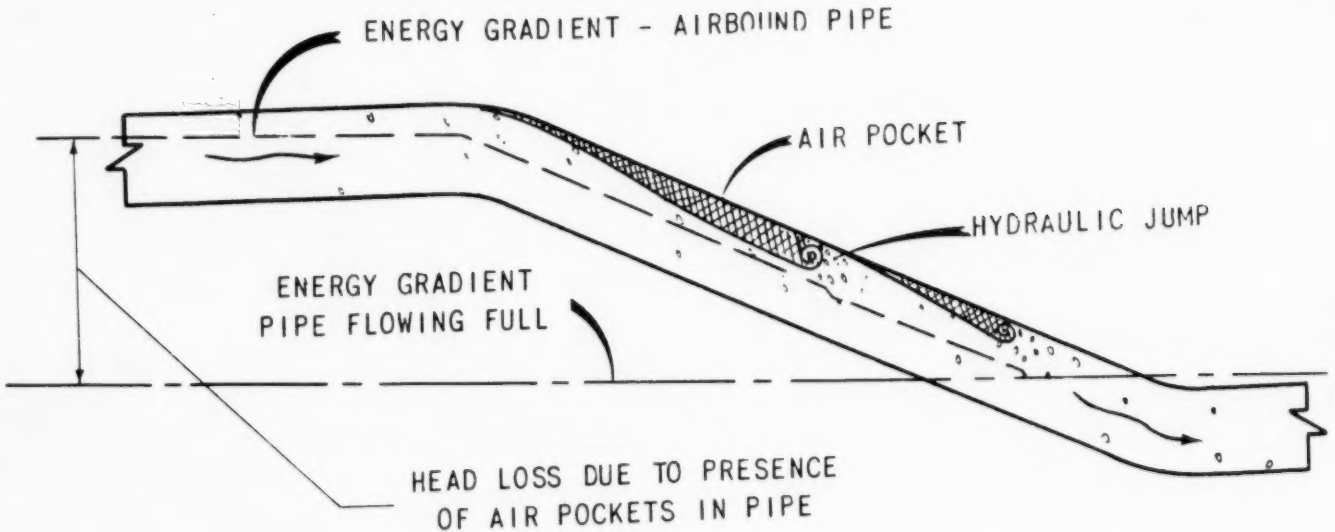
ENERGY GRADIENT - AIRBOUND PIPE
AIR POCKET
HYDRAULIC JUMP
ENERGY GRADIENT
PIPE FLOWING FULL
HEAD LOSS DUE TO PRESENCE
OF AIR POCKETS IN PIPE

FIGURE 1

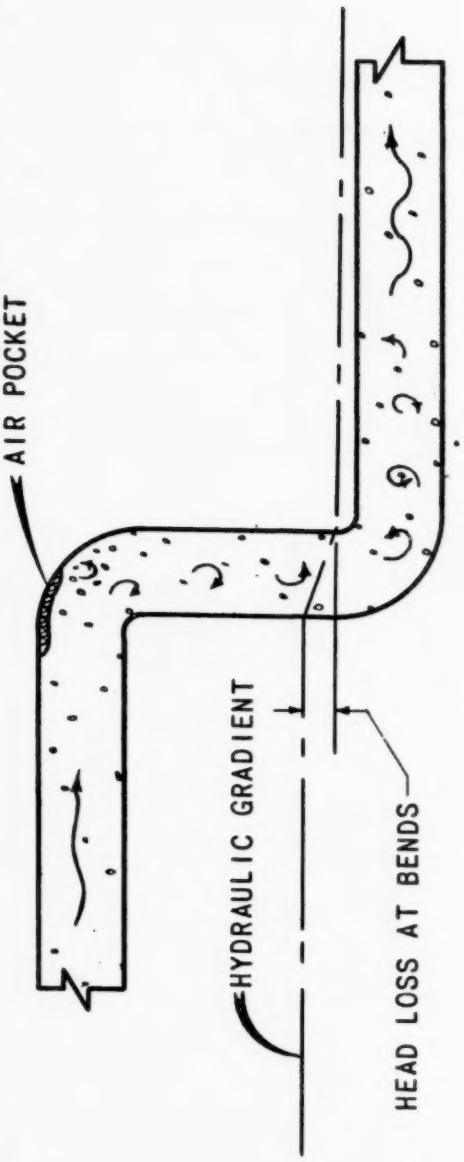

FIGURE 2

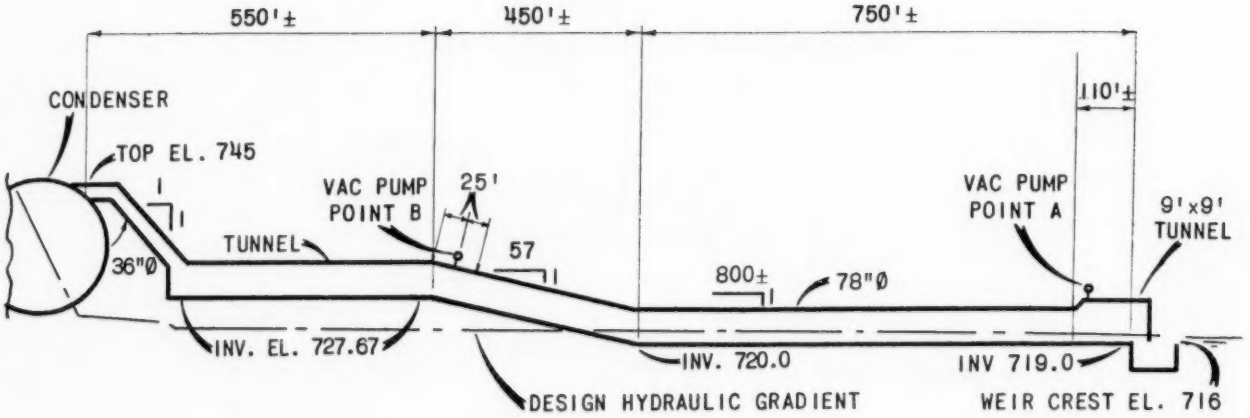

PROFILE OF DISCHARGE CONDUIT - STATION A

FIGURE 3

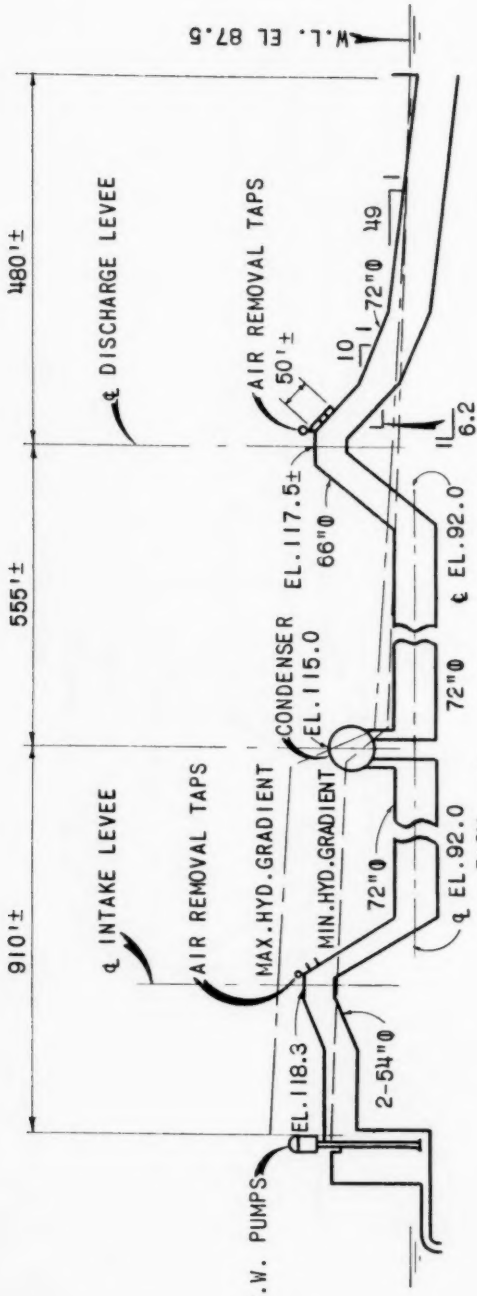

PROFILE OF CIRCULATING WATER SYSTEM - STATION B

FIGURE 4

Paper 1455 December, 1957 HY 6

Journal of the
HYDRAULICS DIVISION
Proceedings of the American Society of Civil Engineers

FLOW THROUGH CIRCULAR WEIRS

J. C. Stevens,[1] M. ASCE
(Proc. Paper 1455)

SYNOPSIS

There are certain advantages inherent in the use of the circular weir. However it has not come into general usage in this country. It is more extensively used in Europe where there has been developed a rigid, accurate formula by which the flow can be determined.

There is presented herein a formula for the theoretical flow through sharp crested circular weirs which involves the use of elliptic functions. Most of the European treatises on such weirs are not generally available now. Tables appended give (1) a summary of available experimental data with discharge coefficients, (2) the flow through weirs of various diameters based on these coefficients and (3) values of the elliptic functions involved by which the flow through a circular weir of any diameter may be found.

INTRODUCTION

Weirs with circular crests have the advantage that the crest can be turned and beveled with precision in a lathe. Moreover the weir crest does not have to be leveled, hence the point of zero flow is readily determined.

When wells are tested by pumping the pump discharge is usually measured by an orifice fixed to the end of the discharge pipe. The flow is determined by the orifice formula in which the down-stream head is constant—that of one atmosphere. When the pipe is not running full the orifice becomes a circular weir and it is often important to know the flow under such conditions.

The problem of circular weir discharge first thrust itself upon the author's attention in connection with a rather novel fishway where the discharge from it was to be carried in a pipe to a power canal a short distance away. This

Note: Discussion open until May 1, 1958. Paper 1455 is part of the copyrighted Journal of the Hydraulics Division of the American Society of Civil Engineers, Vol. 83, No. HY 6, December, 1957.

1. M. Past Pres., ASCE; Cons. Eng., Stevens & Thompson, also Leupold & Stevens Instruments, Inc. Portland, Ore.

flow had to be measured. The circular orifice in the end of the pipe would be running partly full most of the time, and therefore became a circular weir.

Experimental Data

A few laboratory experiments are available on the flow through circular and semi-circular weirs. A summary of all such experiments the author could find appears in Appendix A. Doubtless others were made in European countries, but are not available to the author. There is also given in Appendix B a table of flows through such weirs from 0.25 to 5.0 feet in diameter. The theoretical flow was first determined by the rigid formula presented herein which was then modified by an average discharge coefficient disclosed by the above laboratory experiments. Appendix C presents a table of the elliptic function involved in the formula by which the theoretical flow for a weir of any diameter can easily be tabulated.

The following laboratory experiments to determine the flow through circular and semi-circular weirs have been found in available technical papers.

Experiments by H. V. Cone[1]

Experiments on the flow through two circular and two semi-circular weirs are reported. The results are given graphically by 4 curves. No attempt was made to develop a flow formula for them.

Experiments by F. V. Greve[2]

Extensive experiments on the flow through circular, parabolic, and triangular weirs were conducted by the late F. V. Greve at the Engineering Experiment Station of Purdue University, Lafayette, Indiana.

The differential formula he developed for the flow through such weirs, he states, could not be solved but the flow through semi-circular weirs was found by mechanical integration of his differential equations for several diameters.

The flows in Greve's bulletin are all given in pounds per second but they have been converted to cubic feet per second herein.

Experiments by Eldon R. Dodge[3]

These were made to determine the flow through circular orifices in steel plates fixed to the outlet end of sewer pipes intended for storm drain culverts. The orifice plates were attached to the pipe with various eccentricities, that is with the centers of some orifices concentric and others not concentric with the centers of the pipes. Only the flows for concentric orifices are tabulated herein. Flows were determined under heads with orifices flowing partly full and also under surcharged heads wherein the discharge changes from weir flow to orifice flow.

Mr. Dodge presents a trigonometrical series formula, aided by curves, by which the theoretical flows through his weirs were approximately found. He also presents curves of his discharge coefficients.

It is doubtful whether any of the above authors and experimenters were aware of the work done in Europe on flow through circular weirs. It is practically certain that the first one in this country to make recorded tests of such weir flow was H. V. Cone who made his experiments in 1916 at Fort Collins, Colorado. Dr. Eng A. Staus' first publication of which the writer has knowledge appeared in 1926, while G. H. Gulliver made flow tests in England on small circular weirs as early as 1909. (See References)

Experiments by G. H. Gulliver[4]

These were made on a small circular weir 2-1/2 inches diameter. The differential formula developed is

$$q = 12.05 \int_0^h \sqrt{h(H-h)\ [D-(H-h)]}\ dh$$

where D = diameter of the circular weir-inches; H = head above the lowest point of the weir-inches, q = discharge - gpm; h = distance to elementary area above the circular weir invert. The formula was mechanically integrated and the results are given by curves. Flow coefficients found were between .625 and .630. The curves were on too small a scale to be read with accuracy and his results are not included in this paper.

Experiments by H. Th. Thijsse[5]

Circular weirs have been in use for many years in his laboratory to measure the flow through hydraulic models of structures and other devices. They were adopted because of their ease of construction but more particularly because they did not have to be leveled and the point of zero is so readily determined.

The formula given is

$$Q = m\ \sqrt{gR} = kH^2$$

Where Q, flow in liters per second
g, the metric gravity constant
R, radius of Circular Weir - centimeters
H, head on the Weir invert - centimeters
m, discharge coefficient

The value of m was found by calibration in place. Curves were prepared for values of k vs H^2 from the calibration for each size of weir. These curves however have no general validity if the conditions of use depart materially from those under which they are obtained.

These data are given in metric units but they have been converted to English units in the tables herein.

The Elliptic Formula

The articles by Dr. Eng Staus do not give the transformation to the Elliptic form which is rather involved. This however was developed entirely independently by the author with substantial assistance from Dr. W. E. Milne, retired, formerly head of the mathematics department of Oregon State College. This transformation is given in Appendix D.

Referring to Fig. 1 it is obvious that

$$1 = 2\sqrt{\left(\frac{D}{2}\right)^2 - \left(\frac{D}{2} - y\right)^2} = 2\sqrt{y\ (D-y)} \qquad (1)$$

The head on the elementary area 1 dy is H - y and the elementary theoretical flow becomes

$$dQ_t = 2\sqrt{2g}\ \sqrt{(D-y)\ y\ (H-y)}\ dy$$

This is true whether H is greater or less than the radius of the circle. Then

$$Q_t = 2\sqrt{2g}\int_0^H \sqrt{(D - y)\, y\, (H - y)}\, dy \qquad (2)$$

This can be developed into a series and integrated[6] term by term obtaining as was done by E. R. Dodge but not in a trigometric form

$$Q_t = 2\sqrt{2g}\, D^{5/2}\pi\left(\tfrac{1}{8} z^2 - \tfrac{1}{32} z^3 - \tfrac{5}{1024} z^4 \cdots\cdots\right)$$ Pierce 214, 218,

Where z = H/D

This, however, is an infinite series and laborous to deal with.

The elliptic formula for the theoretical flow through circular weirs is

$$Q_t = \frac{4}{15}\sqrt{2g} D^{5/2}\left[2(1 - k^2 + k^4)E - (2 - k^2)(1 - k^2) K\right] \qquad (3)$$

Application of the Elliptic Formula

In equation (3) the modulus k depends solely on the head and diameter of the weir. In brief the formula may be written

$$Q_t = B\Delta$$

where

$$B = 4/15\sqrt{2g}D^{5/2} = 2.14D^{5/2}$$

and Δ is the quantity in [ ]

In evaluating (3) for various diameters a table of k^2 vs Δ was prepared (see Appendix C). This table gives Δ to 4 decimal places for values of D/H to 3 decimal places. If we multiply the values of Δ by 2.14 we obtain the theoretical flow for a 1-foot diameter weir since

$$B = 4/15\sqrt{2g}D^{5/2} = 2.14$$

The value of the factor B for any other diameter is obtained by

$$B = 2.14D^{5/2}$$

Discharge Coefficients

The tabulation of experimental data in Appendix A gives the discharge coefficients obtained by

$$c = Q/Q_t$$

These values are plotted in Fig. 2. While there is some evidence of a nonlinear trend it is not definable in the evidence at hand. No coefficients have been discarded. The average of each experimenter's coefficients for each weir diameter is also indicated in Fig. 2. From this it appears that an average coefficient of 59 per cent is justified for the experimental data presented.

The coefficients from the Thijsse experiments indicate that the flows were influenced by velocity of approach. However this would not affect the validity

of his experiments since his weirs were all calibrated in place and the flows observed include this factor. The Dodge experiments also appear to show this same effect since the orifices were in the end of drain pipes.

The experiments by H. V. Cone are all near the 59 per cent line except those for the 3-foot weir for which there is no evident explanation unless his zero point was in error.

The Greve experiments are the most consistent of all and are believed to be entirely trustworthy.

It is hoped that some laboratories in this country will make more experiments on the flow through circular sharp-crested weirs and thereby obtain more discharge coefficients.

Notation

In this paper the letter symbols for Hydraulics, approved by the American Standards Association January 1942 has been used as far as practicable. The foot-seconds system has been used throughout. See also Fig. 1.

- D, diameter of sharp crested weir opening
- H, head on weir above the invert measured upstream of the surface curve of approach
- Q_t, theoretical flow through weir
- Q, observed flow
- C, coefficient of discharge = Q/Q_t
- g, acceleration of gravity
- l, length of chord of elementary area
- y, distance above circle invert to an elementary area
- k, modulus of the elliptic integrals = $\sqrt{H/D}$
- K, the complete elliptic integral of the first kind
- E, the complete elliptic integral of the second kind
- Δ, Value of the elliptic function involved such that $Q_t = B\Delta$ and $Q = BC\Delta$

REFERENCES

1. Cone, H. V., Circular Weirs, Journal of Agricultural Research USDA March 6, 1916.
2. Greve, F. V., Flow of Water through Circular, Parabolic, and Triangular Vertical Notch Weirs, Engineering Bulletin, Research Series No. 40. Purdue University, Lafayette, Indiana. This bulletin also contains a bibliography with summaries.
3. Dodge, Eldon R., A Thesis Submitted for a Masters Degree, University of Wisconsin, Madison, Wisconsin. 1935. (Not published.)
4. Gulliver, G. H., PRSE, "On the Discharge of Water from Circular Weirs and Orifices," London Engineering January 8, 1909.
5. Thijsse, J. Th., Discharge Meters, Director Hydraulic Laboratory (Waterloopkundig Laboratorium) Delft, The Netherlands.
6. Pierce, B. O., A Short Table of Integrals. Ginn and Company, New York. E and K to 4 decimal places; also $E(k\phi)$ and $F(k, \phi)$ to 10, 5 and 1 degree intervals.

7. Dwight, Herbert Bristol, Tables of Integrals and Other Mathematical Data. Dsc Revised Edition—The Macmillan Company, New York. E and K to 3 decimal places by 1^0 and 0.1^0—No tables of $E(k,\phi)$ or $F(k,\phi)$.

8. Legendres' Tables for complete elliptic integrals E and K to 8 decimal places and k^2 by .01 intervals 0 to 1.00; also $E(k,\phi)$ and $F(k,\phi)$ to 10 decimal places. Published in Paris in 1826. (Out of print)

9. Staus, A., Der Kreisrunde Uberfall und seine Abarten. (The Circular Weir and Its Variations). Gas—und Wasserfach H. 27-28, 29 and 30 1926.

10. Staus, A., Zur Berechnung kreisrunder Uberfälle (concerning computations for Circular Weirs) 5 p. 1f. 1 tab. Wasserkr. und Wasserw. 1930 H 11.

11. Gradstein, S. and Walther, A., Zeichnerische Behandlung des kreisrunden Uberfälle. (Graphic Treatment of Circular Weirs) Das Gas—und Wasserfach. Nr. 10 1931.

12. Staus, A., Der Beiwert kreisrunder Uberfälle (Coefficients for Circular Weirs) 3 p. Wasserkr. und Wasserw. 1931 p. 42 N. 4.

13. Jorinssen, Andre, Le Déversoir Circulaireen Mince Poroi (A Study of the Reasons for Variations of the Flow Coefficient), Revue Universelle des Mines, 8 me Serie Tome XIV No. 12 Décembre 1938.

ACKNOWLEDGMENTS

The author is especially grateful to Dr. W. E. Milne (retired) formerly head of the Mathematics Department of Oregon State College, for substantial assistance in the transformation and application of elliptic functions to theoretical flow through circular weirs.

To Dr. James R. Villemonte, head of the Hydraulics Laboratory at the University of Wisconsin for the loan of the thesis by Eldon R. Dodge containing the results of his experiments on Circular weirs; also to Dr. J. Th. Thijsse for the flow through circular weirs used in his laboratory.

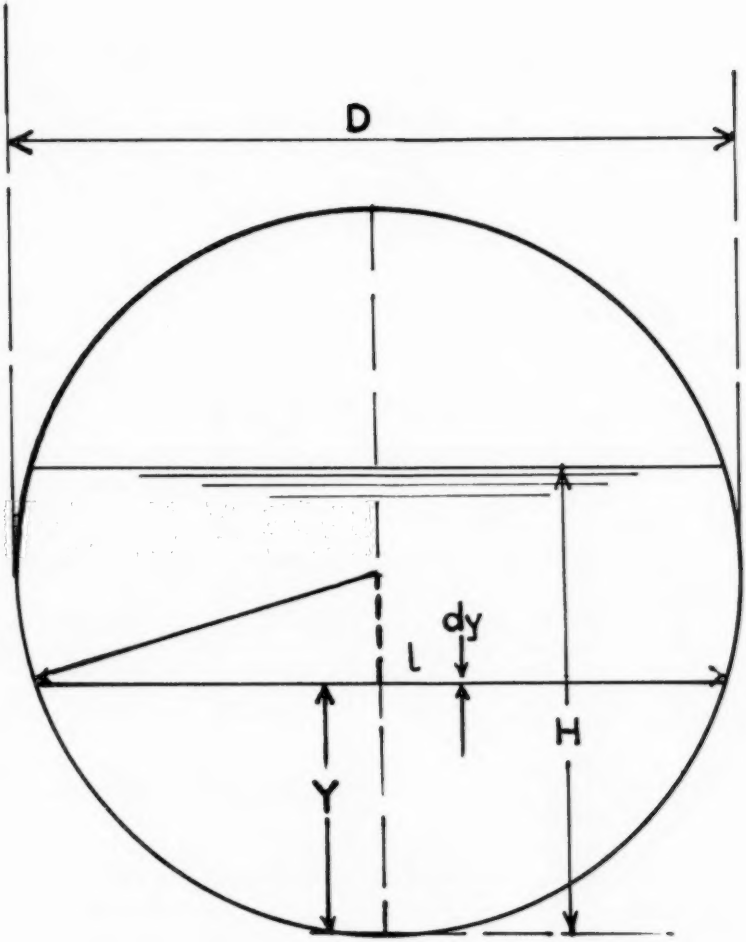

FIG. 1

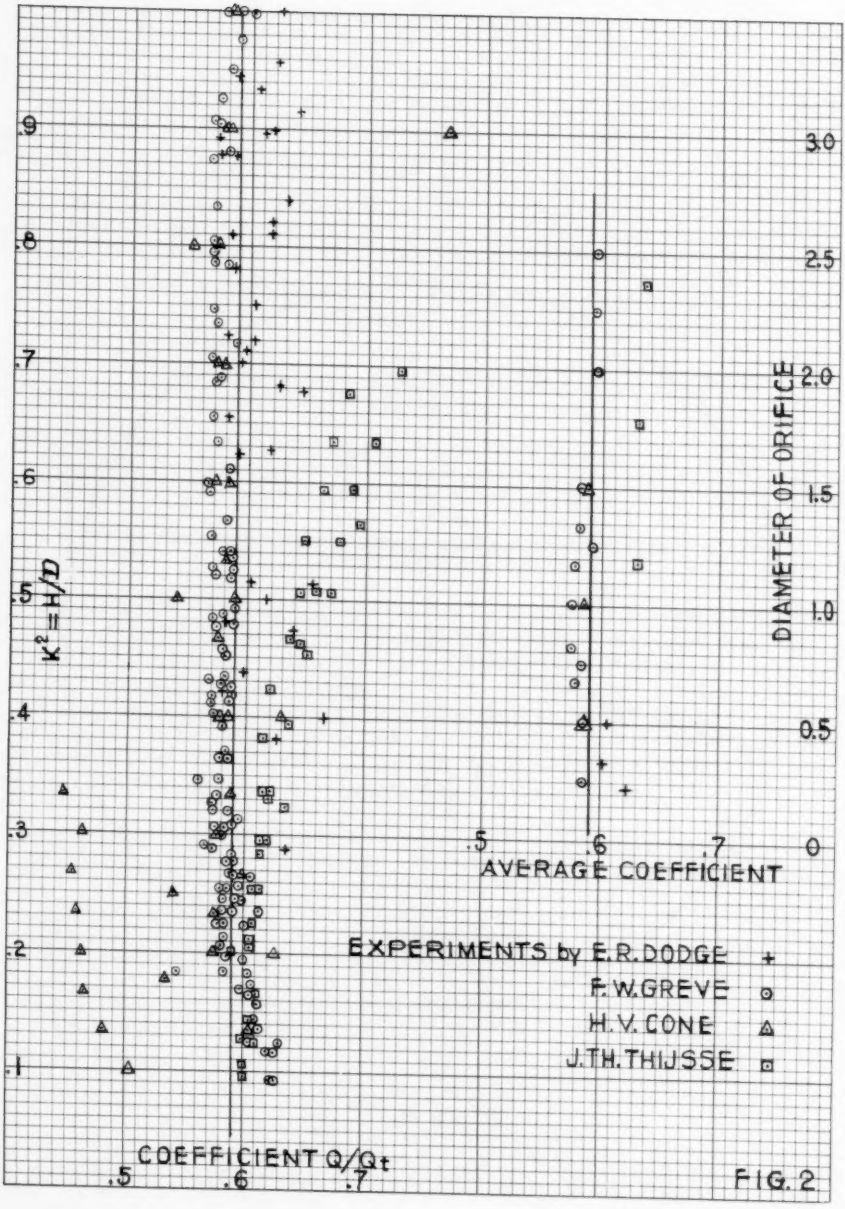
.9
.8
.7
.6
.5
.4
.3
.2
.1
$K^2 = H/D$
.5
.6
.7
COEFFICIENT Q/Qt
3.0
2.5
2.0
1.5
1.0
0.5
0
DIAMETER OF ORIFICE
.5
.6
.7
AVERAGE COEFFICIENT
EXPERIMENTS by E.R.DODGE +
F.W.GREVE ○
H.V.CONE △
J.TH.THIJSSE ⊡

FIG. 2

APPENDIX A

Flow through Circular Weirs and discharge coefficients determined by laboratory experiments.

See text for description of each author's experiments.

E. R. Dodge

D	H	H/D	Q_t	Q	C
.211	.084	.398	.018	.012	.666
	.100	.474	.025	.016	.640
	.108	.512	.029	.019	.655
	.132	.626	.042	.026	.619
	.143	.677	.048	.031	.646
	.150	.711	.052	.031	.596
	.152	.720	.053	.032	.604
	.169	.802	.063	.036	.572
	.171	.810	.064	.039	.619
	.177	.839	.068	.043	.633
	.189	.896	.075	.046	.614
	.193	.915	.078	.050	.640
	.202	.958	.082	.051	.623
	.211	1.000	.088	.055	.625
					.624

F. W. Greve

D	H	H/D	Q_t	Q	C
.25	.131	.525	.046	.027	.587
	.133	.533	.048	.028	.584
	.137	.548	.050	.029	.580
	.146	.576	.055	.032	.582
	.176	.704	.078	.045	.577
	.179	.716	.080	.047	.588
	.240	.960	.127	.074	.583
	.244	.976	.129	.076	.590
					.585

E. R. Dodge

D	H	H/D	Q_t	Q	C
.336	.128	.380	.054	.034	.628
	.142	.423	.069	.040	.580
	.161	.478	.085	.050	.588
	.168	.500	.089	.055	.618
	.219	.652	.144	.084	.583
	.229	.682	.155	.097	.625
	.235	.700	.162	.096	.593
	.243	.723	.174	.101	.580
	.262	.780	.195	.114	.584
	.273	.812	.208	.122	.587
	.294	.875	.233	.136	.585
	.299	.888	.239	.139	.583
	.302	.900	.244	.151	.619
	.321	.955	.265	.156	.589
					.602

F. W. Greve

D	H	H/D	Q_t	Q	C
.50	.131	.262	.071	.043	.606
	.157	.314	.101	.060	.594
	.160	.320	.105	.061	.580
	.206	.412	.168	.098	.583
	.212	.424	.177	.104	.588
	.273	.546	.282	.164	.580
	.305	.610	.344	.200	.580
	.344	.688	.424	.244	.575
	.391	.782	.525	.304	.580
	.440	.880	.633	.368	.580
					.585

H. V. Cone

D	H	H/D	Q_t	Q	C
.50	.20	.40	.159	.10	.628
	.25	.50	.241	.13	.540
	.30	.60	.334	.19	.568
	.35	.70	.437	.25	.572
	.40	.80	.545	.30	.550
	.45	.90	.655	.38	.580
	.50	1.00	.758	.44	.580
					.585

E. R. Dodge

D	H	H/D	Q_t	Q	C
.50	.145	.289	.085	.054	.635
	.219	.437	.189	.113	.598
	.259	.516	.256	.154	.602
	.317	.633	.369	.218	.592
	.376	.750	.493	.297	.603
	.407	.814	.563	.340	.605
	.461	.920	.680	.421	.619
	.467	.933	.694	.421	.606
					.607

F. W. Greve

D	H	H/D	Q_t	Q	C
.666	.156	.234	.117	.068	.581
	.163	.244	.127	.074	.582
	.198	.298	.187	.108	.579
	.217	.326	.222	.127	.572
	.253	.380	.296	.172	.581
	.300	.451	.408	.236	.579
	.368	.553	.591	.336	.569
	.437	.656	.799	.454	.569
	.498	.748	.998	.568	.569
	.554	.832	1.186	.675	.570
	.615	.924	1.392	.798	.573
	.665	1.000	1.550	.922	.594
					.578
.75	.191	.254	.185	.107	.579
	.223	.297	.250	.145	.580
	.308	.411	.461	.263	.570
	.312	.416	.471	.268	.570
	.356	.475	.603	.345	.572
	.363	.484	.624	.356	.570
					.584
.833	.189	.227	.194	.112	.578
	.224	.269	.269	.158	.587
	.276	.332	.402	.231	.575
	.290	.348	.440	.254	.578
	.348	.418	.620	.358	.577
	.417	.502	.869	.495	.570
	.491	.590	1.162	.659	.568
	.495	.595	1.183	.671	.567
	.571	.685	1.508	.864	.573
	.654	.785	1.894	1.076	.569
	.661	.794	1.929	1.093	.567
	.669	.803	1.965	1.114	.568
	.752	.902	2.354	1.345	.571
	.755	.906	2.376	1.352	.569
	.833	1.000	2.750	1.570	.574
					.574

F. W. Greve

D	H	H/D	Q_t	Q	C
1.00	.205	.205	.251	.146	.580
	.254	.254	.379	.220	.580
	.307	.307	.546	.314	.576
	.364	.364	.754	.435	.577
	.430	.430	1.029	.594	.578
	.520	.520	1.461	.836	.572
	.526	.526	1.491	.850	.570
	.634	.634	2.079	1.190	.573
	.732	.732	2.659	1.520	.572
	.873	.873	3.530	2.000	.566
	1.000	1.000	4.280	2.520	.588
					.576

H. V. Cone

D	H	H/D	Q_t	Q	C
1.00	.2	.2	.239	.15	.628
	.3	.3	.523	.30	.575
	.4	.4	.899	.52	.577
	.5	.5	1.360	.80	.588
	.6	.6	1.887	1.10	.583
	.7	.7	2.466	1.41	.572
	.8	.8	3.077	1.76	.572
	.9	.9	3.698	2.15	.581
	1.0	1.0	4.280	2.50	.584
					.585

F. W. Greve

D	H	H/D	Q_t	Q	C
1.167	.253	.217	.413	.247	.598
	.316	.271	.633	.377	.595
	.390	.334	.944	.553	.585
	.492	.422	1.463	.870	.594
	.603	.517	2.128	1.300	.610
	.708	.606	2.827	1.684	.596
	.825	.708	3.701	2.168	.586
	.947	.812	4.639	2.700	.585
	1.166	1.000	6.300	3.788	.602
					.578

J. Th. Thijsse

D	H	H/D	Q_t	Q	C
1.181	.236	.200	.363	.210	.578
	.25	.212	.406	.246	.605
	.30	.254	.576	.350	.607
	.35	.296	.773	.473	.612
	.40	.338	.995	.613	.616
	.45	.381	1.246	.767	.616
	.50	.424	1.521	.944	.620
	.55	.466	1.813	1.155	.638
	.60	.507	2.116	1.365	.645
	.65	.550	2.452	1.590	.649
	.70	.592	2.796	1.860	.664
	.75	.635	3.163	2.110	.666
	.80	.676	3.526	2.410	.680
					.630

F. W. Greve

D	H	H/D	Q_t	Q	C
1.333	.280	.210	.540	.322	.597
	.322	.242	.709	.417	.588
	.415	.311	1.149	.675	.588
	.495	.372	1.611	.935	.580
	.577	.433	2.139	1.244	.580
	.582	.437	2.176	1.260	.580
	.703	.527	3.069	1.797	.586
	.814	.610	3.986	2.296	.575
	.967	.726	5.380	3.055	.568
	1.124	.844	6.873	3.900	.567
	1.146	.860	7.077	3.995	.565
	1.332	1.000	8.780	5.070	.578
					.580

H. V. Cone

D	H	H/D	Q_t	Q	C
1.50	.20	.133	.298	.18	.604
	.25	.167	.467	.25	.535
	.30	.200	.660	.38	.575
	.35	.233	.886	.51	.575
	.40	.267	1.152	.69	.598
	.50	.333	1.758	1.03	.586
	.60	.400	2.480	1.45	.584
	.70	.467	3.308	1.90	.575
	.80	.533	4.211	2.44	.580
					.588

F. W. Greve

D	H	H/D	Q_t	Q	C
1.50	.214	.143	.345	.207	.600
	.226	.151	.384	.230	.599
	.248	.165	.456	.272	.596
	.273	.182	.551	.330	.599
	.309	.206	.700	.417	.596
	.349	.232	.879	.526	.598
	.388	.259	1.086	.643	.592
	.424	.283	1.289	.755	.586
	.470	.314	1.574	.916	.582
	.503	.335	1.779	1.035	.582
	.548	.365	2.091	1.205	.576
	.590	.393	2.401	1.383	.576
	.642	.428	2.815	1.620	.576
	.674	.449	3.077	1.780	.579
	.720	.480	3.481	2.003	.575
	.920	.614	5.422	3.070	.567
	1.050	.700	6.804	3.800	.559
	1.196	.798	8.456	4.780	.565
	1.406	.938	10.830	6.250	.576
					.582
1.748	.159	.091	.204	.128	.627
	.207	.118	.345	.214	.620
	.254	.145	.520	.316	.608
	.321	.184	.825	.482	.584
	.388	.222	1.183	.710	.600
	.435	.249	1.476	.875	.593
	.487	.279	1.837	1.080	.589
	.528	.302	2.141	1.250	.584
	.588	.345	2.756	1.540	.560
	.647	.370	3.143	1.830	.582
	.703	.402	3.670	2.140	.583
	.750	.429	4.142	2.390	.577
	.801	.458	4.677	2.710	.579
	.853	.488	5.257	3.050	.580
	.907	.519	5.883	3.420	.582
					.591

J. Th. Thijsse

D	H	H/D	Q_t	Q	C
1.770	.223	.126	.406	.246	.606
	.25	.141	.507	.306	.604
	.30	.169	.722	.437	.605
	.40	.226	1.263	.768	.608
	.50	.282	1.935	1.185	.613
	.60	.339	2.749	1.700	.618
	.70	.395	3.663	2.330	.636
	.80	.452	4.707	3.060	.650
	.90	.508	5.835	3.910	.670
	1.00	.565	7.068	4.920	.695
					.630

F. W. Greve

2.00	.185	.092	.293	.186	.635
	.237	.118	.483	.300	.622
	.273	.136	.640	.392	.612
	.345	.172	1.014	.615	.607
	.396	.198	1.328	.792	.596
	.470	.235	1.846	1.097	.595
	.515	.257	2.195	1.305	.595
	.567	.288	2.733	1.560	.571
	.613	.306	3.071	1.808	.589
	.661	.330	3.544	2.070	.585
	.730	.365	4.286	2.504	.585
	.778	.389	4.828	2.810	.583
	.873	.436	5.971	3.485	.583
	.960	.480	7.134	4.223	.592
	.988	.494	7.520	4.430	.589
					.595
2.25	.280	.124	.715	.450	.630
	.351	.156	1.128	.690	.611
	.413	.183	1.534	.840	.548
	.525	.238	2.441	1.50	.614
	.627	.279	3.451	2.02	.585
					.592

J. Th. Thijsse

D	H	H/D	Q_t	Q	C
2.36	.223	.095	.473	.283	.600
	.25	.106	.590	.354	.600
	.30	.127	.846	.507	.600
	.40	.169	1.484	.894	.603
	.50	.212	2.294	1.380	.603
	.60	.254	3.248	1.975	.608
	.70	.296	4.362	2.680	.615
	.80	.339	5.646	3.470	.615
	.90	.382	7.066	4.360	.617
	1.00	.424	8.583	5.430	.633
	1.10	.466	10.23	6.580	.643
	1.20	.508	11.98	7.900	.659
	1.30	.550	13.85	9.330	.675
	1.40	.594	15.87	10.90	.685
	1.50	.635	17.85	12.60	.706
	1.64	.695	20.86	15.20	.728
					.636

F. W. Greve

2.495	.311	.125	.942	.573	.608
	.409	.164	1.607	.966	.601
	.453	.181	1.943	1.175	.604
	.490	.196	2.265	1.359	.600
	.526	.211	2.608	1.550	.594
	.563	.226	2.978	1.765	.593
	.585	.235	3.209	1.895	.590
	.620	.248	3.560	2.118	.594
	.665	.267	4.105	2.424	.590
	.699	.280	4.498	2.648	.589
	.723	.290	4.814	2.823	.566
					.594

H. V. Cone

3.00	.30	.100	.953	.48	.504
	.40	.133	1.686	.81	.481
	.50	.167	2.640	1.22	.463
	.60	.200	3.730	1.72	.462
	.70	.233	5.006	2.30	.459
	.80	.267	6.506	2.95	.454
	.90	.300	8.142	3.67	.452
	1.00	.333	9.932	4.44	.447
					.467

APPENDIX B

Flow Through Circular Weirs as Calculated from the Following Formula

$$Q = 1.262\, D^{5/2} \left[2(1 - k^2 - k^4)\, E - (2 - k^2)(1 - k^2)\, K \right]$$

where

Q is the flow in ft^3/sec
D, the diameter of the Circular Weir - feet
H, the head on the Weir invert - feet
k^2, H/D the head in terms of diameter
E and K taken from tables of complete elliptic integrals
$b = \frac{4}{15}\, C\, \sqrt{2g}\, D^{5/2}$ where C = .59
based on the experiments in Appendix A

Values of b

D	$D^{5/2}$	b	D	$D^{5/2}$	b
.25	.0312	.039	2.00	5.656	7.14
.50	.1768	.223	2.50	9.882	12.47
.75	.4871	.615	3.00	15.588	19.67
1.00	1.000	1.262	4.00	32.000	40.38
1.50	2.756	3.48	5.00	55.900	70.55

D = .25		D = .50		D = .75	D = 1.00	D = 1.50	D = 2.00		D = 2.50	D = 3.00
H	Q	H	Q	Q	Q	Q	H	Q	Q	Q
.02	.001	.05	.006	.008	.009	.011	.1	.051	.054	.063
.04	.003	.10	.025	.031	.036	.045	.2	.204	.227	.252
.06	.006	.15	.054	.069	.081	.099	.3	.458	.514	.563
.08	.011	.20	.094	.121	.141	.176	.4	.799	.908	.995
.10	.017	.25	.142	.184	.217	.275	.5	1.227	1.395	1.558
.12	.023	.30	.197	.259	.308	.389	.6	1.744	1.981	2.201
.14	.031	.35	.257	.346	.413	.522	.7	2.336	2.667	2.954
.16	.039	.40	.321	.441	.530	.679	.8	3.000	3.445	3.840
.18	.048	.45	.385	.544	.661	.850	.9	3.739	4.303	4.305
.20	.057	.50	.446	.655	.802	1.036	1.0	4.535	5.241	5.862
.22	.066	.55		.769	.953	1.244	1.1	5.390	6.259	7.038
.24	.075	.60		.888	1.113	1.462	1.2	6.294	7.352	8.267
.25	.079	.65		1.008	1.281	1.694	1.3	7.245	8.511	9.583
		.70		1.124	1.454	1.950	1.4	8.222	9.725	11.03
		.75		1.235	1.633	2.210	1.5	9.237	11.00	12.50
		.80			1.815	2.482	1.6	10.26	12.32	14.04
		.85			2.000	2.774	1.7	10.98	13.68	15.69
		.90			2.181	3.067	1.8	12.33	15.06	17.35
		.95			2.357	3.369	1.9	13.33	16.50	19.06
		1.00			2.524	3.690	2.0	14.28	17.93	20.87
		1.05				4.007	2.1		19.38	22.66
		1.10				4.330	2.2		20.82	24.49
		1.15				4.671	2.3		22.25	26.42
		1.20				5.001	2.4		23.63	28.29
		1.25				5.335	2.5		24.94	30.17
		1.30				5.676	2.6			32.10
		1.35				6.010	2.7			33.99
		1.40				6.333	2.8			35.82
		1.45				6.657	2.9			37.65
		1.50				6.956	3.0			39.34

H	Q D = 4.00	Q D = 5.0	H	Q D = 4.00	Q D = 5.00
.1	.081	.092	3.1	55.16	65.91
.2	.295	.325	3.2	58.07	69.68
.3	.646	.720	3.3	60.97	73.51
.4	1.155	1.284	3.4	63.92	77.39
.5	1.809	2.018	3.5	66.83	81.27
.6	2.592	2.907	3.6	69.78	85.22
.7	3.497	3.951	3.7	72.60	89.24
.8	4.518	5.136	3.8	75.83	93.34
.9	5.669	6.448	3.9	78.14	97.28
1.0	6.941	7.895	4.0	80.76	101.5
1.1	8.342	9.482	4.1		105.5
1.2	9.865	11.21	4.2		109.6
1.3	11.49	13.08	4.3		113.7
1.4	13.22	15.09	4.4		117.8
1.5	15.04	17.24	4.5		121.9
1.6	16.97	19.49	4.6		125.9
1.7	19.00	21.86	4.7		129.8
1.8	21.25	24.35	4.8		133.7
1.9	23.36	26.94	4.9		137.4
2.0	25.66	29.65	5.0		141.1
2.1	28.04	32.47			
2.2	30.49	35.41			
2.3	33.02	38.46			
2.4	35.61	41.60			
2.5	38.26	44.83			
2.6	40.99	48.15			
2.7	43.73	51.54			
2.8	46.52	55.22			
2.9	49.38	58.58			
3.0	52.25	62.21			

Note: Although Q is given for the complete circle of the weir, the flow begins to increase at about 70% of the diameter beyond that given by the formula, thus, partaking of a transition between weir flow and orifice flow as the weir becomes surcharged.

APPENDIX C

Values of $\Delta = 2(1 - k^2 - k^4)\,E - (2 - k^2)(1 - k^2)\,K$

where $k^2 = H/D$; E and K to be taken from tables of complete elliptic integrals.

Note: for k^2 values the 3d decimal is at the top.

k^2	0	1	2	3	4	5	6	7	8	9	Diff for k^2 = .001
0	0	.0000	.0001	.0001	.0002	.0002	.0002	.0003	.0003	.0004	0.4
.01	.0004	.0005	.0006	.0007	.0008	.0009	.0010	.0011	.0011	.0012	0.9
.02	.0013	.0015	.0016	.0018	.0019	.0020	.0022	.0023	.0025	.0026	1.4
.03	.0027	.0028	.0030	.0032	.0034	.0035	.0037	.0039	.0041	.0043	1.9
.04	.0046	.0048	.0050	.0053	.0055	.0058	.0060	.0063	.0065	.0068	2.5
.05	.0071	.0074	.0077	.0080	.0083	.0087	.0090	.0093	.0096	.0099	3.1
.06	.0102	.0106	.0109	.0113	.0117	.0120	.0124	.0128	.0132	.0135	3.7
.07	.0139	.0144	.0148	.0152	.0156	.0160	.0165	.0169	.0173	.0178	4.3
.08	.0182	.0187	.0192	.0197	.0202	.0206	.0211	.0216	.0221	.0226	4.9
.09	.0231	.0236	.0242	.0248	.0253	.0258	.0264	.0270	.0275	.0281	5.5
.10	.0286	.0292	.0298	.0304	.0310	.0316	.0322	.0328	.0334	.0340	6.0
.11	.0346	.0353	.0359	.0366	.0372	.0379	.0386	.0392	.0399	.0405	6.6
.12	.0412	.0419	.0462	.0433	.0440	.0448	.0455	.0462	.0469	.0476	7.1
.13	.0483	.0491	.0498	.0506	.0514	.0522	.0529	.0537	.0545	.0552	7.7
.14	.0560	.0568	.0576	.0585	.0593	.0601	.0609	.0617	.0626	.0634	8.2
.15	.0642	.0651	.0659	.0668	.0676	.0685	.0694	.0702	.0711	.0719	8.6
.16	.0728	.0737	.0746	.0755	.0764	.0773	.0783	.0792	.0801	.0810	9.1
.17	.0819	.0828	.0838	.0847	.0857	.0866	.0876	.0886	.0895	.0904	9.5
.18	.0914	.0924	.0934	.0944	.0954	.0964	.0974	.0984	.0994	.1004	10.0
.19	.1014	.1024	.1035	.1046	.1056	.1066	.1077	.1088	.1098	.1108	10.5
.20	.1119	.1130	.1141	.1152	.1163	.1174	.1185	.1196	.1207	.1218	11.0
.21	.1229	.1240	.1252	.1264	.1275	.1286	.1298	.1310	.1321	.1332	11.5
.22	.1344	.1356	.1368	.1380	.1392	.1404	.1416	.1428	.1440	.1452	12.0
.23	.1464	.1476	.1489	.1502	.1514	.1526	.1539	.1552	.1564	.1576	12.5
.24	.1589	.1602	.1615	.1628	.1641	.1654	.1667	.1680	.1693	.1706	13.0
.25	.1719	.1732	.1746	.1760	.1773	.1786	.1800	.1814	.1827	.1840	13.5
.26	.1854	.1868	.1882	.1869	.1910	.1924	.1938	.1952	.1966	.1980	14.0
.27	.1994	.2008	.2023	.2038	.2052	.2066	.2081	.2095	.2110	.2124	14.5
.28	.2139	.2154	.2169	.2184	.2199	.2214	.2229	.2244	.2259	.2274	15.0
.29	.2289	.2304	.2320	.2335	.2351	.2366	.2381	.2397	.2412	.2428	15.4
.30	.2443	.2459	.2475	.2490	.2506	.2522	.2538	.2554	.2569	.2585	15.8
.31	.2601	.2617	.2633	.2650	.2666	.2682	.2698	.2714	.2731	.2747	16.2
.32	.2763	.2780	.2796	.2813	.2829	.2846	.2863	.2879	.2896	.2912	16.6
.33	.2929	.2946	.2963	.2980	.2997	.3014	.3031	.3048	.3065	.3082	17.0
.34	.3099	.3116	.3134	.3151	.3169	.3186	.3203	.3221	.3238	.3256	17.4
.35	.3273	.3291	.3309	.3326	.3344	.3362	.3380	.3398	.3415	.3432	17.8
.36	.3451	.3469	.3487	.3506	.3524	.3542	.3560	.3578	.3597	.3615	18.2
.37	.3633	.3652	.3670	.3689	.3707	.3725	.3745	.3763	.3782	.3800	18.6
.38	.3819	.3838	.3857	.3876	.3895	.3914	.3933	.3952	.3971	.3990	19.0
.39	.4009	.4028	.4048	.4067	.4087	.4106	.4125	.4145	.4164	.4184	19.4
.40	.4203	.4223	.4243	.4262	.4282	.4302	.4322	.4342	.4361	.4381	19.8
.41	.4401	.4421	.4441	.4462	.4482	.4502	.4522	.4542	.4563	.4583	20.2
.42	.4603	.4624	.4644	.4665	.4685	.4706	.4727	.4747	.4768	.4788	20.6
.43	.4809	.4830	.4851	.4872	.4893	.4914	.4935	.4956	.4977	.4998	21.0
.44	.5019	.5040	.5062	.5083	.5105	.5126	.5147	.5169	.5190	.5212	21.4
.45	.5233	.5255	.5277	.5298	.5320	.5342	.5364	.5386	.5407	.5429	21.8
.46	.5451	.5473	.5495	.5517	.5539	.5561	.5584	.5606	.5628	.5650	22.1
.47	.5672	.5694	.5717	.5739	.5762	.5784	.5806	.5829	.5851	.5874	22.4
.48	.5896	.5919	.5941	.5964	.5987	.6010	.6032	.6055	.6078	.6100	22.7
.49	.6123	.6146	.6169	.6192	.6215	.6238	.6262	.6285	.6308	.6331	23.1
.50	.6354	.6377	.6401	.6424	.6448	.6471	.6494	.6518	.6541	.6565	23.4

k^2	0	1	2	3	4	5	6	7	8	9	Diff for k^2 = .001
.51	.6588	.6612	.6635	.6659	.6683	.6706	.6730	.6754	.6778	.6801	23.7
.52	.6825	.6849	.6873	.6897	.6921	.6944	.6968	.6992	.7016	.7040	23.9
.53	.7064	.7088	.7112	.7137	.7161	.7185	.7209	.7233	.7258	.7282	24.2
.54	.7306	.7330	.7355	.7380	.7404	.7428	.7453	.7478	.7502	.7526	24.5
.55	.7551	.7576	.7601	.7625	.7650	.7675	.7700	.7725	.7749	.7774	24.8
.56	.7799	.7824	.7849	.7874	.7899	.7924	.7950	.7975	.8000	.8025	25.1
.57	.8050	.8075	.8101	.8126	.8152	.8177	.8202	.8228	.8253	.8279	25.4
.58	.8304	.8330	.8355	.8381	.8406	.8432	.8458	.8483	.8509	.8534	25.6
.59	.8560	.8586	.8612	.8637	.8663	.8689	.8715	.8741	.8766	.8792	25.8
.60	.8818	.8844	.8870	.8896	.8922	.8948	.8975	.9001	.9027	.9053	26.1
.61	.9079	.9105	.9132	.9158	.9184	.9210	.9237	.9263	.9289	.9316	26.3
.62	.9342	.9369	.9395	.9422	.9448	.9475	.9502	.9528	.9555	.9581	26.6
.63	.9608	.9635	.9662	.9688	.9715	.9742	.9769	.9796	.9822	.9849	26.8
.64	.9876	.9903	.9930	.9957	.9984	1.0012	1.0039	1.0066	1.0093	1.0120	27.1
.65	1.0147	1.0174	1.0202	1.0229	1.0256	1.0284	1.0311	1.0338	1.0365	1.0393	27.3
.66	1.0420	1.0447	1.0475	1.0502	1.0530	1.0557	1.0584	1.0612	1.0639	1.0667	27.4
.67	1.0694	1.0721	1.0749	1.0777	1.0804	1.0832	1.0859	1.0886	1.0914	1.0941	27.5
.68	1.0969	1.0997	1.1024	1.1052	1.1080	1.1108	1.1135	1.1163	1.1191	1.1218	27.7
.69	1.1246	1.1274	1.1302	1.1329	1.1357	1.1385	1.1413	1.1441	1.1468	1.1496	27.8
.70	1.1524	1.1552	1.1580	1.1608	1.1636	1.1664	1.1692	1.1720	1.1748	1.1776	28.0
.71	1.1804	1.1832	1.1860	1.1888	1.1916	1.1944	1.1973	1.2001	1.2029	1.2057	28.1
.72	1.2085	1.2113	1.2142	1.2170	1.2198	1.2226	1.2255	1.2283	1.2311	1.2340	28.3
.73	1.2368	1.2396	1.2425	1.2453	1.2482	1.2510	1.2539	1.2568	1.2596	1.2624	28.5
.74	1.2653	1.2682	1.2710	1.2739	1.2767	1.2796	1.2825	1.2853	1.2882	1.2910	28.6
.75	1.2939	1.2968	1.2996	1.3025	1.3054	1.3082	1.3111	1.3140	1.3169	1.3197	28.7
.76	1.3226	1.3255	1.3284	1.3312	1.3341	1.3370	1.3399	1.3428	1.3456	1.3485	28.8
.77	1.3514	1.3543	1.3572	1.3600	1.3629	1.3658	1.3687	1.3716	1.3744	1.3773	28.8
.78	1.3802	1.3831	1.3860	1.3889	1.3918	1.3946	1.3975	1.4004	1.4033	1.4062	28.9
.79	1.4091	1.4120	1.4149	1.4178	1.4207	1.4236	1.4264	1.4293	1.4322	1.4351	28.9
.80	1.4380	1.4409	1.4438	1.4467	1.4496	1.4525	1.4554	1.4583	1.4612	1.4641	29.0
.81	1.4670	1.4699	1.4728	1.4757	1.4786	1.4815	1.4844	1.4873	1.4902	1.4931	29.0
.82	1.4960	1.4989	1.5018	1.5047	1.5076	1.5105	1.5134	1.5163	1.5192	1.5221	29.0
.83	1.5250	1.5279	1.5308	1.5337	1.5366	1.5395	1.5424	1.5453	1.5482	1.5511	29.0
.84	1.5540	1.5569	1.5598	1.5627	1.5656	1.5685	1.5714	1.5743	1.5772	1.5801	29.0
.85	1.5830	1.5858	1.5880	1.5917	1.5946	1.5975	1.6004	1.6033	1.6062	1.6091	29.0
.86	1.6120	1.6149	1.6178	1.6207	1.6236	1.6265	1.6294	1.6323	1.6352	1.6381	29.0
.87	1.6410	1.6439	1.6468	1.6497	1.6526	1.6554	1.6583	1.6612	1.6641	1.6670	28.9
.88	1.6699	1.6728	1.6757	1.6786	1.6815	1.6843	1.6872	1.6901	1.6930	1.6959	28.9
.89	1.6988	1.7017	1.7046	1.7074	1.7103	1.7132	1.7161	1.7190	1.7218	1.7247	28.8
.90	1.7276	1.7304	1.7333	1.7362	1.7390	1.7418	1.7447	1.7475	1.7504	1.7532	28.5
.91	1.7561	1.7589	1.7618	1.7650	1.7674	1.7702	1.7731	1.7759	1.7787	1.7816	28.3
.92	1.7844	1.7872	1.7900	1.7928	1.7956	1.7984	1.8013	1.8041	1.8069	1.8097	28.1
.93	1.8125	1.8153	1.8181	1.8208	1.8236	1.8264	1.8292	1.8320	1.8347	1.8375	27.8
.94	1.8403	1.8430	1.8458	1.8485	1.8513	1.8540	1.8568	1.8596	1.8623	1.8650	27.5
.95	1.8678	1.8705	1.8732	1.8760	1.8787	1.8814	1.8841	1.8868	1.8896	1.8923	27.2
.96	1.8950	1.8977	1.9004	1.9031	1.9058	1.9084	1.9111	1.9138	1.9165	1.9192	26.9
.97	1.9219	1.9246	1.9272	1.9298	1.9325	1.9352	1.9378	1.9404	1.9431	1.9458	26.5
.98	1.9484	1.9510	1.9536	1.9562	1.9588	1.9614	1.9640	1.9667	1.9692	1.9718	26.0
.99	1.9744	1.9770	1.9795	1.9821	1.9846	1.9872	1.9900	1.9923	1.9949	1.9974	25.6
1.00	2.0000										

APPENDIX D

Transformation of the basic hydraulic equation (2) to the elliptic equation (3) in the text; (20) in this appendix.

Transformation to Elliptical Integrals

Equation (2) may be transformed into a form of complete elliptic integral and a solution found to almost any degree of precision desired. Tables are available of these elliptic functions to 8 or more decimal places.

Following are a few fundamental relationships that are essential to this transformation. The elliptic integral of the first kind is

$$F(\phi,k) = u = \int_0^{\phi} \frac{d\phi}{\sqrt{1 - k^2 \sin \phi}} \qquad [k < 1] \quad , \quad [x = \sin \phi]$$

$$= \int_0^{x} \frac{dx}{\sqrt{(1 - x^2)(1 - k^2x^2)}}$$

Dwight 750

ϕ is the amplitude and k the modulus			751.1
$\phi = \text{am } u$			751.2
$\sin \phi = \text{sn } u = x$			751.3
$\cos \phi = \text{cn } u = \sqrt{1 - x^2}$			751.4
$\text{dn } u = \sqrt{1 - k^2x^2}$			751.5
$\text{am} - u = - \text{am } u$	753.1	$\text{am } 0 = 0$	754.1
$\text{sn} - u = -\text{sn } u$	753.2	$\text{sn } 0 = 0$	754.2
$\text{cn} - u = \text{cn } u$	753.3	$\text{cn } 0 = 1$	754.3
$\text{dn} - u = \text{dn } u$	753.4	$\text{dn } 0 = 1$	754.4
$\text{sn}^2 u + \text{cn}^2 u = 1$			755.1
$\text{dn}^2 u + k^2 \text{sn}^2 u = 1$			755.2
$\text{dn}^2 u - k^2 \text{cn}^2 u = 1 - k^2$			751.7 and 755.3
$\frac{d}{dx} \text{sn } x = \text{cn } x \text{ dn } x$			768.1

The elliptic integral of the second kind is

$$E(\phi, k) = \int_0^{\phi} \sqrt{1 - k^2 \sin^2 \phi} \; d\phi$$

$$= \int_0^{x} \frac{\sqrt{1 - k^2 x^2}}{\sqrt{1 - x^2}} \; dx \qquad [x = \sin \phi]$$

Dwight 771

If the integration is taken between the limits 0 and $\pi/2$ we obtain complete elliptic integrals thus

$$K = \int_0^{\pi/2} \frac{d\phi}{\sqrt{1 - k^2 \sin^2 \phi}}$$

Dwight 773.1

and

$$E = \int_0^{\frac{\pi}{2}} \sqrt{1 - k^2 \sin^2 \phi} \; d\phi \qquad \text{Dwight 774.1}$$

Let

$$y = H sn^2 x = D k^2 sn^2 x \tag{3A}$$

$$H = Dk^2 \tag{4}$$

The first derivative of (3) is

$$dy = 2 H sn x \frac{d}{dx} sn x \tag{5}$$

and from (4) and Dwight 768.1

$$dy = 2 D k^2 sn x \, cn x \, dn x \, dx \tag{6}$$

from (3) and 755.1

$$H - y = H(1 - sn^2 x) = D k^2 cn^2 x \tag{7}$$

from (4) and 755.2

$$D - y = D(1 - k^2 sn^2 x) = D \, dn^2 x \tag{8}$$

From (3), (4), (6), (7) and (8)

$$\begin{aligned} &\left[(D - y)\, y\, (H - y)\right]^{\frac{1}{2}} \, dy \\ &= \left[D \, dn^2 x \; Dk^2 sn^2 x \; D k^2 \, cn^2 x\right]^{\frac{1}{2}} (2Dk^2 sn \, x \, cn \, x \, dn \, x)\, dx \\ &= \left[4D^5 k^8 sn^4 x \, cn^4 x \, dn^4 x\right]^{\frac{1}{2}} dx \end{aligned} \tag{9}$$

(3) may be written $y = H \, sn^2 (\sin^{-1} \phi)$. Hence when $y = 0$, $\sin^{-1} \phi = x = 0$ also when $y = H$, from Dwight 751.3 since $y/H = 1$

$x = sn^{-1} u = K$ the complete elliptic integral of the first kind.

Adding the limits of integration and substituting (9), (2) becomes

$$Q_t = 4 \sqrt{2g} \; D^{5/2} \; k^4 \int_0^K sn^2 cn^2 dn^2 dx \tag{10}$$

But by Dwight 755.1 and 755.2

$$cn^2 x = 1 - sn^2 x \text{ and } dn^2 x = 1 - k^2 sn^2 x$$

substituting in (10)

$$Q_t = 4 \sqrt{2g} \; D^{5/2} \; k^4 \; I \tag{11}$$

where

$$I = \int_0^{\kappa} sn^2x\,dx - (1 - k^2)\int_0^{\kappa} sn^4x\,dx + k^2\int_0^{\kappa} sn^6dx \qquad (12)$$

Reverting to Pierce[6] we have

$$(m+1)\int sn^m x\,dx = (m+2)(1+k^2)\int sn^{m+2}x\,dx$$

$$-(m+3)k^2\int sn^{m+4}x\,dx + sn^{m+1}x\,cn\,x\,dn\,x, \qquad \text{Pierce 567}$$

which for m = 2, and adding the limits of integration becomes

$$3\int_0^{\kappa} sn^2x\,dx = 4(1+k^2)\int_0^{\kappa} sn^4dx - 5k^2\int_0^{\kappa} sn^6x\,dx + sn^3x\,cn\,x\,dn\,x$$

since by Dwight 751.3 and 754.2 sn 0 - 0 and cn K = x = 0 the integrated terms (the last one) of Pierce 567 disappears and there remains

$$5k^2\int_0^{\kappa} sn^6x\,dx = 4(1+k^2)\int_0^{\kappa} sin^4x\,dx - 3\int_0^{\kappa} sn^2x\,dx \qquad (13)$$

also for m = 0 in Pierce 567

$$\int_0^{\kappa} dx = 2(1+k^2)\int_0^{\kappa} sn^2x\,dx - 3k^2\int_0^{\kappa} sn^4x\,dy \qquad (14)$$

Since the left hand term = K we obtain by Pierce 564

$$\int_0^{\kappa} sn^2x = \frac{1}{k^2}(K - E) \qquad (15)$$

since

$$E(o, k) = 0 \text{ and } E(am\ k, H) = E$$

substitute (15) in (14)

$$3k^2\int_0^{\kappa} sn^4x\,dx = \frac{2(1+k^2)}{k^2}(K - E) - K \qquad (16)$$

or

$$\int_0^{\kappa} sn^4dx = \frac{2(1+k^2)}{3k^4}(K - E) - \frac{K}{3k^2} \qquad (17)$$

substitute (15) in (17) and (13)

$$5k^2\int_0^{\kappa} sn^6x\,dx = 4(1+k^2)\left[\frac{2(1+k^2)}{3k^4}(K - E) - \frac{K}{3k^2}\right]$$

$$= \frac{8(1+k^2)^2}{3k^4}(K - E) - \frac{4(1+k^2)}{3k^2}K - \frac{3}{k^2}(K - E)$$

whence

$$k^2\int_0^{\kappa} sn^6x\,dx = \left[\frac{8}{15}\frac{(1+k^2)^2}{k^2} - \frac{3}{5k^2}\right]\left[K - E\right] - \frac{4}{15}\frac{1+k^2}{k^2}K \qquad (18)$$

substitute (15), (17) and (8) in (12) and obtain

$$I = \frac{1}{k^2}\ (K - E) - (1+k^2)\left[\frac{2(1+k^2)}{3k^4}\ (K - E) - \frac{K}{3k^2}\right]$$

$$= \frac{2(1+k^2)^2}{3k^4}\ (K - E) + \frac{1+k^2}{3k^2}\ K$$

$$+ \left(\frac{8}{15}\ \frac{(1+k^2)^2}{k^4} - \frac{3}{5k^2}\right)(K-E) - \frac{4}{15}\ \frac{1+k^2}{k^2}\ K$$

collecting E - terms

$$\frac{E}{15k^4}\ (-15k^2 + 10 + 20k^2 - 8 - 16k^2 - 8k^4 + 9k^2)$$

$$= \frac{1}{15k^4}\ 2(1 - k^2 + k^4)\,E$$

collecting K - terms

$$\frac{K}{15k^4}\ (15k^2 - 10 - 20k^2 - 10k + 5k^2 + 5k^4 + 8 + 16k^2$$

$$+ 8k^4 - 9k^2 + 4 + 4k^2) = \frac{1}{15k^4}\ (2 - 3k^2 + k^4)$$

combining E - and K - terms

$$I = \frac{1}{15k^4}\ \left[2(1 - k^2 + k^4)\ E - (2 - k^2)(1 - k^2)\ K\right] \qquad (19)$$

substitute (19) in (11) and obtain finally

$$Q_t = \frac{4}{15}\sqrt{2g}\ D^{5/2}\ \left[2(1 - k^2 + k^4)E - (2 - k^2)(1 - k^2)\ K\right] \qquad (20)$$

a rigid formula for the theoretical flow through a sharp edged circular weir with complete contractions and no appreciable velocity of approach.

In (20) k^2 = H/D the head on the invert of the circle in terms of the diameter. E and K may be taken from tables (see references).

Paper 1456 December, 1957 HY 6

Journal of the

HYDRAULICS DIVISION

Proceedings of the American Society of Civil Engineers

CONTENTS

DISCUSSION
(Proc. Paper 1456)

Page

Proportional Weirs for Sedimentation Tanks, by J. C. Stevens. (Proc. Paper 1015. June, 1956. Prior discussion: 1177. Discussion closed.)
by J. C. Stevens (closure) 1456-3

The Problem of Reservoir Capacity for Long-Term Storage, by Aly Fathy and Aly Salem Shukry. (Proc. Paper 1082. October, 1956. Prior discussion: 1230, 1283. Discussion closed.)
by Aly Fathy and Aly Salem Shukry (closure). 1456-7

Technical Problems of Flood Insurance, by H. Alden Foster. (Proc. Paper 1165. February, 1957. Prior discussion: 1348. Discussion closed.)
by H. Alden Foster (closure) 1456-11

A High-Head Cavitation Test Stand for Hydraulic Turbines, by W. G. Whippen and G. D. Johnson. (Proc. Paper 1201. April, 1957. Prior discussion: 1417. Discussion closed.)
by Robert T. Knapp 1456-13

The Efficacy of Floor Sills under Drowned Hydraulic Jumps, by Ahmed Shukry. (Proc. Paper 1260. June, 1957. Prior discussion: 1417. Discussion closed.)
by Alvin J. Peterka 1456-15
by Alfred C. Ingersoll 1456-16
by S. Leliavsky 1456-18

Stilling Basin Experiences of the Corps of Engineers, by R. H. Berryhill. (Proc. Paper 1264. June, 1957. Prior discussion: none. Discussion closed.)
by Alvin J. Peterka 1456-25

Note: Paper 1456 is part of the copyrighted Journal of the Hydraulics Division of the American Society of Civil Engineers, Vol. 83, HY 6, December, 1957.

PROPORTIONAL WEIRS FOR SEDIMENTATION TANKS[a]

Closure by J. C. Stevens

J. C. Stevens,[1] M. ASCE.—The author is grateful indeed to Prof. Guido Di Ricco of the University of Rome, for his contribution to the subject of proportional weirs.

He is quite correct in assuming that the author was entirely unaware of the very extensive work done by him in this field. This must be charged to the handicap of the language barrier that separates us. To illustrate: when Prof. Ricco's discussion appeared any attempt to obtain copies of his papers only met with frustration. From his footnotes, they could not be found in the Engineering Societies Library in New York nor any other library where inquiries were made. They were finally obtained through ASCE for whom Prof. Ricco had photostat copies made of some of the papers cited, which were passed on to the writer. Two translations of the principal paper were obtained from two local Italian sources, but both had to be retranslated by the author into the King's English no doubt because neither translator know hydraulic terms — more frustrations.

The credit for inventing the proportional weir must undoubtedly be given to the late Dr. Oscar Van Pelt Stout, M. ASCE, while he was Professor of Civil Engineering at the University of Nebraska. He designed, tested and put to practical use such a weir in 1896 and presented a paper on it at the first meeting of the Nebraska Engineering Society held in Lincoln in 1897.

These facts were submitted to the author by Prof. Steponas Kolupaila of Notre Dame University, who also submitted a bibliography on the subject which, with his permission, is being appended hereto. It is always best to give full credit where credit is due.

The writer was a student under Prof. Stout. He faintly remembers being told about the Stout proportional weir while in college, but did not know or had forgotten that its mathematical details had been made public some 8 years prior. During the intervening 50 years it was easy to forget until Prof. Kolupaila's most excellent system of references brought the facts cogently to mind, for which grateful acknowledgment is hereby made.

There is a typographical error in the footnote to Prof. Ricco's discussion as printed in No. HY 1, Feb. 1957 p 1177-41. The date of his paper in L'Energia Elettrica should be October 1936 instead of 1956.

Beginning with the author's basic equation(7) Prof. Ricco presents his generalized formula(2) in which the lateral width of the weir (x) for any depth (y) is evolved in his equation(4) in terms of the gamma function.

---

a. Proc. Paper 1015, June, 1956, by J. C. Stevens.

1. Cons. Hydro. Engr., Stevens & Thompson Engrs., Portland, Ore.

Had the author known of this he might have saved himself much of the laborious series developments with which his paper is adorned.

The use of a series of chords instead of a purely curvilinear profile for the weir is also an innovation that may well be adopted in this country. Compare Figs 4 and 5 with the author's Fig 2. It appears that by this expedient the proportional weir can be designed to produce almost any desired pattern of outflow from a tank or reservoir and might, with profit, be applied to some cases of river regulation.

It is hoped that this paper and the discussion will stimulate a more extensive use of the proportional weir than exists at present in this country. It has many advantages and could well be used more extensively.

REFERENCES

American Literature

1. O. V. P. Stout, A New Form of Weir Notch. Transactions of the Nebraska Engineering Society, Lincoln, Nebr. Vol. 1 No. 1 pp.13-16 1897, Jacob North & Co For the Stout weir the flow is directly proportional to the head on the weir. Theoretically the width (x) of the weir becomes infinite for zero depth (y) but Dr. Stout showed in this paper how this effect could be compensated for by a rectangular base and indicated how the dimensions of this rectangle could be readily determined.

2. E. H. Breidenback treats of the Sutro weir. Proc. Am. WW Assoc. 1912, p. 212.

3. E. W. Rettger, A Proportional-flow Weir. Eng. News Vol. 71 1914 June 29, p.1409. The weir herein described is identical in all respects with the Stout weir which preceded it by 17 years. He did however outline a worthwhile feature regarding flow coefficients.

4. O. V. P. Stout, The Proportional Weir Devised in 1896. Eng. News Vol. 72, 1914, July 16, p.148. This prompt rejoinder, just one month later than reference (3), was doubtless made in defense of his unrecognized claim to priority.

5. E. W. Pratt, Another Proportional-flow Weir. One devised in 1908 by Henry Sutro. It had a rectangular base of arbitrary depth and the proportionality to flow obtained above a datum 1/3 the height of the rectangle. Because of this innovation no doubt these weirs have become known as "Sutro Weirs." Eng. News Vol. 72, 1914 Aug. 27, p.462.

6. E. W. Rettgar, The Inverted Weir, Eng. News Vol. 73, Jan 14, 1915.

7. B. D. Moses, Large Sutro Weir under test, Eng. News Vol. 74, 1915 Aug. 16, p. 277.

8. E. W. Debler and F. H. Bayfield, Tests of a proportional weir, Eng. News Vol. 74, 1915, Nov. 22, p. 1018.

9. John Gregory, Proportional weir in grit chambers, Eng. News-Record Vol. 116, 1936 Feb. 13 p. 257.

10. Ch. H. Capen, History of Sutro Weirs, Eng. News-Record Vol. 131, 1943, Oct. 21, p. 585.

11. Messrs. Soucek, Howe, and Mavis, Sutro Weir Investigations to Furnish Discharge Coefficients, Eng. News-Record. Vol 117, Nov. 12, 1936, p. 1679. Tests of 11 proportional weirs were made at Iowa Institute of Hydraulic Research at Iowa City, Ia.

12. L. Pearse, More on Sutro Weirs, Eng. News-Record, Vol. 131, 1943, Nov. 18, p. 735.

13. F. T. Mavis, There's No Mystery in Weir Flow Calculations, Eng. News-Record, Vol. 142, 1949, Jan. 6, p. 76.

14. R. B. Banks, A Note on the generalized weir equation, Northwestern University, Evanston, Ill. 1954, Ms. eight pages.

15. J. C. Stevens, Proportional weirs for sedimentation tanks, Journal Hydraulics Division ASCE Paper 1015, 1956.

European Literature

16. M. Rother, Einschnittsform von Uberfällen (Über die Eischnittsform von Überfällen, deren Durchflussmenge proportional mit der Strahlhöhe zunimmt). In German: Weir-notch; on a notch whose discharge increases proportionally with the nappe height. Wasser und Gas, 11 (1920-21), No. 41-42, pp. 1213-1231. Berlin 1921.

17. R. Lummert, Proportionalschreibwerk für Überfälle, Wasser und Gas, 12 (1921-22), No. 10, pp. 249-252. Berlin 1921; same: Das Gas- und Wasser fach, 64 (1921), No 48, p. 787. München-Berlin, In German: Proportional recorder for weirs.
Comment: M. Rother, Wasser und Gas, 12 (1921-22), No. 10, pp. 251-252. Berlin 1921.

18. H. Janert, Dränwassermessungen. In German: Water measurement in drains. Der Kulturtechniker, 33 (1930), No. 1, pp. 19-27. Breslau.

19. R. Ehrenberger, Genauere Ermittlung der Wassermengen mit Hilfe des Dränwassermessers von Janert. In German: More exact determination of water discharge by drainage-water meter of Janert. Wasserwirtschaft und Technik, 4 (1937), No. 17-19, pp. 180-185. Wien.

20. G. Di Ricco, Edificio di misura ad equazione di portata lineare. In Italian: Measurement structure with linear equation of discharge. Rivista del Catasto e di Servici Tecnici Erariali. (1940), No. 3, pp 293- ; No. 4, pp. 416- . Roma
A German abstract:

21. C. Reindl, Mess-Ausflussoffnung mit linearer Ausfluss-Gleichung. Wasserkraft und Wasserwirtshaft, 36 (1941), No. 4, pp. 110-111. München.

22. S. Barocio Barrios, La détermination d'un déversoir devant respecter une loi hauteur-débit dennée. In French: Design of a weir capable to follow a given law height-discharge. La Houille Blanche, 8 (1953), No. 4, Apr.-Sep., pp. 515-520. Discussions: G di Ricco, No. 6, Nov.-Dec. p. 839; S. B. Barrios, 9 (1954), No. 3, June, pp. 515-516. Grenoble.

THE PROBLEM OF RESERVOIR CAPACITY FOR LONG-TERM STORAGE[a]

Closure by Aly Fathy and Aly Salem Shukry

ALY FATHY[1] and ALY SALEM SHUKRY[2].—The authors find that the discussions of their paper have brought forth no consequential information on the subject under study with the exception of Mr. Hanna's exposition on the question of sub-annual storage. That exposition fills a gap in the inquiry that was passed over rather lightly.

In Mr. Mostafa's discussion an attempt was made to demonstrate the inadequacy of a normal capacity of 45 milld. m^3, as arrived at through application of the authors' method to the projected long-term reservoir on the Nile at Aswan. In that attempt, however, sub-annual effects were introduced. In the light of Mr. Hanna's observations it will be seen that when these effects are taken into consideration the extra capacity provided for flood relief should be included in the working capacity. According to Mr. Mostafa's own calculations the total capacity of 75 milliards (45 + 30) would be more than sufficient.

The discussion by Messrs. Simaika and Boulos is devoted mainly to demonstrating the unreliability of conditions derived from past observations as a guide in forecasting the future behaviour of a natural event. In a field of enquiry where probability considerations play the leading part such an attempt is really superfluous. As far as hydrological phenomena are concerned, the principal criteria to which reference may be made are:

1. The Mean.
2. The Standard Deviation.
3. The Maximum Deviation of a single observation from the Mean.
4. The Maximum Deviations of the arithmetic mean for groups of observations of varying number.

Of these criteria, the Standard Deviation is the most erratic and the least amenable to provisional adjustment. Thus a method of treatment which depends primarily on that parameter would be the least reliable.

In Dr. Hurst's discussion a slip has been made in the attempt to reconstruct the expression of the ideal range (Eq. b). As the length of the critical period is supposed = N/2, the derived expression should be multiplied by $\sqrt{2}$. That would raise the numerical factor to the same value as given by the authors in Eq. 15.

Dr. Hurst considers it faulty to adopt the mean value N/2 as a standard for the length of the critical period. It would certainly be more legitimate to do so with regard to a parameter that fluctuates about a definite mean than to

a. Proc. Paper 1082, October, 1956, by Aly Fathy and Aly Salem Shukry.

1. Part-time Prof., Faculty of Eng., Alexandria Univ., Alexandria, Egypt.
2. Asst. Prof., Faculty of Eng., Alexandria Univ., Alexandria, Egypt.

one that varies progressively such as the range R. According to Dr. Hurst's "Century Storage" theory a standard value is assigned to R corresponding to a working period of 100 years. It is here that disregard of the variability of R may be questioned.

Incidentally, it may be noted that by assigning a standard value of 1/2 to the relative length of the critical period the resultant expression of R is brought to the same form (though not the same value) as arrived at by Dr. Hurst himself through a very elaborate mathematical analysis. Mr. Hanna's observations on that point will be found most illuminating.

The authors wish to stress the fact, however, that in the practical application of their method of treatment no reference at all is made to the ideal range which is an indeterminate quantity. The capacity S needed to guarantee a draft less than the mean (as would always be the case) is derived straightforward from the deviation-curve. The tying up of S with R, as proposed by Dr. Hurst, greatly complicates the problem. Both of his expressions of S (Eq. 8 in the original paper and Eq. 27 in Mr. Hanna's discussion) will be found to lead to absurd results when the difference between the guaranteed draft and the mean is large. According to (8), S becomes zero when $(M - B) = 1.04\ \sigma$. That quantity is usually much in excess of the maximum deviation of one observation or of the mean for a small group. For the Nile at Aswan, $M = 93$ and $\sigma = 19.8$. Thus S becomes zero when $B = 72.4$. That figure is 30.4 milliards greater than the observed minimum supply of one year, which is 42. Evidently, the storage provided should cover the deficit in one year at least.

The logarithmic relation (27) yields a value of $S = 4.9$ for a guaranteed draft of 60 millds./ann. Actually, the storage needed to cover the deficit in the worst year would be 18 milliards.

The above examples bear sufficient evidence of the need for a totally different line of approach. It is the authors' belief that the line they have suggested is the only alternative.

Corrections: Fig. 7 of the original paper did not contain the construction referred to in the text. The correct figure is reproduced herewith.

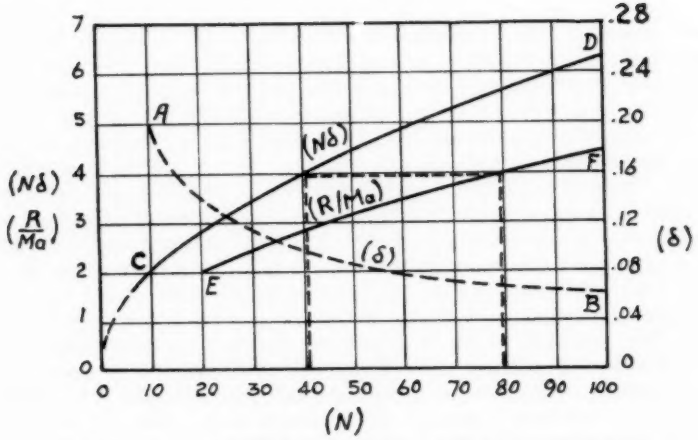

Fig. 7 - DERIVATION OF THE RANGE FROM THE DEVIATION-CURVE

TECHNICAL PROBLEMS OF FLOOD INSURANCE[a]

Closure by H. Alden Foster

H. ALDEN FOSTER,* M. ASCE.—The discussion by Mr. Alexander emphasizes some of the difficulties encountered in preparing probability estimates for floods. From a practical viewpoint, it is impossible to prepare an absolutely reliable probability curve from a limited flood record. The record itself may be represented by a "standard" flood-frequency curve; but the corresponding curve for any future "sample" of equal length may be appreciably different within so-called "tolerance limits" or "confidence limits."

It has been pointed out by numerous writers that the probability method is not suitable for the determination of the flood magnitude for design of the spillway of an important dam. As pointed out by the writer, however, in the present paper and on other occasions,(1) probability methods have a proper and useful application in certain fields, particularly in estimating average annual flood benefits for a flood-control project or in the design of cofferdams for sites subject to floods, where precision of the estimate is not of primary importance. For satisfactory determination of flood-insurance rates, some kind of probability estimate is essential. In this case, however, the possible range of the probability estimate between the confidence limits may add appreciably to the risk assumed by the insuring agency.

Mr. Alexander points out the differences of opinion among mathematicians as to the proper method of estimating the confidence limits for a particular record which is essentially a statistical problem. A fellow-countryman of Mr. Alexander(2) has discussed methods for determining such confidence limits for the log-normal and Pearson Type III distributions.

The writer agrees with Mr. Alexander that the method of estimating floods by use of the "maximum possible precipitation" requires clarification, particularly as to its relation to probability estimates. It is understood that a paper by Mr. Alexander discussing this question, together with the interesting subject of the relation of probability estimates to "factors of safety" for dams, will soon be published by the Institution of Civil Engineers of Australia.

Professor Kolupaila's remarks about the writer's 1924 paper are greatly appreciated. The problem of "sampling errors" and confidence limits was not well understood by most engineers and hydrologists 30 years ago. An appreciation of the importance of these problems would doubtless have prevented unsuitable application of the theoretical probability methods in hydrological studies.

---

a. Proc. Paper 1165, February, 1957, by H. Alden Foster.

*Prin. Associate, Parsons, Brinckerhoff, Hall & Macdonald, New York, N. Y.

REFERENCES

1. "Frequency Analyses of Streamflow Data" by David K. Todd, Proc. Paper 1166; discussion by H. Alden Foster, Proc. Paper 1283, June 1957, p. 9.

2. "The Statistical Treatment of Flood Flows"; P. A. P. Moran; Trans. AGU, Aug. 1957, p. 519.

A HIGH-HEAD CAVITATION TEST STAND FOR HYDRAULIC TURBINES[a]

Discussion by Robert T. Knapp

ROBERT T. KNAPP,[1] M. ASCE.—The authors are to be congratulated upon the design and construction of a fine cavitation laboratory for the testing of hydraulic turbines. Their careful planning should pay dividends for a long time. The design of the dynamometer and the method of mounting the test machine are particularly noteworthy. There are many other nice things that can be said about this new laboratory. However, in a discussion it sometimes seems more fitting to raise differences in viewpoint.

One of the possibilities sacrificed in the unique turbine mounting is that of visual observation of cavitation in the wicket gates or in any part of the installation except the draft tube and the discharge edges of the runner vane. This may be serious in the use of the laboratory as a development tool. Another unfortunate limitation, in the writer's opinion, is that the test machine cannot be operated as a pump and that transient conditions cannot be investigated. This seems unfortunate in light of the growing interest in pump-turbines.

The writer is surprised at the weight put on the simulation of field test techniques. Such techniques are often dictated by necessity rather than by desirability. It should not be difficult, with properly selected instruments, to get at least equal accuracy and reliability with one operator, with or without an assistant, and possibly require less time to make the same run. In this connection, it would be interesting to know whether the laboratory has a planned program for the regular recalibration of the venturi meters by the same agencies using the same test installations that were employed in the original calibration. Such a program would appear necessary if the quantity measurements are to be maintained at the same high standard of accuracy as that obtainable with the other test measurements.

The writer does not feel that it is permissible to adjust the air content solely on the basis of preventing the accumulation of air in the manometer connections. Unfortunately, there is as yet not enough known about the relationship between air content and cavitation performance to establish a better criterion. It is hoped that the laboratory operators will bear this possible relationship in mind so as not to become too enamoured of their current technique.

The samples of test results presented in Figs. 4 and 5 are very interesting. The authors are to be complimented on not using a "step-up" factor on their measured efficiencies. At the Reynolds numbers at which these tests were made a step-up would be questionable. The paper seems to imply that

---

a. Proc. Paper 1201, April, 1957, by W. G. Whippen and G. D. Johnson.
1. Prof., Hydr. Eng., California Inst. of Technology, Pasadena, Calif.

continuous operation of the turbine at "critical σ " would not produce significant cavitation damage. Further comments on this point would be appreciated. It would be interesting to see "sigma break" curves for a series of turbines of differing designs. The writer is under the impression that it is not uncommon to obtain appreciably steeper breaks. In this connection it would seem desirable to emphasize the authors' warning that if emergency operation at very low sigma values is anticipated, the permissible limits of operation must be based on a complete and reliable set of model test curves covering the sigma values likely to be encountered.

The writer agrees with the authors that it is most desirable to test the efficiency and cavitation performance of hydraulic machines at prototype heads and velocities. He made the same choice in 1933-34 during the design of the Hydraulic Machinery Laboratory of the California Institute of Technology and has yet to regret it. However, it must be remembered that this approach ignores several facets of the cavitation process. For example, the vertical dimensions of large machines are great enough to affect the extent of the areas subjected to cavitation. To simulate these effects model tests at prototype Froude numbers are necessary. But experiments show that such tests also fail to agree with the cavitation performance of the prototype, primarily because they fail to alter the properties of the test liquid to correspond to the changed scale. It is feared that this dilemma will continue to confront not only the authors, but also all other workers in cavitation laboratories for some time to come.

In their concluding paragraphs the authors propose that accurate model tests, carried out in adequate laboratories such as the one they describe, can be substituted for the more expensive and the consuming field tests. In general, the writer agrees with this proposal. He would like to emphasize, however, that such model tests to be acceptable must include all of the hydraulically significant features of the field installation. Furthermore, the model turbine must be a true model of the machine as installed in the field. In many cases this would require the construction of a new model turbine, since the model used in the design study may not be geometrically similar to the turbine as installed. Two common deviations from similarity are: (1) design changes introduced between the model test and the prototype construction, and (2) errors introduced in the manufacture and installation of the full-sized machine that cause it to differ from the final design drawings. In the opinion of the writer, if model acceptance tests are to replace field tests, the laboratory responsible for making these tests should also have the responsibility of ascertaining and certifying to the geometric similarity of the model and field installations, as well as to the laboratory accuracy of the test measurements.

THE EFFICACY OF FLOOR SILLS UNDER DROWNED HYDRAULIC JUMPS[a]

Discussion by Alvin J. Peterka, Alfred C. Ingersoll, and S. Leliavsky

ALVIN J. PETERKA,[1] M. ASCE.—The conclusions drawn by Mr. Shukry are contrary to general practice procedures which have been developed over a period of years from hydraulic laboratory tests, prototype tests, and other prototype experiences. From a limited number of velocity measurements on a small hydraulic model, Mr. Shukry has concluded that a sill placed near the middle of the apron is in the optimum position. His conclusion is based on an unproved assumption that "The efficiency of any sill against bed erosion is indicated by the rate of adjustment of the flow to the normal distribution in the downstream channel." In addition, the tests were conducted on a fixed-bed model where erosion could not be measured, and the conclusions are contrary to test results obtained from a movable bed model of the same structure, Figure 2.

It is not clearly stated in the paper whether the difficulty in reconciling erosion test results was between several models of the same structure or between the models and the prototypes. The "erratic results" of the prototype scour tests are not described. It is not clear, therefore, why Mr. Shukry abandoned the conventional movable bed tests and used velocity traverses to indicate scour tendencies. It is also not clear why Mr. Shukry has mathematically defined a scour hole since he used a fixed-bed model in his tests. However, certain impressions are obtained in reading this paper, and it is on these impressions the writer must base his discussion.

The fact that agreement between model and prototype erosion tests was not found may be due to any one of several factors. It should be remembered that models are mechanical devices and that the interpretation of the model test results is often as important as the model itself. A 3-bay model will represent a 46-bay prototype spillway only if all factors concerning operating procedures are considered. By proper selection of model scale and bed material size, it is possible to predict qualitatively where the most severe erosion will occur in a prototype structure. It is also possible to construct several or more models of the same structure and obtain identical erosion patterns. Contrary to the statement in the paper, it is possible, therefore, to obtain qualitative similarity between model and prototype and between different models of the same structure. On the other hand, it is not generally believed that an ordinary movable bed model can be used to determine quantitative

a. Proc. Paper 1260, June, 1957, by Ahmed Shukry.

1. Hydr. Engr., Bureau of Reclamation, U. S. Dept. of the Interior, Denver, Colo.

erosion test results that are directly transferable to the prototype structure. Mr. Shukry infers in his paper that this was to be expected.

If prototype erosion was greater than that predicted by the original sectional model, unsymmetrical operation of the 46 bays could have produced almost any conceivable scour pattern. Degradation of the prototype riverbed could also account for lack of agreement between model and prototype erosion patterns. Clear water released from a reservoir tends to pick up a silt load as soon as possible. The riverbed below a dam is sometimes attacked in this manner when the bed material is very fine. This action has nothing in common with the erosive action encountered downstream from stilling basins. Prototype riverbeds have been lowered several feet in a few years as a result of degradation.

Mr. Shukry states that for the Edfina barrage and others that the best location for the sill is in the middle of the floor. This statement is meaningless unless the length of the solid floor is defined in terms of the flow depth or in some dimensionless number. Sufficient data are not presented to allow the reader to compute the probable length of apron required, but it appears from Figure 1 that the aprons are longer than those usually required for discharges and heads of this magnitude. For example, it appears that a floor extending to Section IV or V, Figure 1a, would provide a sufficiently long paved floor. A sill at the end of the apron and riprap downstream from the sill would ordinarily provide ample protection to the riverbed, since the total energy in the flow is relatively small.

A sill is most effective in preventing scour when it is located so that mild bottom velocities strike the sill and are directed away from the riverbed in a positive and gentle manner. Near-zero velocity then prevails at the bed and water interface and optimum conditions for the prevention of scour are present. With the sill located in the middle of the apron, a redistribution of velocity occurs before the flow contacts the riverbed and possibly before a boundary layer is established, resulting in greater scour. Broad sloping sills usually produce weaker ground rollers than steep sills, reducing the circulation and loss of bed material at the end of the apron. A properly shaped dentated sill also helps to produce zero velocity at the interface and a negligible ground roller. Scores of stilling basins with dentated sills have been tested in various laboratories and have been found to be superior to solid sills.

It should also be pointed out that the action described on the Edfina apron should not be classed as hydraulic jump action. It appears (sufficient data are not given) that the Froude number of the incoming flow is very low, perhaps no greater than 2. In a hydraulic jump, the energy loss is only 6 percent of the total when the Froude number is 2. If the jump is drowned, the loss would be even less. The action on the apron in the Edfina tests would probably be better described, therefore, as a roller action where energy loss is related to the turbulence developed on the apron. Statements concerning the shape and placement of sills should therefore be applied, at best, to the structures tested and should not be considered to be generally true for hydraulic jump aprons.

ALFRED C. INGERSOLL,[1] M. ASCE.—In this paper Mr. Shukry has contributed greatly to the hudraulic designer's understanding of the effectiveness

1. Associate Prof. of Civ. Eng., California Inst. of Technology, Pasadena, Calif.

of barrage floor sills at various locations in minimizing downstream scour. The need for a clarification of the previously existing multifarious and conflicting design criteria is admirably demonstrated by the tests on a movable bed model of the old Esna Barrage. The model tests predicted scour behavior that has been largely refuted by experience on full-scale structures.

As sound as the author's principal conclusion - that anti-scour sills can be investigated by means of fixed-bed model studies - appears to be, it is nontheless unfortunate that no case is cited wherein either a movable-bed model or a prototype structure behaves clearly according to the fixed-bed predictions. It is true that the fixed-bed studies on the Edfina Barrage seem to bear out the earlier of the two sets of movable-bed studies, but the more recent set of tests, shown in Fig. 2, gives results diametrically opposed to the conclusions of the fixed-bed studies, with the mid-floor (or edge) position of the sill being the best by one test method and the worst by the other. It would seem that this all-important question cannot be truly resolved until the behavior of this and similar prototype structures can be observed.

In Eq. (6) the author appears to have evolved an expression for the shear stress that is independent of the viscosity or Reynolds number, and he therefore proceeds to apply the Froude law to the fixed-bed model studies, comparing one model test qualitatively with another, to predict which prototype structure will experience the least scour. The writer feels that there is a danger in this, and that it lies in the effect of the Reynolds number upon the velocity distribution (especially that downstream) and consequently upon β and therefore upon τ_0.

Although the analogy is admittedly rough, one may seek a relation between β and R from information on smooth pipes. Inasmuch as the scale of the Edfina Barrage model is 1:66.7, the Reynolds number scale, when tested by the Froude law, is $1:(66.7)^{3/2}$ or 1:543. As shown by Rouse,[1] the variation to be expected in β for this change in Reynolds number is on the order of from 1.01 at the prototype scale to 1.03 at the model scale.

While this magnitude of difference in itself may be negligible, it may be observed that it probably applies more to the downstream condition, e.g. Station VII, than to the upstream condition at Station I. That is, the velocity distribution immediately downstream from the gate is affected most by the gate opening and position, the viscous forces having little opportunity to come into play in the short distance before Station I. As the flow continues over the long floor and the bed-protection works, however, the viscous forces tend to establish a more normal velocity distribution, as is shown in Fig. 6. Thus when the slightly differing values of β_2 are subtracted (as in Eq. 6) from a value of β_1 which is the same for both model and prototype, the resulting difference in τ_0 could be significant. The net effect of this would be for the prototype to develop a higher relative bed shear stress than the model and it could conceivably occur that fixed-bed model studies of competing prototype designs would lead to an erroneous evaluation on this account.

The curves of Fig. 7 are especially interesting to the student of open-channel hydraulics. The rising surface profiles for tranquil flow over a horizontal bed are, of course, impossible for normal channel velocity distributions. For the marked maldistributions observed, however, the validity of these profiles may be confirmed by an energy analysis applied to the reach between Stations I and VII.

Considering condition (a), with discharge passed under the gate, the velocity distribution curve at Station VII may be analyzed to yield a value for the energy correction factor,

$$\alpha = \frac{\int_o^Y \int_o^b v_x^3 \, dz \, dy}{V_x^3 \; b \, Y} \tag{1}$$

of 1.32. With a depth of 4.50 meters and average velocity of 2.13 ms. per sec, the specific energy,

$$E_o = Y_o + \alpha \frac{V_o^2}{2g} \tag{2}$$

is 4.81 ms.

Allowing for a reasonable loss of, say, 5 cm between Stations I and VII, the specific energy at Station I must be about 4.86 ms. From Fig. 7(a) the depth at I may be scaled at 0.68 x 4.50 or 3.06 ms. The kinetic energy must then be 1.80 ms. Inasmuch as the average velocity at this section is 3.14 ms. per sec., the velocity head is only 0.501 ms. and clearly this will require a value of α of 1.80/0.501 or 3.59.

Turning to the velocity distribution diagram for Station I of Fig. 6(a), it is possible to compute a value for α by scaling the diagram, provided it be assumed that this diagram is representative of the velocity distribution across the entire 10.5-meter width of one vent and pier. The value of α so obtained is approximately 2.92, not sufficient to account for the high kinetic energy of 1.80 meters.

The explanation for this discrepancy seems to lie in the lateral distribution of velocity as it is badly distorted at the downstream edge of the 2.5-meter wide pier, just at Station I. If, then one assumes that the distribution diagram shown applies only to the 8-meter width of the channel upstream, while the average velocity, V, applies to the full 10.5-meter width downstream, the value of α becomes 4.85. This is indeed more than enough to account for the kinetic energy. The difference between this and the minimum requirement for α of 3.59 is readily absorbed in considering lateral velocity distributions between the two extreme cases postulated.

This paper is extremely valuable in opening new vistas of research, wherein the elusive scour phenomenon can be studied with the fixed-bed model and the pitot tube. It is to be hoped that the author will continue these significant studies and that he will, whenever possible, relate the predictions so obtained to observations of scour on prototype structures.

REFERENCES

1. "Engineering Hydraulics," edited by Hunter Rouse, John Wiley & Sons, Inc., New York, N. Y. 1950 Fig. 9, p. 401.

S. LELIAVSKY*.—For over twenty years the writer held the post of Director, Designing Service, in the Department in charge of the construction

*Civ. and Hydr. Eng., formerly in the employ of the Egyptian Government.

and remodelling of the barrages shown in the authors Fig. 1, and in this capacity, he ventures to make some constructive remarks about Professor Shukry's interesting and timely paper.

The authors' argument is roughly this: since it is impossible to reproduce in the model the true ratio of the structural dimensions of the prototype to the size of the particles of the granular soil, let us drop this material altogether, and carry out the model tests within rigid boundaries, deriving our conclusions from the observed behaviour of the flowing water.

This is not a new approach, but it was usually believed to be particularly suitable for simpler structures, such for instance, as the Gully Control works, which were the subject of the experiments of B. T. Morris and D. C. Johnson(1); but whether it is also applicable to works of the size and importance of the Nile Barrages—on the safety of each of which may easily depend the welfare of as much as a million rural population—is a matter requiring much thought, and consideration of the various aspects of the relevant problems.

Had the author been personally responsible for such designs, he would have certainly realised the complexity of these problems and might have then, very probably, abstained from veiled complaints against the alleged monotony of the adopted design solutions. (Which remark should not be interpreted as adverse criticism, but only as an attempt to clarify the writers argument.)

Let us begin with the Assiut Barrage (d in Fig. 1) the remodelling of which was the first among the large Nile Works, to be designed according to model tests completed before the drawings were prepared and actual work began. The author has envisaged, in his experiments, three alternatives—flow above, in between and below the gates—but he has not considered the fourth alternative, i.e., flow above the undergate weir; and yet, such a weir formed (according to the model tests referred to) a significant part of the anti-scour-devices arrangement, adopted for the remodelling of this work.

Originally, the object of this weir was a matter of gate design. In fact, the new regulation order, for which the Barrage was then being remodelled, called for a greater total height of obstruction than the old one, but the permissible height for the new gates was limited by considerations pertinent to the housing space available behind the parapet. Hence the weir.

But when the consulting engineers, Messrs. Coode, Wilson, Mitchell and Vaughan Lee, suggested metal trestles above the parapet level and in spite of strong opposition the suggestion was adopted (see Fig. 2),(2) the housing space problem was ipso facto solved, and the weir was therefore capable of being dispensed with.

This should have been, apparently, the proper solution from the hydraulic standpoint, since it yielded a more regular pattern of flow lines, but a general analysis of all the then available evidence, derived from numerous model tests with granular material, tended to show the merits of the undergate weir in fighting tail-erosion; and the results in practice, confirmed entirely this conclusion, notwithstanding the fact that it had been derived from experiments with sand, which the author appears to condemn.

In the pre-modelling period, the Inspector in charge lived, during the flood months, in constant terror of what that blessed Barrage would do next, for apart from a permanent scour-hole ("bayarah"), local scour in closer vicinity to the apron was not unfrequent, and had to be immediately levelled out with rubble-stone dipped from barges, of which more than 130,000 cub.met.

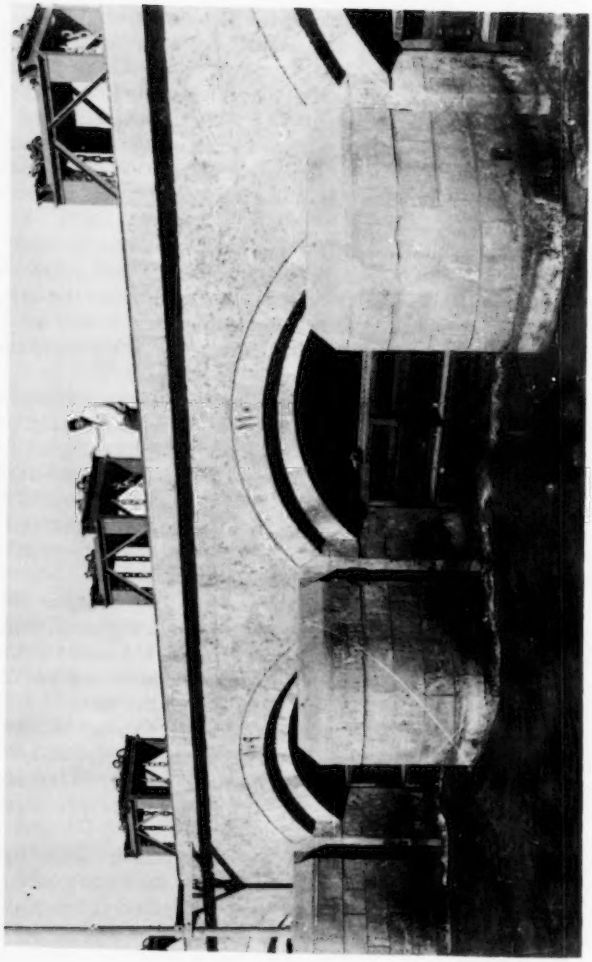

Fig. a

had been thrown into the water, since the barrage had been built. Little wonder, therefore, that when we saw that after the remodelling, the surface of the earthen channel behind the barrage remained almost scourless, we began believing in miracles.

Of course, model tests with sand are not to be interpreted too literally, but with a certain experience in the subject, you may very well distinguish in examining the information they supply, the basic and substantial, from the accidental and inaccurate. In fact, inconsistencies and inaccuracies in such experiments when they occur are not so much the result of differences in compactness and cohesion and other systematic causes, as the author seems to believe, but are chiefly due to the fact that it is difficult (if not impossible) to reproduce accurately in a very small size experiment, the true case history of the phenomenon.

The only way of dealing with such essentially accidental inaccuracies is to increase the scale of the tests; which means that for important works, such as the Nile Barrages, the scale of an experiment with sand, must not be less than 1/10. This explains that, immediately after the completion of the Assiut Barrage Remodelling, we included in the project of Mohammad Aly Barrages, a generously proportioned test-laboratory, in which such large scale experiments could easily be carried out. It may be unfortunate that, for administrative reasons, this laboratory was not completed, until after the second world war.

Reverting to the author's tests, it might be of interest to find out whether their method is sensitive enough to perceive the effect of the undergate weir on downstream erosion? Additional experiments to clarify this point appear to be, certainly, desirable.

The writer wishes to emphasize that he has no intention whatever of objecting against the author's solution, but he believes that the more usual type of model-test with sand, must take precedence on it, and that the two systems can then be used in parallel, according to a consistent, self-contained program, aiming at mutual verification of the results.

The next important work on the Nile, after the Remodelling of Assiut Barrage was completed, was the construction of the Mohammad Aly Barrages. The hydraulic lay-out of this project, for which the writer was particularly responsible, incorporated two main requirements: -

A) To take advantage of the lesson of Assiut Barrage.
B) To take, also, into account that the backwater curve of the new barrage extended beyond Cairo, a large city with over a million population and many valuable old buildings resting on very dubious, if any, foundations.

Thus, as the yearly flood began to subside and the water table started to receed, frequent instances occurred in which such buildings fell, causing loss of life and property. It was, therefore, essential not to widen the range of water level variations, i.e. reduce the additional heading-up, consequent on the construction of the new barrage, to a minimum.

The success of the solution of this problem deserves, perhaps, being placed on record: during the highest flood after construction, the afflux on this barrage did not exceed 2 cm (3/4"). To achieve this result the writer removed (or smoothed out) all solid surfaces exposed to the direct action of the shock of water, or causing separation of flow from solid boundary.

Thus, though the Remodelling Project of Assiut Barrage was taken as basis, the sill of the hypothetical undergate weir was joined with the

downstream and upstream edges of the floor, by straight lines; thus yielding two sloping surfaces on each side of the highest point under the gates.

Better to explain this semi-intuitive solution, attention is called to Fig. b(3) in which the profiles of the three main Nile Barrages are superposed upon one another. In this drawing, the method of the sloping flour of the Mohammad Aly Barrages, as used in loco of the weir of Assiut Barrage, is quite obvious, and the solution seems to be evident but. . . the writer was, at the time, severely criticized for using it, because it was then alleged that sloping floors intensified downstream scour, and the designs for Gebel Aulia Dam, on the White Nile, which was then in course of construction, were modified accordingly.

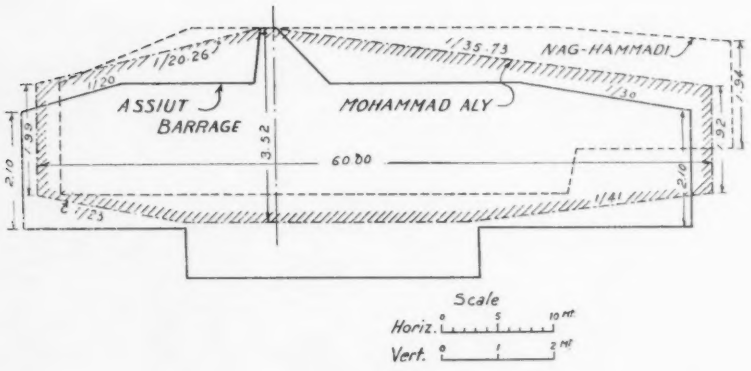

Fig. b

The heresy, in fact, arose from a wrong interpretation of another set of model experiments with sand, and since subsequent practice fully vindicated the writers views on the matter, this problem is another subject on which Prof. Shukry's experiments could throw more welcome, additional light. In fact sloping floors seem not to have been considered by him at all.

It remains to analyse the conditions prevailing at the barrage of Nag-Hammadi (see Fig. 1-e). This is a sui generis case, because the floor of this barrage is built to three different levels (58.50, 59.50 and 60,50 metres above the conventional irrigation datum, which at some time was believed to be the mean sea level at Alexandria).

As regards downstream scour, this floor arrangement is by no means a negligible contingency; in fact, as shown by both, the writer's calculations of the probable depth of scour (see Fig. c),(4) and also by actual soundings taken in the channel of the river, downstream of the apron, the depth of scour decreases gradually with the discharge in the part with the highest floor level, but in the deepest portion of the barrage, it begins to increase again as the river drops to its summer levels.

This is another aspect of the scour problem for the Nile Barrages, which might be covered by Professor Shukry's valuable tests.

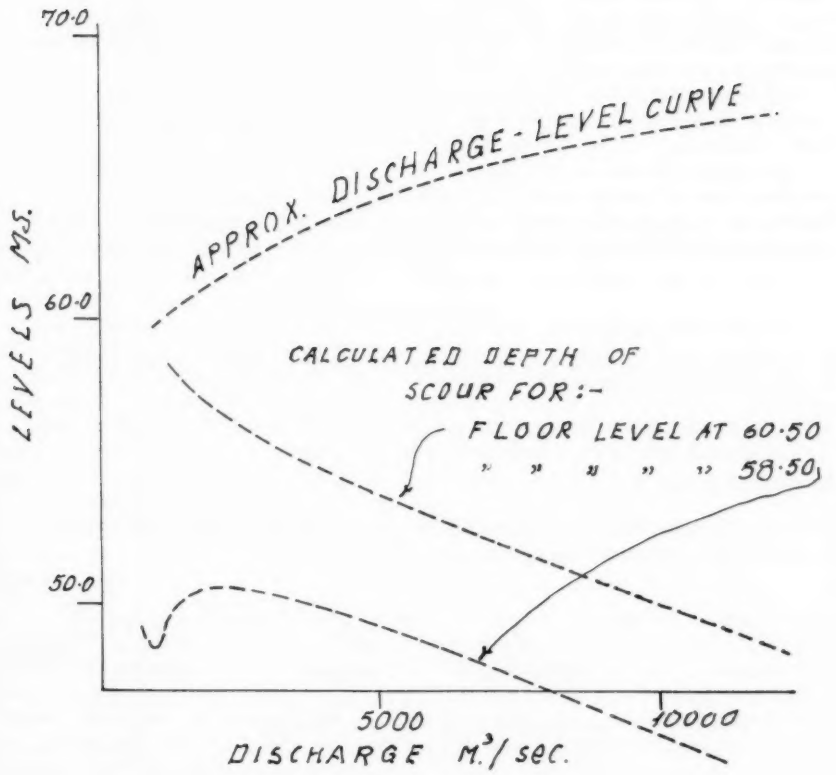

Fig. c

But, the main point on which further experiments of the same type appear to be necessary, is that the scour-hole itself will basically affect the flow pattern, and therefore, to be able to draw significant conclusions from Prof. Shukry's tests, we must possess, in addition to the results obtained for a level channel-bed, full information obtained in the same manner for scour-holes of various depths; viz., using available empirical information on the profiles of the most probable scour-holes, the solid bed, which in these experiments replaces the earthen channel, must be shaped accordingly, and then, tests carried out and diagrams prepared as for a level channel for various assumed depths of the scour-hole. This will then supply exhaustive information on the matter and may, possibly, yield a convincing result.

In fact, it must be realised that scouring action may be started at any time and for any accidental reasons, and we must be sure that if this occurs, the hole will be filled in naturally, or will not attain a dangerous depth, before we have had time enough to fill it in with rubble.

Broadly speaking, the Nile Barrages must not be visualised as granite castles built on a rocky foundation, but rather, as islands made of friable material, which are held in precarious equilbrium, afload on an immense sea of almost oily, semi-liquid misture of water and very fine sediment. Granted that this description is an obvious exaggeration, from the designers standpoint the exaggeration is in the right direction.

Every precaution must, consequently, be taken to ensure stability of granular material, and departures from established practice must be carefully considered.

The writer, therefore, concludes that it is too early to dispense with the standard type of model-tests with sand altogether, replacing them by Professor Shukry's interesting method; but this last method must be used to interpret, and sometimes explain, the older type of such experiments.

REFERENCES

1. "Hydraulic Design of Drop Structures for Gully Control," Trans. ASCE., Vol. 108, pp. 887 and foll.

2. From S. Leliavsky, "Irrigation and Hydraulic Design," Vol. II, 1957, Ed. Chapman & Hall Ltd., London, Fig. 82.

3. Leliavsky, loc. cit., Fig. 123.

4. Fig. c is computed from Figs. 170 to 172 in the same book referred to in Reference 2, but in Vol. I, pages 218-220.

STILLING BASIN EXPERIENCES OF THE CORPS OF ENGINEERS[a]

Discussion by Alvin J. Peterka

ALVIN J. PETERKA,[1] M. ASCE.—The paper by Mr. Berryhill is an excellent summary of "how things have worked out." With a few exceptions, it appears that design procedures based on hydraulic model tests have provided relatively trouble-free operation.

The writer wishes to raise a question, however, concerning the proper depth of tail water, D_2, for a stilling basin containing baffle piers. It has been common practice in some offices to reduce the conjugate depth, D_2, by 10 to 20 percent because of the restraining effect of the baffle piers. Certain economies result; the basin floor may be set at a higher elevation reducing excavation costs, and the training walls may be correspondingly reduced in height. In some cases these savings result in a lowered basin cost. In other cases, however, the savings, in terms of other costs, are minor.

In either case, the writer believes that full conjugate depth or more (about 10 percent more) should be used when setting the floor elevation, for the following reasons:

1. The safety of the entire structure may hinge on whether the baffle piers remain fully effective after they have been subjected to the wear of abrasion and/or the erosion caused by cavitation. Rounded baffle piers are considerably less effective than square-edged piers and only nominal damage may render the baffle piers ineffective. With the baffle piers ineffective, the apron is too high and the tail water too low to produce the proper jump action. Dangerous riverbed erosion may result. Difficulties typical of a high apron are illustrated by Lock and Dam No. 1, Missouri River and Bull Shoals Dam.

2. Due to degradation of the river channel after the dam is constructed, the tail water elevation becomes progressively lower over a period of years, reducing the factor of safety against jump sweepout and lowering the efficiency of the jump. On the other hand, an apron designed for conjugate depth will operate properly even if the baffle piers are not replaced.

3. Experience has shown that actual tail water elevations are often lower than the computed values, used for design or model testing of the basin. This may have been true for Kanopolis Dam, which was found by the author to be operating at 0.7 D_2. Unless the tail water curve is known to be correct, extra tail water depth should be provided in the design.

4. In the temporal sense, the actual tail water depth lags the depth shown on the tail water curve during periods of increasing discharge. On some

a. Proc. Paper 1264, June, 1957, by R. H. Berryhill.

1. Hydr. Engr., Bureau of Reclamation, U. S. Dept of the Interior, Denver, Colo.

rivers, it may take several hours for the tail water to stabilize after the discharge is set. When it is necessary to open spillway gates rapidly, the basin must be capable of performing satisfactorily with tail water elevations below the stable values.

5. A slightly drowned jump, in the writer's opinion, produces a better all-around energy dissipator than one at conjugate depth. The slight loss in efficiency (energy dissipation) is more than offset by the smoother downstream water surface conditions and the reduction in splash and surging. A slight excess of tail water also moves the toe of the jump against the sloping face of the spillway (if one is present), stabilizing the jump and producing smoother overall operation.

On the Center Hill, Conchos, Norfork and Fort Gibson Dams, Mr. Berryhill describes damage caused by bed meterial or other debris circulating on the apron. The writer has also witnessed damage of this type on other structures and feels that abrasion damage is more wide spread than generally believed. Every effort should, therefore, be made, particularly by those engaged in hydraulic model testing to eliminate "dead" areas in basins where debris may become trapped. Insofar as possible, basins or buckets should be made self-cleaning and the bed material just downstream from the end sill should be stabilized or reduced in elevation to prevent bed material from being swept into the basin during periods of necessary unsymmetrical operation. It has been common practice on model tested basins to use an end sill which creates a ground roller and moves bed material upstream against the end sill to prevent undermining of the apron. The writer believes that strong ground rollers should be avoided by providing end sills with flatter slopes or dentated or notched sills which tend to neutralize the upstream motion. With continued motion of the bed material against the end sill, some bed material is bound to find its way into the basin and become the source of abrasion damage.

In discussing the damage at Lucky Peak Dam, Mr. Berryhill indicates that perhaps the damage was similar to that found in laboratory tests on concrete specimens subjected to the impingement of high velocity jets. In the case of the laboratory tests, the damaged area was in the form of an annular ring adjacent to the impingement area. The writer believes that at Lucky Peak Dam the damage resulted from an entirely different cause since the damage was located some distance from the impinging jet. It is very possible that a vortex formed at the upstream corners of each slide gate, similar to those which form behind radial gates on a spillway. At small gate openings, the low pressure core of the vortex was directed toward the floor, as mentioned by Mr. Berryhill, and deflected inwardly by the gate slots. Cavitation then occurred in the vortex core near the floor. Downstream, a high pressure area collapsed the cavities and damage resulted as shown in the photographs. The extreme damage further downstream was probably a progressive result of the damage which began closer to the gate. The eroded areas in Figure 13a indicate that the low pressure area originated behind the gate. The vortex theory should be investigated at the first opportunity in a hydraulic model.

Paper 1492 December, 1957 HY 6

Journal of the
HYDRAULICS DIVISION
Proceedings of the American Society of Civil Engineers

DIVIDED FLOW THROUGH A DIVERGENT INLET CONDUIT*

Stavros Tsakonas,** A.M. ASCE
(Proc. Paper 1492)

SYNOPSIS

This investigation is concerned with the determination of the characteristics of divided flow phenomena. Two models have been analytically and experimentally investigated. One is a conduit with a constant cross-section having an opening perpendicular to its length. The other is a conduit with a divergent inlet having a side opening at the end of the divergent. The analysis is developed by means of the free stream line theory, assuming two-dimensional irrotational flow of an incompressible fluid. The experiments were conducted under approximately two-dimensional flow conditions. The theory, together with the experiments, has shown quantitatively the influence of the velocity distribution in the inlet on the characteristics of the divided flow phenomena.

INTRODUCTION

Efficient diversion of a portion of a main flow for auxiliary purposes is vitally important in designing large scale hydraulic systems. Experiments have shown that a unique angle exists for a branch conduit which will keep losses at a minimum. A conduit with a slit or hole in its side produces a free jet stream at a certain natural angle to the main flow. This angle corresponds to the angle of least loss for the case of a branch conduit.

The objective of this investigation was to determine the parameters affecting this natural angle and other flow characteristics and to study their influence on the jet diverted through the slit opening.

Earlier experimental work(1,2) and analytic studies(3,4,5) have shown that the natural angle and other flow characteristics such as the contraction coefficient, width of jet etc. depend on two factors. These are (a) the geometry of the junction and (b) the ratio (r) of the discharge diverted into the branch to

Note: Discussion open until May 1, 1958. Paper 1492 is part of the copyrighted Journal of the Hydraulics Division of the American Society of Civil Engineers, Vol. 83, No. HY 6, December, 1957.

* The material is essentially an extract of that presented in "Divided Flow Through A Divergent Inlet Conduit," by Stavros Tsakonas; Ph.D. Dissertation, Columbia University, N. Y., October 1956.

** Research Engr., E.T.T. Stevens Inst. of Technology, Hoboken, N. Y.

the total discharge in the main conduit beyond the junction point. Previous scale model tests conducted by the Bureau of Reclamation[6] have shown large discrepancies with the results obtained in small laboratory tests and also have differed with prototype measurements.

At the suggestion of Professor A. Craya, the present study was initiated to determine the influence of the velocity distribution in the upstream sections of the main conduit on the natural angle and other characteristics of the flow diverted through the slit. No known experimental or analytical work had considered this effect in the past.

The problem of a general velocity distribution in a main conduit preceding the junction point is neither theoretically tractable nor experimentally feasible. The mathematical difficulties of the problem are increased greatly because the use of the complex variable technique is not possible in a rotational flow. In addition the problem of altering the velocity distribution at the inlet of the conduit by laboratory means is difficult.[7] However, the use of a divergent inlet conduit offers a means of altering the velocity distribution. The divergent inlet conduit is advantageous in that a small angle of divergence produces considerable changes in the velocity distribution, as shown by Nikuradge.[8] Ordinarily such velocity distribution changes would require an inlet length of 20 to 50 feet before the actual experimental section. The influence of the angle of divergence itself, i.e., in the case of irrotational flow on the jet characteristics can be determined analytically. This influence has been shown to be small for small angles of divergence.

The theoretical part of this investigation dealt with two models. One is a conduit with a constant cross-section and a side opening, while the other is a conduit with a divergent inlet having a side opening at the end of the sloping part. Both cases were investigated as problems in two-dimensional irrotational flow of an ideal incompressible fluid by means of the free streamline theory. The experimental part of this investigation dealt with the same two cases of straight and divergent inlet conduits under approximate two-dimensional flow conditions.

Comparison of theoretical and experimental results obtained for the straight conduit model served to determine the degree of the validity of the free streamline theory together with the previously stated assumptions. The second model with the divergent inlet conduit was used to determine the influence of the non-uniform velocity distributions.

If the deviation between the theory and the experiments in the case of the divergent channel is greater than the differences observed between the theory and the experiments in the case of the straight conduit, this deviation may be attributed to the influence of the velocity distribution. This was assumed since all other parameters (ratio of discharges, geometry of the opening and property of the fluid) were kept constant and only the velocity distribution was changed.

In summary, the present investigation was concerned with:

1. the theoretical determination of the natural angle of the jet and other flow characteristics for divided flow through a conduit with a constant cross-section as well as for a divergent inlet conduit, based on the free streamline theory of irrotational flow;
2. the experimental determination of the natural angle of the jet in both models. The angles used were: $\phi = 0^{o}$, $\phi = 2^{o}45'48''$, $\phi = 6^{o}25'43''$;
3. the magnitude of the influence of the velocity distribution at the inlet on

the characteristics of the jet diverted through the side opening. This also required measurement of velocity distributions in the experiments.

The experimental results showed agreement with the free streamline theory when the velocity distribution at the inlet was uniform as in the case of the straight conduit. However, when the velocity distribution was non-uniform as in the divergent conduit, the experiments showed a deviation from the theory, but they remained similar in their general aspects.

The experiments thus showed that the velocity distribution in a inlet conduit has a definite influence on the flow pattern of a divided flow field.

Analysis

The derivation of a theoretical solution for the flow characteristics of the problem of a divided flow through a divergent inlet conduit will be considered in the following analysis.

The inflow through the divergent channel A'', A' , N and P was divided into a flow through a slit (PQ) and a straight conduit (NBQ) as shown in Figure 1. By successive transformations the physical plane was transformed to the hodograph plane (Figure 2), then to the logarithmic plane (Figure 3), and finally, by the Schwartz - Christoffel transformation, to the ζ -plane (Figure 4) where physical properties of the flow pattern could be identified easily.

By considering the physical plane with a source of strength (q) at the point of intersection of the sides (AP and AN) of the divergent channel, the resulting idealized flow is such that the field of interest is bounded by streamlines along which the velocity is either constant in direction or constant in magnitude. The line AO (O is a stagnation point) is the boundary which divides the flow field into an upper part discharged through the side opening (PQ) and a lower part conveyed through the main conduit (NBQ). The point N is another stagnation point of a different nature since it does not split the flow field.

The hodograph plane represents the complex conjugate velocities of the flow field, hence

$$W = u - iv \ , \tag{1-1}$$

where u and v are the velocity components of the point (x,y) in the z-plane. The logrithmic plane is related to the W-plane by

$$U = \log W. \tag{1-2}$$

The origin is chosen at the point P. This requires the magnitude of the velocity at P to be equal to unity as well as to the points Q and C. This involves no loss of generality.

The ζ -plane is the result of the Schwartz-Christoffel transformation:

$$\frac{dU}{d\zeta} = \rho\, \zeta^{-1/2}(\zeta+\omega)^{-1}(\zeta+\beta)(\zeta+\nu)^{-1}(\zeta+\alpha)^{-1}(\zeta+\mu) \ , \tag{1-3}$$

where ρ is a complex constant and the points Q, P and N have been chosen at $\zeta = 0, \pm\infty, -1$, respectively.

Equation (1-3) may be written in a partial fraction form as

$$\frac{dU}{d\zeta} = \frac{1}{\sqrt{\zeta}}\left(\frac{A}{\zeta+\alpha} + \frac{B}{\zeta+\nu} + \frac{C}{\zeta+\omega}\right) \ , \tag{1-4}$$

where

$$A = \frac{\rho(\alpha-\mu)(\alpha-\beta)}{(\alpha-\omega)(\alpha-\nu)}$$

$$B = \frac{\rho(\nu-\beta)(\mu-\nu)}{(\alpha-\nu)(\nu-\omega)} \qquad (1\text{-}5)$$

$$C = \frac{\rho(\mu-\omega)(\beta-\omega)}{(\alpha-\omega)(\nu-\omega)}$$

Using $t = \sqrt{\zeta}$ and spliting the terms of Equation (1-4) into complex conjugate forms and then integrating them yields:

$$U = \frac{A}{i\sqrt{\alpha}}\log\left(\frac{\sqrt{\zeta}-i\sqrt{\alpha}}{\sqrt{\zeta}+i\sqrt{\alpha}}\right) + \frac{B}{i\sqrt{\nu}}\log\left(\frac{\sqrt{\zeta}-i\sqrt{\nu}}{\sqrt{\zeta}+i\sqrt{\nu}}\right) + \frac{C}{i\sqrt{\omega}}\log\left(\frac{\sqrt{\zeta}-i\sqrt{\omega}}{\sqrt{\zeta}+i\sqrt{\omega}}\right) \qquad (1\text{-}6)$$

The condition $U_p = 0$ at $t = \pm\infty$ has been used to eliminate the constant of integration.

The constants of the transformations have been determined by relating the ζ -plane to the U-plane, since on traversing the boundary in the U-plane the change of arguments of U is known.

Using Equation (1-6) in the following form

$$\arg(U) = \frac{A}{i\sqrt{\alpha}}\arg\left(\frac{\sqrt{\zeta}-i\sqrt{\alpha}}{\sqrt{\zeta}+i\sqrt{\alpha}}\right) + \frac{B}{i\sqrt{\nu}}\arg\left(\frac{\sqrt{\zeta}-i\sqrt{\nu}}{\sqrt{\zeta}+i\sqrt{\nu}}\right) + \frac{C}{i\sqrt{\omega}}\arg\left(\frac{\sqrt{\zeta}-i\sqrt{\omega}}{\sqrt{\zeta}+i\sqrt{\omega}}\right)$$

in order to describe the singular points O, A and N leads to

$$\frac{C}{i\sqrt{\omega}} = 1, \quad \frac{A}{i\sqrt{\alpha}} = -\frac{\phi}{\pi} = -k, \quad \frac{B}{i\sqrt{\nu}} = k \qquad (1\text{-}7)$$

However, it must be kept in mind that the constants A, B and C of the transformation are purely imaginary since ρ can be readily shown to be imaginary.(10)

Combination of Equations (1-5) and (1-7) yields

$$-\frac{1}{\sqrt{\alpha}} = \frac{B}{A} = \frac{(1-\beta)(\mu-1)(\alpha-\omega)}{(\alpha-\mu)(\alpha-\beta)(1-\omega)} \qquad \text{(a)}$$

$$\frac{\sqrt{\omega}}{k} = \frac{C}{B} = \frac{(\mu-\omega)(\beta-\omega)(\alpha-1)}{(\alpha-\omega)(1-\beta)(\mu-1)} \qquad \text{(b)} \qquad (1\text{-}8)$$

where $\nu = 1$ is due to the transformation.

The substitution of $\sqrt{\alpha} = a$ and $\sqrt{\omega} = w$ in Equation (1-8) leads to:

$$\beta = \frac{a^2\mu + a^3 + a\mu w^2 - aw^2(a^2 + a + 1)}{\mu(a^2 + a + 1) - a^2 - \mu w^2 - aw^2} \qquad (1\text{-}9)$$

and

$$k(\mu - w^2)(\mu + a)(a - 1) = w(\mu - 1)(\mu - a^2) \quad . \tag{1-10}$$

Equation (1-10) is quadratic in μ and yields the solution

$$\mu = \frac{-[k(a-1)(a-w^2)+(1+a^2)w] \mp \sqrt{[k(a-1)(a-w^2)+(1+a^2)w]^2+4[k(a-1)-w][k(a-1)aw^2+a^2w]}}{2[k(a-1)-w]} \tag{1-11}$$

where the negative sign is the proper one satisfying the relation $\mu > \alpha$, imposed by the transformation. (See Figure 4)

The complex potential function (Z) in the ζ -plane for a source of strength q at $\zeta = -\alpha$ and sinks of strength q' and q'' at $\zeta = -\beta$ and $\zeta = \gamma$ respectively is given by

$$Z = -\frac{q}{\pi} \log(\zeta + \alpha) + \frac{q'}{\pi} \log(\zeta + \beta) + \frac{q''}{\pi} \log(\zeta - \gamma) \quad . \tag{1-12}$$

The complex conjugate velocity and complex potential are related by

$$W = -\frac{dZ}{dz} = -\frac{dZ}{d\zeta}\frac{d\zeta}{dz} \tag{1-13}$$

Setting W = O at the stagnation point ($\zeta = -\omega$) leads to

$$\frac{\alpha - \beta}{\alpha - \omega} = r\,\frac{\gamma + \beta}{\gamma + \omega} \quad , \tag{1-14}$$

where $r = \frac{q''}{q}$, with r being the ratio of the discharge diverted into the branch to the discharge into the main conduit before the junction point.

Substitution of Equation (1-7) for the values of A, B and C in Equation (1-6) and use of Equation (1-2) gives the velocity at any point in the field by the following:

$$W = \left(\frac{\sqrt{\zeta} + i\sqrt{\alpha}}{\sqrt{\zeta} - i\sqrt{\alpha}}\right)^k \left(\frac{\sqrt{\zeta} - i}{\sqrt{\zeta} + i}\right)^k \left(\frac{\sqrt{\zeta} - i\sqrt{\omega}}{\sqrt{\zeta} + i\sqrt{\omega}}\right) \tag{1-15}$$

As a result of this Equation (1-13) leads to

$$dz = \frac{q}{\pi}\left[\frac{1}{\zeta+\alpha} - \frac{1-r}{\zeta+\beta} - \frac{r}{\zeta-\gamma}\right] G(\zeta)\,d\zeta \quad , \tag{1-16}$$

where

$$G(\zeta) = \left(\frac{\sqrt{\zeta} - i\sqrt{\alpha}}{\sqrt{\zeta} + i\sqrt{\alpha}}\right)^k \left(\frac{\sqrt{\zeta} + i}{\sqrt{\zeta} - i}\right)^k \left(\frac{\sqrt{\zeta} + i\sqrt{\omega}}{\sqrt{\zeta} - i\sqrt{\omega}}\right) \quad .$$

Equation (1-16), which relates the ζ -plane to the physical plane through a differential form, becomes

$$dz = -\frac{q}{\pi}\frac{(\alpha-\beta)(\alpha+\gamma)}{(\alpha-\omega)}\frac{\zeta+\omega}{(\zeta+\alpha)(\zeta+\beta)(\zeta-\gamma)}G(\zeta)d\zeta \quad , \qquad (1\text{-}17)$$

after using Equation (1-14). At this stage of the development the parameters α, ω, and γ are still undetermined. An additional relation between these parameters is evident from the geometry of the configuration shown in Figure 1.

$$AP = \frac{h'}{\tan\phi} \quad ,$$

which, by means of Equation (1-17), yields

$$\frac{(\alpha-\beta)(\alpha+\gamma)}{\alpha-\omega}\frac{\tan\phi}{\pi r}\int_{-\alpha}^{-\infty}\frac{(\zeta+\omega)G(\zeta)}{(\zeta+\alpha)(\zeta+\beta)(\zeta-\gamma)}d\zeta = \frac{h'}{h''} \quad . \qquad (1\text{-}18)$$

Combining the expression of the velocity at B, found from Equation (1-15) for $\zeta = -\beta$, with

$$\frac{V}{1} = \frac{q'/h'}{q''/h''} = \frac{1-r}{r}\frac{h''}{h'}$$

leads to

$$\frac{h''}{h'} = \frac{r}{1-r}\left(\frac{\sqrt{\alpha}+\sqrt{\beta}}{\sqrt{\alpha}-\sqrt{\beta}}\right)^k\left(\frac{1-\sqrt{\beta}}{1+\sqrt{\beta}}\right)^k\left(\frac{\sqrt{\beta}-\sqrt{\omega}}{\sqrt{\beta}+\sqrt{\omega}}\right) \quad . \qquad (1\text{-}19)$$

This relates the width of the diverted jet to the height of the conduit.

Use of Equation (1-19) together with (1-14), changes (1-18) into the form:

$$-\int_{-\alpha}^{-\infty}\frac{(\zeta+\omega)G(\zeta)}{(\zeta+\alpha)(\zeta+\beta)(\zeta-\gamma)}d\zeta = \qquad (1\text{-}20)$$

$$\frac{\pi(\beta-\omega)}{\tan\phi(\alpha-\beta)(\beta+\gamma)}\left(\frac{\sqrt{\alpha}-\sqrt{\beta}}{\sqrt{\alpha}+\sqrt{\beta}}\right)^k\left(\frac{1+\sqrt{\beta}}{1-\sqrt{\beta}}\right)^k\left(\frac{\sqrt{\beta}+\sqrt{\omega}}{\sqrt{\beta}-\sqrt{\omega}}\right) \quad .$$

This integral relation will determine the parameter γ for given α, β, ω.

Using the intermediate relation

$$q = \frac{h''}{r} = h'\frac{(\alpha-\omega)(\beta+\gamma)}{(\alpha+\gamma)(\beta-\omega)}\left(\frac{\sqrt{\alpha}+\sqrt{\beta}}{\sqrt{\alpha}-\sqrt{\beta}}\right)^k\left(\frac{1-\sqrt{\beta}}{1+\sqrt{\beta}}\right)^k\left(\frac{\sqrt{\beta}-\sqrt{\omega}}{\sqrt{\beta}+\sqrt{\omega}}\right),$$

the width of the slit is given by Equation (1-21) after the integration of Equation (1-17) from $\zeta = 0$ to $\zeta = +\infty$.

$$\frac{\ell}{h'} = \frac{(\beta+\gamma)(\alpha-\beta)}{\pi(\sqrt{\beta}+\sqrt{\omega})^2}\left(\frac{\sqrt{\alpha}+\sqrt{\beta}}{\sqrt{\alpha}-\sqrt{\beta}}\right)^k\left(\frac{1-\sqrt{\beta}}{1+\sqrt{\beta}}\right)^k(-1)\int_0^{\infty}\frac{(\zeta+\omega)G(\zeta)}{(\zeta+\alpha)(\zeta+\beta)(\zeta-\gamma)}d\zeta \quad (1\text{-}21)$$

The position of the stagnation point of the flow pattern is given by:

$$S = -\frac{q}{\pi}\frac{(\alpha-\beta)(\alpha+\gamma)}{\alpha-\omega}\int_{-\omega}^{0}\frac{(\zeta+\omega)G(\zeta)d\zeta}{(\zeta+\alpha)(\zeta+\beta)(\zeta-\gamma)} \quad . \quad (1\text{-}22)$$

The contraction coefficient "c" of diverted flow is defined as

$$C = \frac{h''}{\ell} \quad , \quad (1\text{-}23)$$

where ℓ and h'' are given by Equation (1-21) and Equation (1-19), respectively.

The angle of the diverted jet at ∞ is given by setting $\zeta = \gamma$ in Equation (1-15)

$$W_c = \left(\frac{\sqrt{\gamma}+i\sqrt{\alpha}}{\sqrt{\gamma}-i\sqrt{\alpha}}\right)^k\left(\frac{\sqrt{\gamma}-i}{\sqrt{\gamma}+i}\right)^k\left(\frac{\sqrt{\gamma}-i\sqrt{\omega}}{\sqrt{\gamma}+i\sqrt{\omega}}\right) = e^{-i\theta} \quad .$$

Since $W_c = |v_c|\, e^{-i\theta}$ and $|v_c| = 1$,

then

$$e^{-i\theta} = e^{i2k\tan^{-1}\frac{\sqrt{\alpha}}{\sqrt{\gamma}} - i2k\tan^{-1}\frac{1}{\sqrt{\gamma}} - i2\tan^{-1}\frac{\sqrt{\omega}}{\sqrt{\gamma}}} \quad .$$

Taking the principal values of the multivalued functions, the angle of the impinging jet is given by

$$\theta = 2k\tan^{-1}\frac{1}{\sqrt{\gamma}} - 2k\tan^{-1}\frac{\sqrt{\alpha}}{\sqrt{\gamma}} + 2\tan^{-1}\frac{\sqrt{\omega}}{\sqrt{\gamma}} \quad . \quad (1\text{-}24)$$

The analysis developed thus far permits determination of all characteristics of the flow pattern providing the ratio of discharge and the geometry of the configuration are known.

For simplicity the following method of computation was adopted in this investigation.

Assuming values of $\alpha > 1$ and $0 < \omega < 1$, μ was determined by Equation (1-11), β by Equation (1-9) and γ by the integral relation of Equation (1-20). The flow characteristics and the corresponding boundaries were obtained as follows:

θ by Equation (1-24), ℓ/h by Equation (1-21), C by Equation (1-23), h''/h' by Equation (1-19), S by Equation (1-22) and r by Equation (1-14). This computation procedure has the advantage of eliminating all but one of the integral relations between the parameters. The integral relation which must be used is given by Equation (1-20).

2 - Solution for a Straight Conduit

Using the expression evolved for the general case of the divergent inlet channel, the flow characteristics for the straight conduit ($k = \frac{\phi}{\pi} = 0$) will be developed.

For the case of k = 0 Equation (1-11) gives

$$\mu = 1 \quad \text{or} \quad \mu = \alpha .$$

The former case requires $\mu = \alpha = \beta = \omega = 1$ and is a special case which will be discussed later. The latter case ($\mu = \alpha$) requires $\beta = 1$, thus allowing Equation (1-15) to be reduced to

$$W = \frac{\sqrt{\zeta} - i\sqrt{\omega}}{\sqrt{\zeta} + i\sqrt{\omega}} \quad . \tag{2-1}$$

When $\zeta = -\beta = -1$ and $\zeta = -\alpha$, Equation (2-1) becomes, respectively,

$$W_B = \left|V_B\right| = \frac{1 - \sqrt{\omega}}{1 + \sqrt{\omega}}$$

and

$$W_A = \left|V_A\right| = \frac{\sqrt{\alpha} - \sqrt{\omega}}{\sqrt{\alpha} + \sqrt{\omega}} \quad .$$

Using the latter expressions, h and h' can be determined as

$$h = \frac{q}{V_A} = q\,\frac{\sqrt{\alpha} + \sqrt{\omega}}{\sqrt{\alpha} - \sqrt{\omega}}$$

and

$$h' = \frac{(1-r)q}{V_B} = q(1-r)\,\frac{1 + \sqrt{\omega}}{1 - \sqrt{\omega}} \quad . \tag{2-2}$$

Since h = h' , Equation (2-2) takes the form

$$\frac{(\sqrt{\alpha} + \sqrt{\omega})^2}{\alpha + \gamma}\;\frac{(1 + \sqrt{\omega})^2}{1 + \gamma} \tag{2-3}$$

after using Equation (1-14). Once the values for α and ω are chosen, the value of γ may be obtained from Equation (2-3).

The angle of diverted jet is determined by Equation (1-24) as

$$\theta = 2\,\tan^{-1}\frac{\sqrt{\omega}}{\sqrt{\gamma}} \quad . \tag{2-4}$$

The corresponding ratio of discharges is given by Equation (1-14) as

$$r = \frac{\alpha - 1}{\alpha - \omega} \frac{\gamma + \omega}{\gamma + 1} \tag{2-5}$$

The width of the slit, upon integration of Equation (1-14)[10] leads to:

$$\ell/h' = \frac{1}{\pi(1+\sqrt{\omega})^2(\alpha+\gamma)} \left[(\alpha+\omega)(\gamma+1)\log\alpha - (\gamma-\omega)(\alpha-1)\log\gamma + 2\sqrt{\omega}\sqrt{\gamma}(\alpha-1)\pi\right] \tag{2-6}$$

The corresponding contraction coefficient given by

$$C = \frac{\pi(\alpha-1)(\gamma+\omega)}{(\alpha+\omega)(\gamma+1)\log\alpha - (\gamma-\omega)(\alpha-1)\log\gamma + 2\sqrt{\omega}\sqrt{\gamma}(\alpha-1)\pi} \tag{2-7}$$

and the ratio of the width of the jet to the height of conduit is determined by Equation (1-19) as

$$\frac{h''}{h'} = \frac{(\alpha-1)(\gamma+\omega)}{(\alpha+\gamma)(1+\sqrt{\omega})^2} \quad . \tag{2-8}$$

Two limited cases ($r = 1$ and $\alpha \to \infty$ with $0 < r < 1$) were investigated and are described as follows:

1) Case $r = 1$,

$$\text{then } \omega = 1 \quad \text{and} \quad \gamma = \frac{4\alpha - (\sqrt{\alpha}-1)^2}{(\sqrt{\alpha}+1)^2 - 4} \quad . \tag{2-9}$$

If $\alpha \to 1$,

$$\text{then} \quad \lim_{\alpha \to 1} \gamma = 1$$

and

$$\theta = 90^\circ \quad \lim_{\alpha \to 1} \frac{\ell}{h'} \to 0 \quad \text{and} \quad C = \frac{\pi}{2+\pi} = 0.611 \quad . \tag{2-10}$$

This limiting case corresponds to a flow through an orifice on an infinitely large container.

If $\alpha \to \infty$

$$\text{then } \lim_{\alpha \to \infty} \gamma = 3, \quad \theta = 60^\circ, \quad \lim_{\alpha \to \infty} \frac{\ell}{h'} \to \infty \quad ,$$

independently of the values of γ and ω,

$$\text{and} \quad \lim_{\alpha \to \infty} C = 0.$$

This case ($r = 1, \alpha \to \infty$) corresponds to the flow pattern through an orifice, the dimensions of which may be considered infinitely large in respect to the height of the conduit. The jet is diverted through an angle of 60° without any contraction.

2) Case $\alpha \to \infty$ and $0 < r < 1$,

then parameters γ and ω are determined, respectively, by

$$\frac{1-\sqrt{\omega}}{1+\sqrt{\omega}} = 1 - r \qquad \text{and} \qquad \frac{(1+\sqrt{\omega})^2}{1+\sqrt{\gamma}} = 1$$

and the characteristics of the flow field are determined by Equations (2-4), (2-6), (2-7) and (2-8). Noticing that ω decreases to zero faster than γ, it follows from the characteristic relations of the flow pattern that $\theta = 0$, $\frac{h''}{h'} = 0$ and $C = 0$ independently of the values ℓ / h', when $\omega = 0$.

The case $\alpha \to \infty$ corresponds to an orifice with an infinitely large opening compared to the height of the conduit. The jet is diverted without any contraction and the quantity h''/h' takes a maximum value for each ratio of discharge. The jet emerges through the free surface in the vicinity of the downstream edge of the slit which extends an infinite distance from the upstream leading edge.

Results for a straight conduit solution as well as for its limiting cases, are plotted in Figures 5, 6 and 7. Although it does not seem possible to show the identity of the expressions developed in the present analysis with the corresponding expressions developed by Craya[3] and McNown,[5] the plotted results show complete agreement with Craya's results and good agreement with McNown's results. The small discrepancy in the latter case is probably due to the fact that, in reducing the results to the same basis, use was made of values obtained from the graphs plotted by McNown.

3 - Solutions for a Small Angle of Divergence

After the successive transformations of $\zeta = -\sigma$ and $\sqrt{\sigma} = t$ the integral relation (1-20), which determines the parameter γ, leads to

$$2\int_{\sqrt{\alpha}}^{\infty} \frac{t(t+\sqrt{\omega})^2}{(t^2-\alpha)(t^2-\beta)(t^2+\gamma)} \left(\frac{t-\sqrt{\alpha}}{t+\sqrt{\alpha}}\right)^k \left(\frac{t+1}{t-1}\right)^k dt = \frac{\pi(\sqrt{\beta}+\sqrt{\omega})^2}{\tan\Phi(\alpha-\beta)(\beta+\gamma)} \left(\frac{\sqrt{\alpha}-\sqrt{\beta}}{\sqrt{\alpha}+\sqrt{\beta}}\right)^k \left(\frac{1+\sqrt{\beta}}{1-\sqrt{\beta}}\right)^k \tag{3-1}$$

Upon integration and substitution for β by Equation (1-9) this takes the form

$$f(\alpha, \gamma, \omega, k) = \Phi(\alpha, \gamma, \omega, k). \tag{3-2}$$

Having these two functions $f(\alpha, \gamma, \omega, k)$ and $\phi(\alpha, \gamma, \omega, k)$ which are

analytic functions of k in some common region (R) with respect to all parameters (α, γ, ω) and the independent variable k, we actually postulate that only on some surface $S(\alpha, \gamma, \omega)$, which belongs to the regions of analyticity, does the equality (3-2) hold. The functions may be expressed as power series in k in the region of common analyticity:

$$f(\alpha, \gamma, \omega, k) = A_o(\alpha, \gamma, \omega) + A_1(\alpha, \gamma, \omega)k + A_2(\alpha, \gamma, \omega)k^2+\ldots$$

$$\Phi(\alpha, \gamma, \omega, k) = B_o(\alpha, \gamma, \omega) + B_1(\alpha, \gamma, \omega)k + B_2(\alpha, \gamma, \omega)k^2+\ldots$$

Then on the surface (S), the equality (3-2) implies that coefficients of like powers of k are equal

$$A_o(\alpha, \gamma, \omega) = B_o(\alpha, \gamma, \omega) \qquad \text{(a)}$$

$$A_1(\alpha, \gamma, \omega) = B_1(\alpha, \gamma, \omega) \qquad \text{(b)} \qquad (3\text{-}3)$$

$$A_2(\alpha, \gamma, \omega) = B_2(\alpha, \gamma, \omega) \qquad \text{(c)}$$

Equations a, b, c, etc. define several surfaces in α, γ, ω space. If any two of the surfaces differ they may or may not intersect. If they do intersect, Equation (3-2) would apply only to restricted values of one of the parameters, namely those satisfying the equation of the intersection. However, this contradicts the postulate based on physical grounds that no restriction exists on any of the parameters in the region P of the analyticity.

If the surfaces do not intersect, no values of the parameter exist which are common to both surfaces. Hence, there is no surface for which (3-2) holds. This also contradicts the postulate that $S(\alpha, \gamma, \omega)$ must exist.

Consequently, the remaining equations in (3-3) must be identically satisfied or equivalent to (3-3a) which is the only one that specifies $S(\alpha, \gamma, \omega)$.

Equation (3-1), expressed in k powers with attention being concentrated on only the first term,(10) leads to:

$$\frac{1}{k}\,\frac{(\sqrt{\alpha}+\sqrt{\omega})^2}{(\alpha-\beta)(\alpha+\gamma)} + E_1(\alpha, \beta, \gamma, \omega)+kE_2(\alpha, \beta, \gamma, \omega)+\ldots =$$

$$\frac{1}{k}\,\frac{(\sqrt{\beta}+\sqrt{\omega})^2}{(\alpha-\beta)(\beta+\gamma)}\,\Phi_1(\alpha, \beta, \gamma, \omega) + k\Phi_2(\alpha, \beta, \gamma, \omega)+\ldots \qquad (3\text{-}4)$$

On the other hand were Equation (1-9) written as

$$\beta = 1 - \frac{(a+1)(\mu-a^2)(1-w^2)}{\mu(a^2+a+1) - a^2 - \mu w^2 - a w^2} \sim 1 - k \quad , \qquad (3\text{-}5)$$

Equation (3-4) then obtains its final form:

$$\frac{1}{k}\,\frac{(\sqrt{\alpha}+\sqrt{\omega})^2}{(\alpha-1)(\alpha+\gamma)} + F_1(\alpha, \gamma, \omega)+kF_2(\alpha, \gamma, \omega)+\ldots =$$

$$\frac{1}{k}\,\frac{(1+\sqrt{\omega})^2}{(\alpha-1)(1+\gamma)}\,\Phi_1(\alpha, \gamma, \omega)+k\Phi_2(\alpha, \gamma, \omega)+\ldots \qquad (3\text{-}6)$$

Therefore by the argument stated above, the surface $S(\alpha, \gamma, \omega)$ to which Equation (3-1) holds is given by

$$\frac{(\sqrt{\alpha}+\sqrt{\omega})^2}{\alpha+\gamma} = \frac{(1+\sqrt{\omega})^2}{1+\gamma} \quad . \tag{3-7}$$

This is the same relationship as Equation (2-3) found in the analysis for the case of k = 0, without using the integral relation (1-20).

It can be readily found that the integral relation should include the case of k = 0 by means of Equation (3-5), since

$$\lim_{\substack{k\to 0 \\ \beta\to 1}} \left(\frac{1+\sqrt{\beta}}{1-\sqrt{\beta}}\right)^k \to 1$$

and the right hand side of Equation (3-1) does not vanish.

The discussion in the preceding paragraphs eliminates the need for evaluating the integral in Equation (3-1), which was attempted both by a closed-form method and by numerical computations. The closed-form method was not tractable, while numerical computations were arduous, difficult and did not maintain the required accuracy.

By means of Equations (1-9), (1-11) and 3-7) the values of β, μ and γ can be determined for assumed values of $\alpha > 1$ and $0 < \omega < 1$. The flow characteristics then can be computed in close-form except for the ratio of the slit opening to the height of conduit (ℓ/h') and the contraction coefficient (c).

The investigation of some limiting cases leads to:

1) when $\mu \to \infty$,
Equations (1-11), (1-9) and 3-7) yield, respectively,

$$\alpha = \left(\frac{\sqrt{\omega}}{k}+1\right)^2 \tag{a}$$

and

$$\beta = \frac{\alpha+\sqrt{\alpha\,\omega}}{\alpha+\sqrt{\alpha}+1-\omega} \tag{b}$$

and

$$\gamma = \frac{\left[2\sqrt{\alpha}+(\sqrt{\alpha}+1)\sqrt{\omega}\right]\sqrt{\omega}}{\sqrt{\alpha}+1+2\sqrt{\omega}} \tag{c}$$

(3-8)

For the case $\mu \to \infty$ and assumed values of $0 < \omega < 1$, the values of α, β, and γ can be computed by Equation (3-8 a, b, c) afterwhich the flow characteristics θ, r, h''/h' can be determined by the general expressions given in section 1. This case physically corresponds to a conduit with an extremely large opening in its side. The width of the diverted jet is smaller than that attained in the case of straight conduit. Furthermore, it is noticeable that, as the size of the slit opening increases and tends to infinity, the width of the jet diverted through the opening approaches zero.

2) When $\mu \to \infty$ and $\alpha = 1$,

Equations (3-8) leads to: $\omega \to o\, \beta \to 0.3333$ and $\gamma \to 0$ (γ does not approach zero as quickly as ω)
For this case $\theta = 0$, $h''/h' = 0$ and $r = 0$. The entire discharge is conveyed through the main conduit.

3) When $\alpha \to 1$,

Equation (1-10) leads to $\mu = \alpha = 1$, independent of the value of ω. Then Equation (1-9) gives β the value of 1 for any value of ω, while Equation (3-7) or (3-8c) yields $\gamma = \sqrt{\omega}$. However, Equation (1-14) has meaning only if $\omega = 1$, which leads to:

$$r = 1 \quad \theta \to \frac{\pi}{2} \quad \text{and } h''/h' \to 0$$

This case corresponds to the physical case of an infinitely large container with a small side opening. The jet is diverted through an angle of 90^o and the angle of divergence has no influence on the jet's characteristics.

Up to this stage of the analysis no approximation has been made. The flow characteristics r, θ, h''/h' have been determined in closed-form expressions and the results are plotted in Figure 7 for the cases of $\phi = \frac{\pi}{64}$ and $\phi = \frac{\pi}{32}$.

In order to reach a conclusion on the influence of the angle of divergence in the case of an irrotational solution, the study of the physical characteristics ℓ/h' must be considered. At this stage it is assumed that k is small, i.e., the angle of divergence (ϕ) is smaller than $\frac{\pi}{32} = 6^o26'$. Equation (1-21) can be written in an expanded form, where only the two first terms are taken into account(10) as

$$\ell/h' = C\int_o^\infty f(\zeta)d\zeta + i2ck \int_o^\infty f(\zeta)\Phi(\zeta)d\zeta + \ldots \text{ , or} \qquad (3\text{-}9)$$
$$\ell/h' = CI_1 + i2ckI_2 \text{ ,}$$

where

$$f(\zeta) = \frac{(\sqrt{\zeta} + i\sqrt{\omega})^2}{(\zeta+\alpha)(\zeta+\beta)(\zeta-\gamma)}$$
$$\Phi(\zeta) = \tan^{-1}\frac{1}{\sqrt{\zeta}} - \tan^{-1}\frac{\sqrt{\alpha}}{\sqrt{\zeta}}$$

and

$$C = \frac{(\beta+\gamma)(\alpha-\beta)}{\pi(\sqrt{\beta}+\sqrt{\omega})^2}\left(\frac{\sqrt{\alpha}+\sqrt{\beta}}{\sqrt{\alpha}-\sqrt{\beta}}\right)^k\left(\frac{1-\sqrt{\beta}}{1+\sqrt{\beta}}\right)^k .$$

The first term (I_1) of Equation (3-9) is the value of ℓ/h' for k = 0 and its coefficient (c) reduces to

$$C_1 = \frac{1}{\pi(\alpha+\gamma)(1+\sqrt{\omega})^2} .$$

The integrand of the second term I_2 is a combination of the integrand of I_1 and the function $\phi(\zeta)$ which is bounded. Its maximum value is attained as $\zeta = \sqrt{\alpha}$. As a result

$$\max.\Phi(\zeta) = \tan^{-1}\frac{1}{4\sqrt{\alpha}} - \tan^{-1}4\sqrt{\alpha} \quad .$$

Therefore, the following inequality holds:

$$\left|2ck\int_0^\infty f(\zeta)\Phi(\zeta)d\zeta\right| < 2c_2k\Phi(\sqrt{\alpha}) \left|c_1\int_0^\infty f(\zeta)d\zeta\right| \sim 2c_2k\Phi(\sqrt{\alpha})\left|I_1\right| = I'_2,$$

where

$$c_2 = \left(\frac{\sqrt{\alpha}+\sqrt{\beta}}{\sqrt{\alpha}-\sqrt{\beta}}\right)^k \left(\frac{1-\sqrt{\beta}}{1+\sqrt{\beta}}\right)^k \quad .$$

The actual value of the second term of Equation (3-9) is much smaller than I'_2. It can be shown by calculation that $I'_2 = (1.5 = 3\%)\, I_1$. Since $I_1 < 1$, the use of the second term (I_2) in Equation (3-9) with the first term (I_1) will alter the values of ℓ/h' to the second or third decimal point.

Therefore, for the case of a small angle of divergence and for $\alpha \leq 9$ which covers the range of practical applications, it can be assumed that the lines of ℓ/h' remain almost invariable as k varies from 0 to $\frac{\pi}{32}$.

Using this fact the theoretical results obtained from $\frac{h''}{h'}$ versus θ plane (Figure 7) can be transferred to θ versus r plane (Figures 10 and 11) which has been used for comparison with experimental work.

4 - Experimental Investigation

The main features of the equipment and instrumentations as well as the experimental procedure are discussed briefly in this section. The entire experimental work was conducted in the Fluid Laboratory at Columbia University. The fluid used in the experimental work was water. The open channel in which the experiments were conducted was 21 feet long, 15 inches wide and 37 inches deep. It is part of a circuit formed by a reservoir, pump, constant head tank, entrance section, two exit tanks with measuring weirs and a returning channel leading to the reservoir or to a volumetric measuring tank.

The actual test section was made by inserting two carriers (Figure 8) and a partially movable bottom into the channel so that it was divided into four parts: (1) an entrance chamber, (2) a main conduit, (3) an upper chamber and (4) the remainder of the channel. The lifting mechanism under the partially movable bottom provided a maximum angle of convergence and divergence of some seven degrees in the inlet section of the main conduit.

The measuring equipment consisted of a pitot-tube with a traversing mechanism, standard point gages, a protractor, a micromanometer, a set of tubing to feed sufficient quantity of dye into the test section and a pair of triangular weirs to measure the two discharges.

The pitot-tube consisted of a streamlined stem and three removable tips to permit reading of the differential pressures at three different stations of the inlet conduit.

The protractor consisted of a quadrant which was divided into one degree divisions, a carriage which bore the pointer and a micrometer head used for small adjustments. The protractor was used for measuring the angle of the diverted jet. This was done by centering the pointer in the jet flow and by making it parallel to the jet.

The main problem in the experimental work was to regulate and control the discharge of water passing through the slit and the main conduit, to read the angle of the diverting jets and to determine the fluid's velocity at different sections in the inlet conduit.

Regulation of the discharge was achieved by calibrated weirs of known discharge coefficients. Main readings were taken of the two discharges, the angle of the side jet, and the velocity distribution in the upstream inlet section. In order to read the angle of the jet, a sufficient quantity of dye was inserted to make the jet visible. A picture also was taken of each test. Another important feature of this investigation was the velocity distributions used for comparing the results of straight and divergent inlet conduits. Differential pressure between the pitot-tube and hydrostatic wall tap was measured by means of the pitot-tube and micromanometer. The velocity distributions was obtained by

$$V^2 = \frac{10.40}{\rho} \Delta p \quad \text{ft.}^2/\text{sec.}^2 \quad ,$$

where Δp = differential pressure in inches of water
and ρ = density in slug / ft.^{3}.

Velocity distributions were taken at three different stations, 2 7/16, 6 3/8 and 12 5/16 inches from the leading edge of the opening. The results were plotted in a non-dimensional form y/d versus u/u_m (see as an example Figure 9) where

y = distance from the central line of the conduit
d = 1/2 of the corresponding height of the conduit
u = velocity at the point under consideration
u_m = maximum velocity at the section under consideration

Table I gives values of h_i, d_i, 1_i, and the corresponding area (A_i) for the various cases under consideration.

Experimental work was carried out for a straight conduit as well as for a divergent inlet channel with angles of divergence $\phi = \frac{\pi}{64} = 2^{\circ}45' 48''$ and $\phi = \frac{\pi}{32} = 6^{\circ}25' 40''$. Several slit openings and various discharge ratios were used for each geometry.

In the straight conduit case the velocity distribution was almost uniform except at the boundary later. When an angle of divergence was used, the deviation of the velocity distribution from uniform became more and more pronounced as the angle was increased. In most cases the velocity distribution was nearly symmetric, the exceptions being cases in which separation was imminent.

The plot of the experimental results on charts representing the theoretical

Table I

Angle of divergence	Scheme	Station 1 ℓ_1 = 2 7/16"	Station 2 ℓ_2 = 6 3/8"	Station 3 ℓ_3 = 12 5/16"
$\phi = 0$	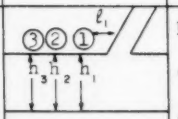	h_1 = 1.905" d_1 = 0.9525" A_1 = 0.1984ft.^{2}	h_2 = 1.905" d_2 = 0.9525" A_2 = 0.1984ft.^{2}	h_3 = 1.905" d_3 = 0.9525" A_3 = 1984ft.^{2}
$\phi = 2^o45'48"$	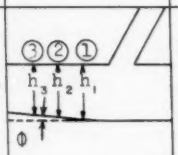	h_1 = 1.9852" d_1 = 0.8926" A_1 = 0.1859ft.^{2}	h_2 = 1.5918" d_2 = 0.796" A_2 = 0.1658ft.^{2}	h_3 = 1.3001" d_3 = 0.6506" A_3 = 0.1354ft.^{2}
$\phi = 6^o25'43"$	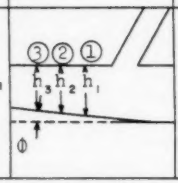	h_1 = 1.6303" d_1 = 0.8152" A_1 = 0.1698ft.^{2}	h_2 = 1.1867" d_2 = 0.5934" A_2 = 0.1236ft.^{2}	h_3 = 0.5177" d_3 = 0.2588" A_3 = 0.0539ft.^{2}

solution shows a close agreement in the case of a straight conduit with uniform velocity distribution (Figure 5), but depicts a definite deviation in the case of a divergent conduit with non-uniform velocity distribution. As the velocity distribution becomes more and more non-uniform the deviation of the theoretical and experimental points becomes more and more pronounced. (Figures 10 and 11).

CONCLUSIONS

The free-streamline theory is the only one which offers an analytic solution to the divided flow phenomena, but the stumbling-block for the generalization of its principles was believed to be attributed to the velocity distribution in the inlet. The main goal of this investigation was to determine qualitatively the influence of the velocity distribution on the solution obtained by the free-streamline theory.

Both the experimental work and the analysis established the fact that the upstream velocity distribution is another essential factor for the determination of the divided flow pattern by the free streamline theory.

This conclusion has been established by comparison of the theoretical solution, obtained by the free streamline, with corresponding experiments for several different angles of divergence, which are equivalent to considering several different velocity distributions.

As long as the upstream distribution remains essentially uniform, the free streamline solution is verified fully by the experiments. However, when the velocity distribution is not uniform, the characteristics of the diverted jet

shows a systematic difference, but remain similar in general aspects.

An angle of divergence of $\phi = 2^{O}45' 48''$, which alters the velocity distribution slightly from uniformity, lowers the angle of diverting jet by 1 1/2 to 4 degrees. An angle of divergence of $\phi = 6^{O}25' 43''$, which alters the velocity distribution considerably, lowers the angle of the jet inclination by 2 1/2 to 6 degrees.

The similarity in results found between analysis and experiments suggests an attempt to incorporate the velocity factor to the principle of the free streamline theory. This may lead to a generalization of the free streamline theory for rotational flow, which at the present is relatively intractable from a theoretical stand-point.

The analysis used in this investigation leads to a close-form solution for the flow characteristics in a straight conduit case as well as in the case of a divergent inlet conduit with a small angle of divergence ($\phi \leqslant \frac{\pi}{32}$). However, for any angle of divergence $\frac{\pi}{32} < \phi < \frac{\pi}{2}$ close-form expressions are obtained for the natural angle, the ratio of discharges and the ratio of the width of the jet to the height of the conduit.

Figures 5 through 10 show the variation of the flow characteristics for different slit openings and discharge ratios. These variations are discussed in Reference 11 as a function of the pressure variation.

The analysis developed herein, based on the free streamline theory and applied to a small angle of divergence of the inlet conduit, is expected to be useful for design purposes or/and as a guide for the interpretation of experimental data for similar geometrical configurations.

ACKNOWLEDGMENT

The author is grateful to Professor A. Craya, M. Friedman, R. Skalak and J. Weiner for their valuable advice and criticism throughout this investigation. The author also expresses a special gratitude to Professor R. Skalak under whose supervision and advise the work was carried out. This project was partially supported by the Office of Naval Research under Contract Nonr 266(10).

REFERENCES

1. Thomas, D.: "Hydraulic Losses in Pipe Fittings," Trans. of the Tokyo Sectional Meeting, World Power Conference.

2. Vogel, G.; "Untersuchungen über der Verlust in rechtwinklingen Rohrverzweigungen," Inst. der Tech. Hock., Munich, Germany, Vol. I, 1926, pp. 75-90 and Vol. II, 1928, pp. 51-54.

3. Craya, A.: "Ecoulement Potentiel," Unpublished Manuscript, 1940.

4. McNown, J. and En-Yum Hsu: "Application of Conformal Mapping to Divided Flow," Proc. of the Midwestern Conference on Fluid Dynamics, 1951, pp. 143-155.

5. McNown, J. and Chia-Shun Yih: "Free Streamline Analyses of Transition Flow and Jet Defection," State University of Iowa, Studies in Engin., Bul. 35, No. 427, 1953.

6. Bureau of Reclamation: "Model Studies of Penstocks and Outlet Works, and Penstocks and Outlet Pipes," Boulder Canyon Project, Final Report, Part IV, Vol. 2, 1938 and Bul. 5, 1940.

7. Schlichting, H.: "Boundary Layer Theory," McGraw-Hill, 1955, p. 400.

8. Nikuradsi, J.: "Untersuchungen über die Stromungen des Wassers in Konvergenten Divergenten Kanalen," Forchungsarbeiten des Vereines Deutcher Ingenieur, Heft, 289, 1929.

9. Milne-Thomson, L. M.: "Theoretical Hydrodynamics," MacMillan Co., 1950.

10. Tsakonas, S.: "Divided Flow through a Divergent Inlet Conduit," Ph.D. Dissertation, Columbia University, 1956.

11. McNown, J.: "Mechanics of Manifold Flow," A.S.C.E. Trans. 1954, pp. 1103-1118.

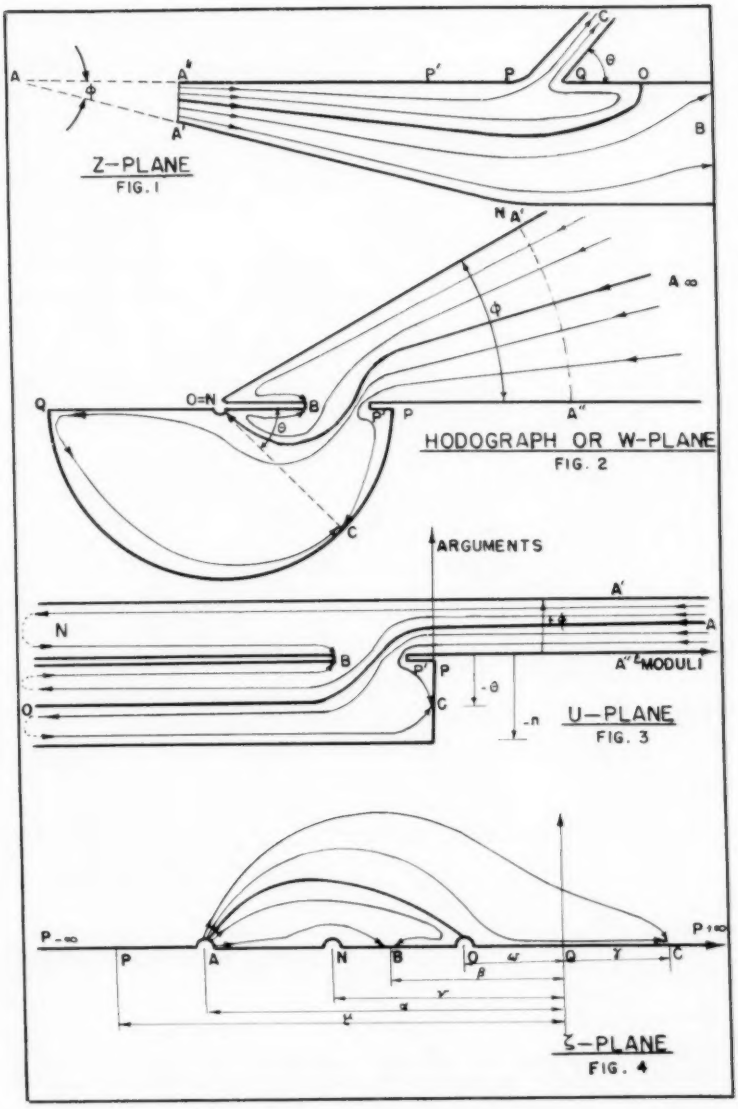
A
Φ
A'
P'
P
Q
θ
O
C
B
Z-PLANE
FIG. 1
N
A'
A∞
Φ
Q
O=N
B
θ
P'
P
A''
C
HODOGRAPH OR W-PLANE
FIG. 2
ARGUMENTS
A'
N
B
A
P'
P
A''
MODULI
Q
C
-θ
-n
U-PLANE
FIG. 3
P-∞
P+∞
P
A
N
B
O
Q
C
β
γ
α
ζ
ζ-PLANE
FIG. 4

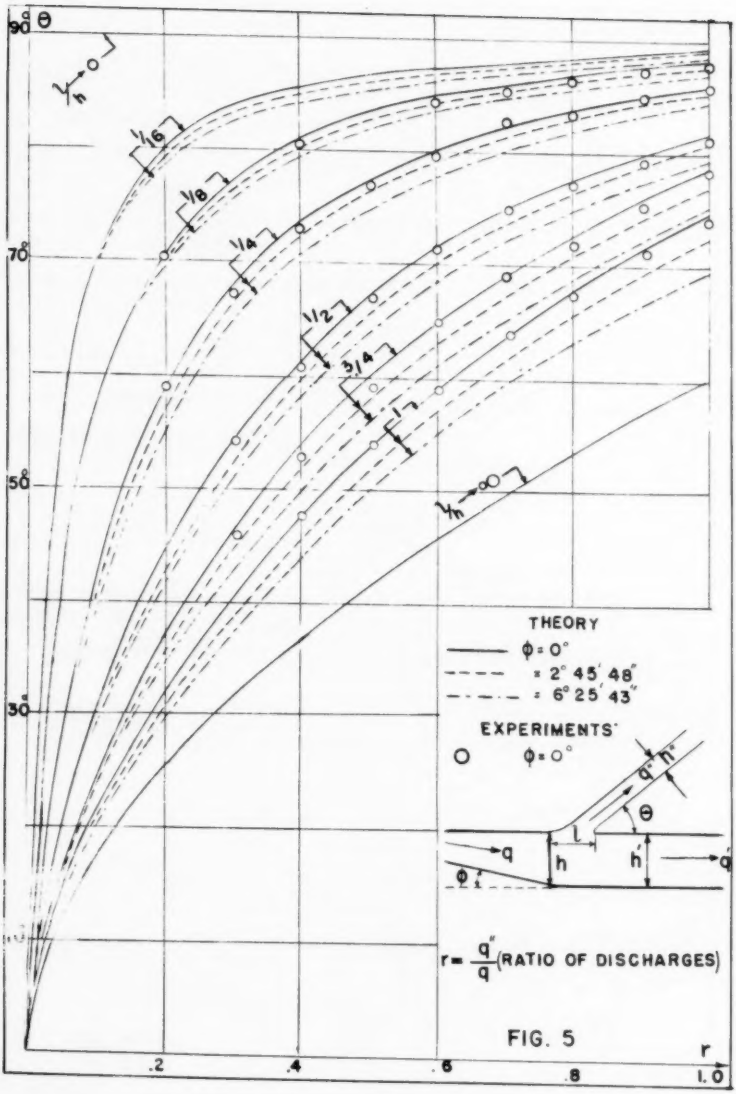
90°
θ
70°
50°
30°
1/16
1/8
1/4
1/2
3/4
1
1/h
THEORY
φ = 0°
= 2° 45' 48"
= 6° 25' 43"
EXPERIMENTS
φ = 0°
q''
h''
θ
l
q
h
h'
q'
φ
r = q''/q (RATIO OF DISCHARGES)
.2
.4
.6
.8
1.0
r

FIG. 5

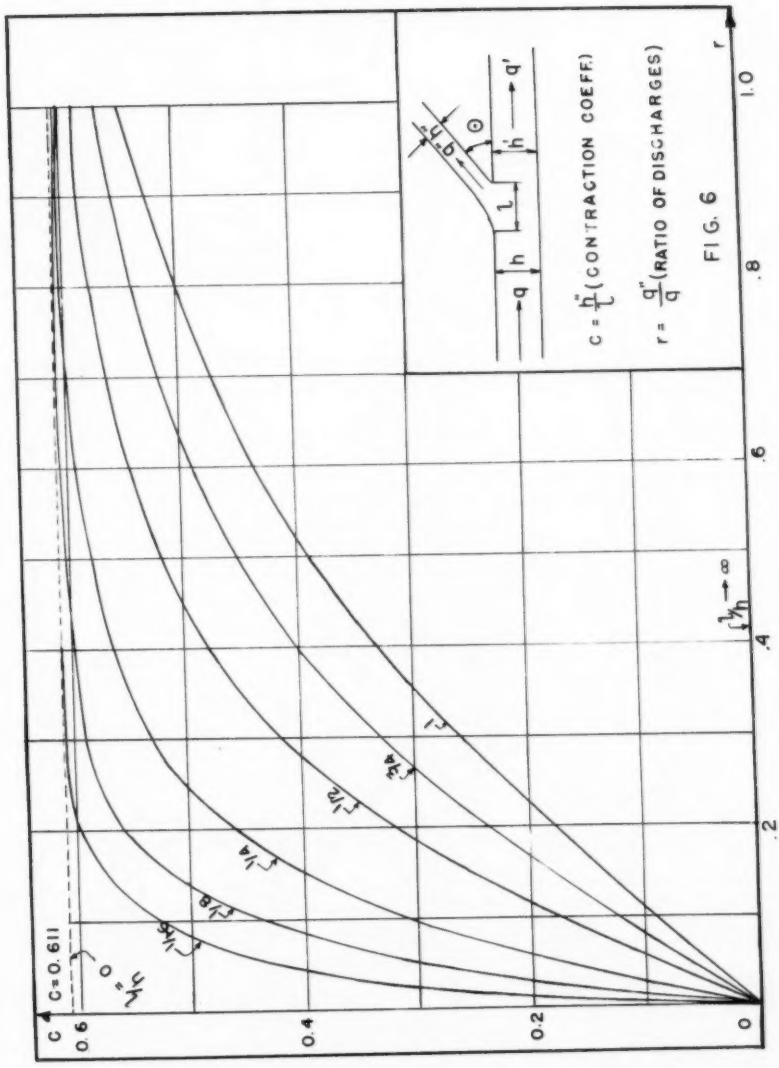
c
C=0.611
θ=π/2
3π/4
π
2π/3
π/4
π/6
π/8
π/12
0
0.2
0.4
0.6
.2
.4
.6
.8
1.0
r
h/h → ∞
q
h
l
h'
q'
θ
4b
c = h''/h' (CONTRACTION COEFF.)
r = q''/q (RATIO OF DISCHARGES)

FIG. 6

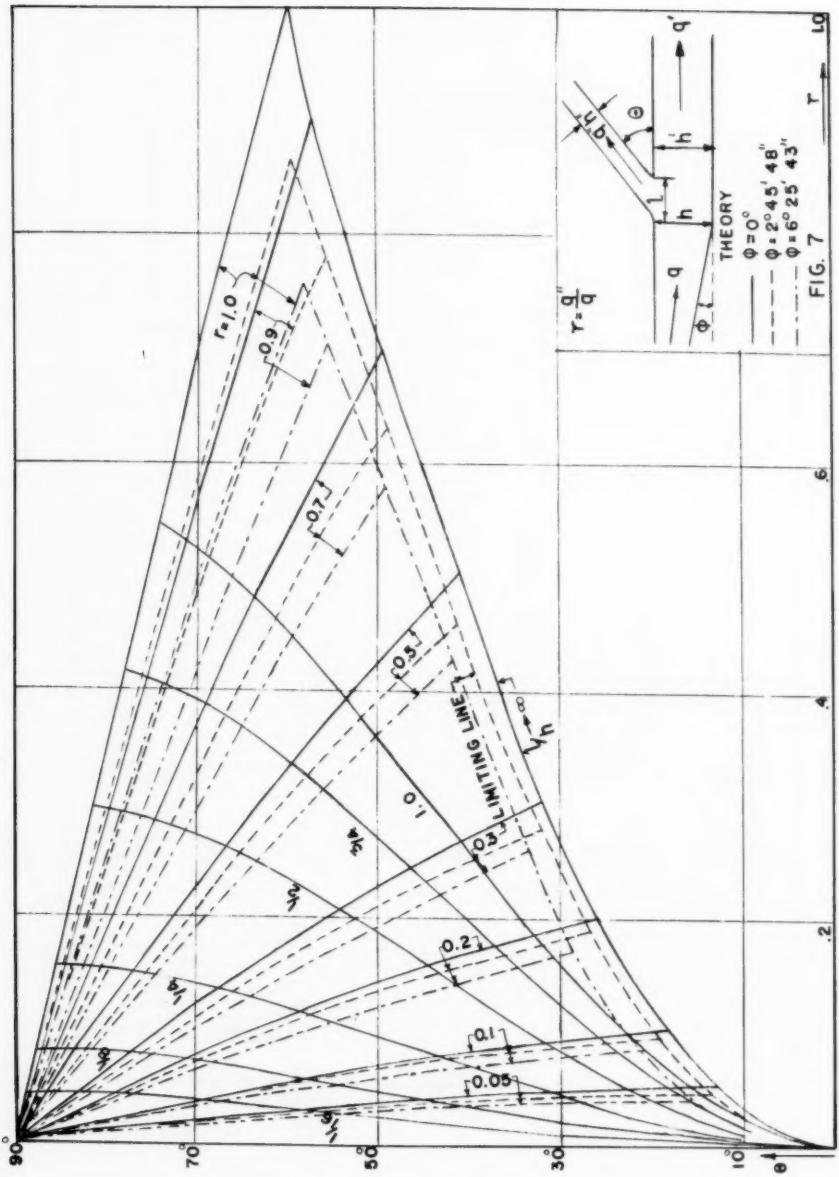
r=1.0
0.9
0.7
0.5
0.3
0.2
0.1
0.05
LIMITING LINE
h/l
∞
90°
70°
50°
30°
10°
θ
.6
.4
.2
r=q''/q
q
q'
θ
h'
h
l
b
φ
THEORY
φ=0°
φ=2°45' 48"
φ=6°25' 43"
r
1.0

FIG. 7

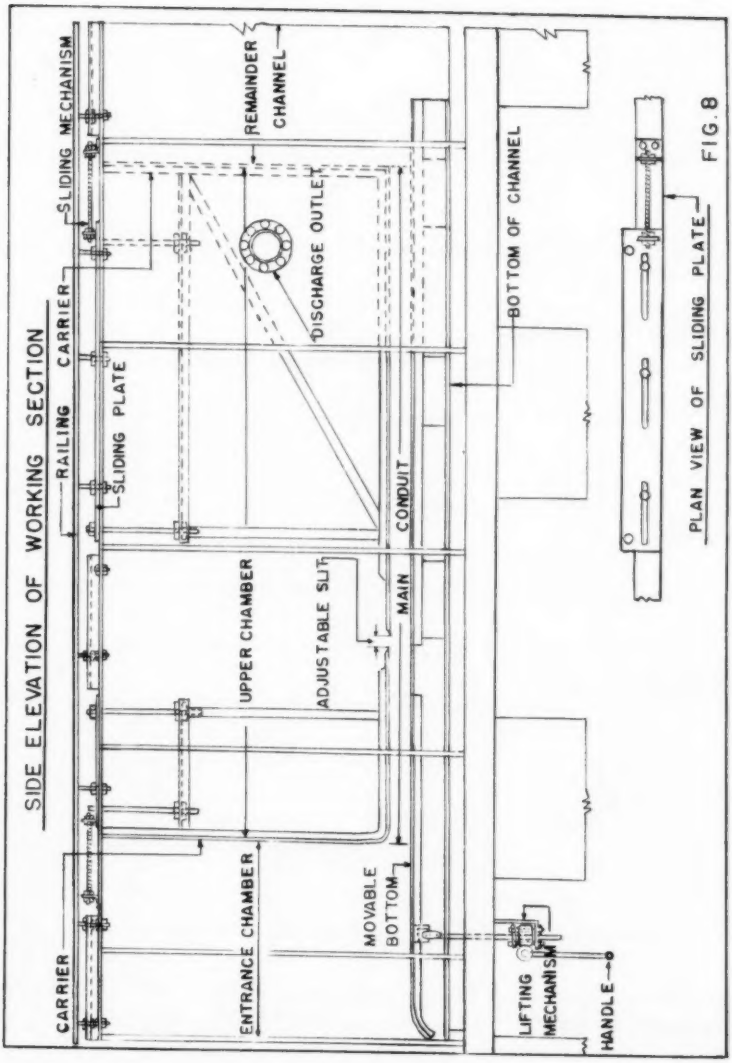
SIDE ELEVATION OF WORKING SECTION
SLIDING MECHANISM
RAILING
CARRIER
SLIDING PLATE
REMAINDER CHANNEL
DISCHARGE OUTLET
BOTTOM OF CHANNEL
CONDUIT
UPPER CHAMBER
ADJUSTABLE SLIT
MAIN
CARRIER
ENTRANCE CHAMBER
MOVABLE BOTTOM
LIFTING MECHANISM
HANDLE
PLAN VIEW OF SLIDING PLATE

FIG. 8

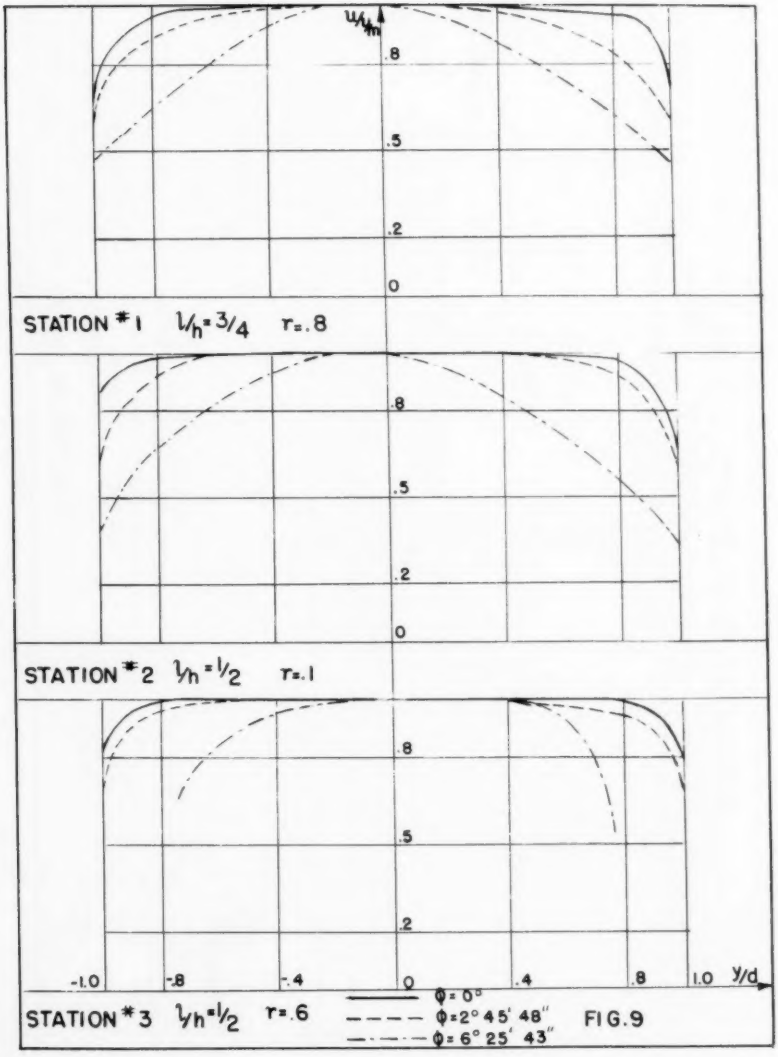
u/u_m
.8
.5
.2
0
STATION #1 l/h=3/4 r=.8
.8
.5
.2
0
STATION #2 l/h=1/2 r=.1
.8
.5
.2
-1.0
-.8
-.4
0
.4
.8
1.0
y/d
STATION #3 l/h=1/2 r=.6
φ=0°
φ=2°45'48"
φ=6°25'43"

FIG.9

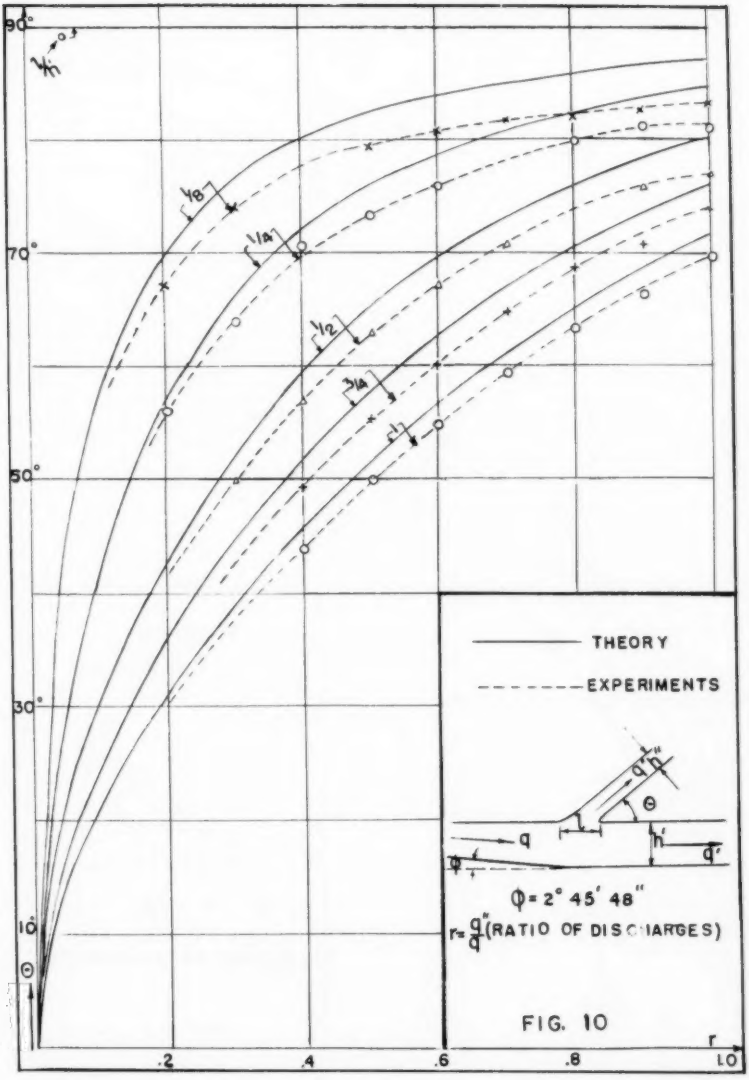
90°
70°
50°
30°
10°
Θ
.2
.4
.6
.8
1.0
r
1/8
1/4
1/2
3/4
1
THEORY
EXPERIMENTS
q
q'
q''
h'
Θ
Φ = 2° 45' 48"
r = q''/q (RATIO OF DISCHARGES)

FIG. 10

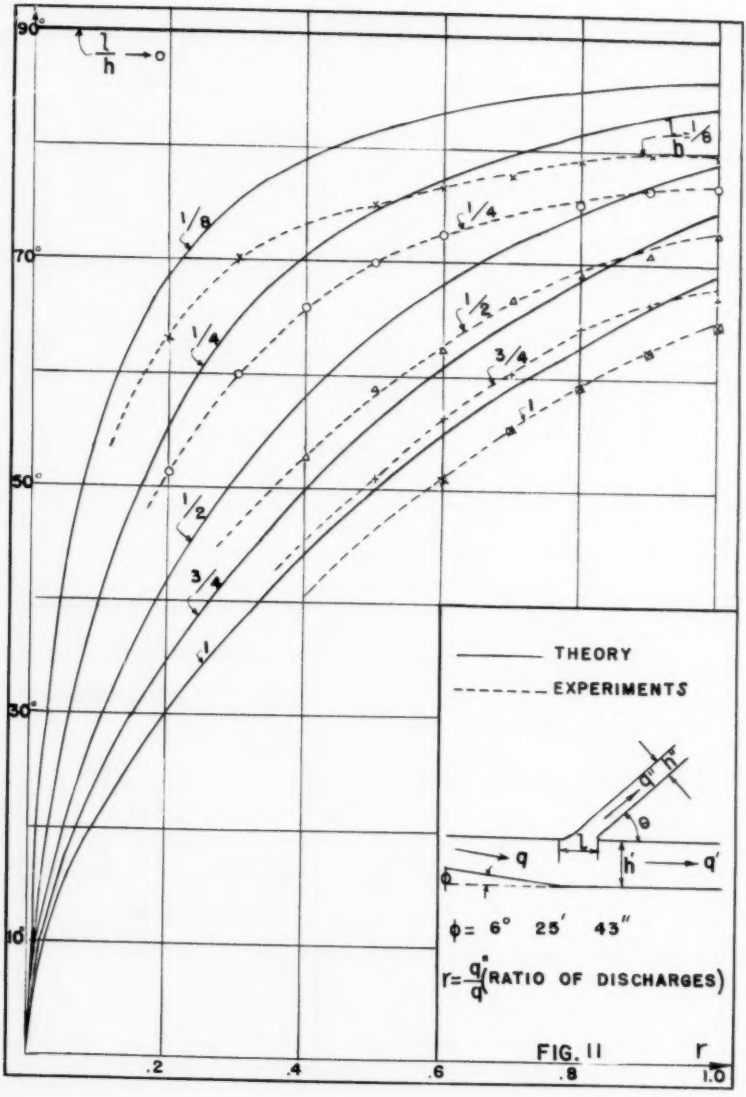
90°
70°
50°
30°
10°
.2
.4
.6
.8
1.0
r
l/h → 0
1/8
1/4
1/2
3/4
1
l/h = 1/8
THEORY
EXPERIMENTS
q''
h''
θ
q
h'
q'
φ
r
φ = 6° 25' 43"
r = q'/q (RATIO OF DISCHARGES)

FIG. 11